USAAVLABS TECHNICAL REPORT 68-44

WIND TUNNEL TESTS OF FULL-SCALE ROTORS OPERATING AT HIGH ADVANCING TIP MACH NUMBERS AND ADVANCE RATIOS

By

W. H. TANNER
J. F. VAN WYCKHOUSE

JULY 1968

U. S. ARMY AVIATION MATERIEL LABORATORIES
FORT EUSTIS, VIRGINIA

CONTRACT DA 44-177-AMC-291(T)
CONTRACT DAAJ02-67-C-0018

BELL HELICOPTER COMPANY
FORT WORTH, TEXAS

Disclaimers

The findings in this report are not to be construed as an official Department of the Army position unless so designated by other authorized documents.

When Government drawings, specifications, or other data are used for any purpose other than in connection with a definitely related Government procurement operation, the United States Government thereby incurs no responsibility nor any obligation whatsoever; and the fact that the Government may have formulated, furnished, or in any way supplied the said drawings, specifications, or other data is not to be regarded by implication or otherwise as in any manner licensing the holder or any other person or corporation, or conveying any rights or permission, to manufacture, use, or sell any patented invention that may in any way be related thereto.

Disposition Instructions

Destroy this report when no longer needed. Do not return it to originator.

DEPARTMENT OF THE ARMY
U. S. ARMY AVIATION MATERIEL LABORATORIES
FORT EUSTIS, VIRGINIA 23604

This report has been reviewed by the U. S. Army Aviation Materiel Laboratories and is considered to be technically sound. The report is published for the exchange of information and the stimulation of ideas.

TASK IF125901A13903
Contract DA 44-177-AMC-291(T)

Task IF125901A14231
Contract DAAJ02-67-C-0018

USAAVLABS Technical Report 68-44
July 1968

WIND TUNNEL TESTS OF FULL-SCALE ROTORS OPERATING AT HIGH ADVANCING TIP MACH NUMBERS AND ADVANCE RATIOS

Bell Helicopter Report 576-099-001

By

W. H. Tanner
J. F. Van Wyckhouse

Prepared by

Bell Helicopter Company
A Division of Bell Aerospace Corporation
Fort Worth, Texas

for

U. S. ARMY AVIATION MATERIEL LABORATORIES
FORT EUSTIS, VIRGINIA

SUMMARY

A joint U. S. Army Aviation Materiel Laboratories/NASA-Ames/Bell Helicopter Company experimental investigation of three full-scale sets of rotor blades was conducted in the NASA-Ames Large Scale Wind Tunnel. Tested were: (1) production UH-1D (NACA 0012 profile) 48-foot-diameter blades, (2) modified UH-1D blades reduced in thickness at the tip, and (3) UH-1D blades reduced in diameter to 34 feet. The production blades were evaluated at Mach numbers up to 0.95, the thin-tipped blades to Mach 1.025, and the 34-foot rotor to advance ratios of 0.79. The production and thin-tipped blades are compared to show the compressibility effects. At higher tip Mach numbers, a significant reduction in power required was obtained with the thin-tipped blades. Additionally, the state of the art of calculating rotorcraft performance at high tip speeds and advance ratio is reviewed, and limited experimental data obtained with special boundary layer instrumentation installed at the 3/4 radius and surface pressure instrumentation installed near the blade tip are presented.

FOREWORD

The results from the full-scale rotor performance tests of a two-bladed semirigid rotor system are contained in this report. The tests were conducted in the Large Scale Wind Tunnel at NASA-Ames Research Center. The project was performed under Contracts DA 44-177-AMC-291(T) and DAAJ02-67-C-0018 under the technical cognizance of Patrick Cancro, Project Engineer, U. S. Army Aviation Materiel Laboratories.

The assistance and cooperation of Advanced Engineering personnel and the Engineering Laboratories of the Bell Helicopter Company and the active participation of John McCloud, III, and James Biggers of the NASA-Ames Research Center, in organizing and conducting the tests, are gratefully acknowledged. The analytical techniques used in this report and the advanced instrumentation were developed as part of the Bell Helicopter Company Independent Research and Development program.

TABLE OF CONTENTS

LIST OF ILLUSTRATIONS

Figure		Page
15	Theory-Test Comparison, Nondimensional Performance of UH-1D Rotor at Various Combinations of Advance Ratio and Advancing Tip Mach Number	28
16	Theory-Test Comparison, Nondimensional Performance of Thin-Tipped Blades at μ = 0.30 and M(1.0, 90.) = 0.95	33
17	Theory-Test Comparison, Nondimensional Performance of Thin-Tipped Blades at μ = 0.35 and M(1.0, 90.) = 1.00	34
18	Variation of Critical and Drag Divergence Mach Number with Thickness Ratio	35
19	Theory-Test Comparison, Nondimensional Performance of 34-Foot-Diameter Rotor at μ = 0.51, M(1.0, 90.) = 0.65	36
20	Theory-Test Comparison, Nondimensional Performance of 34-Foot-Diameter Rotor at μ = 0.66, M(1.0, 90.) = 0.55	39
21	Theory-Test Comparison, Nondimensional Performance of 34-Foot-Diameter Rotor at μ = 0.79, M(1.0, 90.) = 0.52	42
22	Theory-Test Comparison, Control Positions of UH-1D Rotor at μ = 0.30, M(1.0, 90.) = 0.85	45
23	Boundary Layer Button Details	47
24	Variation of Yaw Angle on the Upper Surface with a Change in Azimuth Position for Two Values of Rotor Lift. μ = 0.27, M(1.0, 90.) = 0.90	48
25	Surface Pressure Distribution at 0.98R for Various Azimuths, μ = 0.20, M(1.0, 90.) = 0.85, C_L/σ = 0.0734, C_D/σ = 0.0051	49
26	Surface Pressure Distribution at 0.98R for Various Azimuths, μ = 0.20, M(1.0, 90.) = 0.85, C_L/σ = 0.0604, C_D/σ = 0.00406	51

LIST OF TABLES

LIST OF SYMBOLS

a	Speed of sound, ft/sec
a_o	Rotor coning angle, the component of flapping which is constant and independent of the blade azimuth position, deg
a_{1_s}, a_{2_s} . . . a_{n_s}	Components of longitudinal flapping with respect to the shaft. Constant coefficients of the cosine terms in the Fourier series expressing flapping with respect to a plane normal to the shaft axis, deg
A_{1_s}	Lateral cyclic pitch control with respect to the shaft axis, deg
b	Number of blades
b_{1_s}, b_{2_s} . . . b_{n_s}	Component of lateral flapping with respect to the shaft axis. Constant coefficients of the sine terms of the Fourier series expressing flapping with respect to a plane normal to the shaft axis, deg
B_{1_s}	Longitudinal cyclic pitch with respect to the shaft axis, deg
c	Blade chord, ft
c_d	Section drag coefficient
c_l	Section lift coefficient
C_D/σ	Rotor drag coefficient, $C_D/\sigma = D/\rho bcR(\Omega R)^2$
C_L/σ	Rotor lift coefficient, $C_L/\sigma = L/\rho bcR(\Omega R)^2$
C_Q/σ	Rotor torque coefficient, $C_Q/\sigma = Q/\rho bcR^2(\Omega R)^2$
D	Drag, the component of the resultant force parallel to the relative wind direction, positive in the downwind direction, lb
f	Equivalent flat plate area, D/q
I	Mass moment of inertia about the flapping hinge, slug-ft^2

L	Lift, the component of rotor resultant force perpendicular to the relative wind direction in the plane of the relative wind and the shaft, positive up, lb
$\mathcal{L}$	Rolling moment, the moment about the x axis, positive clockwise looking upstream, ft-lb
M	Mach number, $M = V/a$
$M_{(1.0,\ 90.)}$	Advancing tip Mach number
$\mathfrak{M}$	Pitching moment, the moment about the y axis, positive nose up, ft-lb
$\mathfrak{N}$	Yawing moment, the moment about the z axis, positive clockwise from above, ft-lb
q	Dynamic pressure, lb/sq ft
Q	Shaft torque, the moment about the shaft z axis, positive when torque tends to accelerate the rotor, ft-lb
R	Rotor radius, ft
t	Airfoil thickness, ft
V	Forward speed, fps
Y	Force perpendicular to L and D forces, positive to the right when viewed from downstream, lb
α_s	Shaft angle of attack, the angle between the relative wind and a plane normal to the shaft axis, positive in nose-up direction, deg
α_c	Control axis angle of attack, the angle between the relative wind, the shaft axis, and the projection of the control axis on the plane of the relative wind axis, positive in nose-up direction, deg
β	Flapping angle at any azimuth position referred to the plane normal to the shaft axis, positive up, deg

$$\beta = a_o - a_{1_s} \cos\psi - b_{1_c} \sin\psi - a_{2_s} \cos 2\psi - b_{2_s} \sin 2\psi \; . \; . \; . - b_{n_s} \sin n\psi$$

γ	Radial flow angle, deg
θ	Blade section pitch angle at any azimuth position referred to the shaft axis, positive leading edge up, deg
θ_o	Blade collective pitch angle measured at root (Blade Sta. 28), constant term of Fourier series representing blade pitch (it is assumed that only the first harmonic cyclic pitch is impressed), deg

$$\theta = \theta_o - A_{1_s} \cos\psi \;\; B_{1_s} \sin\psi$$

$\theta_{.75R}$	Blade collective pitch angle measured at 0.75R, deg
θ_1	Difference between hub (blade extended to center of rotation) and tip pitch angles, positive when tip angle is larger, deg
μ	Advance ratio, $\mu = \frac{V}{\Omega R}$
ρ	Density of air, slugs/ft^3
σ	Rotor solidity, $\sigma = \frac{bc}{\pi R}$
ψ	Blade azimuth angle measured from downwind in the direction of rotation in a plane normal to the shaft axis, deg
Ω	Rotor shaft angular velocity, rad/sec

Systems of Axes

1. Wind axis system:

x_w	Longitudinal Wind Axis. Axis lying along the airstream or relative wind direction.
z_w	Normal Wind Axis. Axis perpendicular to the longitudinal wind axis in the plane of the wind axis and the shaft centerline.
y_w	Lateral Wind Axis. Axis perpendicular to the x_w and z_w axes.

2. Shaft axis system:

z_s — Shaft Axis. Axis coincident with the shaft centerline.

x_s — Longitudinal Shaft Axis. Axis perpendicular to the shaft axis, in the plane of the shaft axis and relative wind direction.

y_s — Lateral Shaft Axis. Axis perpendicular to the x_s and z_s axes. This axis is coincident with the lateral y_w wind axis.

3. Control axis system:

z_c — Control Axis. Axis of no feathering, axis with reference to which there is no first harmonic pitch change with azimuth angle. This axis may be tilted with respect to the shaft longitudinally (with ($B1_s$) and laterally (with $A1_s$), separately or in combination.

x_c — Longitudinal Axis. Axis perpendicular to the control axis in the plane of the control axis and the relative wind direction.

y_c — Lateral Axis. An axis perpendicular to the x_c and z_c axis.

4. Virtual axis system:

z_v — Virtual axis. Axis of no flapping. An axis with respect to which there is no first harmonic blade flapping. This axis is perpendicular to the "tip path plane" for zero flapping hinge offset.

x_v — Longitudinal Axis. An axis perpendicular to the vertical axis in the plane of the virtual axis and the relative wind direction.

y_v — Lateral Axis. An axis perpendicular to the x_v and z_v axis.

INTRODUCTION

For years, the rule "do not exceed an advancing tip Mach number of 0.8" was accepted by most rotary-wing aerodynamicists. However, as with most arbitrary rules, experience has modified this attitude. In References 1 and 2, it is shown that there are real benefits to be obtained from high tip speeds if compressibility power losses can be minimized. Furthermore, in the near future, rotorcraft operation at Mach 1.0 and above will become commonplace with (1) high-performance rotorcraft in maneuvers, especially in cold weather, and (2) many low-disc-loading composite-type aircraft. Because of the high installed power, composite aircraft will have the capability of obtaining high helicopter speeds (in excess of normal conversion speeds), which will result in high advancing tip Mach numbers.

Fixed-wing aerodynamicists have largely been able to avoid the transonic region. Until recently, rotary-wing aerodynamicists, busy with other facets of their unique aircraft, have neglected the complicated and little-understood compressibility effects. Supercritical rotor blade operation is a normal occurrence today. Supersonic rotor blade tip operation can be expected to become commonplace if the speed potential of rotorcraft is to be fully realized.

Also, high advance ratio flight will soon be commonplace. Studies (References 2 through 4 are examples) have shown the compound helicopter to be an attractive configuration for achieving speeds of 250 knots and more. Several compound research aircraft have flown and are flying at the present time. In spite of the success of these research aircraft, experimental full-scale rotor data at high advance ratios taken under controlled conditions are extremely limited. To help fill this gap, experimental information for a two-bladed semirigid rotor operating at high advance ratios is required.

To achieve the ultimate potential as well as to understand the complex aerodynamic environment of today's high-performance rotorcraft, the theoretical and empirical aspects of rotor operation must be extended. From this work, new rotor designs will be evolved which are capable of efficient operation in the transonic-supersonic regions, and at high advance ratios as compound helicopters.

This report presents results for a two-bladed semirigid rotor system for advancing blade tip Mach numbers to 1.025 and advance ratios to 0.79. The tests were conducted in the NASA-Ames Large Scale (40- x 80-foot) Wind Tunnel. In addition to the basic rotor performance investigation, feasibility tests were conducted with a new instrument, the Boundary Layer

Button, for measuring velocity, magnitude, and direction in and out of the boundary layer. Also, some airfoil surface pressure measurements were made at 0.98R, where present theory assumes the lift to be zero (tip loss factor).

TEST EQUIPMENT

ROTOR TEST MODULE

The rotor test module is shown in the NASA-Ames 40- x 80-Foot Wind Tunnel (Figure 1). The stand includes a mounting frame, a UH-1 pylon system, a speed increaser gearbox, an electric drive motor, and an aerodynamic fairing. The mounting frame, pylon, and drive system are enclosed by an aerodynamic fairing of tear-drop shape. The maximum diameter of the fairing is 6.66 feet, and the length is 22 feet.

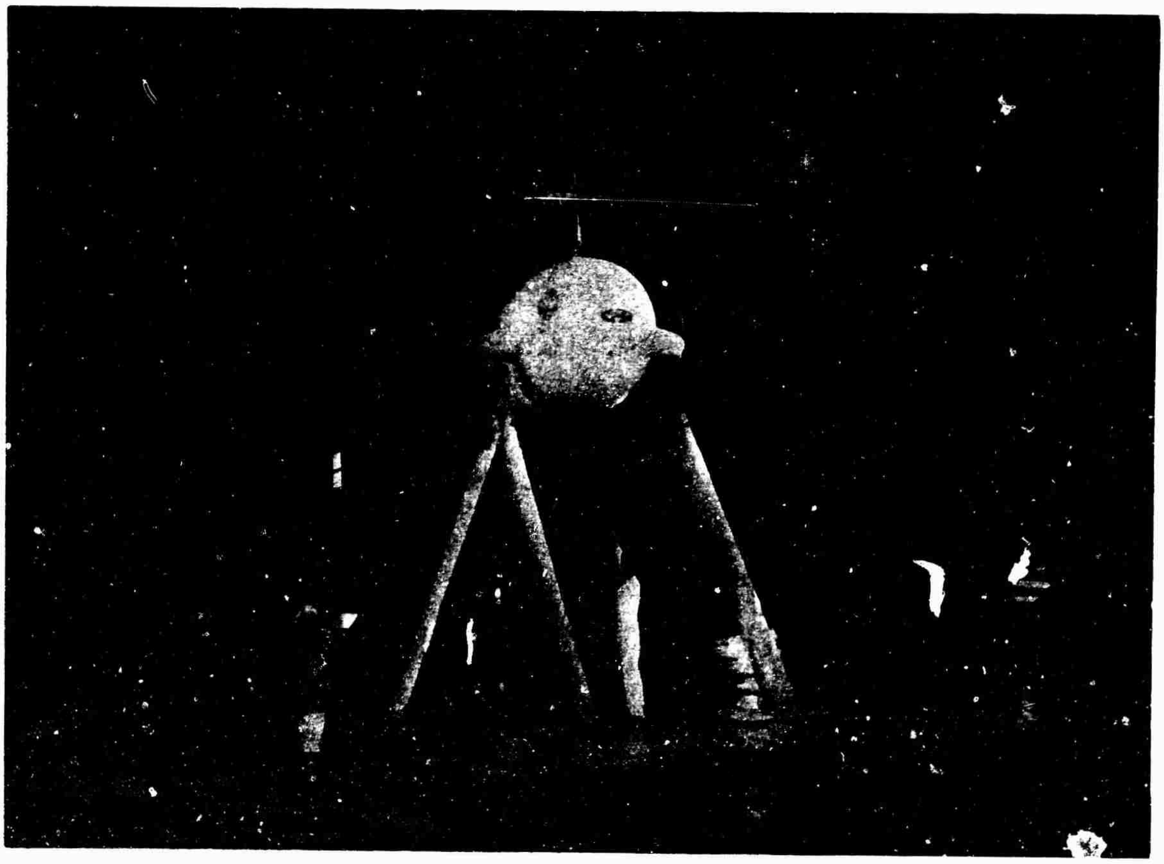

Figure 1. Full-Scale Rotor Wind Tunnel Test Module in NASA-Ames 40- x 80-Foot Wind Tunnel.

ROTORS

Three two-bladed semirigid rotors using a UH-1D underslung feathering axis were tested. The rotors tested were:

- Standard UH-1D 48-foot-diameter, NACA 0012 airfoil
- Modified UH-1D 48-foot-diameter blades incorporating reduced thickness tips
- Standard UH-1D blades reduced to 34-foot diameter

The purpose of the reduced-diameter blades was to reduce the rotational velocity (ΩR) without requiring changes in the standard UH-1 transmission so that high advance ratios ($V/\Omega R$) could be obtained.

Complete details of these rotors are given in Appendix II.

INSTRUMENTATION

Instrumentation was installed to provide rotor and control position data and for monitoring structural loads during the tests. The loads and position data were recorded on direct-write oscillographs provided by NASA-Ames.

Loads data were obtained from foil type (350-ohm) strain gages wired into four active arm bridges and excited by a common DC voltage. The strain gage sensitivities were determined by direct calibration through the expected operating range. The load equivalent electrical output was obtained using a precision resistor shunt on one leg of the bridge. Position data were obtained from potentiometers used as voltage dividers. Position calibrations were performed by moving the hardware incrementally through the full operating ranges and plotting electrical output versus mechanical position. Copies of the calibration data are in permanent file at Bell Helicopter Company.

In conjunction with the basic rotor performance and structural loads experiments, initial results were obtained with a special instrument, the Boundary Layer Button (BLB). Also, 14 pressure transducers were installed at the 0.98 radius on the upper and lower surfaces in order to obtain pressure distribution information.

SHAKE TESTS

Two separate shake tests were conducted to determine the natural frequencies and mode shapes of the combined test module and support system. The purposes of the tests were to: (1) obtain data for predicting the dynamic behavior of the system during wind tunnel operation, (2) establish dynamic

criteria for future test hardware designs, and (3) evaluate the effects of the tunnel balance on the dynamics of the test system. The initial test was conducted with the test module installed on a simulated support system located on the ground floor of the test facility. The second test was conducted in the tunnel test section with the test module and support system mounted on the tunnel balance system.

Complete details of the shake tests are given in Appendix III.

GENERAL STATEMENT OF RESULTS

A joint U. S. Army Aviation Materiel Laboratories/NASA-Ames/Bell Helicopter Company experimental investigation of three full-scale sets of rotor blades was conducted in the NASA-Ames Large Scale Tunnel.

The principal objects of the tests were to, under controlled conditions:

- Provide full-scale rotor performance data to advancing tip Mach numbers greater than 1.0;

- Provide full-scale rotor performance data to advance ratios of 1.0;

- Acquire comparative data for standard UH-1D and thin-tipped blades;

- Conduct feasibility tests on a new instrument, the Boundary Layer Button (BLB), to measure instantaneous velocity, magnitude, and direction on a rotor blade in and out of the boundary layer; and

- Obtain preliminary airfoil pressure distribution in the region where present theory assumes the lift to be zero (tip loss factor).

The basic objectives of the experimental program were accomplished, although the maximum advance ratio obtained was 0.79, not 1.0 as planned. The data are presented herein. In addition to the experimental results included in this report, the state of the art of calculating rotor performance for the tested conditions is reviewed.

Figure 2 gives the range of conditions tested. The maximum tip Mach numbers reached were 0.95 for the standard rotor and 1.025 with the thin-tipped 48-foot rotor. The maximum advance ratio reached for the reduced-diameter blade was 0.79.

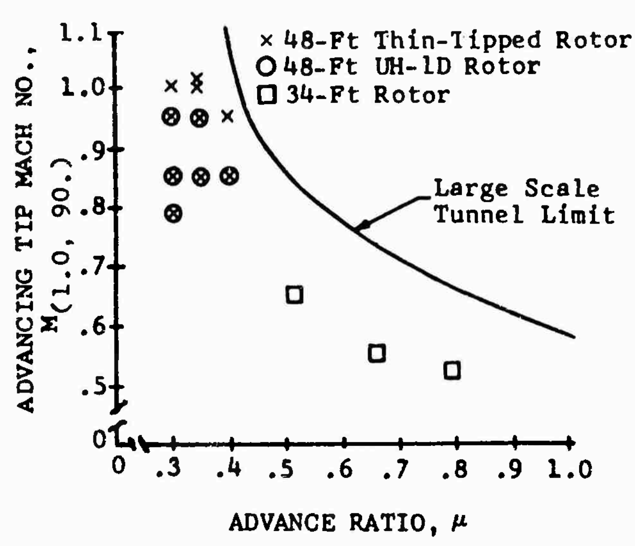

Figure 2. Chart of Test Conditions.

A comparative example of the performance of the standard and thin-tipped blades is given in Figure 3. Horsepower loading (HP/bcR) at constant blade loading (L/bcR) and at parasite drag loading (f/bcR) is shown for advancing blade tip Mach numbers from 0.8 to 1.0. These data are representative of the test results and show that at about $M_{(1.0,\ 90.)} = 0.85$, the thin-tipped blades require less power than the standard blades without compromising the lifting capability of the rotor. Below 0.85 Mach number, a small power penalty is shown for the thin-tipped blades.

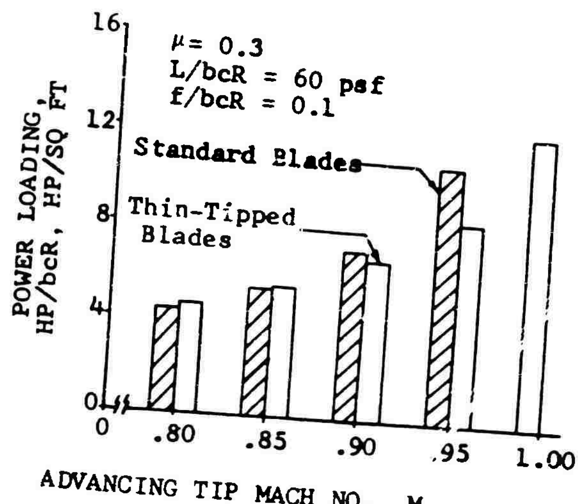

Figure 3. Performance Comparison of Standard and Thin-Tipped Blades.

A theory-experiment comparison for the standard UH-1D blades is shown in Figure 4. These data show that in this low advance ratio range, a present state-of-the-art (blade element

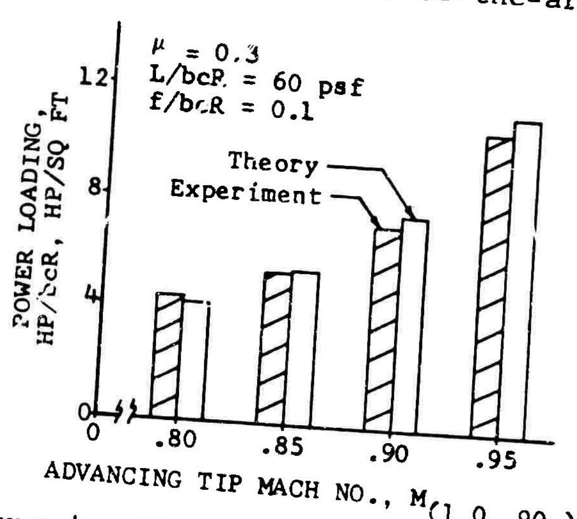

Figure 4. Theory-Experiment Comparison of UH-1D Rotor Performance.

quasi-static) aerodynamic theory gives reasonable performance estimates in the high Mach number realm of operation. It is shown in the main data section of this report that good agreement was obtained to advance ratios of 0.4 throughout the high Mach number range tested.

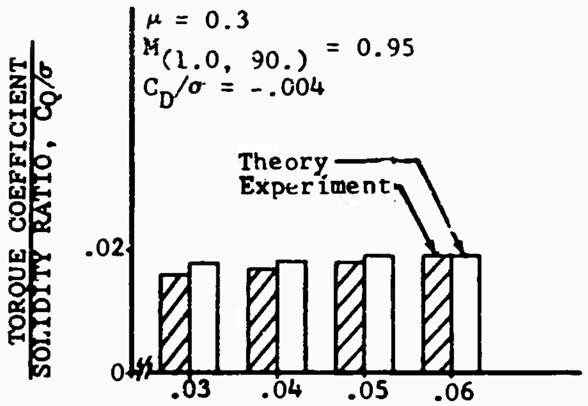

Figure 5. Theory-Experiment Comparison, Thin-Tipped Blades.

Figure 5 is a theory-experiment comparison for the thin-tipped rotor blades. Airfoil data are not available for the tip sections; therefore, for these comparisons the standard NACA 0012 airfoil data were used to the 80-percent radius station, where the thickness taper begins. Outward of this point, the 0012 lift data were assumed to apply, and the drag divergence Mach number was increased in increments as a function of decreased thickness. Experimental data were used to obtain the rate of change of drag divergence with Mach number. This method gave reasonable results and provides a tool for the designer to estimate the performance of rotors with this type of geometry without requiring prior extensive test data as demanded by other methods.

Although good agreement has been shown for the restricted advance ratio range tested at high Mach numbers (high Mach number and high advance ratio cannot be obtained simultaneously in the Ames 40- x 80-Foot Wind Tunnel because of tunnel maximum speed limits), this should not be interpreted as validating agreement throughout the entire rotary-wing spectrum. Analysis of tunnel test data at advance ratios greater than 0.5, given in the next section, indicates that techniques have been tailored to low advance ratios (μ = 0.3 to 0.4; an advance ratio of 0.4 is about the upper limit), because this is within the advance ratio range that has been flight tested for many years. Below μ = 0.2, the uniform inflow assumptions become poor. Above μ = 0.5, the effects which are accounted for in present techniques become nonlinear. Additionally, other effects such as radial flow, boundary layer aeroelasticity, etc., which are not as yet accounted for nor understood, may be important. Developing new predictive techniques in transition or at high advance ratios is beyond the scope of the present report.

Feasibility tests were performed with two BLB's mounted on the standard UH-1D rotor blades at 0.75 radius and 0.80 chord on each surface. The BLB is described on page 18. Some test results and the theoretical yaw angular variation are shown in Figure 6. (The theoretical calculations considered only the rotational and forward velocity components.) The yaw angle variation with azimuth is shown for the upper and lower surfaces and shows that the measured yaw angles are considerably different from the theoretical angles over most of the azimuth. The angles are different on the upper and lower surfaces.

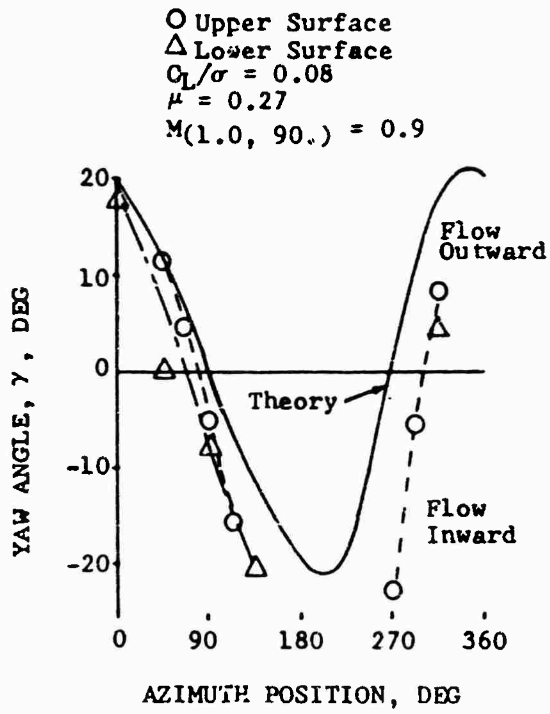

Figure 6. Yaw Angle Variation With Azimuth for Upper and Lower Surfaces.

Also, limited data were obtained from pressure transducers located on both blade surfaces at 98-percent radius to get some preliminary results in the region where present theory assumes the lift to be zero (tip loss factor).

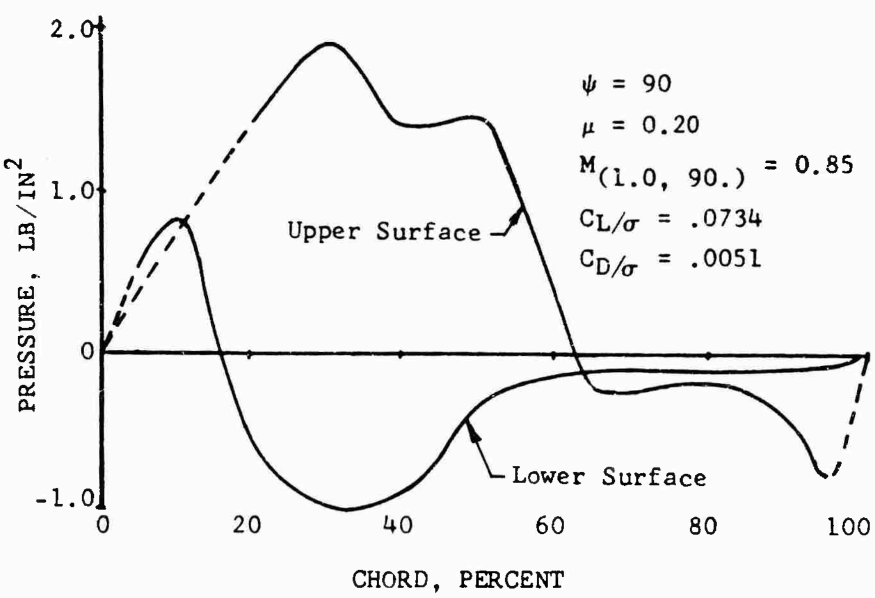

Figure 7. An Example of Pressure Distribution at 0.98 Radius.

Figure 7 is an example of these data and shows that substantial lift is being produced and that the center of pressure is aft of the quarter chord, resulting in a nose-down pitching moment. Lift coefficients as much as 0.9 were measured in the area of the blade

where most current theories assume zero lift. Much study of blade tip aerodynamics is clearly required.

The control system and blade structural loads were monitored throughout the wind tunnel test program. As expected, all loads increased with advancing tip Mach number; however, this was not as great as extrapolation of earlier flight test data would indicate. The oscillatory pitch link loads measured during the wind tunnel tests are shown in Figure 8 as a function of the advancing tip Mach number for the standard and thin-tipped blades. The standard blades show a rapid rise with Mach number and a significant advance ratio effect. The thin-tipped blades, in contrast, show a different trend in that the load does not increase significantly as the Mach number increases. From these data, it is concluded that supersonic speed can be obtained locally on the rotor disc without compromise of structural safety when the blade design parameters are properly selected.

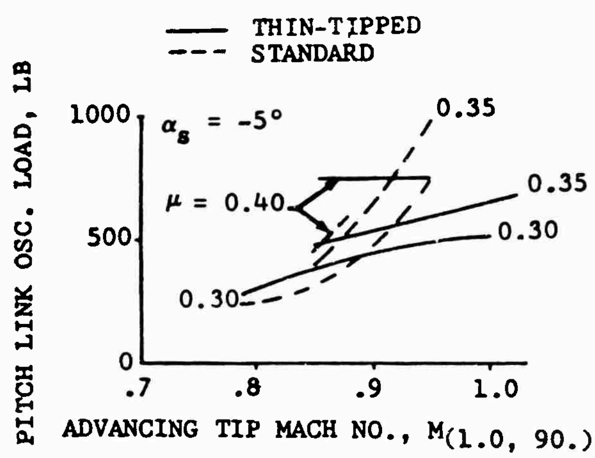

Figure 8. Control Loads Versus Advancing Tip Mach Number for the Standard and Thin-Tipped Blades at Various Advance Ratios.

SPECIFIC TEST RESULTS

GENERAL DISCUSSION

The advance ratio and advancing tip Mach number combinations tested with the three rotors are shown in Tables I and II. The symbols S and T used in Table I refer to the particular combinations tested with the standard UH-1D (S) and thin-tipped (T) rotors. Table II is for the 34-foot rotor.

TABLE I. 48-FOOT-DIAMETER ROTORS

Advance Ratio $\mu = V/\Omega R$	Tip Mach Number $M_{(1.0,\ 90.)}$				
	0.79	0.85	0.95	1.00	1.025
0.30	S,T	S,T	S,T	T	
0.35		S,T	S,T	T	T
0.40		S,T	T		

TABLE II. 34-FOOT-DIAMETER ROTOR

Advance Ratio $\mu = V/\Omega R$	Tip Mach Number $M_{(1.0,\ 90.)}$
0.51	0.65
0.66	0.55
0.79	0.52

The two rotor diameters were required to accomplish the performance objectives of the tests, since the large-scale tunnel is speed limited (see Figure 2). With the 48-foot rotor, supersonic speeds were obtainable within the UH-1B transmission rotational speed range (Table I). However, to obtain high advance ratios, it was necessary to reduce the rotational tip speed (ΩR) because of the tunnel speed limitations. This can be accomplished by a change in transmission gearing or a radius decrease. The latter method is simpler and was chosen.

A graphical presentation of representative performance data and the complete NASA-Ames data reduction tabulation are presented in Appendixes I and IV, respectively.

In addition to the performance data, both rotor system and test module loads and moments were recorded. The principal purposes of monitoring these data were: (1) for flight safety and (2) so that, in the event of a structural failure, an accident analysis could be conducted. No failures occurred, and these data are not reported herein.

TESTING PROCEDURE

For each particular test condition, the rotor rotational speed and the tunnel speed were adjusted to maintain constant values of rotor advance ratio and advancing tip Mach number. The rotor shaft angle (test module pitch) and rotor collective pitch were then varied in even increments to map the test envelope. The rotor cyclic pitch was adjusted to zero the first harmonic flapping with respect to the rotor shaft and data were recorded at each incremental combination of shaft angle and collective pitch.

The wind tunnel balance data were recorded by NASA-Ames. Their data, which are in Appendix IV, were resolved such that all forces were in the relative wind axis system, and all moments were transferred from balance resolving center to the center of rotation of the rotor hub and referenced to the shaft axis system.

Table I shows that for the 48-foot-diameter rotor blades, the data were taken at constant advancing tip Mach number for three advance ratios. This mode of operation was chosen because the primary variable to be investigated was Mach number. Also, by maintaining constant advance ratio, data could be acquired and analyzed void of advance ratio effects.

For the 34-foot rotor tests at high advance ratios and low Mach number, the method of test operation was changed for the convenience of tunnel operation. Constant tunnel speed was set, and the rpm was varied to give the desired advance ratio. This method is acceptable since at low advancing tip Mach numbers, Mach number is not a prime variable.

TEST RESULTS - 48-FOOT ROTOR

Comparisons of the blades with two tip thicknesses at an advance ratio of 0.3 are shown on Figure 9. The form of data presentation chosen is to divide rotor lift (L), horsepower (HP), and equivalent flat-plate propulsive area (f= propulsive force/dynamic pressure) by the total blade area (bcR). In the calculation of blade area, it was assumed that the full chord extended to the center of rotation. Figure 9 shows that above an $M_{(1.0,\ 90.)}$ of about 0.85, there are adverse compressibility effects throughout the blade loading range. For the

standard blades, the power required increases about 100 percent between 0.85 and 0.95 advancing tip Mach number. In terms of speed at the same advance ratio, this represents an increase of 15 knots.

With the thin-tipped blades, the adverse compressibility effects are greatly reduced when compared to the standard blades above an $M_{(1.0,\ 90.)}$ of 0.85. Also, the rate of increase of horsepower with Mach number is substantially less. Figure 9 shows that there is a crossover Mach number where the thin tips require slightly more power than the standard blades.

SUPERCRITICAL FLOW STATES

Before proceeding with a discussion of the subject test results, the supercritical flow states and their relation to rotorcraft will be reviewed briefly in the following paragraphs. There are three supercritical flow states for an airfoil relating to the critical, drag divergence, and shock stall Mach numbers (Reference 7). These are defined below:

- The critical Mach number (M_{cr}) - Free-stream Mach number at which local sonic velocity is first reached on airfoil surface.
- The drag-divergence Mach number (M_d) - Free-stream Mach number at which slope of curve of drag coefficient versus Mach number attains a value of 0.10.
- The shock-stall Mach number (M_s) - Free-stream Mach number at which full separation first occurs at rear of airfoil.

The effects of supercritical flow states on the two-dimensional airfoil characteristics are illustrated by Figure 10. The figure shows that the critical Mach number (M_{cr}) is not the "critical" Mach number as far as power required is concerned. There is no drag rise at M_{cr}, and the lift is still rising. The "critical" Mach number with respect to power is the drag-divergence Mach number at which there is a rapid increase in drag for a small Mach number or angle-of-attack change. The lift curve has not as yet peaked at M_d. M_s is the Mach number where complete separation occurs, with the consequent abrupt lift decrease and drag rise.

Figure 11 shows the portion of the UH-1D (48-foot diameter) rotor disc area that is affected by supercritical flow for various flight conditions. The disc area outboard of the line labeled M_{cr} is above Mach critical, and the area outboard from the line labeled M_d is above drag divergence. For reference,

the 80-percent radius is also shown, and it should be remembered that this is the location where the thickness taper begins on the thin-tipped blades.

Figure 11a, which represents a normal UH-1D operating condition, shows only a small portion of the disc area above drag divergence. Therefore, since little of the disc area is above M_d, thinning the tip airfoil to improve its supercritical flow characteristics would be expected to alter the horsepower required by only a small amount. This is consistent with the flight and wind tunnel experience.

A quite different situation is shown in Figure 11b, which is representative of a flight condition beyond the normal flight envelope of the UH-1D. Now, where $M_{(1.0,\ 90.)} = 0.92$, half of the disc is supercritical and a major portion of the disc outboard of 0.8R is about M_d. A small area on the advancing blade is above shock stall. In this case, thinning the airfoil from 0.8R should have significant effects on the power required, in that the drag divergence line should move outward and the area of shock stall should be eliminated. The latter of itself would significantly reduce the power required. The experimental data at this Mach number (Figure 9) show this to be the case. For both cases, the data show that maximum lift capability of the thin-tipped rotor is not significantly altered.

A very important result from both the flight test and tunnel experience is that, as shown in Figure 9, there is no apparent loss in the lifting capacity of the thin-tipped blades when compared to the standard blades. From the time of original conception of the thin-tipped blades, it was assumed that because of the reduced lift curve slope and lower $C_{L_{max}}$ of the thin airfoil sections, shown by low Mach number two-dimensional results, the overall lifting capability of the rotor would be compromised to obtain the improved supercritical characteristics. These expected penalties have not materialized, and no difference has been found.

COMPARISON WITH THEORY

48-Foot Standard Rotor

Most of the theory-experiment comparisons are for the standard UH-1D (constant NACA 0012 airfoil) blades for which airfoil data are available. The method of data presentation is first to give summary results and then more detailed comparisons. Limited comparisons for the thin-tipped blades are presented in the next section. Figure 12 is a theory-experiment comparison using the performance charts of Reference 8, and it should be noted that there is a 2.9-degree difference in twist between the standard UH-1D blade tested and the rotor of the

theoretical calculations. Also, the solidity correction required for these theoretical data is the maximum recommended by Reference 8. More will be said about the solidity correction effects in the next paragraph. However, Reference 8 is an accepted method of obtaining rotor performance, and the experimental data offered an opportunity to check the trends obtained. As seen on the figure, both trend and magnitude agreement are reasonable, with the largest error occurring at the lowest blade loading.

The effects of the large solidity correction on the results from Reference 8 (theory of Figure 12) were evaluated using the Bell Rotor Aerodynamic Method (BRAM). The conclusion from this study was that at the high blade loadings, a maximum error of HP/bcR = .5 could be made by using the results of Reference 8. The direction of the error is such that the theoretical values would be reduced; thus, there would be an improved agreement between theory and experiment at the high blade loadings. The solidity correction effects at the low blade loading were small.

Figure 13 is a theory-experiment comparison using the BRAM of Reference 9. The theories used for the comparisons shown by Figures 12 and 13 are similar in that both are based on Reference 10. In the comparison shown by Figure 13, the actual UH-1D blade physical characteristics were used with the airfoil data of Reference 8; and as seen, the correlation generally improved. Again, the correlation is best at the higher blade loadings. The 0012 airfoil data were assumed to apply to the blade retention bolts. The reasons for the discrepancies between theory and experiment at the low loading (30 psf) are not known. It appears that the method used in calculating the performance in References 8 and 9 does not adequately represent the rotor where there are sizable negative angles of attack on the advancing blade. Study of predictive techniques in this area is clearly needed. However, the techniques used in Reference 9 appear to give good results at high Mach numbers when compared to full-scale data in the normal helicopter blade loading range. Similar conclusions for small-scale forward flight data were reached in Reference 11.

Figure 14 is a theory-experiment as a function of advance ratio for the standard blades at $M_{(1.0,\ 90.)} = 0.85$ for two blade loadings. These data show that the agreement deteriorates somewhat with advance ratio at the 60-psf blade loading. More will be said about advance ratio effect in a later section of this report.

Theory-experiment performance comparisons, calculated with the BRAM, are given in Figure 15 and support the results presented in the summary graphs.

48-Foot Thin-Tipped Rotor

Two-dimensional airfoil data as a function of Mach number are not available for thin airfoil sections. Therefore, only limited theory-experiment is given in this report. This particular blade varied from 12-percent thickness at 0.8 radius to 6 percent at the tip.

Figures 16 and 17 show these comparisons at 0.95 and 1.0 Mach numbers. Two theoretical sets of data appear on Figure 16, each of which involves empirical corrections to compensate for the lack of applicable airfoil data. The approach used in the short dashed lines (labeled variable drag divergence) was to use the standard 0012 airfoil data to .8 radius; then the drag divergence Mach number was increased as a function of decreased thickness to compensate for the improved super-critical Mach number characteristics of the thin sections. References 7 and 12 were used as empirical guides to obtain the magnitude of this correction, and the variation used is shown in Figure 18.

The second approach, as suggested by Reference 13, to correct empirically for the improved supercritical Mach number characteristics of the thin tip is to increase the drag divergence Mach number by .05 for the entire blade. These results are shown in Figure 16 as dash-dot lines. Both of these methods appear to give reasonable agreement; however, the former is preferable, since the constant drag divergence can only be obtained empirically from the test data and will vary with blade geometry. The variable drag divergence method requires only that reasonable estimates of the change in supercritical flow characteristics from the standard section be made.

34-Foot Rotor

The high advance ratio test results were obtained with the 34-foot-diameter rotor as previously explained. Test-theory comparison for the three conditions is shown in Figures 19 through 21. The carpet form of presentation for these data was unsatisfactory; therefore, C_L/σ, C_D/σ, and C_Q/σ versus α_c for constant collective pitch are presented. These figures show that the correlation is rather poor, especially with respect to drag. However, it must be pointed out that to obtain high advance ratios in the 40- x 80-foot tunnel, reduced rpm must be used because of the tunnel speed restriction, and the drag force generated by the rotor is small compared to the model tare force. (See Appendix IV for tares.)

Present predictive techniques have been tailored to low advance ratios (μ = 0.3 to 0.4; an advance ratio of 0.4 is about the upper limit), because this is within the advance ratio range that has been flight tested for many years. Below μ = 0.2, the uniform inflow assumptions become poor. Above μ = 0.5, the effects which are accounted for by present techniques become nonlinear. Additionally, other effects such as radial flow, boundary layer, aeroelasticity, unsteady airfoil, etc., which are not as yet accounted for may be important. To summarize, in the advance ratio range, where there is vast flight test experience, techniques such as those used in Reference 9, are acceptable in the normal pure helicopter blade loading range (transition excluded). In the high advance ratio region, much basic study of fundamental aerodynamics is required before the predictive technique can be significantly improved.

Control Positions

In a previous section, it was shown that good performance correlation was achieved with the 48-foot rotor blades. Comparisons of theory-test control position (θ.75R and B_{1_s}) were also made, and Figure 22 is an example of these comparisons. Analysis of these data showed that empirical equations could be obtained to correct the theoretical results to the experimental. The equations are:

$$\theta_{.75\ \text{exp}} = \left[\theta_{.75\ \text{theory}}\ (1 + \mu^4)\ (2 - \sqrt{M}\ ) + 1\right] \sqrt[4]{M}$$

$$B_{1_{s\ \text{exp}}} = (B_{1_{s\ \text{theory}}} + 1)\ (1 - \mu^2)\ \sqrt[4]{M}$$

Since poor force agreement was obtained for the high advance ratio condition (i.e., 34-foot rotor), no empirical corrections of control position were attempted for this rotor.

SPECIAL INSTRUMENTATION RESULTS

BOUNDARY LAYER BUTTON (BLB)

The BLB, shown in Figure 23, is a device for measuring the magnitude and direction of the local velocity in or out of the boundary layer on the rotor blade. The BLB is composed of two plates in which are submerged three subminiature pressure transducers. The forward transducer measures static pressure, and the two aft ones are connected to total pressure tubes. The total pressure tubes are oriented 90 degrees apart, and static wind tunnel calibrations of the device have demonstrated that for a 40-degree included angle, both magnitude and direction can be measured with a 3-percent accuracy. The frequency response of the BLB is approximately 400 cps.

Two BLB's were mounted on the standard UH-1D rotor blades at 0.75 radius and 0.8 chord on each surface. The tube height was 0.03 inch above the blade. A comparison of the measured and theoretical yaw angle variation with rotor azimuth has previously been shown in Figure 6. The theoretical yaw angles were calculated based on rotational and forward velocity component considerations only. Figure 6 shows that there is a considerable difference between the measured and calculated values and also that the upper and lower surface angles are not the same. The measured yaw angle variation on the upper surface is shown for two values of lift coefficient in Figure 24. The data show that rotor lift has a significant effect on the retreating blade yaw angle, and the advancing blade yaw angle is unaffected by lift.

The data obtained to date with the BLB are very limited; however, from these results, it is evident that consideration of the forward and rotational velocity components is insufficient to describe the yaw angle variation. In addition to the normal velocity components, the vortex field, spanwise pressure gradient, centrifugal boundary layer forces, and, in all probability, the undeveloped tip vortex must be taken into account for a true representation of the aerodynamic environment of a rotor blade. Discussions of the importance of these effects in hovering are given in Reference 14 and 15, and some information on tip vortex effects in forward flight is given in the next section.

AIRFOIL STATIC PRESSURE DISTRIBUTION AT 0.98 RADIUS

Recent studies (References 14 and 15 are examples) have raised questions about the effect of the forming tip vortex on rotor blade aerodynamics. The cited references give information for hovering but none for forward flight. Thus, in these tests, 14 subminiature pressure transducers were

positioned at 0.98 radius (rotor Station 282.25) on both upper and lower surfaces. The chord locations were as shown below.

Upper Surface Percent Chord	Lower Surface Percent Chord
20	5
30	10
40	20
50	30
65	40
80	50
95	65
	80
	95

Surface pressures were recorded for several test conditions. The measured surface pressure versus chord for several azimuth positions are shown in Figures 25 through 27.

Most theoretical techniques, including the BRAM used for correlation in this report, assume a tip loss factor. The tip loss factor assumes that at some percentage of the outermost span of the rotor blade (0.97R, 1/2 chord, etc.), the lift of the blade is zero and the drag is finite. The experimental data (Figures 25 through 27) show that significant lift still is being produced at 0.98R. It is impossible to integrate the pressure distributions very accurately, since there are no data available forward of the 20-percent chord on the upper surface. However, if the data are faired smoothly to zero chord, the lift coefficient can be of the order of 0.70 or more, not zero as assumed by conventional theory. Secondly, with the above assumption and integration, there will be a nose-down pitching due to the aerodynamic center's being behind the quarter chord. The moment is not accounted for in any known theories and may be especially significant in dynamic response calculations.

Another conclusion from these data is that there is no significant difference between the pressure distributions at $\psi = 0°$ and 180°. One would expect that the influences of the forward velocity would cause notable differences in the forming tip vortex effects at these particular azimuthal positions. From the experimental results, one of two conclusions can be reached: (1) the pressure transducers at 0.98 radius were too far inward to be affected significantly by the forming vortex, or (2) forward velocity is a second-order effect on the forming vortex at these advance ratios (μ = 0.12 and 0.20). The latter means that the first-order effects are those of the rotational and vortex velocities. The proper interpretation of these

results is unknown at this time. More extensive experimental studies are clearly needed in this area.

CONCLUSIONS

The investigation and subsequent analysis of the data for rotor operation to advancing tip Mach number in excess of 1.0 and advance ratios to 0.79 have yielded the following conclusions:

- Thin-tipped rotor blades require significantly less power than constant 12-percent thick blades when operated at advancing tip Mach numbers above 0.85.

- The lifting capability of the rotor was not compromised with the thin-tipped blades.

- No stability limit was encountered to an advancing tip Mach number of 1.025 or an advance ratio of 0.79.

- Control structural loads were reduced with the thin-tipped blades, and the blade structural loads were acceptable.

- Theory-experiment performance comparisons were good at normal blade loading for the low advance ratio of the tests.

- Theoretical predictive techniques appear to be inadequate at low blade loadings at high Mach number and at high advance ratios.

- Empirical equations were determined to correct the theoretically predicted control positions to agree with the experimental results.

- The use of the advanced instrumentation device, the Boundary Layer Button, was shown to be feasible, and the results indicate that:

  - The measured radial flow angles were generally much larger than those calculated by considering forward and rotational velocity components only.

  - There is a strong influence of rotor lift on the radial flow angle of the retreating blade.

- Significant lift and nose-down pitching moments were measured at 0.98R, which is within the region where present theory, using a tip loss, assumes that the lift is zero.

- The variation of lift coefficient with azimuth was small at 0.98R for the limited number of measured conditions.

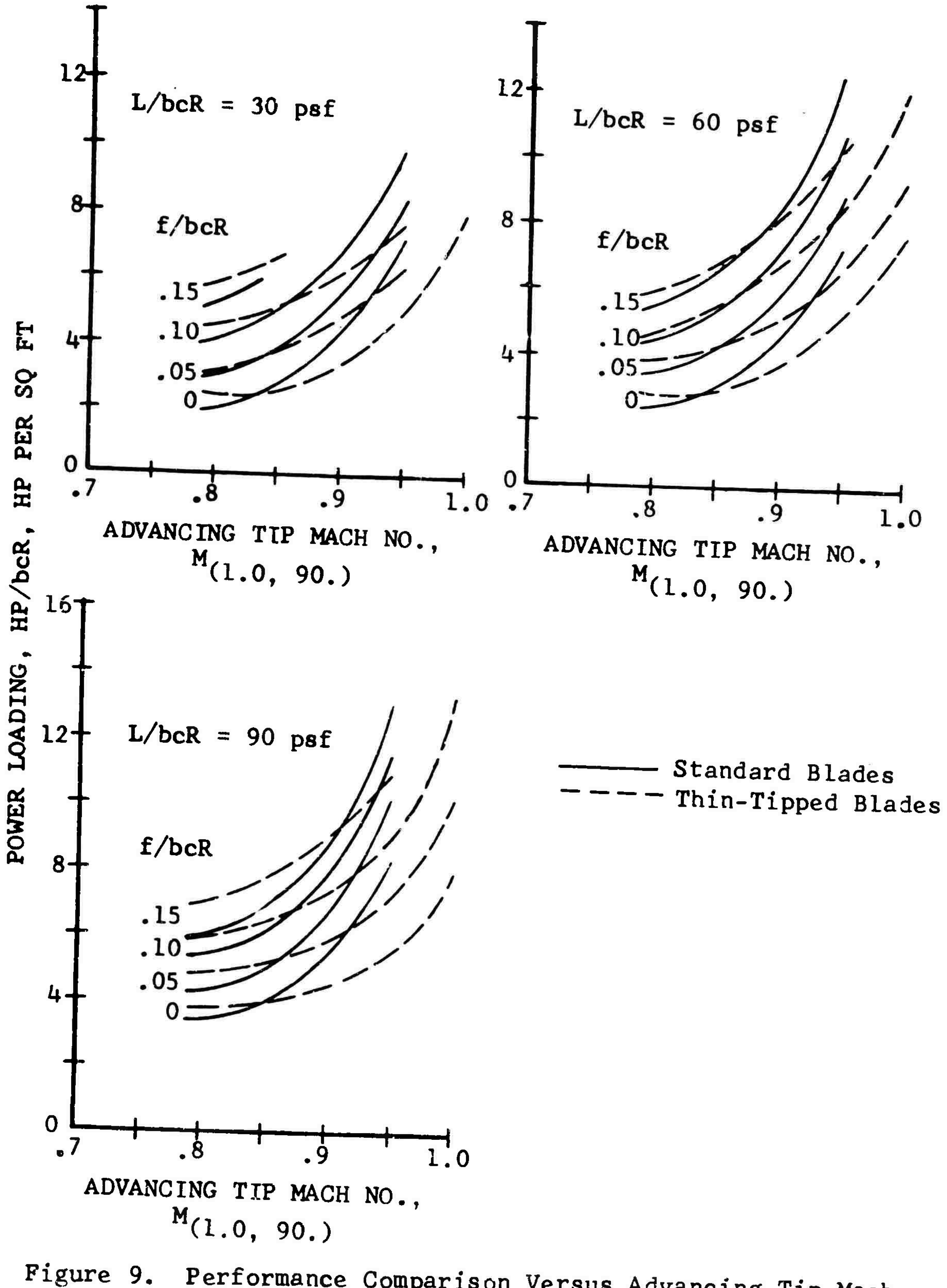

Figure 9. Performance Comparison Versus Advancing Tip Mach Number for Standard and Thin-Tipped Blades at $\mu = 0.30$.

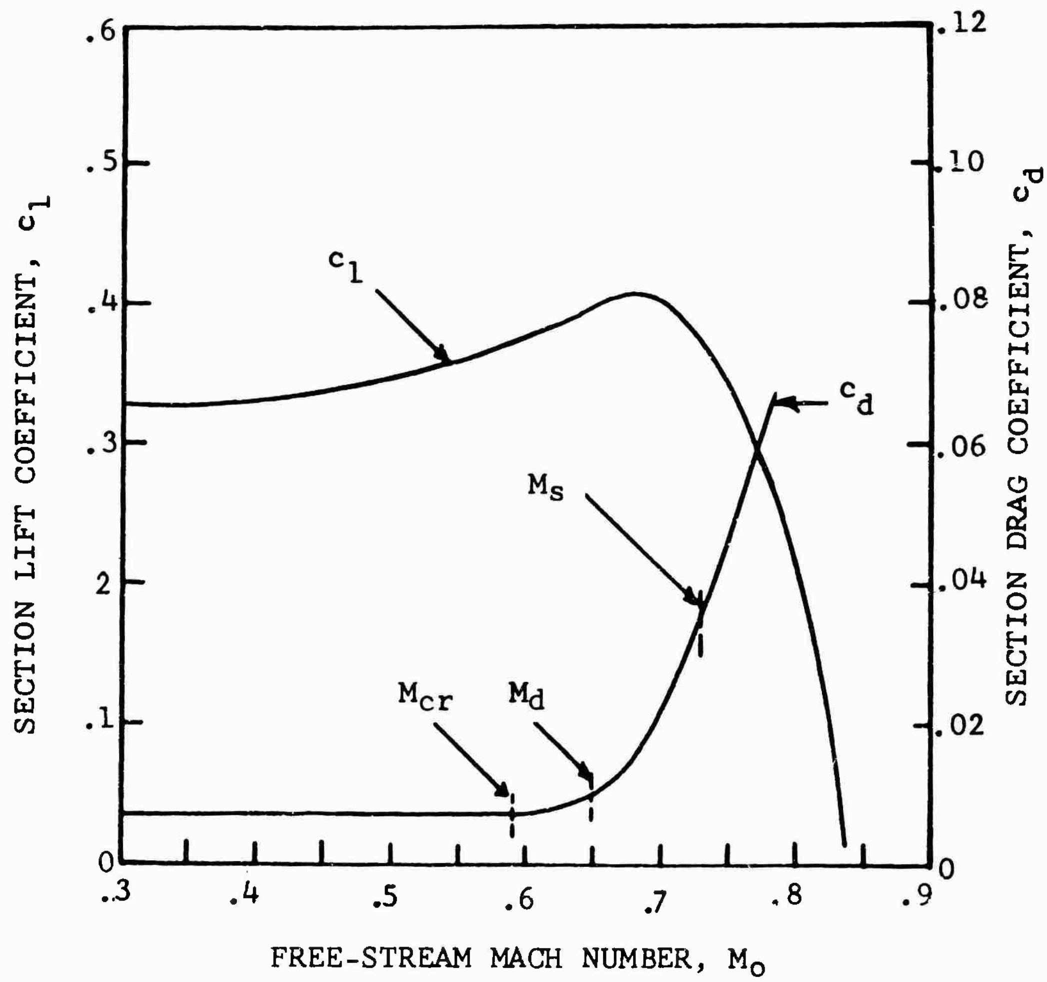

Figure 10. Variation of Representative Airfoil Section Characteristics with Mach Number.

$M_{(1.0,\ 90.)} = 0.83$ L/bcR = 94 lb/sq ft
$\mu = 0.17$ f/bcR = 0.23

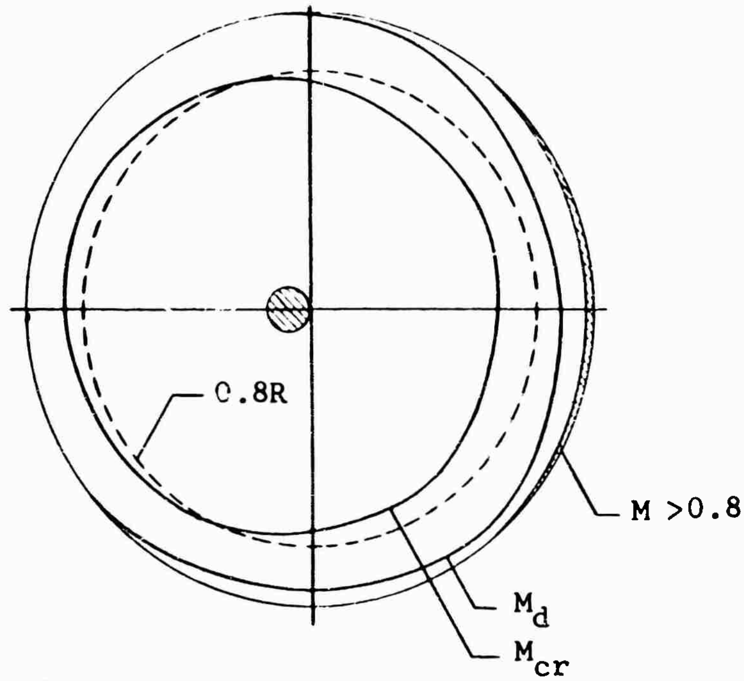

a) Within Normal Flight Envelope

$M_{(1.0,\ 90.)} = 0.92$
$\mu = 0.27$

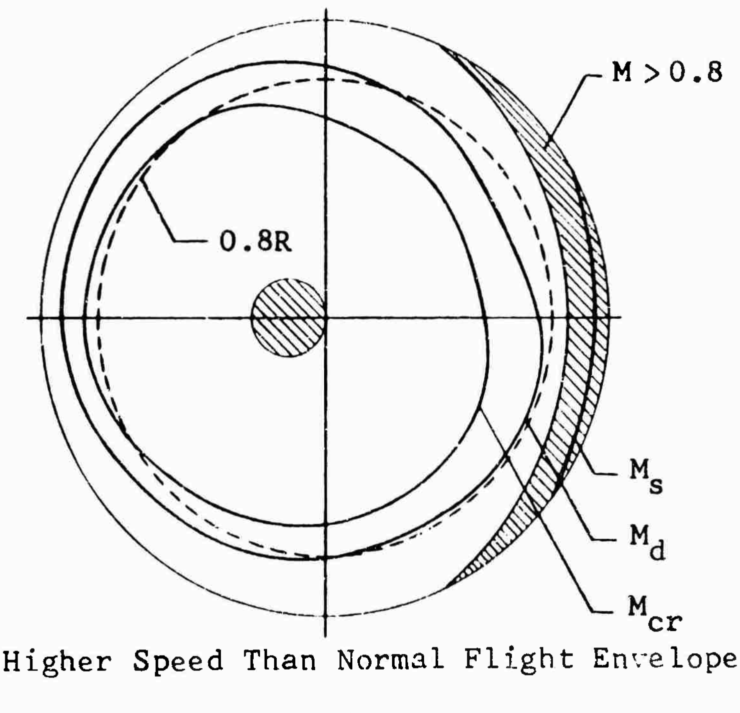

b) Higher Speed Than Normal Flight Envelope

Figure 11. UH-1D Rotor Disc Area Affected by Supercritical Flow.

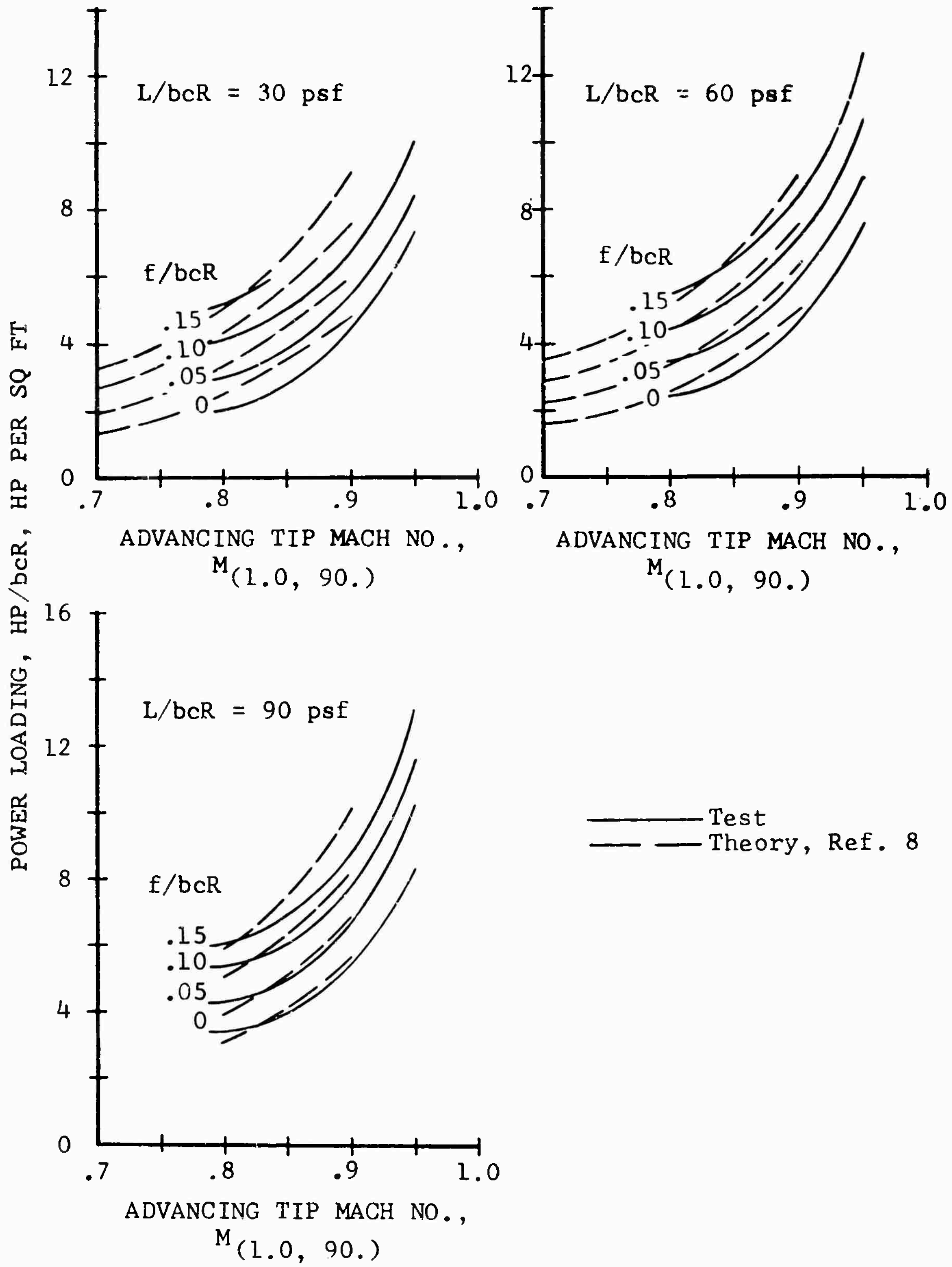

Figure 12. Reference 8 Theory-Test Comparison Versus Advancing Tip Mach Number for UH-1D Rotor at μ = 0.30.

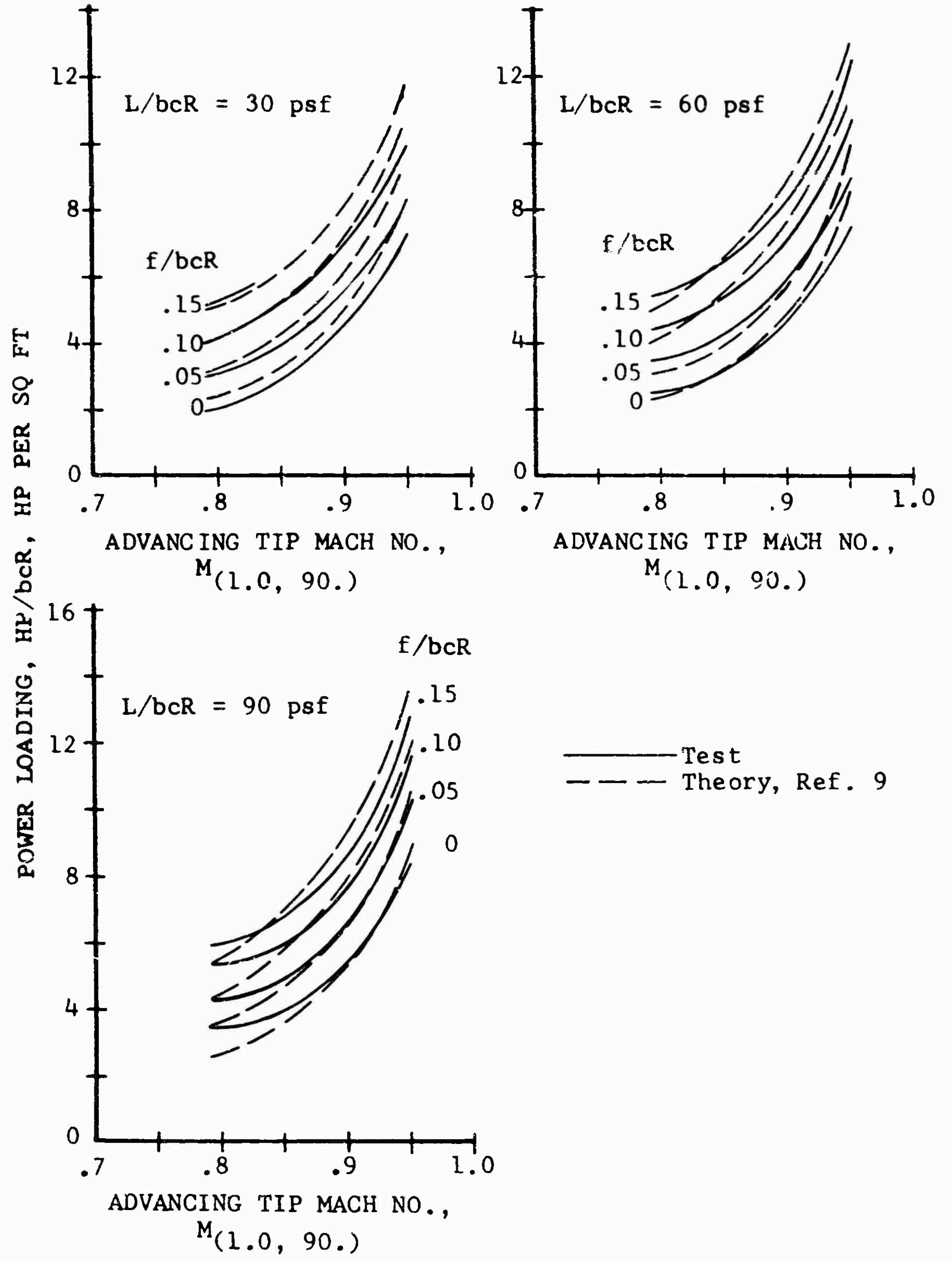

Figure 13. Reference 9 Theory-Test Comparison Versus Advancing Tip Mach Number for UH-1D Rotor at $\mu = 0.30$.

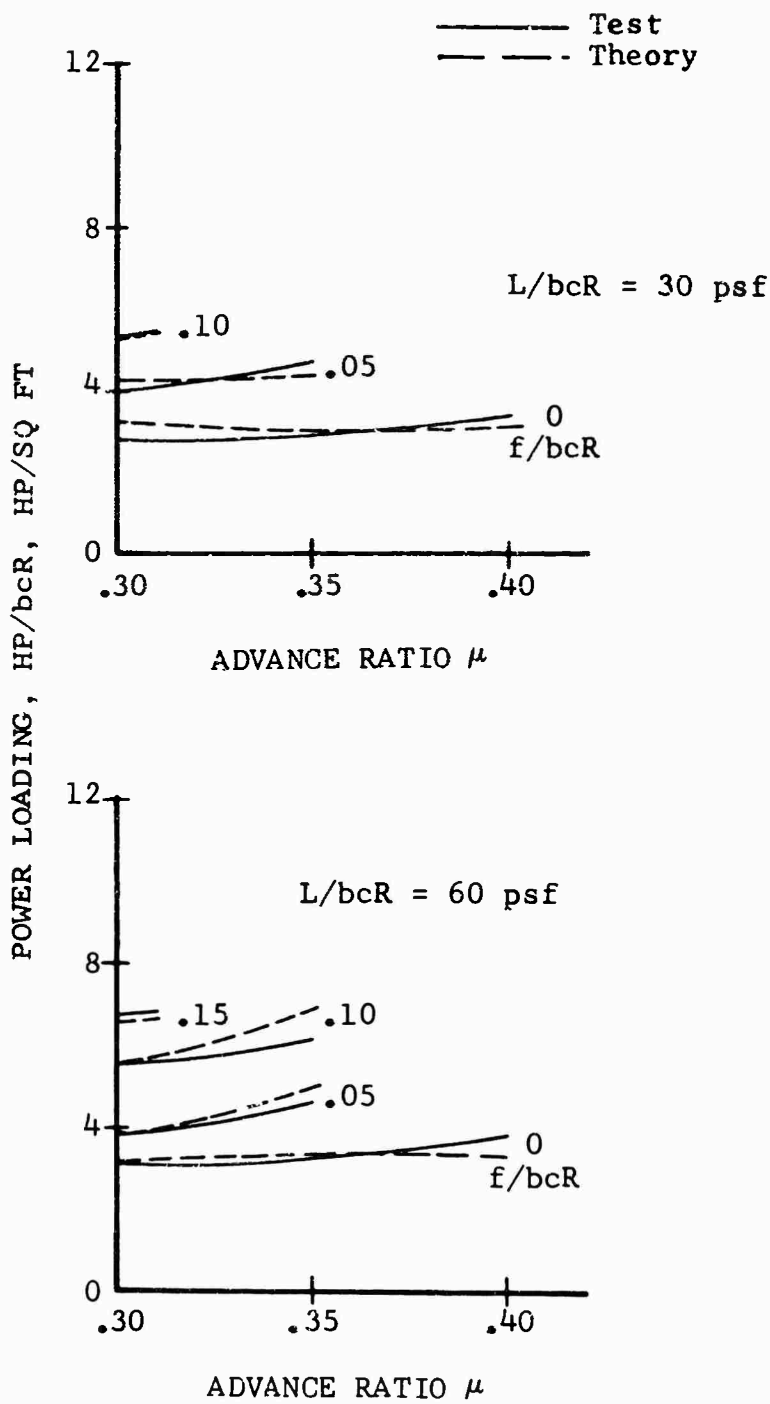

Figure 14. Reference 9 Theory-Test Comparison Versus Rotor Advance Ratio for UH-1D Rotor at $M_{(1.0,\ 90.)} = 0.85$.

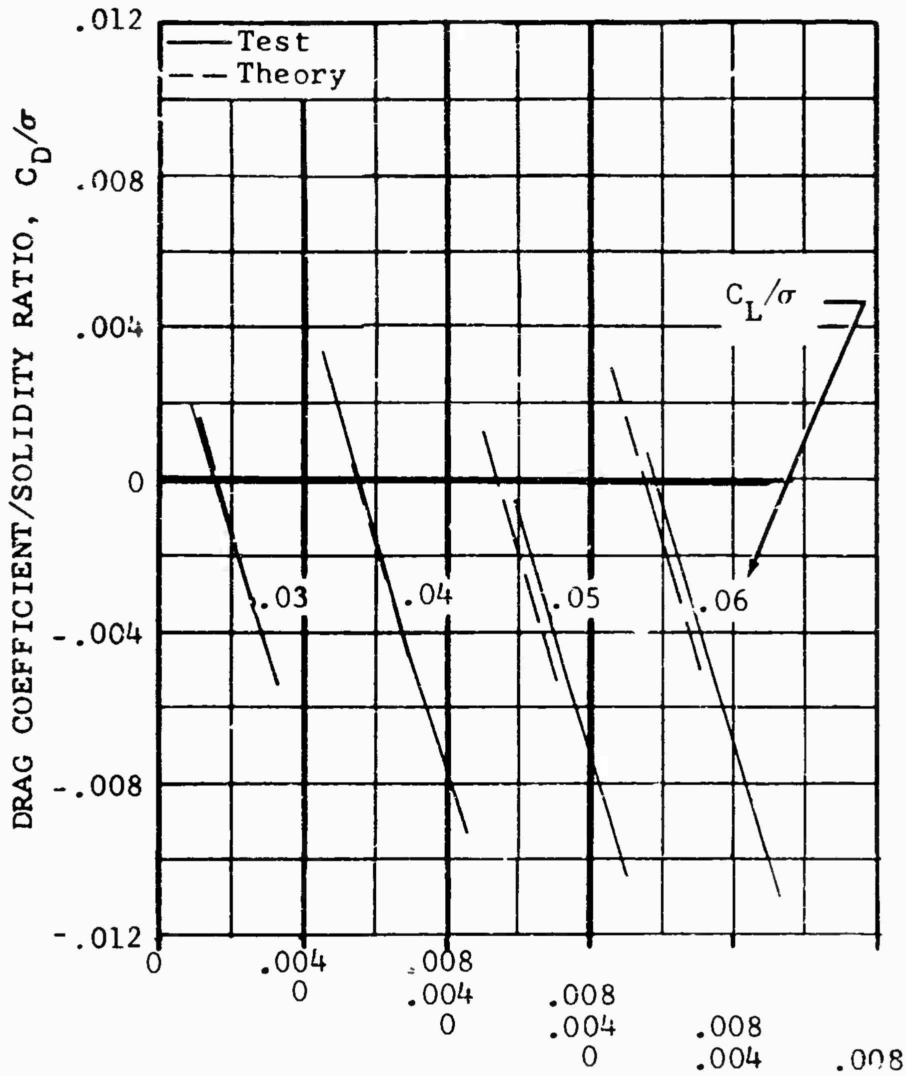

(a) μ = 0.30, $M_{(1.0,\ 90.)}$ = 0.79

Figure 15. Theory-Test Comparison, Nondimensional Performance of UH-1D Rotor at Various Combinations of Advance Ratio and Advancing Tip Mach Number.

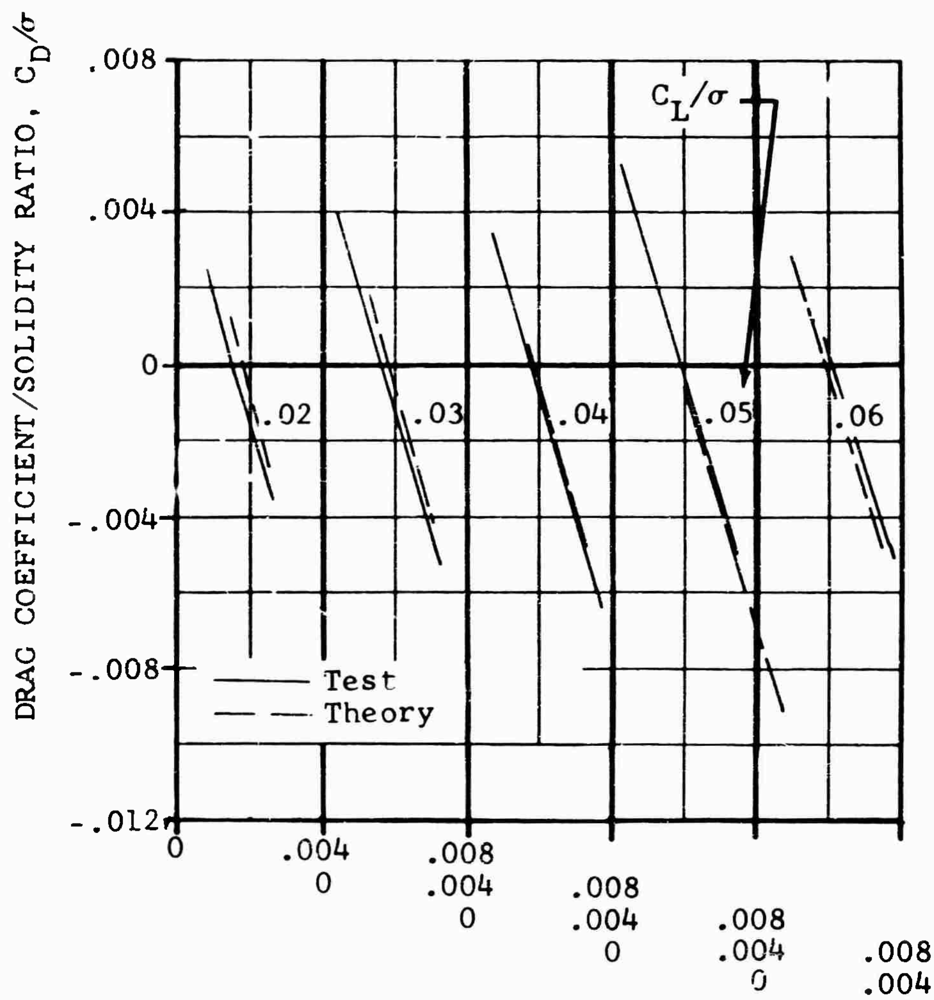

(b) μ = 0.30, $M_{(1.0,\ 90.)}$ = 0.95

Figure 15. Continued.

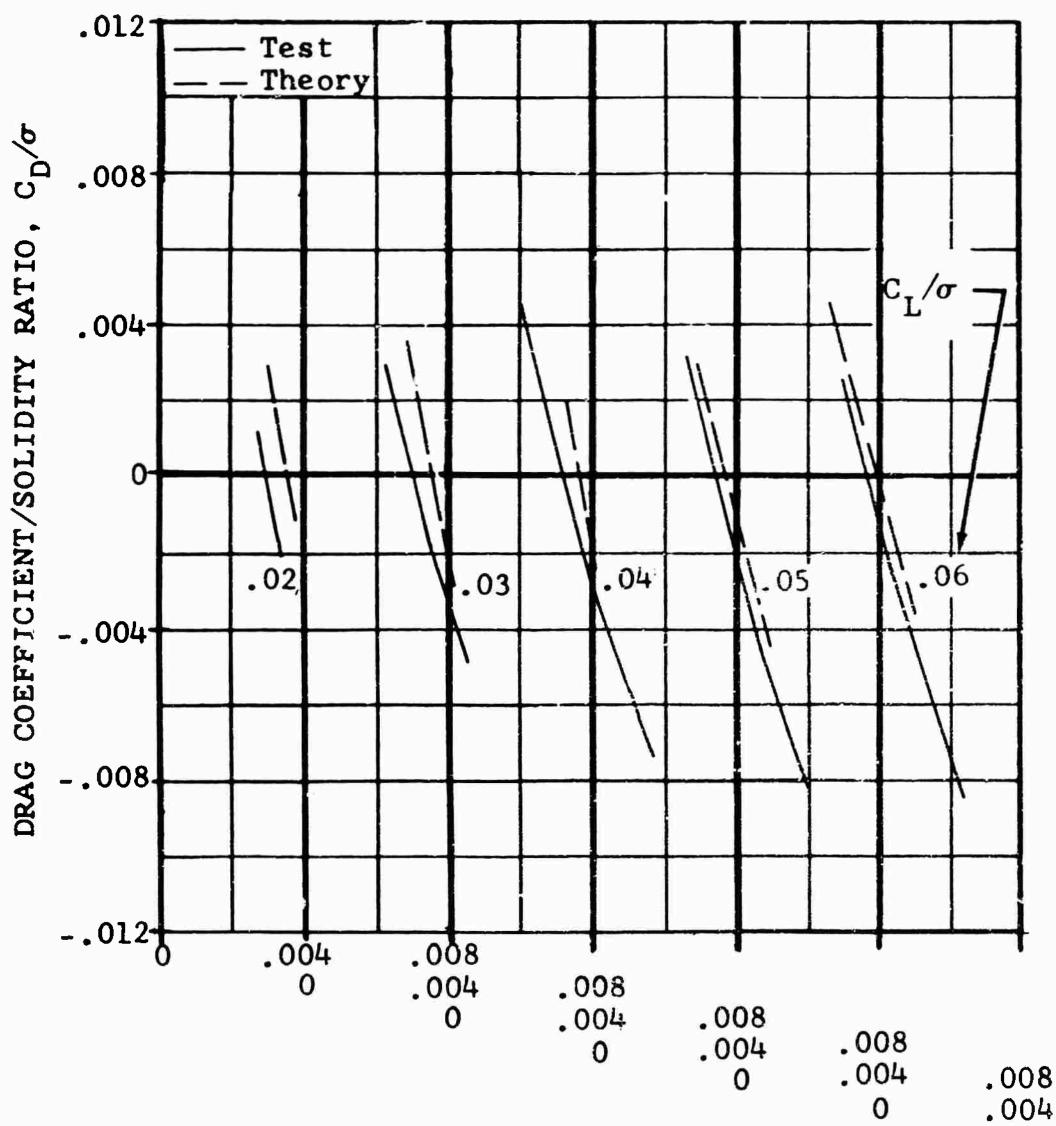

TORQUE COEFFICIENT/SOLIDITY RATIO, C_Q/σ

(c) μ = 0.35, $M_{(1.0,\ 90.)}$ = 0.85

Figure 15. Continued.

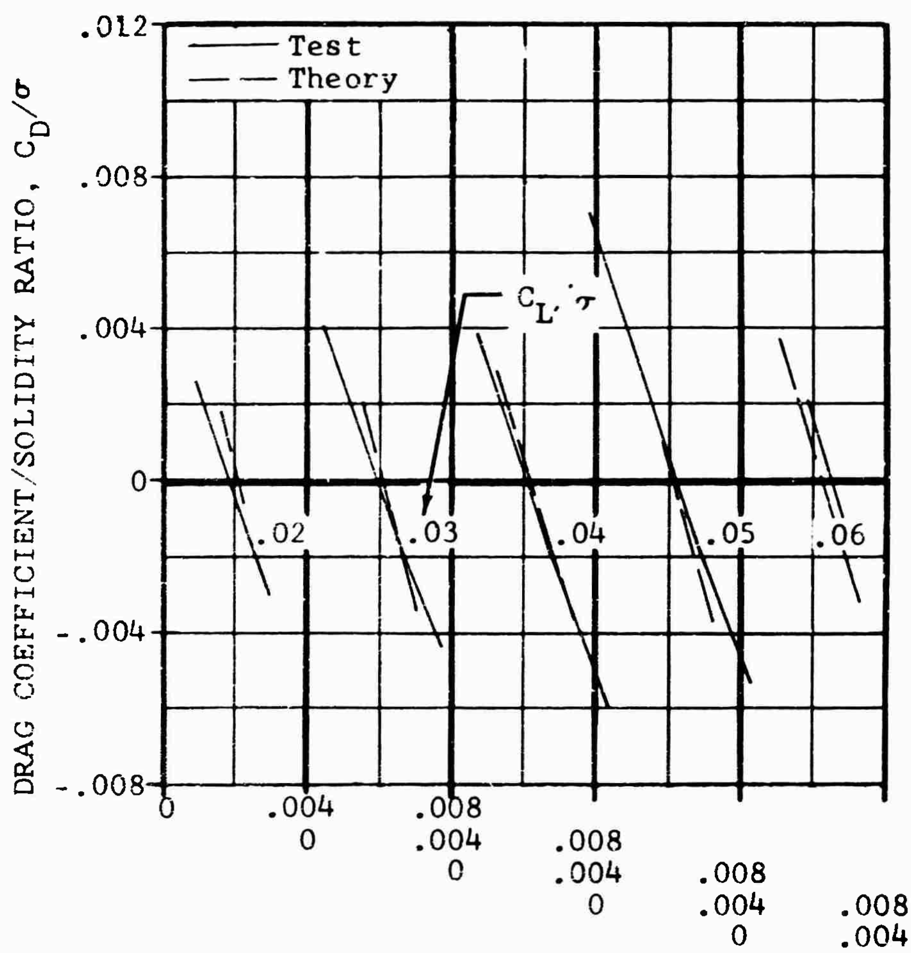

(d) μ = 0.30, $M_{(1.0,\ 90.)}$ = 0.85

Figure 15. Continued.

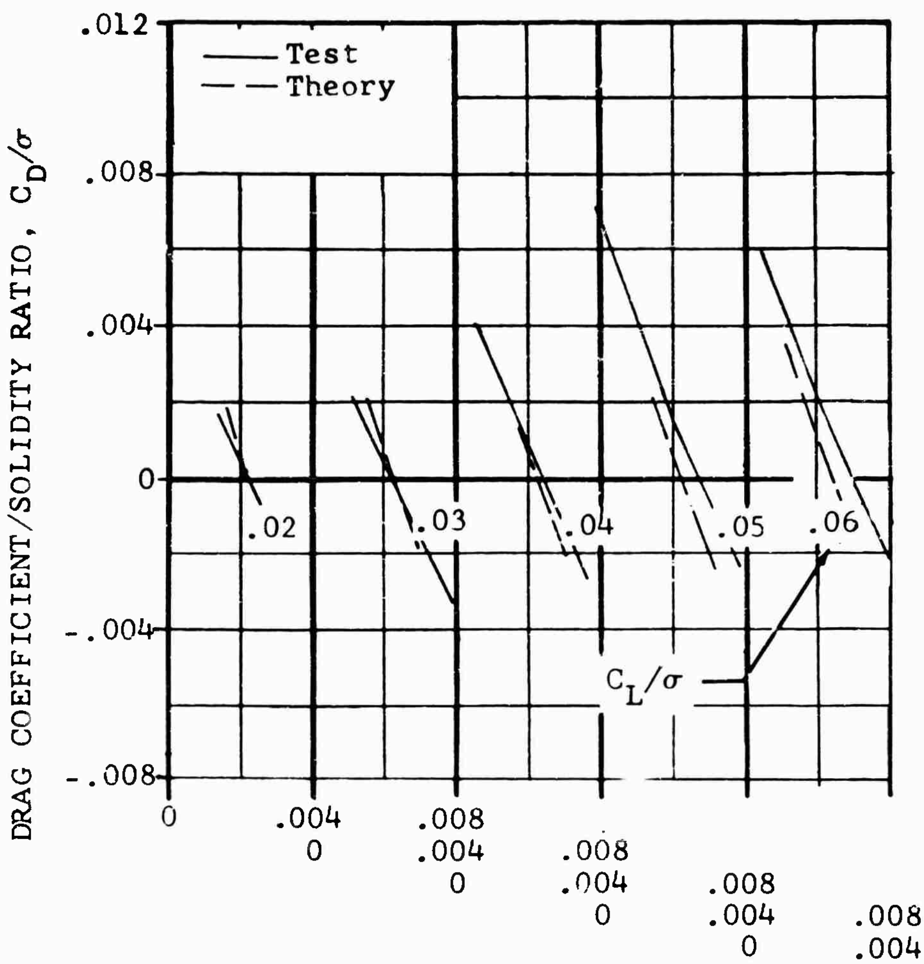

(e) μ = 0.40, $M_{(1.0,\ 90.)}$ = 0.85

Figure 15. Concluded.

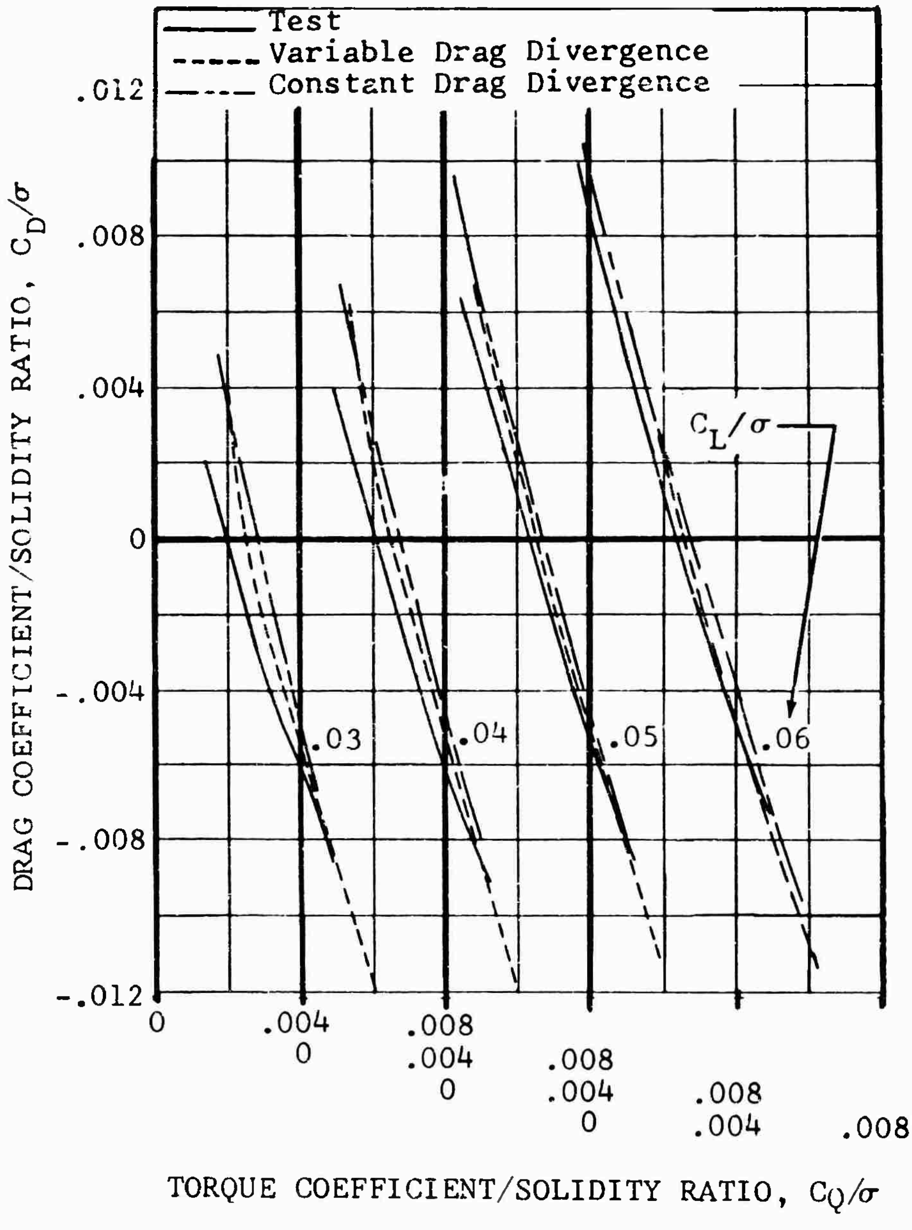

Figure 16. Theory-Test Comparison, Nondimensional Performance of Thin-Tipped Blades at μ = 0.30 and $M_{(1.0,\ 90.)}$ = 0.95.

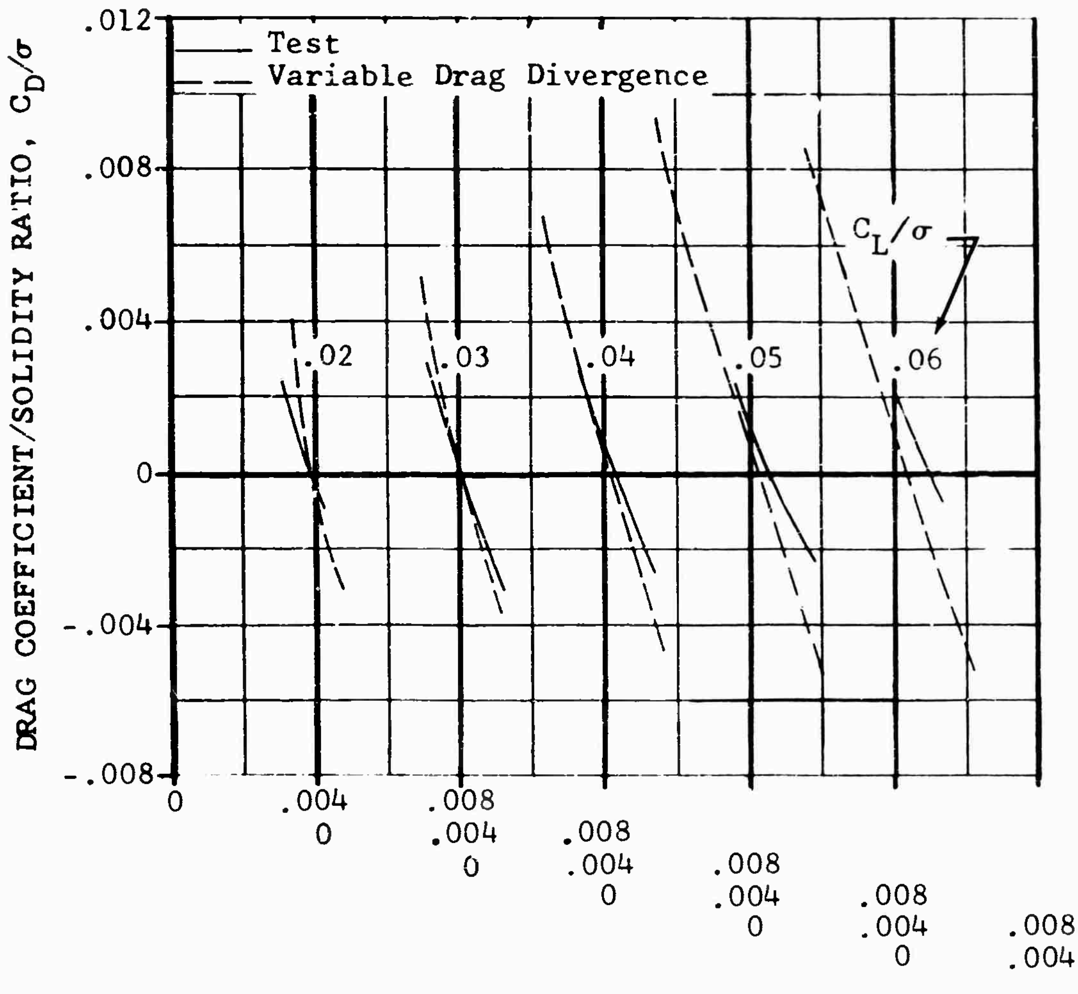

Figure 17. Theory-Test Comparison, Nondimensional Performance of Thin-Tipped Blades at μ = 0.35 and $M_{(1.0,\ 90.)}$ = 1.00.

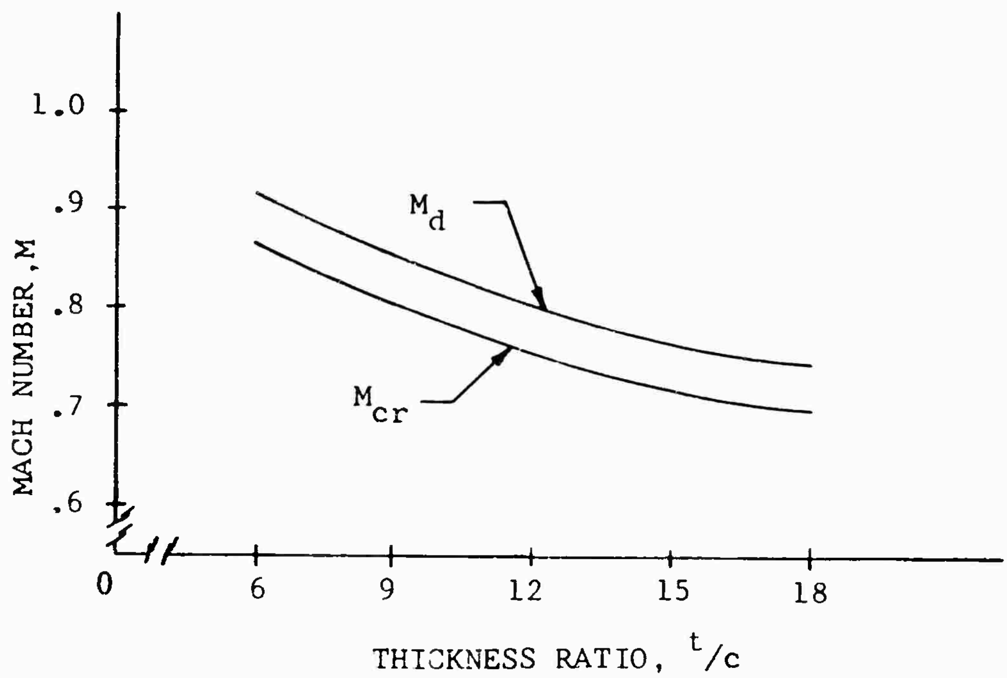

Figure 18. Variation of Critical and Drag Divergence Mach Number with Thickness Ratio.

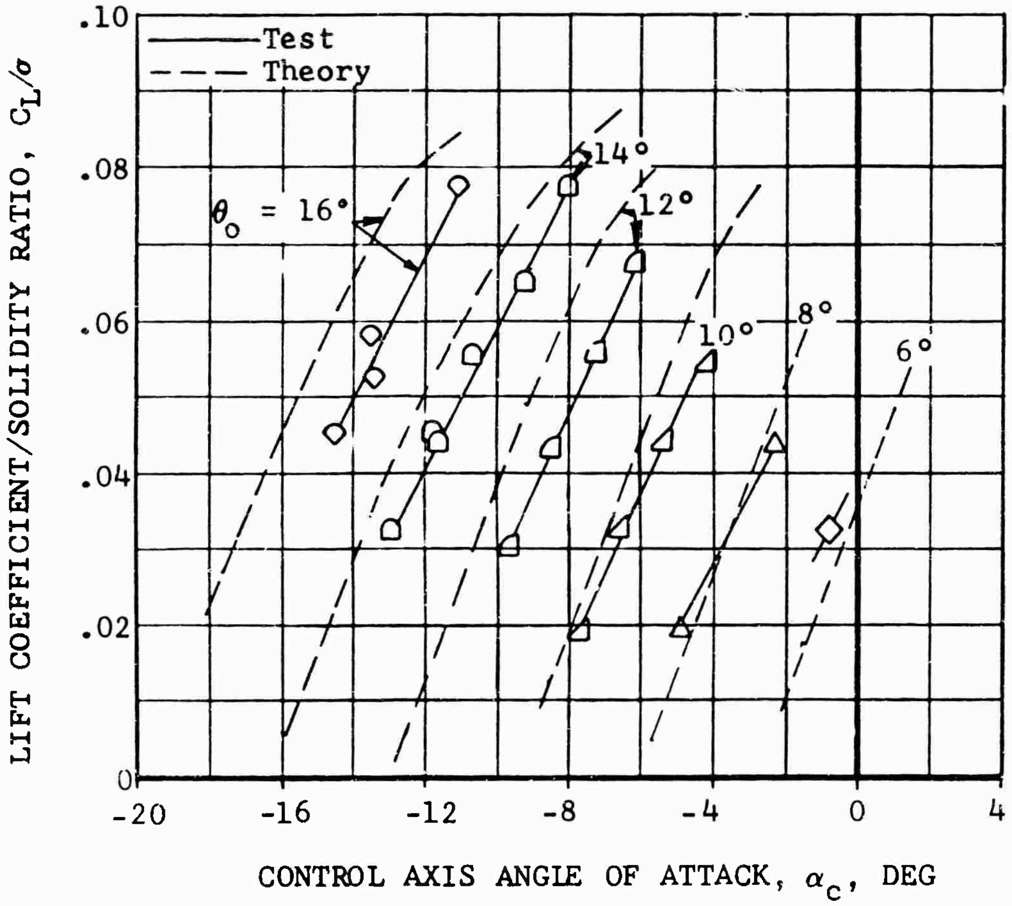

a) C_L/σ vs α_c

Figure 19. Theory-Test Comparison, Nondimensional Performance of 34-Foot-Diameter Rotor at μ = 0.51, $M_{(1.0,\ 90.)}$ = 0.65.

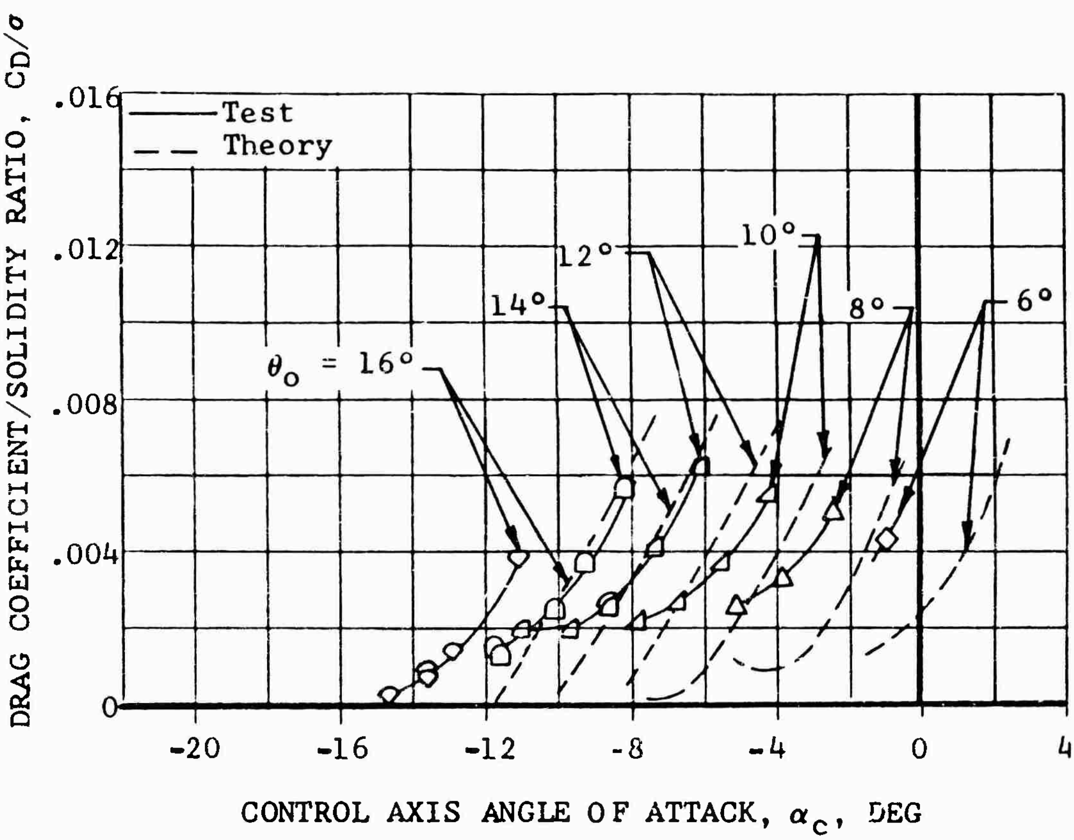

b) C_D/σ vs α_c

Figure 19. Continued.

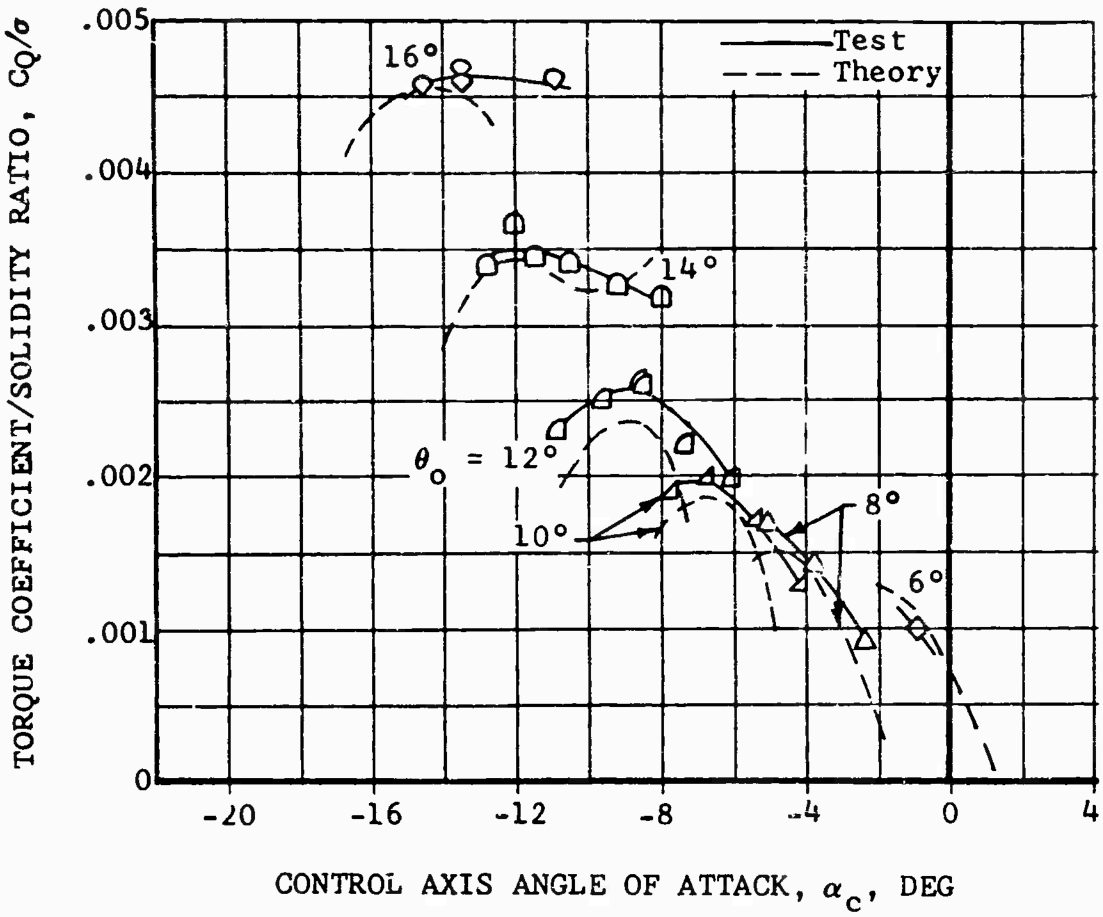

c) C_Q/σ vs α_c

Figure 19. Concluded.

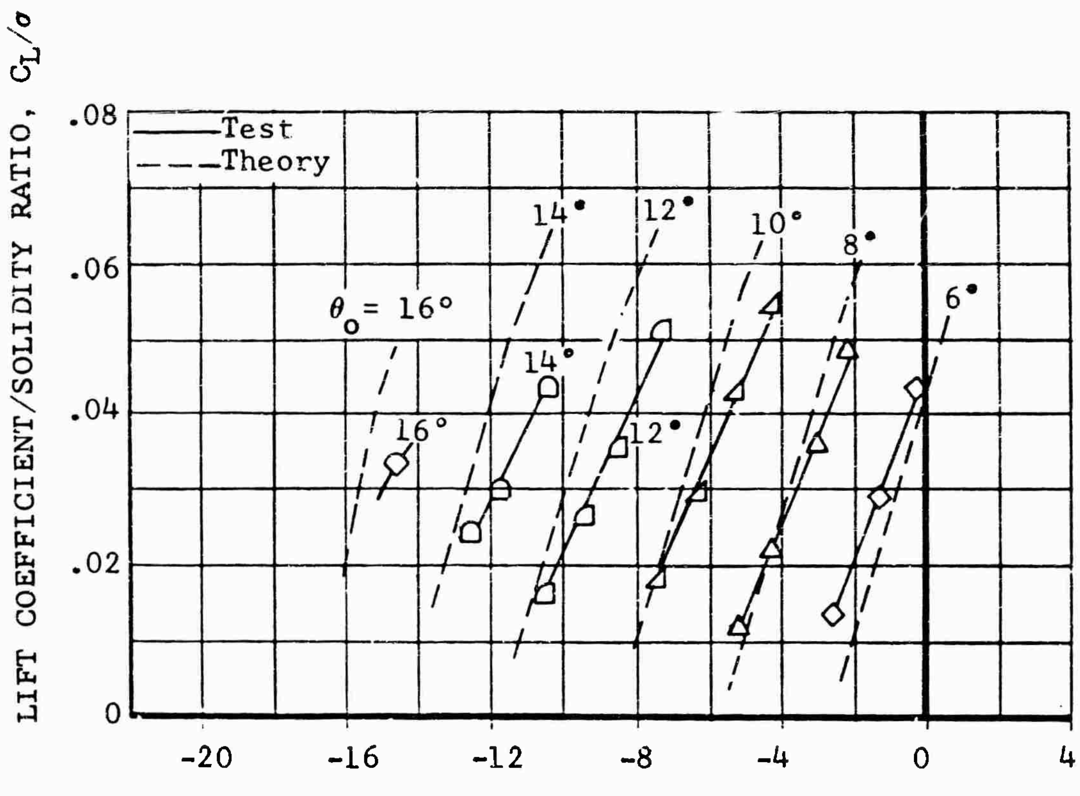

a) C_L/σ vs α_c

Figure 20. Theory-Test Comparison, Nondimensional Performance of 34-Foot-Diameter Rotor at μ = 0.66, $M_{(1.0,\ 90.)}$ = 0.55.

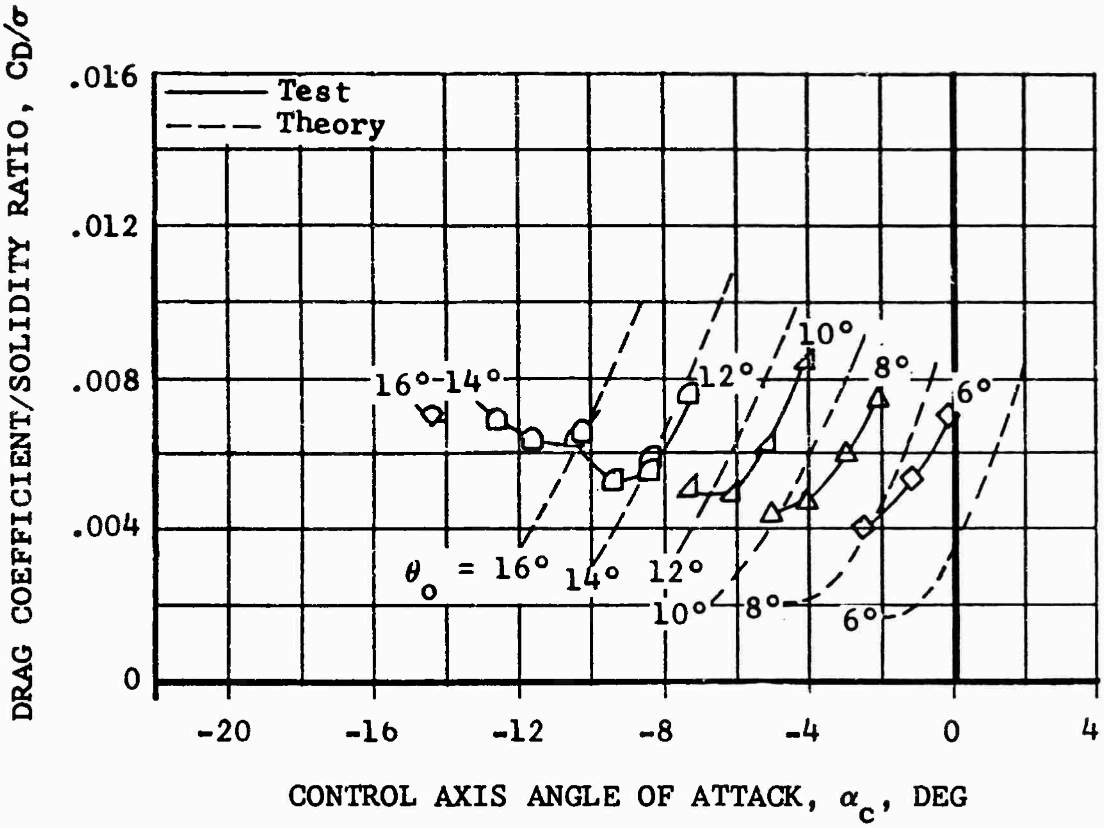

b) C_D/σ vs α_c

Figure 20. Continued.

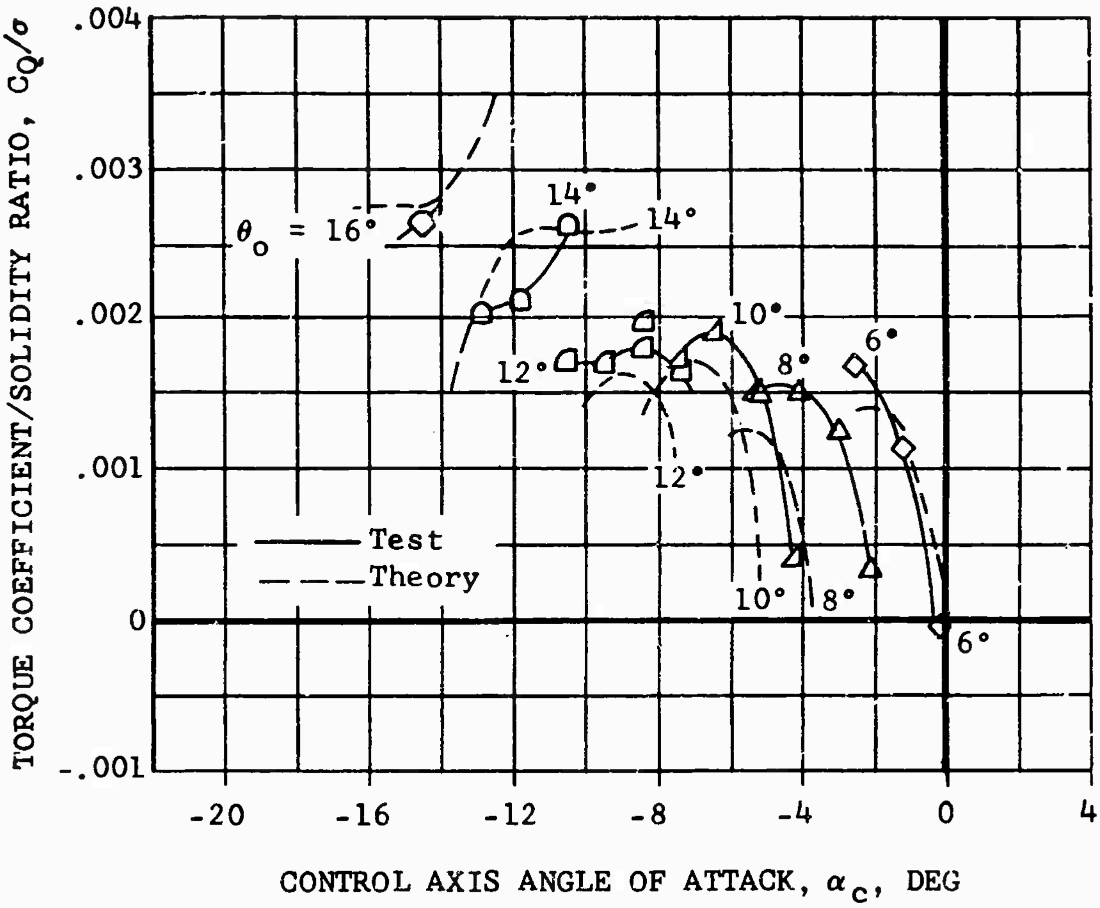

c) C_Q/σ vs α_c

Figure 20. Concluded.

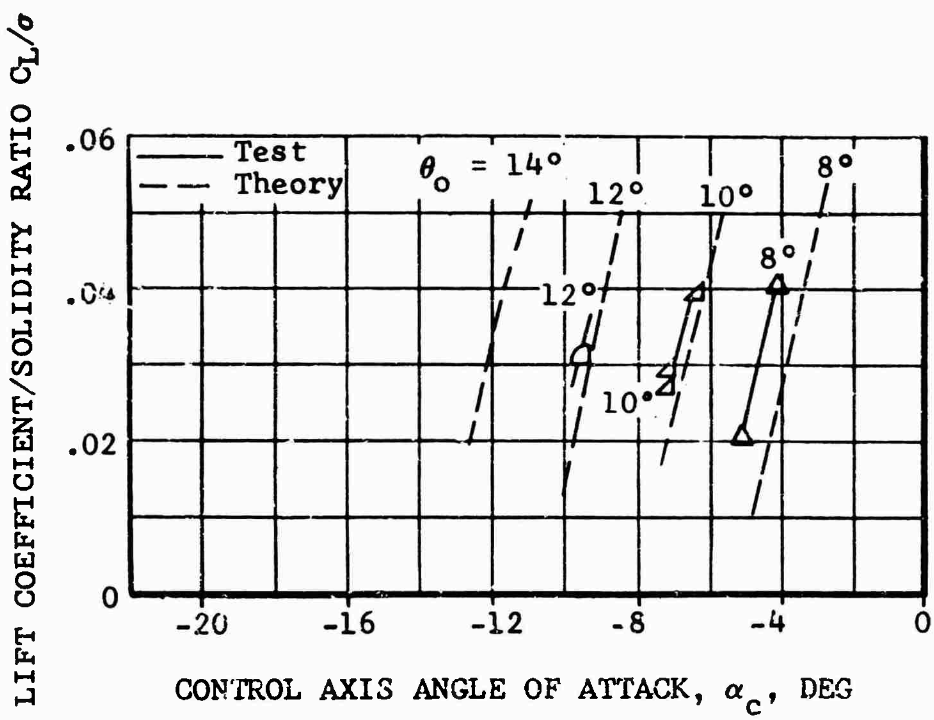

a) C_L/σ vs α_c

Figure 21. Theory-Test Comparison, Nondimensional Performance of 34-Foot-Diameter Rotor at $\mu = 0.79$, $M_{(1.0,\ 90.)} = 0.52$.

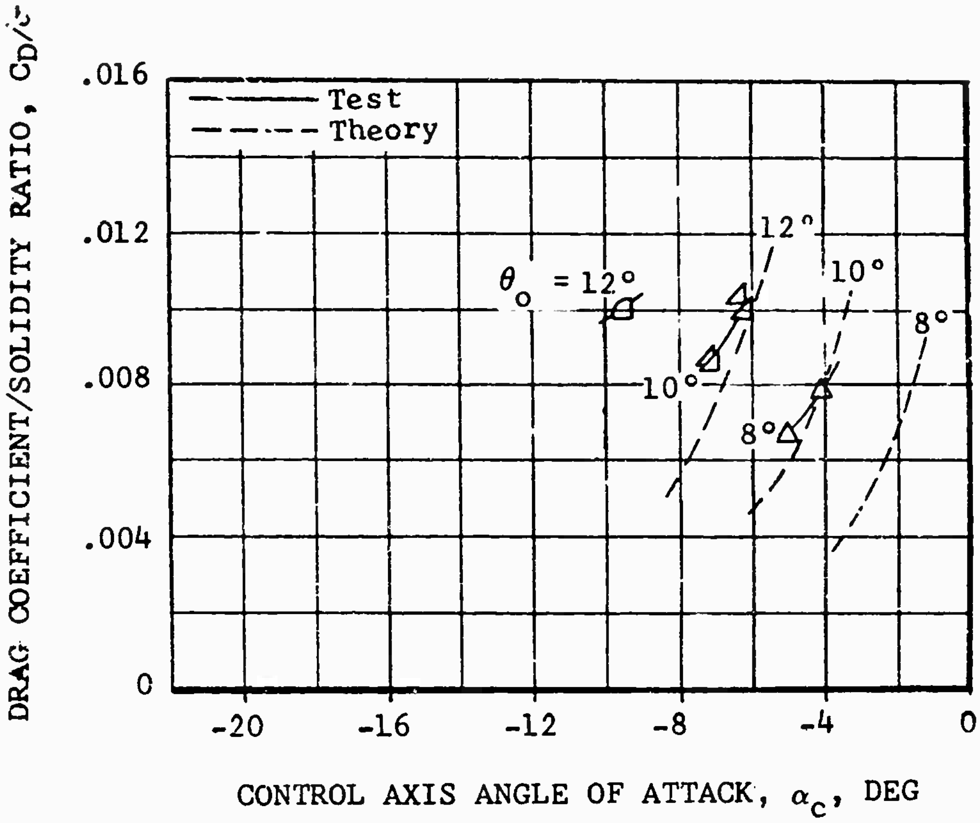

b) C_D/σ vs α_c

Figure 21. Continued.

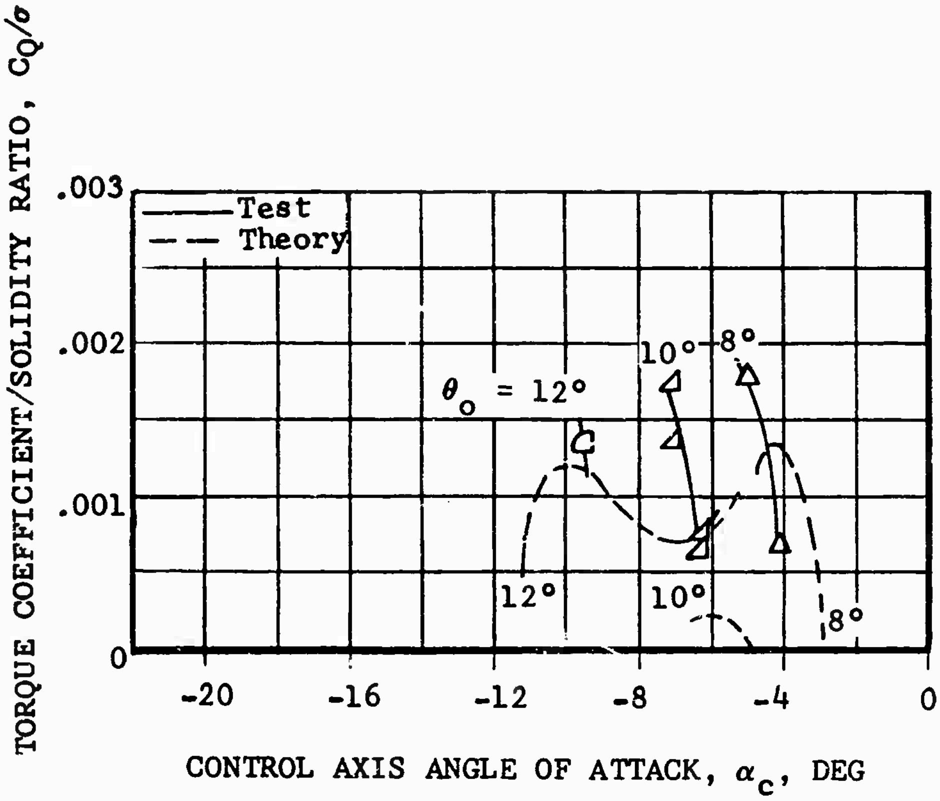

c) C_Q/σ vs α_c

Figure 21. Concluded.

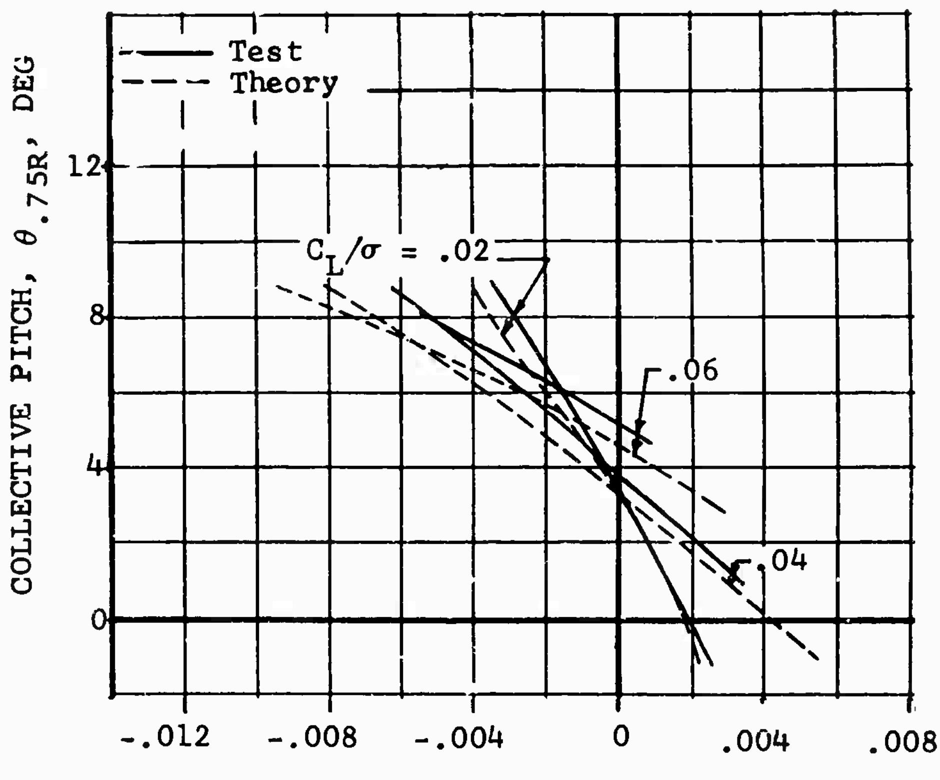

a) $\theta_{.75R}$ vs C_D/σ

Figure 22. Theory-Test Comparison, Control Positions of UH-1D Rotor at μ = 0.30, $M_{(1.0,\ 90.)}$ = 0.85.

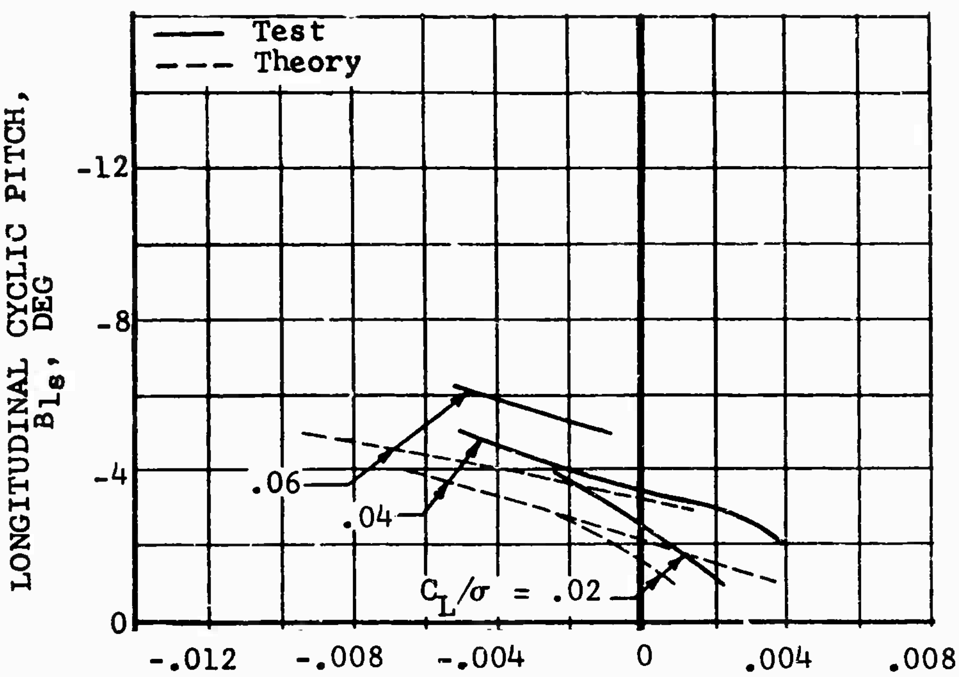

DRAG COEFFICIENT/SOLIDITY RATIO, C_D/σ

b) B_{1s} vs C_D/σ

Figure 22. Concluded.

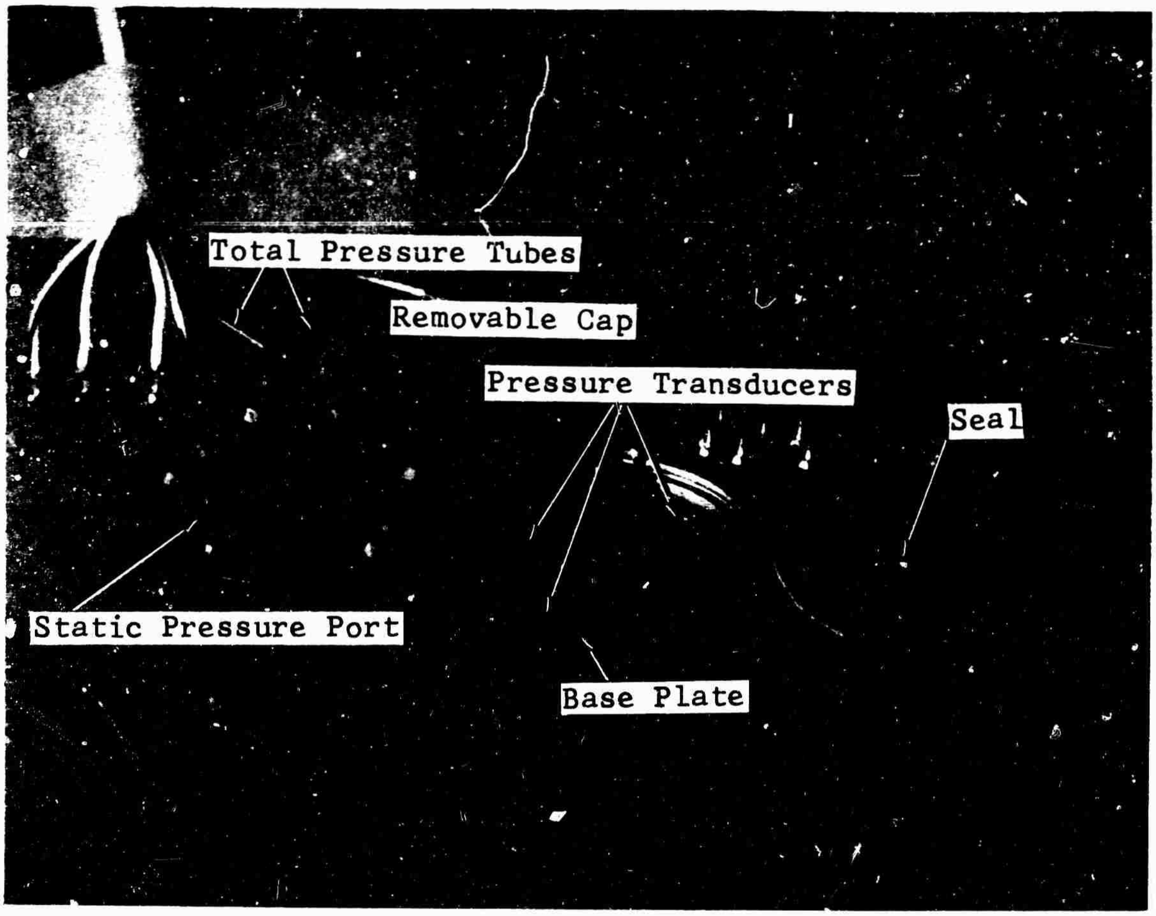

Figure 23. Boundary Layer Button Details.

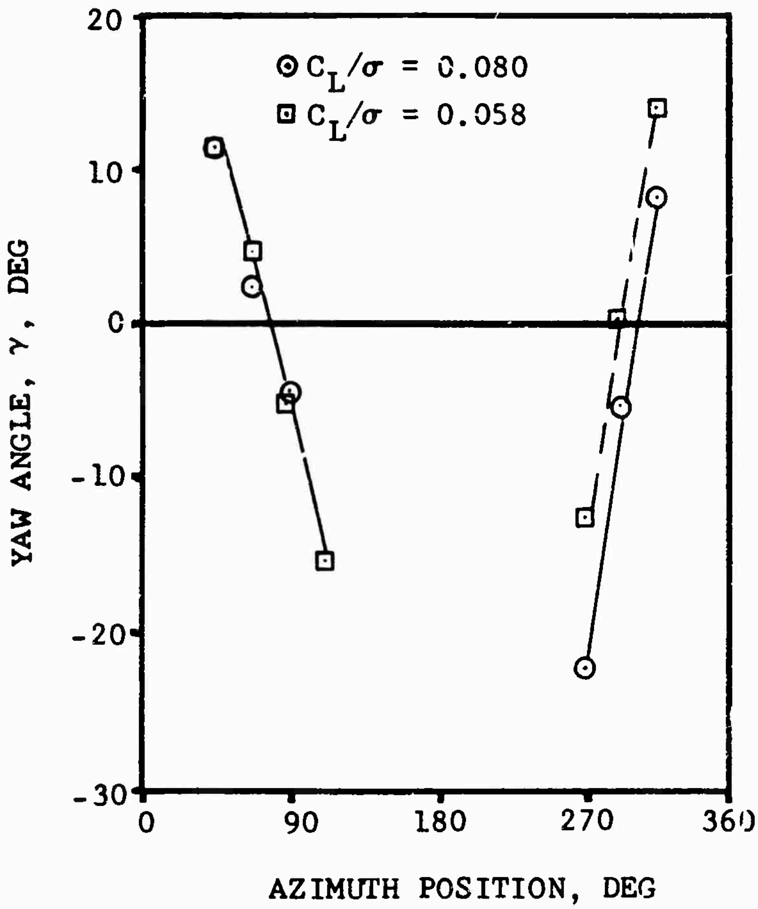

Figure 24. Variation of Yaw Angle on the Upper Surface with a Change in Azimuth Position for Two Values of Rotor Lift. μ = 0.27, $M_{(1.0,\ 90.)}$ = 0.90.

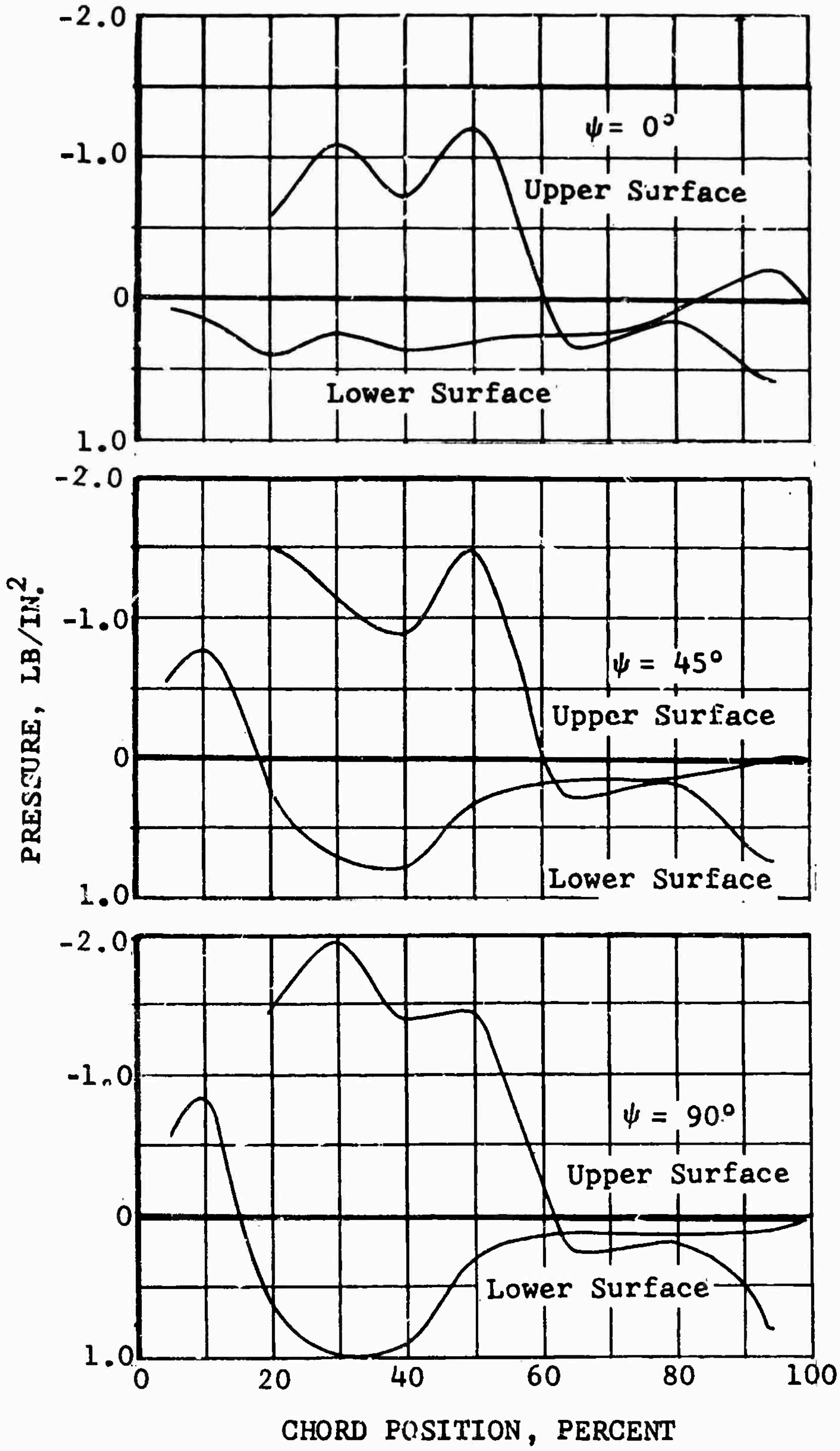

Figure 25. Surface Pressure Distribution at 0.98R for Various Azimuths, μ = 0.20, $M_{(1.0,\ 90.)}$ = 0.85, C_L/σ = 0.0734 C_D/σ = 0.0051.

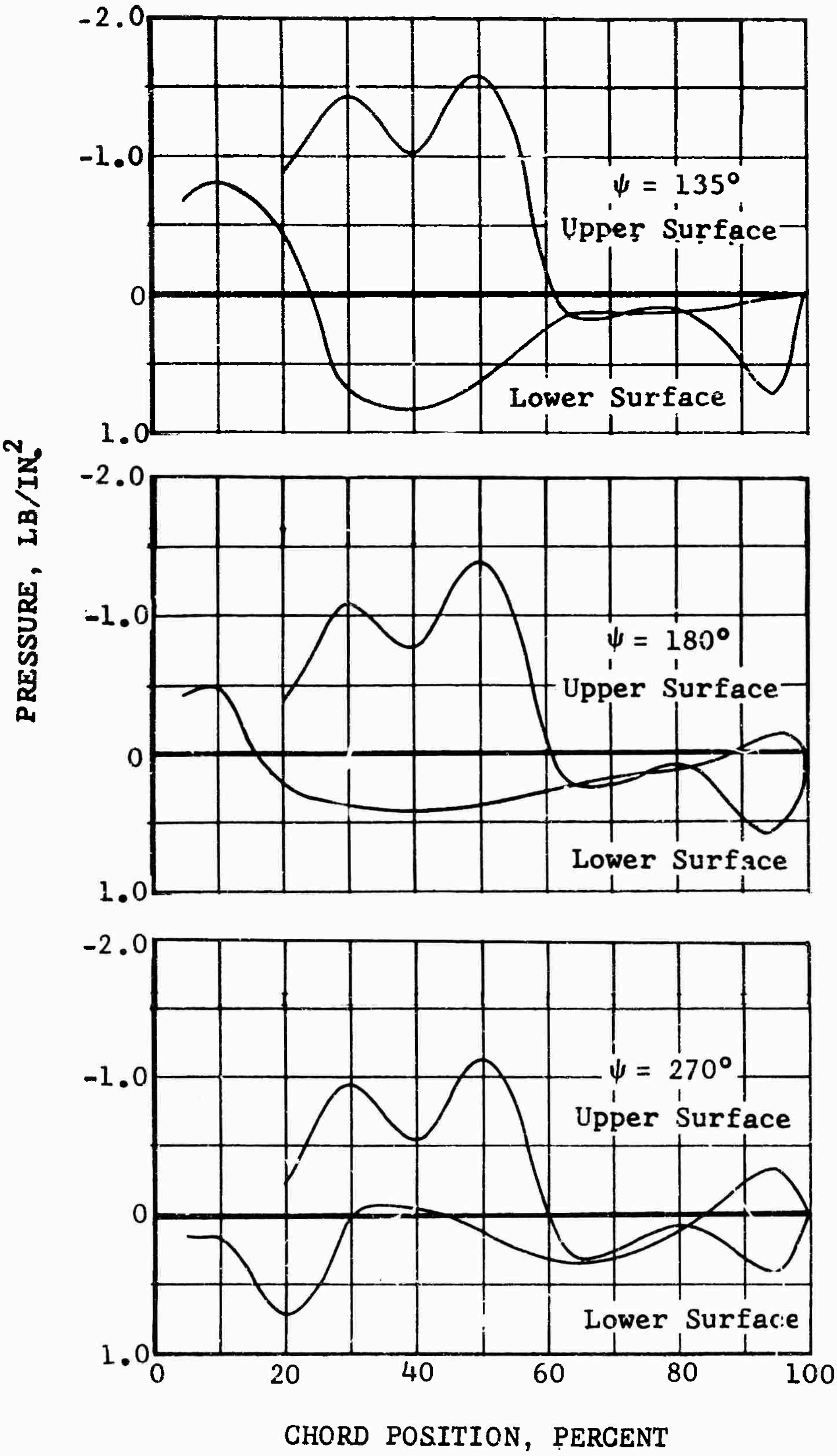

Figure 25. Concluded.

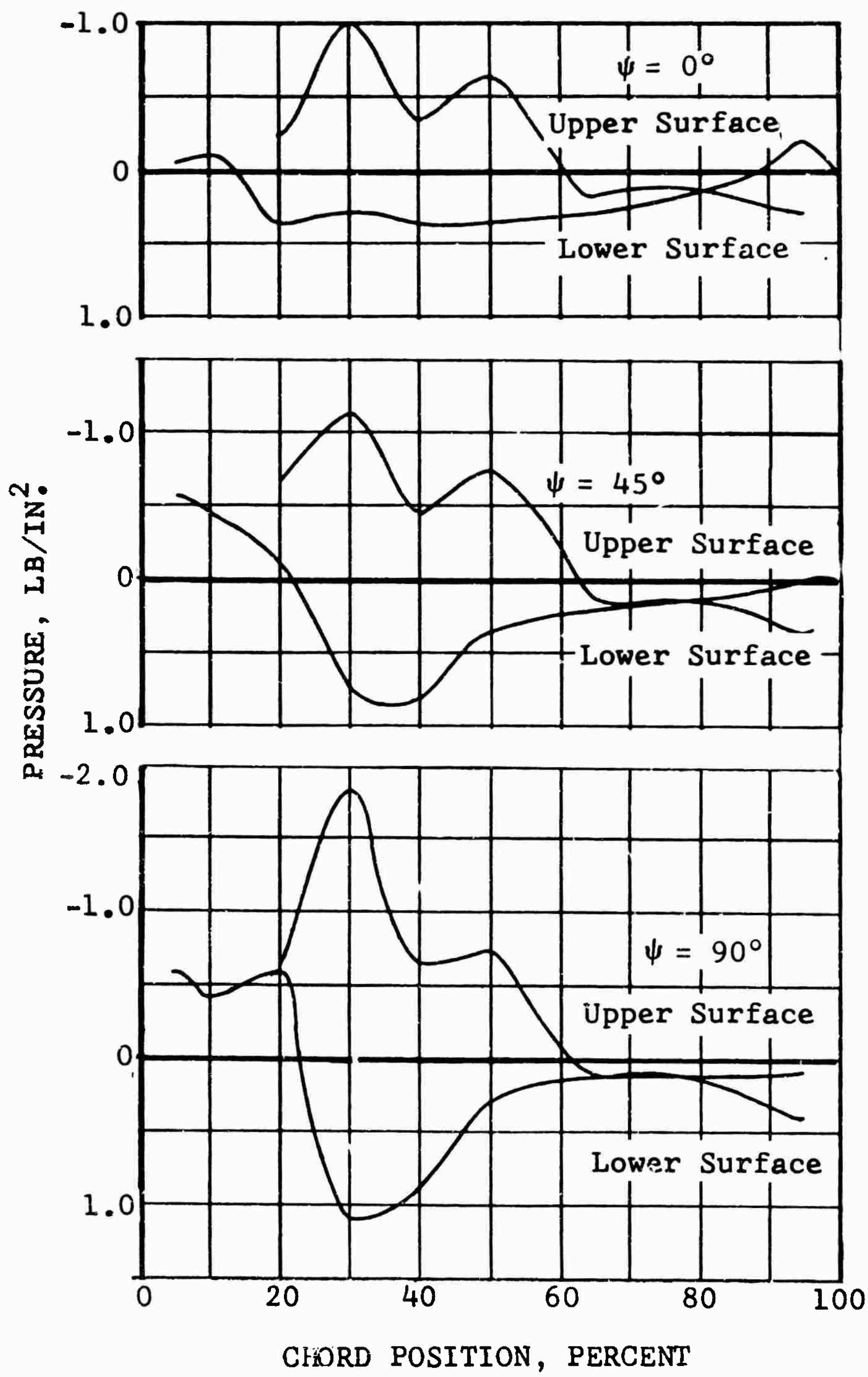

Figure 26. Surface Pressure Distribution at 0.98R for Various Azimuths, μ = 0.20, $M_{(1.0,\ 90.)}$ = 0.85, C_L/σ = 0.0604, C_D/σ = 0.00406.

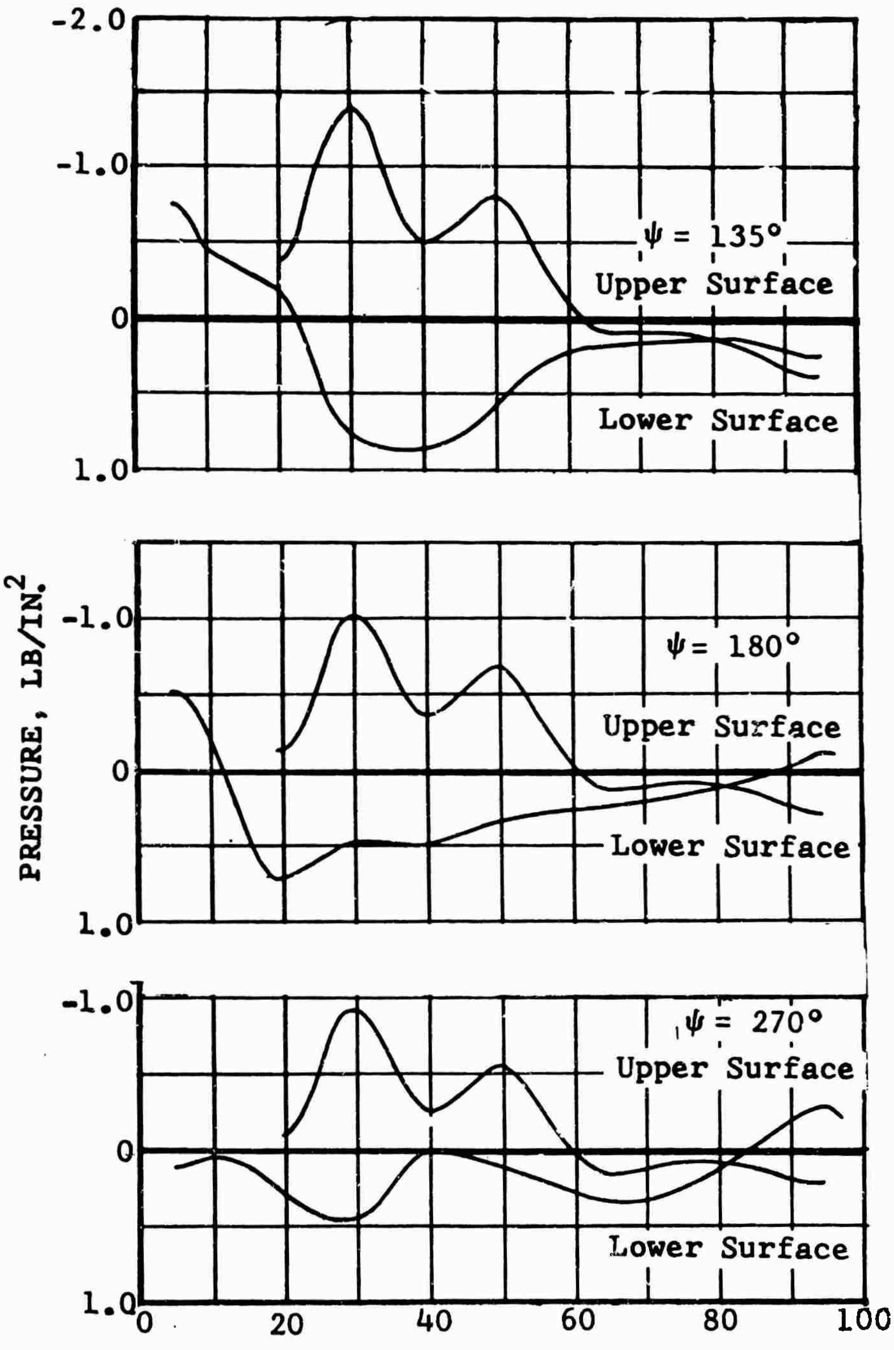

Figure 26. Concluded.

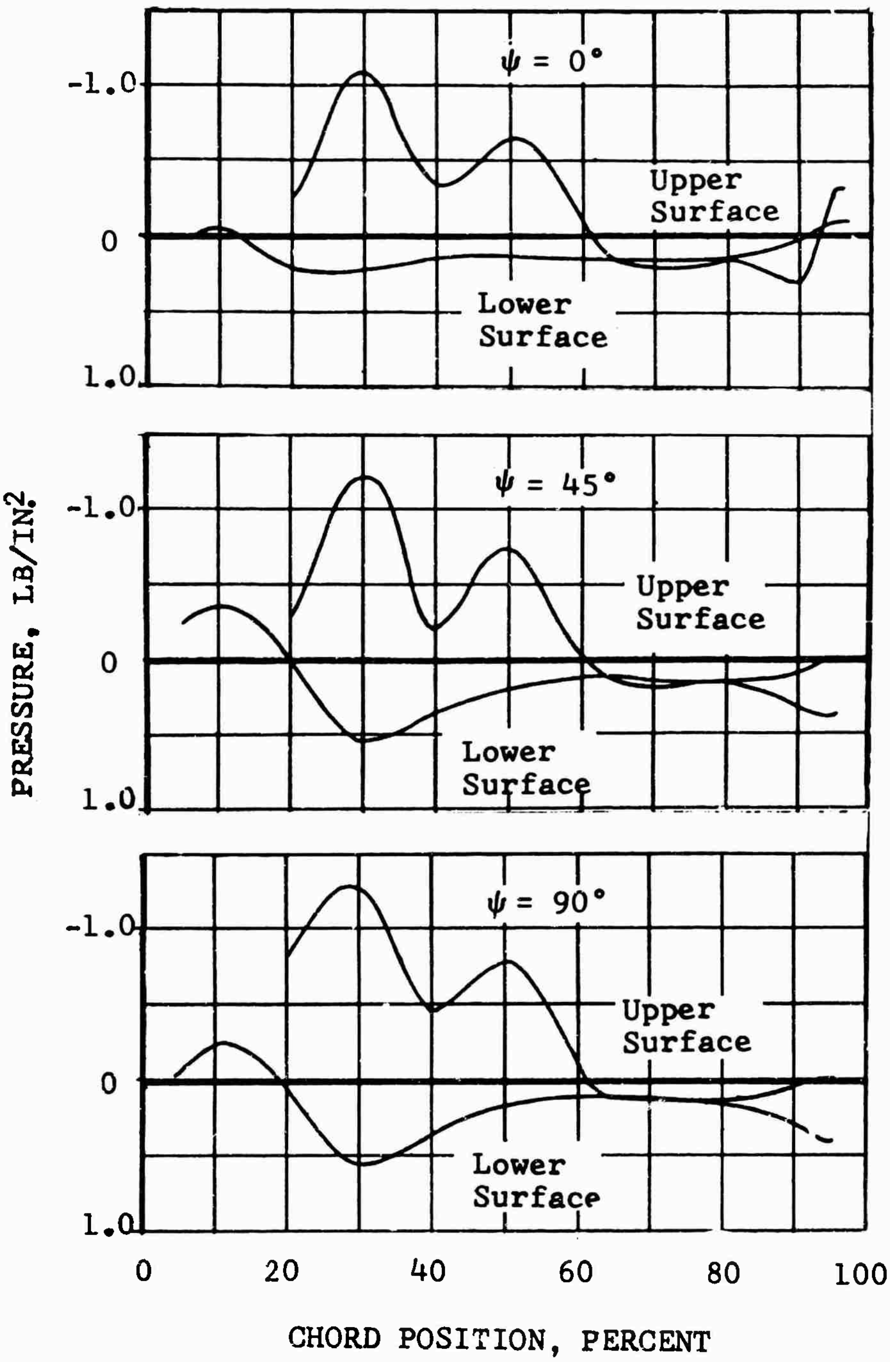

Figure 27. Surface Pressure Distribution at 0.98R for Various Azimuths, $\mu = 0.129$, $M_{(1.0, 90.)} = 0.80$, $C_L/\sigma = 0.077$, $C_D/\sigma = -0.0060$.

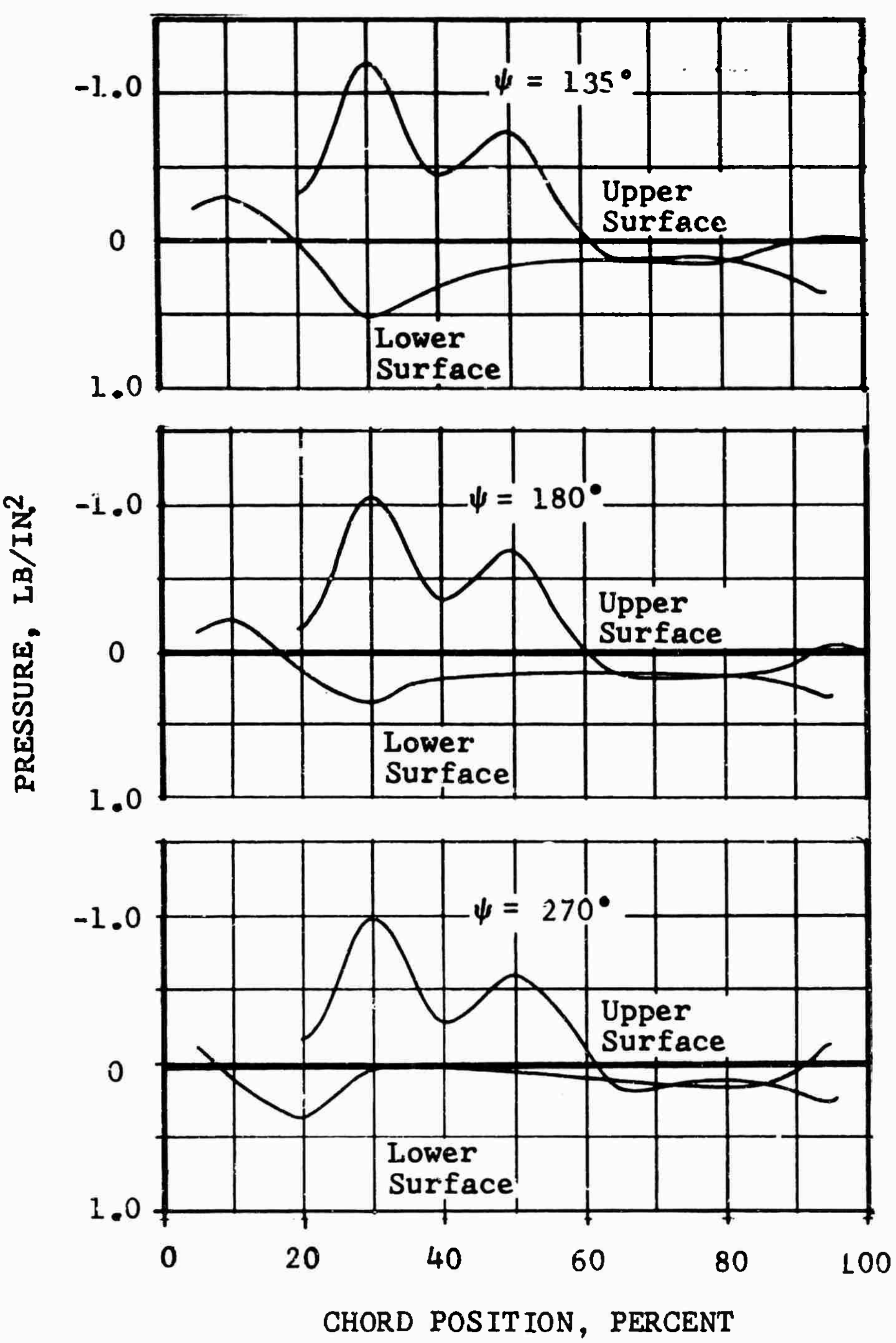

Figure 27. Concluded.

REFERENCES CITED

1. Kelley, B., NOTES ON THE SELECTION OF TIP SPEED AND SOLIDITY, Bell Aircraft Corporation, 18 March 1950.

2. Drees, J. M., and Lynn, R. R., THE PROMISE OF COMPOUNDING, Presented at AGARD, Paris, France, 10-13 January 1966.

3. Fradenburgh, Evan A., AERODYNAMIC EFFICIENCY POTENTIALS OF ROTARY WING AIRCRAFT, Paper presented before the American Helicopter Society's Sixteenth Annual National Forum, Washington, D.C., 11-14 May 1960.

4. Tanner, W. H., and Bergquist, R. R., SOME PROBLEMS OF DESIGN AND OPERATION OF A 250-KNOT COMPOUND HELICOPTER ROTOR, American Institute of Aeronautics and Astronautics Journal of Aircraft, Vol. 1, No. 5, September-October 1964, pp. 252-259.

5. Van Wyckhouse, J. F., and Cresap, W. L., HIGH-PERFORMANCE HELICOPTER PROGRAM SUMMARY REPORT, PHASE II, USATRECOM Technical Report 64-61, October 1964.

6. Van Wyckhouse, J. F., et al., HIGH-PERFORMANCE UH-1 COMPOUND HELICOPTER MANEUVER FLIGHT TEST PROGRAM, USAAVLABS Technical Report 66-17, February 1966, AD630927.

7. Nitzberg, G. E., and Crandall, S., A STUDY OF FLOW CHANGES ASSOCIATED WITH AIRFOIL SECTION DRAG RISE AT SUPERCRITICAL SPEEDS, NACA Technical Note 1813, February 1949.

8. Tanner, W. H., CHARTS FOR ESTIMATING ROTARY WING PERFORMANCE IN HOVER AND AT HIGH FORWARD SPEEDS, NASA Contractor Report CR-114, November 1964.

9. Charles, B. D., BELL ROTOR AERODYNAMIC METHOD, Bell Helicopter Company Report No. 599-102-900, January 1968.

10. Gessow, Alfred, and Crim, Almer D., A METHOD FOR STUDYING THE TRANSIENT BLADE-FLAPPING BEHAVIOR OF LIFTING ROTORS AT EXTREME OPERATING CONDITIONS, NACA Technical Note 3366, January 1955.

11. Fradenburgh, E. A., and Rabbott, J. P., Jr., HIGH SPEED HELICOPTER RESEARCH, Paper presented before the American Helicopter Society's Eighteenth Annual National Forum, Washington, D.C., 1962.

12. Abbott, I. H., Von Doenhoff, A. E., and Stivers, L. S., Jr., SUMMARY OF AIRFOIL DATA, NACA Report No. 824, Langley Memorial Aeronautical Laboratory, Langley Field, Virginia, 1945.

13. Cresap, W. L., Duhon, J. M., Lynn, R. R., and Van Wyckhouse, J. F., THE 200+ KNOT FLIGHT RESEARCH HELICOPTER, Paper presented before the American Helicopter Society's Twenty-First Annual National Forum, Washington, D. C., May 1965.

14. Tanner, W. H., and Yaggy, P. F., EXPERIMENTAL BOUNDARY LAYER STUDY ON HOVERING ROTORS, Paper presented before the American Helicopter Society's Twenty-Second Annual National Forum, Washington, D. C., May 1966.

15. Tanner, W. H., and Buettiker, P., THE BOUNDARY LAYER OF THE HOVERING ROTOR, CAL/USAAVLABS Symposium Proceedings, Vol. III, 22-24 June 1966.

APPENDIX I
GRAPHED DATA

The data presented in this appendix (Figures 28 through 31) are from the wind tunnel balance and model instrumentation as tabulated in Appendix IV. The symbols are actual test points and show lift, drag, and torque as a function of shaft angle, α_s, and root collective pitch (θ_0). These data illustrate the consistency of the experimental results.

Rotor rotational speed and tunnel speed were adjusted to obtain the desired advance ratio and advancing tip Mach number. The cyclic pitch was adjusted to minimize first harmonic rotor flapping; and at each combination of shaft angle and collective pitch, the data were recorded. Collective pitch or shaft angle was then changed, and the above procedure was repeated until the envelope was explored.

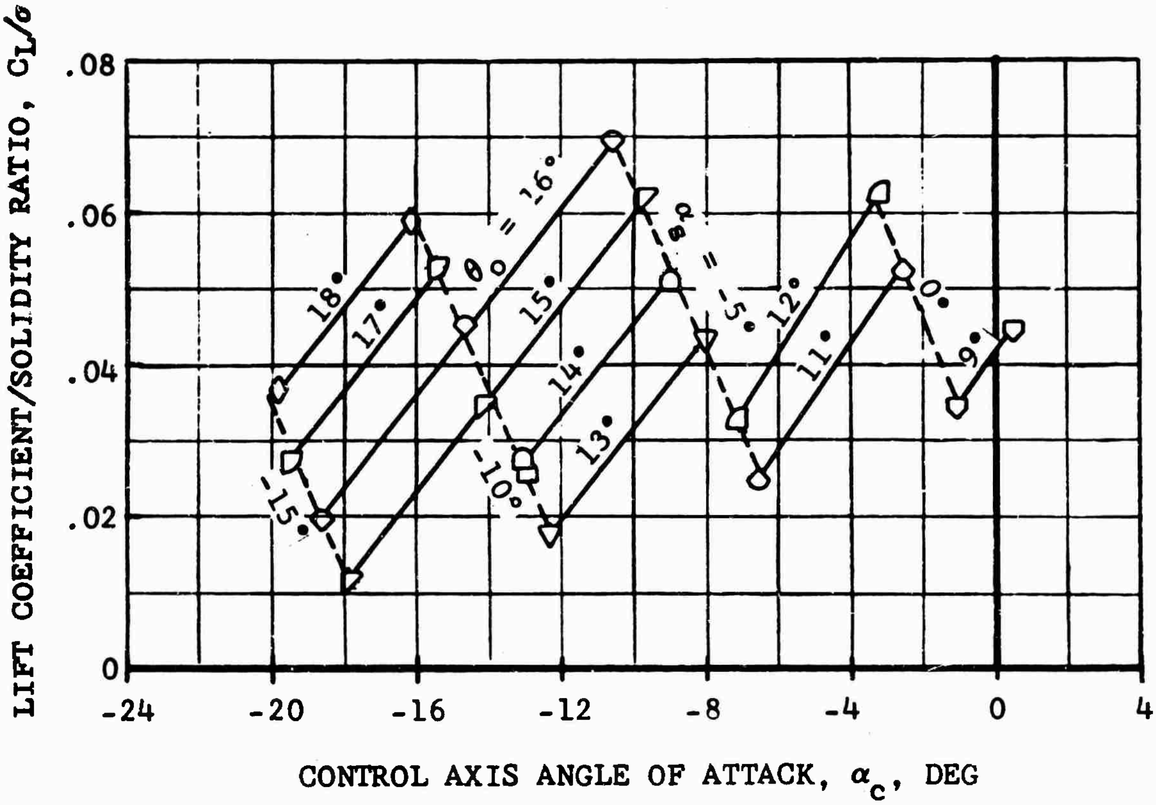

a) C_L/σ vs α_c

Figure 28. The Results of Various Collective Pitch, Shaft and Control Axis Angles on the Performance Characteristics of the Standard Blades. $\mu = 0.30$; $M_{(1.0,\ 90.)} = 0.95$.

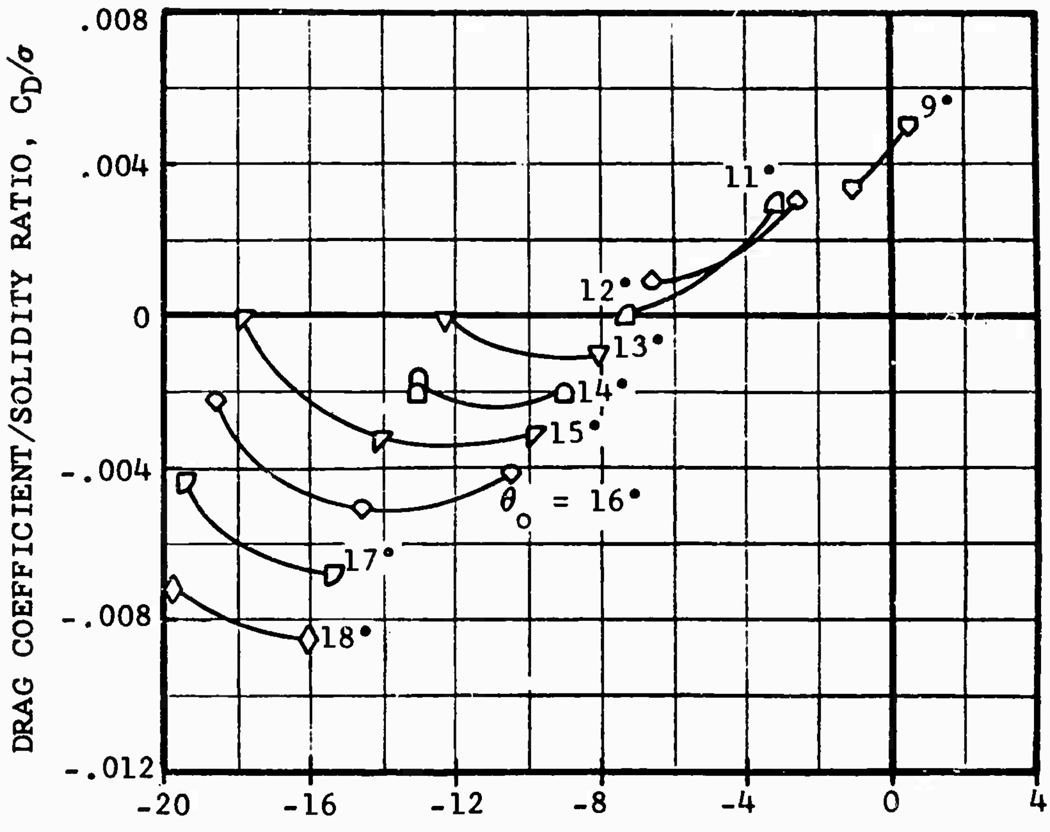

b) C_D/σ vs α_c

Figure 28. Continued.

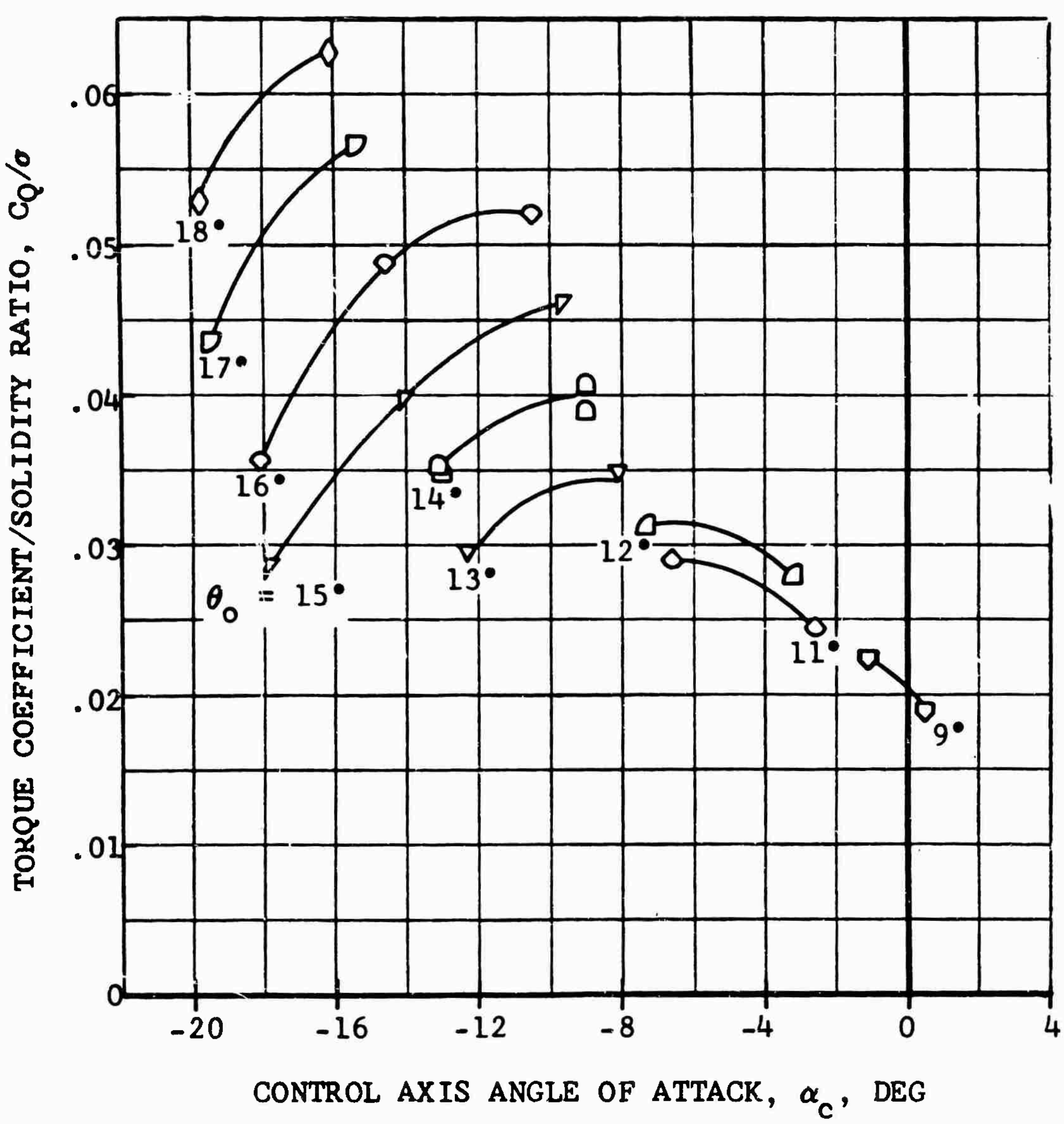

c) C_Q/σ vs α_c

Figure 28. Concluded.

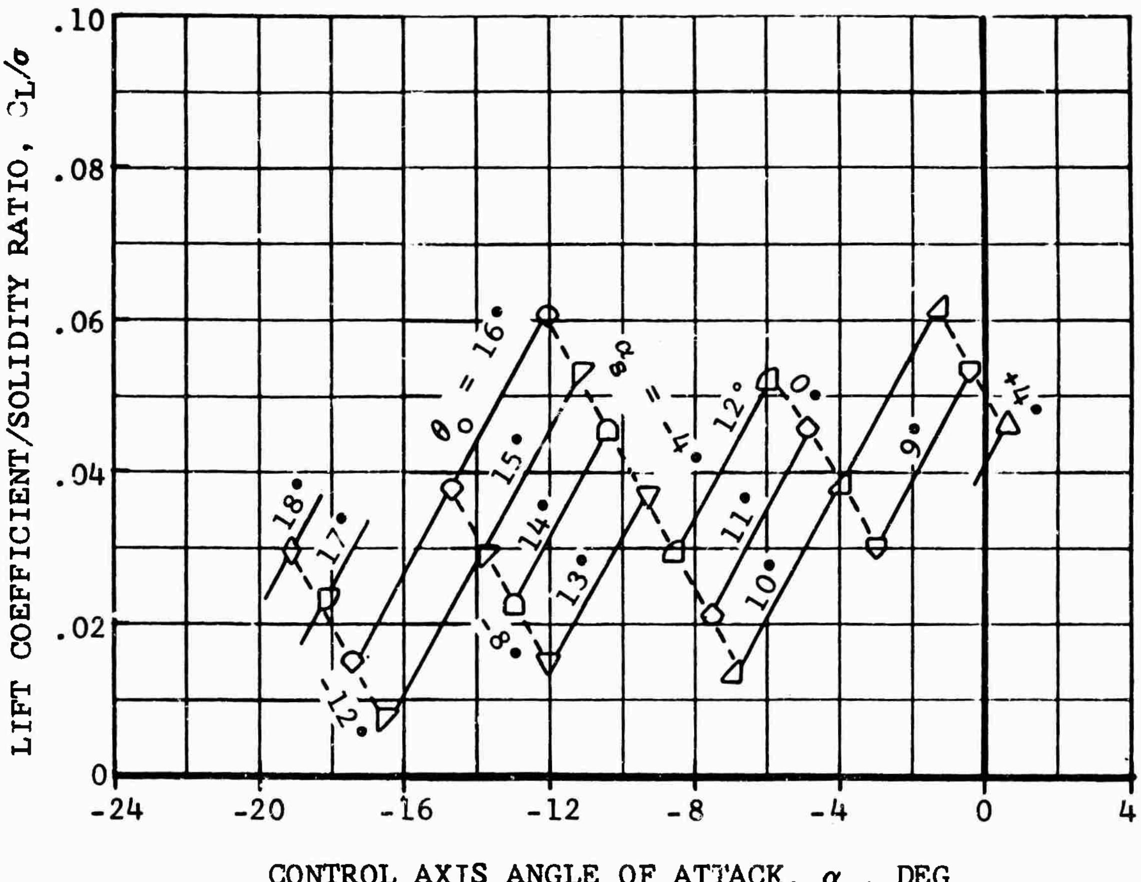

a) C_L/σ vs α_c

Figure 29. The Results of Various Collective Pitch, Shaft and Control Axis Angles on the Performance Characteristics of the Standard Blades. $\mu = 0.40$; $M_{(1.0,\ 90.)} = 0.85$.

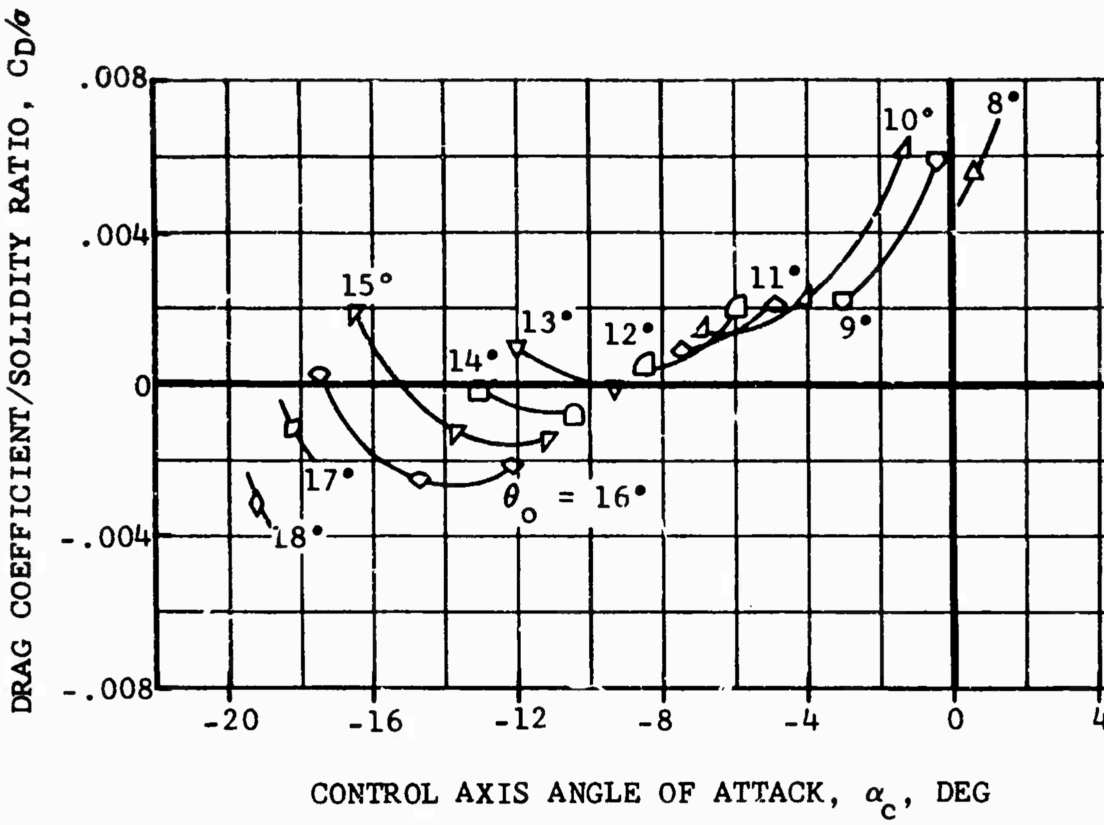

b) C_D/σ vs α_c

Figure 29. Continued.

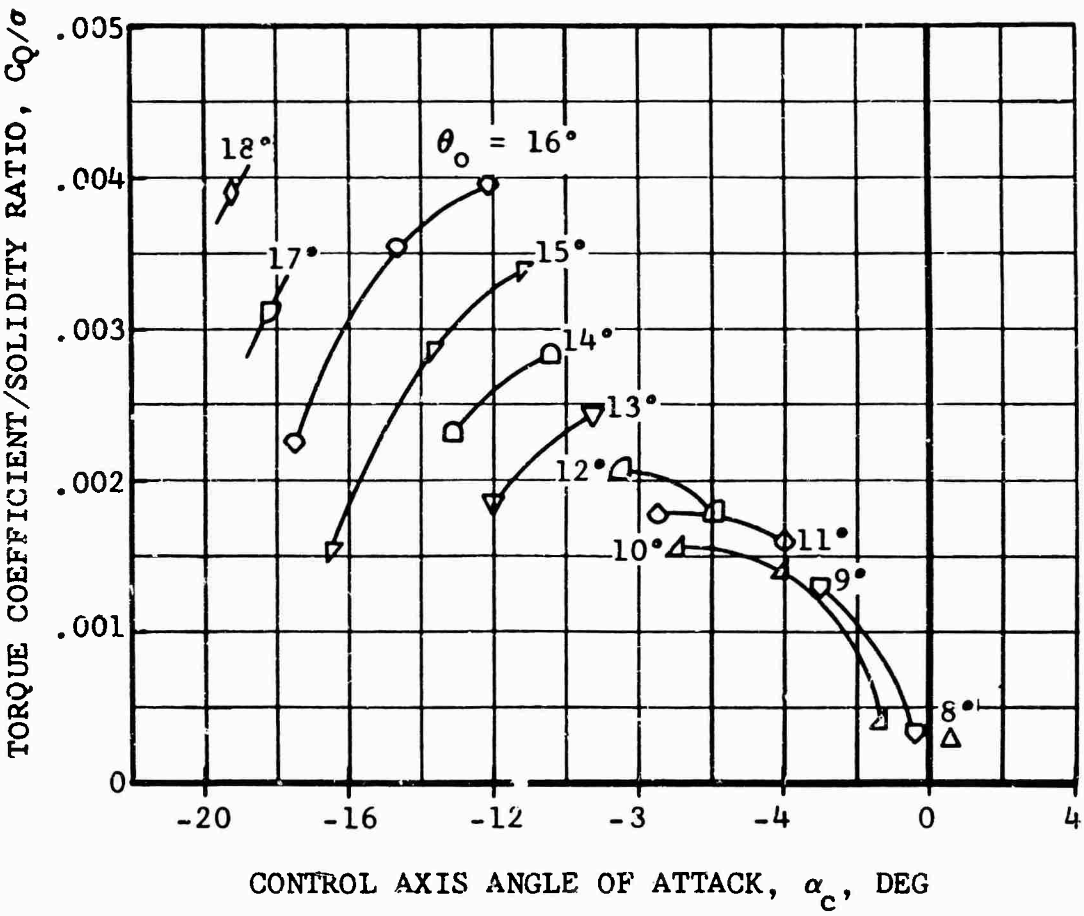

c) C_Q/σ vs α_c

Figure 29. Concluded.

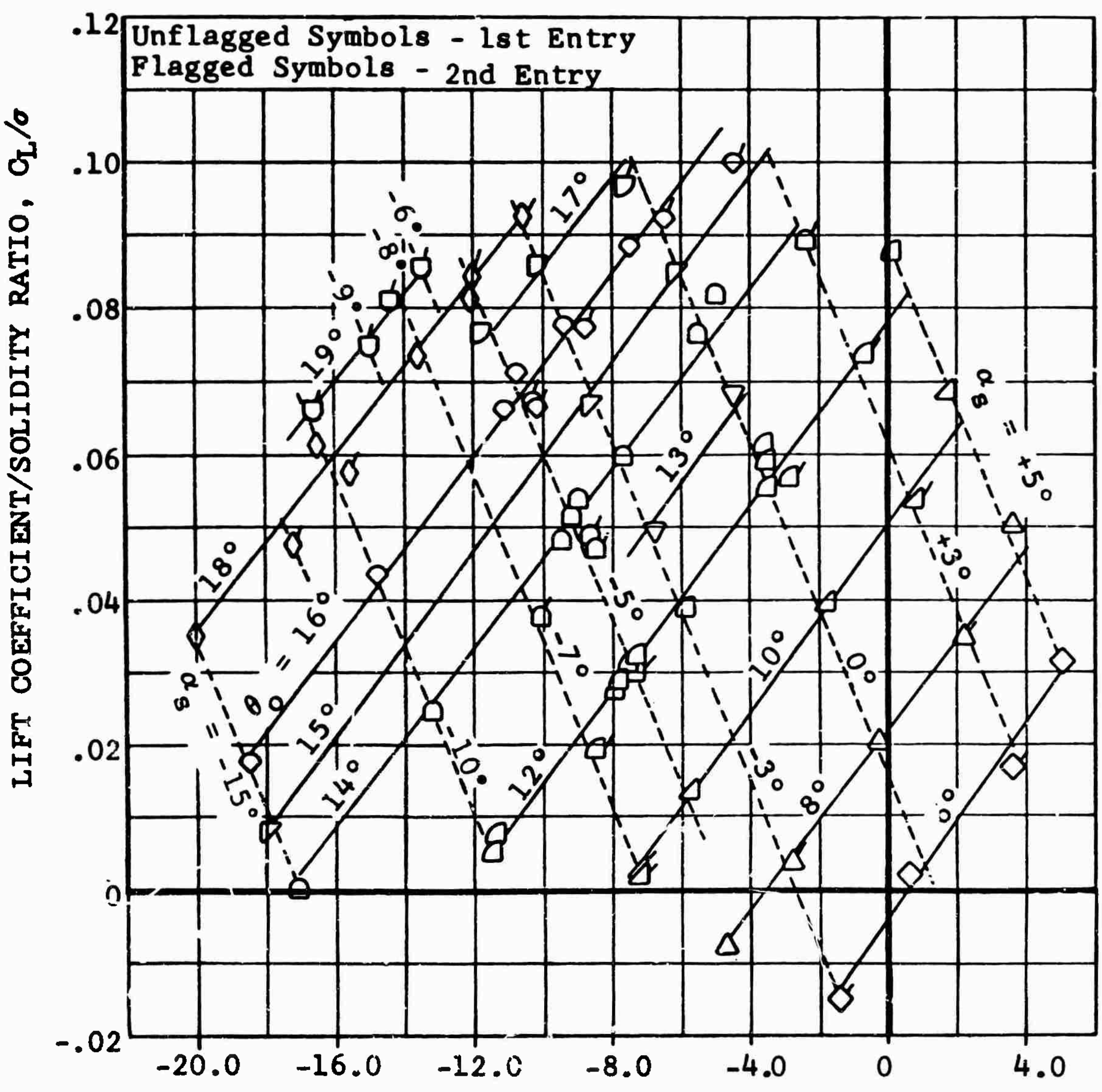

a) C_L/σ vs α_c

Figure 30. The Results of Various Collective Pitch, Shaft and Control Axis Angles on the Performance Characteristics of the Thin-Tipped Blades. $\mu = 0.30$; $M_{(1.0,\ 90.)} = 0.85$.

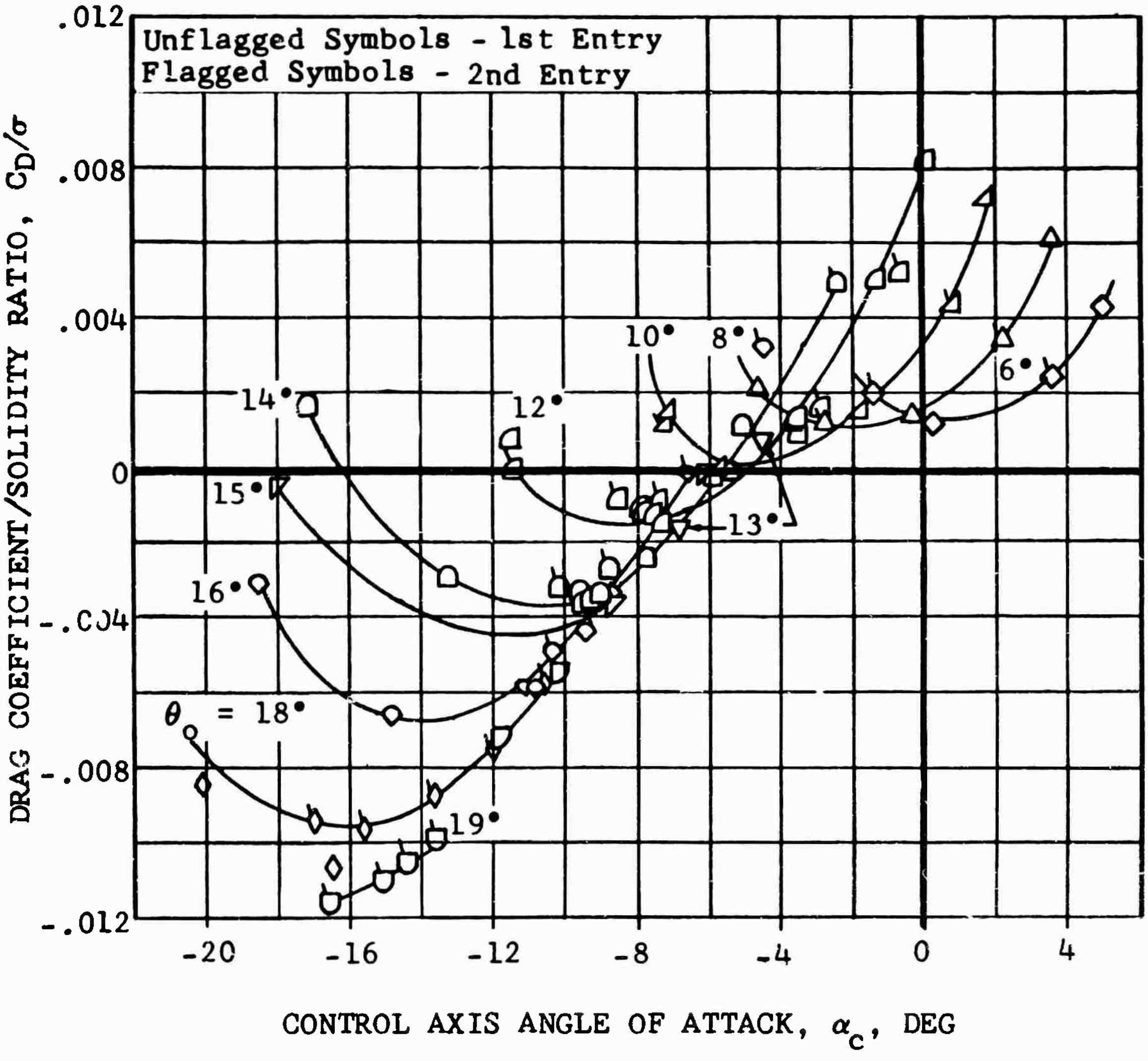

b) C_D/σ vs α_c

Figure 30. Continued

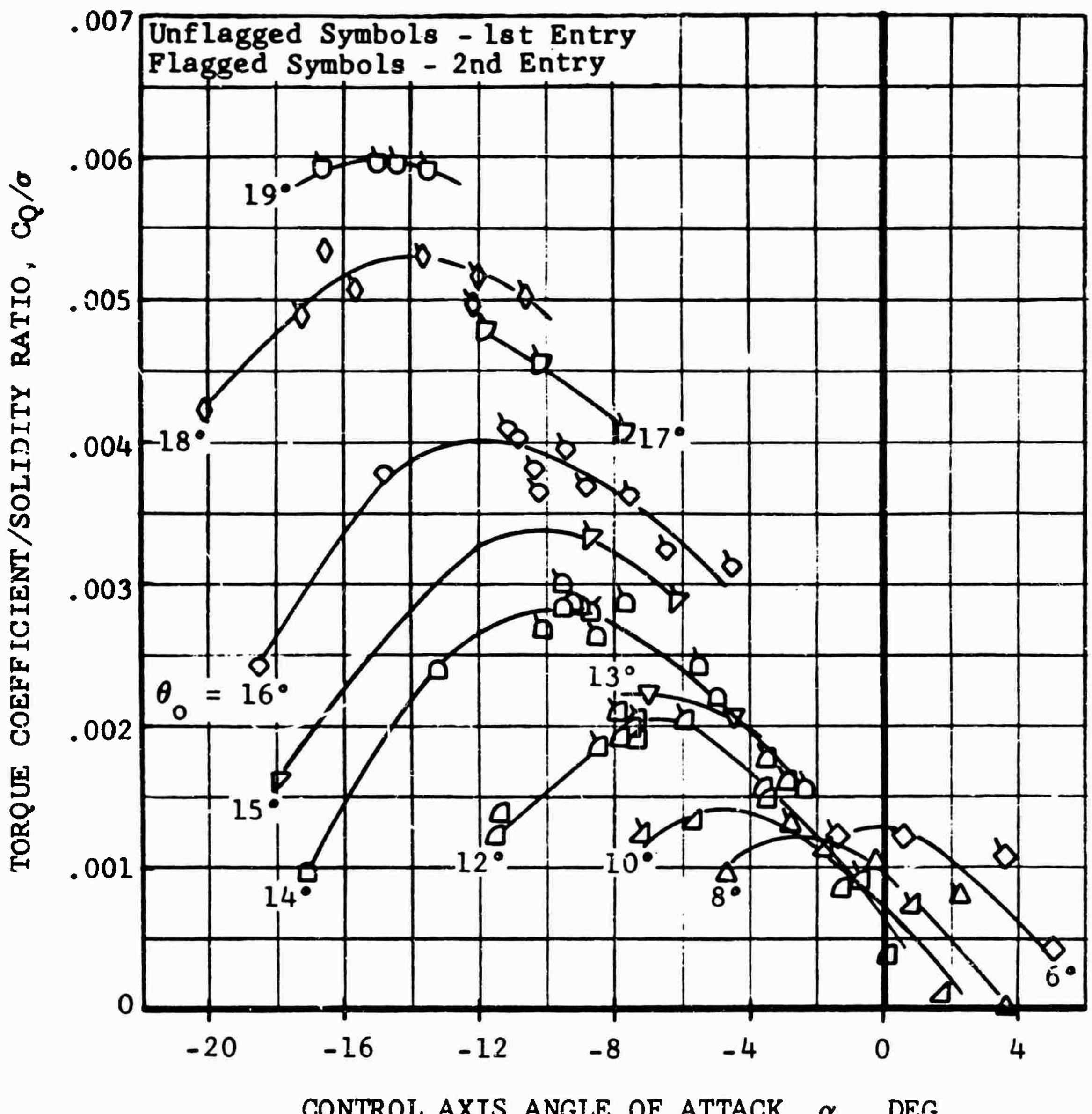

c) C_Q/σ vs α_c

Figure 30. Concluded.

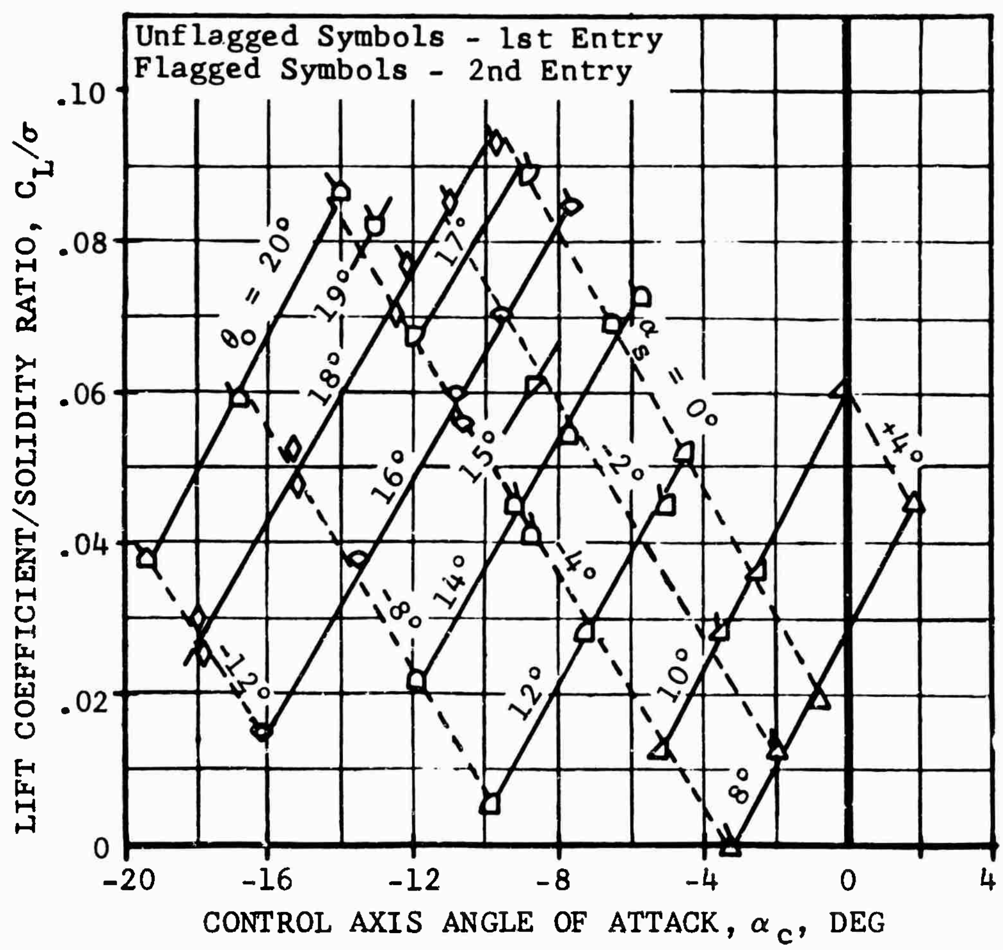

a) C_L/σ vs α_c

Figure 31. The Results of Various Collective Pitch, Shaft and Control Axis Angles on the Performance Characteristics of the Thin-Tipped Blades. $\mu = 0.40$; $M_{(1.0,\ 90.)} = 0.85$.

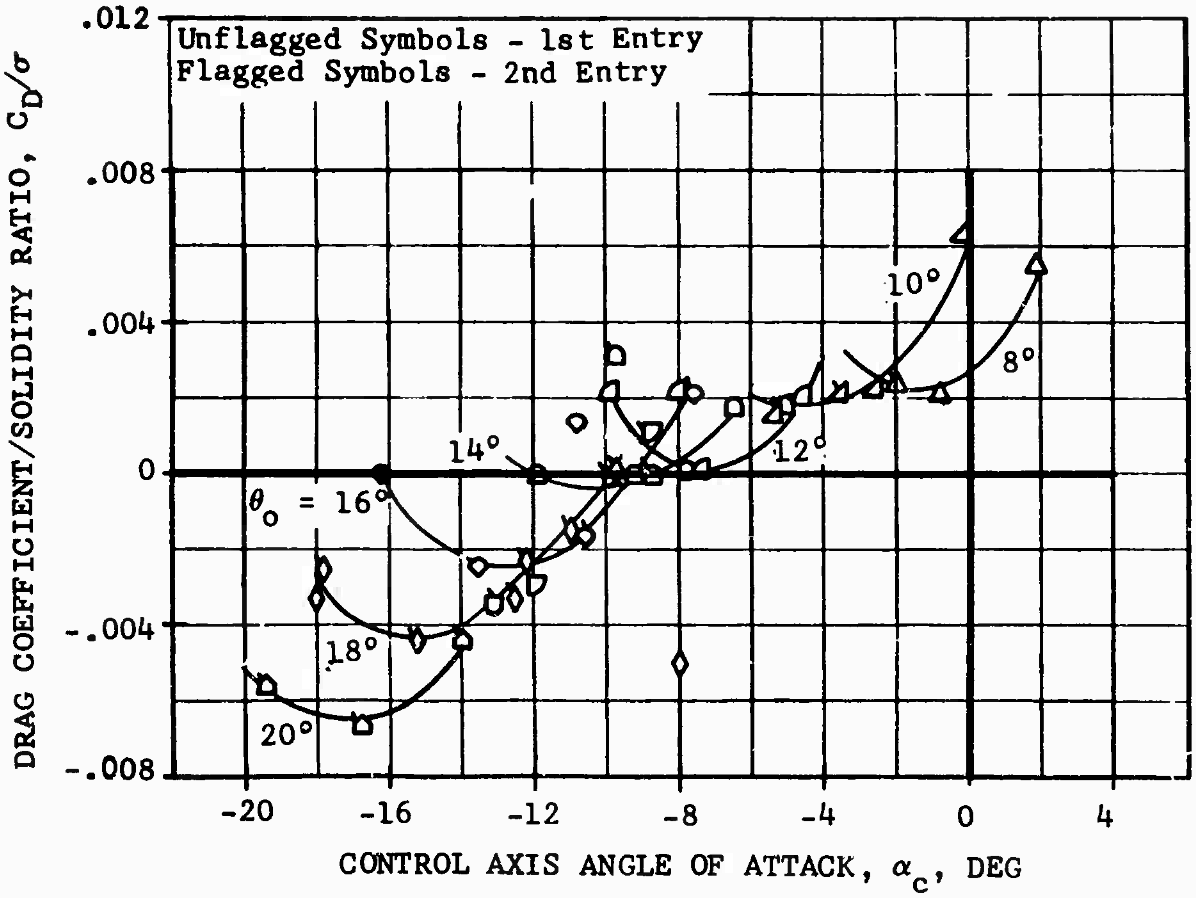

b) C_D/σ vs α_c

Figure 31. Continued.

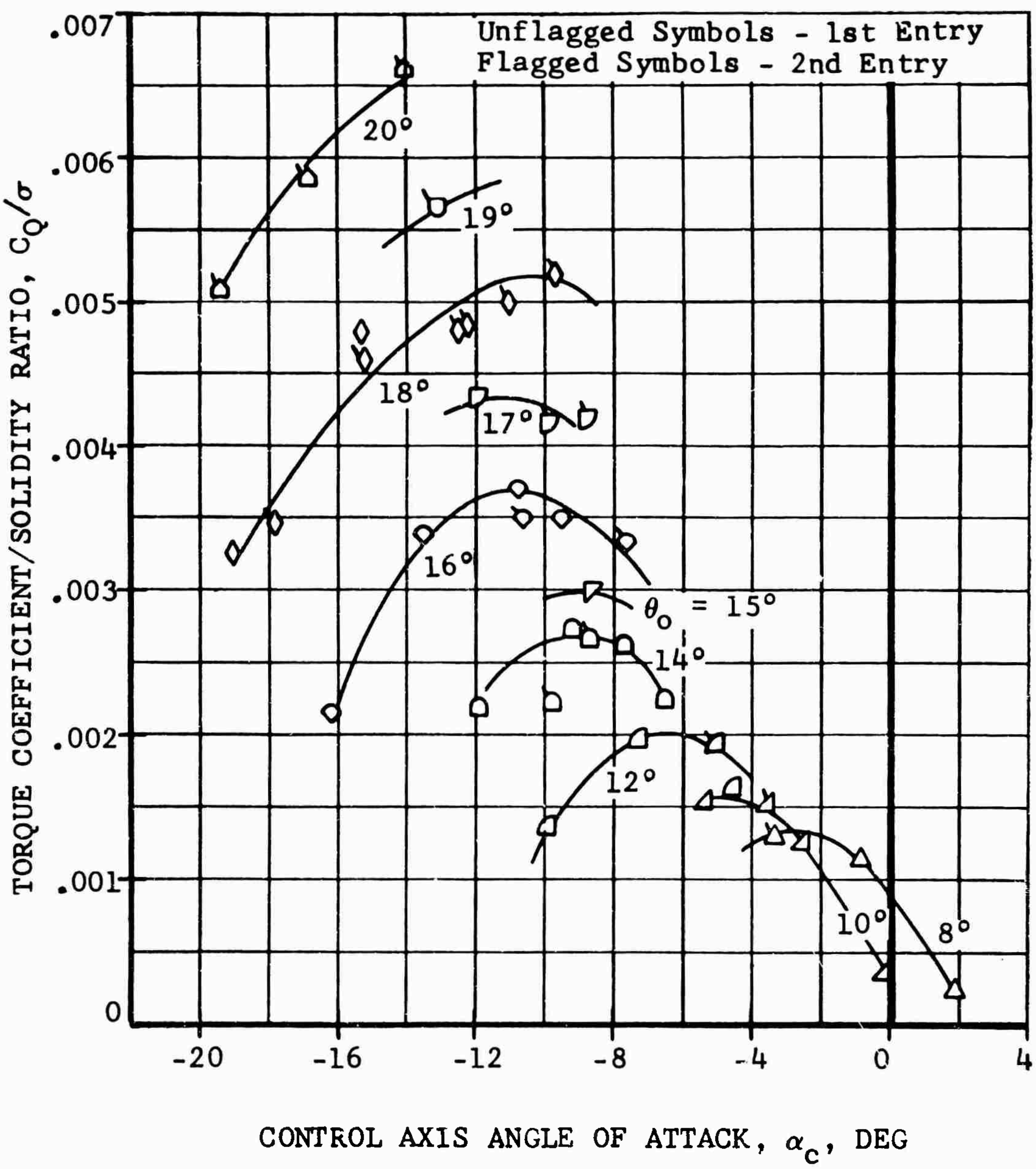

c) C_Q/σ vs α_c

Figure 31. Concluded.

APPENDIX II
DESCRIPTION OF TEST EQUIPMENT

The test equipment consists of a rotor test module, power distribution panel, control module, rotors, and associated instrumentation. This equipment is described in the following paragraphs.

ROTOR TEST MODULE

The rotor test module includes a mounting frame, a rotor pylon, a drive system, and an aerodynamic fairing. The module is designed for mounting on the primary support system in the NASA-Ames 40- x 80-Foot Wind Tunnel. The mounting geometry is shown by Figure 32. The module is supported in the tunnel by two fixed struts and a gimbal-mounted tail strut. The struts attach to the test module through ball and socket joints. The tail strut is extended (or retracted) by an electrically driven jack screw to provide the desired angle-of-attack range. A three-wheeled dolly is provided for transport and storage of the test module when it is not installed in the tunnel test section. Figure 33 shows the test module installed on the transport dolly.

The test module frame mounts the pylon, the speed increaser gearbox, and the drive motor as shown by Figures 34 and 35. The pylon installation consists of a UH-1B transmission and mast assembly and modified rotor controls. The mounting arrangement and the suspension configuration are the same as those of the helicopter installation.

The control system arrangement is shown by Figure 36. Except for the control input linkages, the basic control geometry is the same as that of the helicopter installation. The dimensional data given (Figure 37) are for the UH-1C control system configuration. The module was originally configured with UH-1B control system components. These components were replaced by UH-1C components for increased strength following the initial test program.

Cyclic control is provided by two electric linear actuators connected through independent linkages to the servo control valves of the right- and left-hand cyclic control boost tubes. The amplitude and the phasing of the cyclic input to the rotor are controlled by the relative extension and/or retraction of these two actuators. The actuators are remotely controlled by the switching circuits at the control console.

The rotor collective control is provided by a single electric actuator remotely controlled from the control console connected through a linkage to the servo control valve of the collective control boost tube. The collective or steady

value of rotor blade pitch is controlled by the extension or retraction of the actuator.

Hydraulic control power is supplied from two independent systems on the test module. One system is supplied by a transmission-mounted pump and operates only when the rotor is turning. The second system is supplied by an electric motor-driven pump. The electrically driven system is connected through the power distribution panel and is controlled by the main power switch in the control console. This system provides hydraulic power for control system checkout and calibration in addition to rotor operation.

The rotor drive system consists of a UH-1B transmission, a speed increaser gearbox, and an electric drive motor. The drive motor was provided by NASA-Ames. The drive motor used was originally maximum rated for 1500 hp at 3000 rpm; however, due to the motor bearing life restrictions, the motor has since been derated by NASA to 2800 rpm maximum. The motor speed is controlled by NASA personnel during the tests and is continuously variable from approximately 100 to maximum rpm. The motor output speed is increased to match the transmission speed rating by a 2.606:1 ratio speed increaser gearbox. This gearbox is a commercial unit with a rating of 1295 hp continuous, and 1500 hp intermittent, at 2500 rpm input. The gearbox is mounted to the test module frame between the drive motor and the transmission. Cooling and lubrication are provided by an oil-to-water heat exchanger and an electrically driven oil pump and reservoir mounted below the gearbox. The drive motor and gearbox input shafts are connected by a commercial flexible coupling. The output shaft of the gearbox and the transmission input shaft are connected by a standard UH-1B input drive-shaft coupling. The final speed change is a 1:0.0491 reduction to rotor shaft speed which is provided by the helicopter transmission gearing. The overall speed change from drive motor to rotor shaft is a 1:0.12796 reduction.

The mounting frame, pylon, and drive system are enclosed by an aerodynamic fairing. The fairing, as shown in Figure 38, is a "tear drop" shaped body of revolution with two local protuberances at the lift strut attachment points. The maximum diameter of the fairing body is 6.66 feet, and the overall length is 22 feet. The forward sections (approximately 16 feet) are of molded sandwich construction with fiber-glass inner and outer skins, paper honeycomb cores, and aluminum alloy bulkheads and stiffeners. The tail section of the fairing is a monocoque design with aluminum alloy skins. The fairing is provided with flush panels for access to the struts and also to the controls and fluid connectors located on the underside of the mounting frame. The upper nose

section of the fairing opens upward and pivots forward for access to the transmission, controls, and instrumentation. The upper section of the fairing aft of the mast opens upward and slides aft to provide access to the drive system. The upper access doors are fitted with flush "quick release" latches; all other panels are fitted with flush screw-type fasteners.

POWER DISTRIBUTION PANEL

The test module requires 24 volts DC and 110/220 volts AC power for operation and servicing. The AC power is supplied through a 35-foot-long umbilical cable which connects to the power distribution panel as shown by Figure 39. For wind tunnel testing, the umbilical cable is routed through the left-hand main strut fairing to the distribution panel, which is located below the test section floor. The distribution panel has three coded receptacles which are mated to corresponding plugs on the umbilical. The three connections are for the service outlet, hydraulic pump motor, and oil pump motor on the test module. Power for the three circuits is obtained through the transformer, master switch, and external power cable installed on the panel. The power cable is provided with a connector for attachment to a 440-volt, 60-cycle, 3-phase, AC external power receptacle. The common outlet is "live" whenever the panel master switch is closed and provides power for the tools, lights, etc., for servicing and maintenance of the test module. Power for the pump motor circuits is controlled by two "normally open" 24-volt DC relays mounted on the distribution panel. The hydraulic pump motor relay is series-connected with the master DC power switch on the control module. This arrangement provides hydraulic pressure for control boost whenever DC power is available for control system actuation. The oil pump motor relay is series-connected with a "normally open" pressure-actuated switch in the transmission-driven hydraulic system and the master DC power switch on the control module. Power is supplied to the oil pump motor circuit for lubrication of the speed increaser gearbox whenever the rotor is operating and DC power is available for control system actuation.

CONTROL MODULE

The rotor speed (NASA drive motor) and the module pitch (tail strut actuator) controls are provided by the test facility. All other rotor control and monitoring functions are provided on the desk-type control module shown by Figure 40. The control and monitor functions are arranged in two major panel groups: an operation station and a test engineer station.

The operator's station is on the right-hand section of the control module and includes all the controls and indicators required for operation of the test module. The upper section of the operator's panel mounts, from left to right, a rotor tachometer, the hydraulic and oil systems' warning indicator lights, and the DC power switch. The DC power switch, through its associated relays, controls all the power (except the NASA motor and instrumentation circuits) required for operation of the test module. The system warning indicator lights are series-connected with individual pressure and temperature switches in the two hydraulic systems, the transmission oil system, and the speed increaser gearbox oil system. The warning lights incorporate a "press to test" circuit and are normally "off" unless there is a loss in pressure or excessive temperature rise in their respective system. The rotor tachometer is used to monitor rotor rpm and to provide an indication of rapid power changes such as power failure, inadvertent autorotation entry, or a high rate of control input.

Three control position indicators are mounted in a horizontal row along the center of the panel. The indicators display, from left to right, positions of collective pitch, longitudinal cyclic control, and lateral cyclic control. The collective pitch is controlled by two push-button switches mounted below the collective position indicator. The operator sets collective pitch by depressing and holding either the "UP" or the "DOWN" switch until the desired setting is obtained on the collective pitch indicators. The first harmonic longitudinal and lateral positions of the rotor disc (flapping plane) relative to the shaft are displayed on indicators located immediately below the respective control position indicators. The longitudinal and lateral cyclic pitch is controlled by two spring-centered lever type switches which are located just below the operator's panel and in line with the respective position indicators. The operator moves the switches off-center to the left or right to obtain the desired setting on either the control position indicators or the flapping position indicators as determined by the particular test procedure (see the section on Rotor Test Results).

The test engineer's station is on the left-hand section of the control module and is principally a monitoring station. The test engineer's panel mounts four load meters, a vibration meter, an airspeed indicator, and a three-way selector switch for use with a digital voltmeter. The load meters and vibration meter provide a continuous "on-line" display of oscillatory load and vibration levels for selected critical components. The main rotor yoke flapwise bending moment, pitch link load, drag brace load, and pylon vibration were monitored during initial tunnel entry. The yoke chordwise bending moment was monitored during the initial tests but was replaced

by mast steady torsional moment prior to the second entry test since operation near the system torque limit was expected. A three-way switch installed in the lower right-hand corner of the test engineer's panel is used to select the collective, longitudinal cyclic, or lateral cyclic position signal for display on a digital voltmeter for accurate readout of the control positions. The voltmeter (provided by NASA) mounts immediately above the control module between the operator and test engineer stations.

The switch is normally positioned to display collective positions. The final collective setting for each data point is set based on the digital readout. The digital readout for all control positions is then read and recorded in the test engineer's log.

ROTORS

Three two-bladed, semirigid type rotors utilizing a common UH-1D underslung hub were tested. Basic data for these rotors are tabulated below:

34-Foot-Diameter Rotor

Airfoil Designation	NACA 0012
Chord	1.75 ft
Diameter	34 ft
Twist (Total Aerodynamic)	-7.7 deg
Disc Area	908 sq ft
Solidity	.0656
Effective Root Cutout	11.8 percent span
Lock No.	4.97

UH-1D Rotor (Standard Blade)

Airfoil Designation	NACA 0012
Chord	1.75 ft
Diameter	48 ft
Twist (Total Aerodynamic)	-10.9 deg
Disc Area	1810 sq ft
Solidity	.0464
Effective Root Cutout	8.3 percent span
Lock No.	7.47

Thin-Tipped Rotor

Airfoil Designation	
Root to .8R	NACA 0012
.8R to tip	Uniform Thickness Change
Tip	(See Table III)
Chord	1.75 ft
Diameter	48 ft
Twist (Total Aerodynamic)	-10.9 deg
Disc Area	1810 sq ft
Solidity	.0464
Effective Root Cutout	8.3 percent span
Lock No.	6.91

TABLE III. AIRFOIL CONTOURS,* STATION 288.0, BELL PART NO. 204-018-050 BLADE (in percent of airfoil chord)

Station	Upper Surface Ordinate	Lower Surface Ordinate
0	- 1.190	- 1.190
.5	- .390	- 1.633
1.0	- .095	- 1.776
2.0	.524	- 1.895
3.0	.919	- 1.986
4.0	1.238	- 2.071
5.0	1.514	- 2.148
10.0	2.310	- 2.476
12.5	2.533	- 2.595
15.0	2.676	- 2.676
20.0	2.871	- 2.871
25.0	2.966	- 2.966
30.0	3.000	- 3.000
35.0	2.976	- 2.976
40.0	2.900	- 2.900
50.0	2.647	- 2.647
60.0	2.281	- 2.281
70.0	1.833	- 1.833
80.0	1.309	- 1.309
90.0	.724	- .724
95.0	.405	- .405
100.0	.095	- .095

*NOTE: NACA Airfoil Conventions Observed

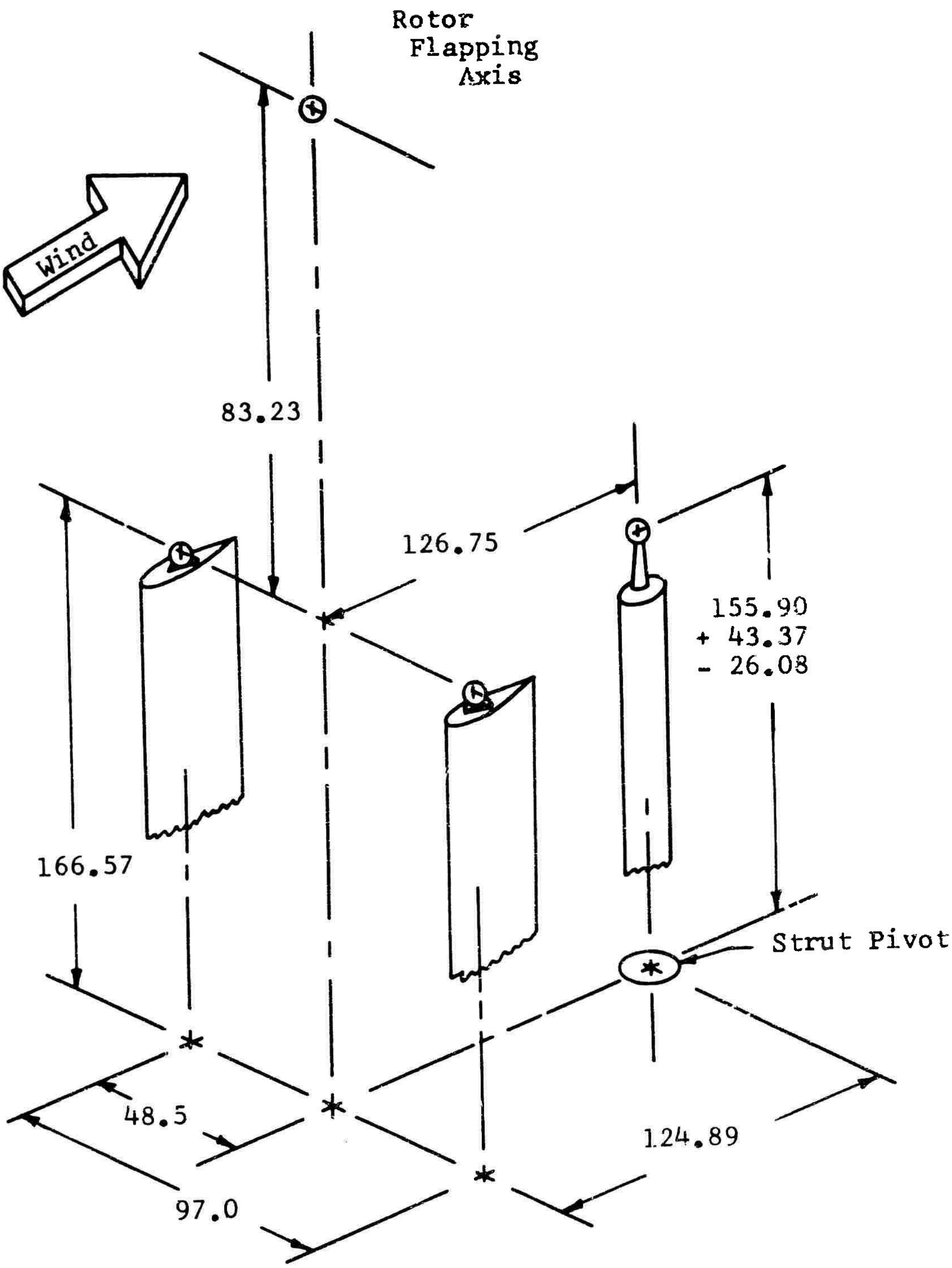

All Dimensions Are in Inches.

Figure 32. Wind Tunnel Strut Arrangement.

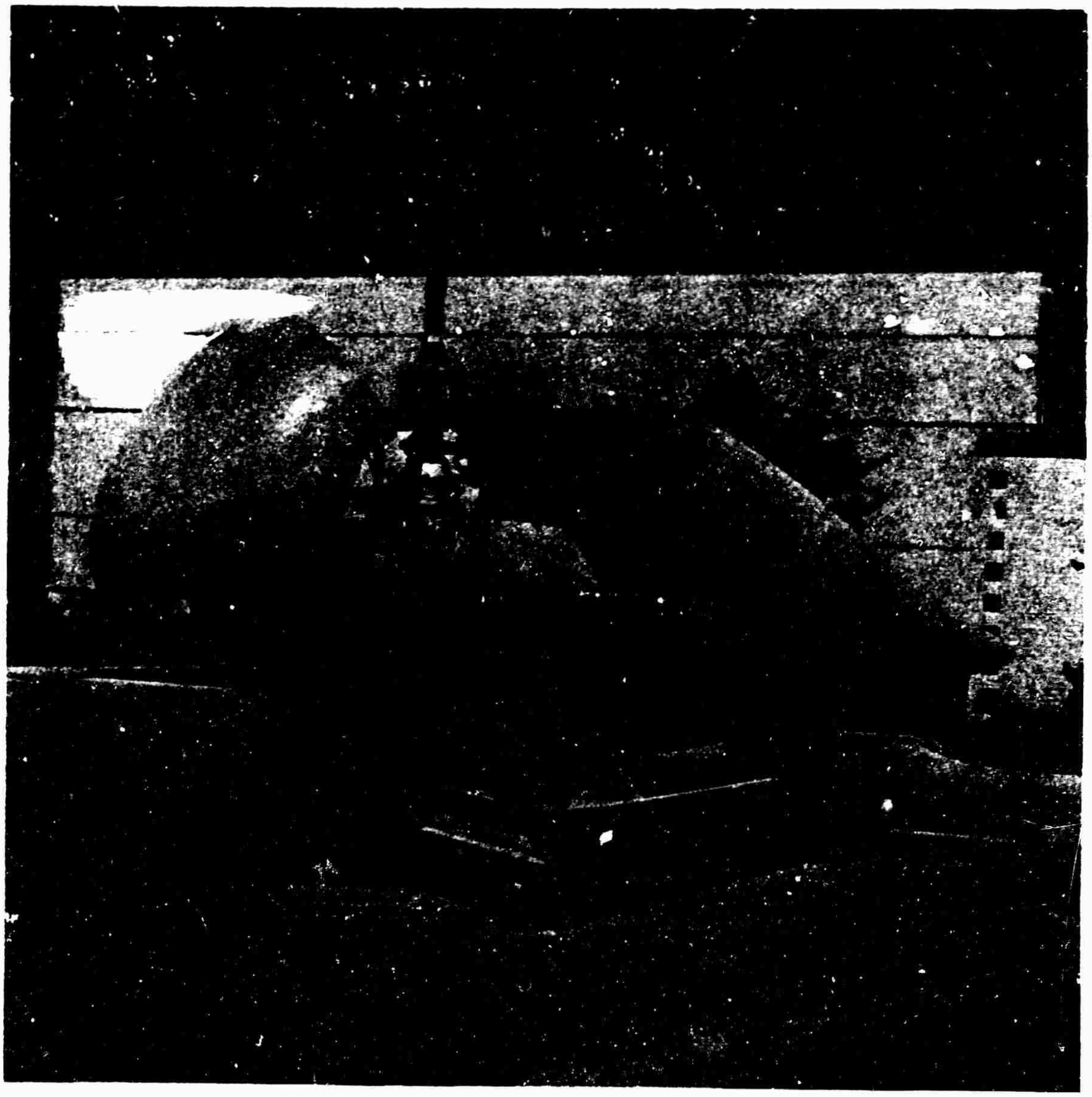

Figure 33. Test Module on Transport Dolly.

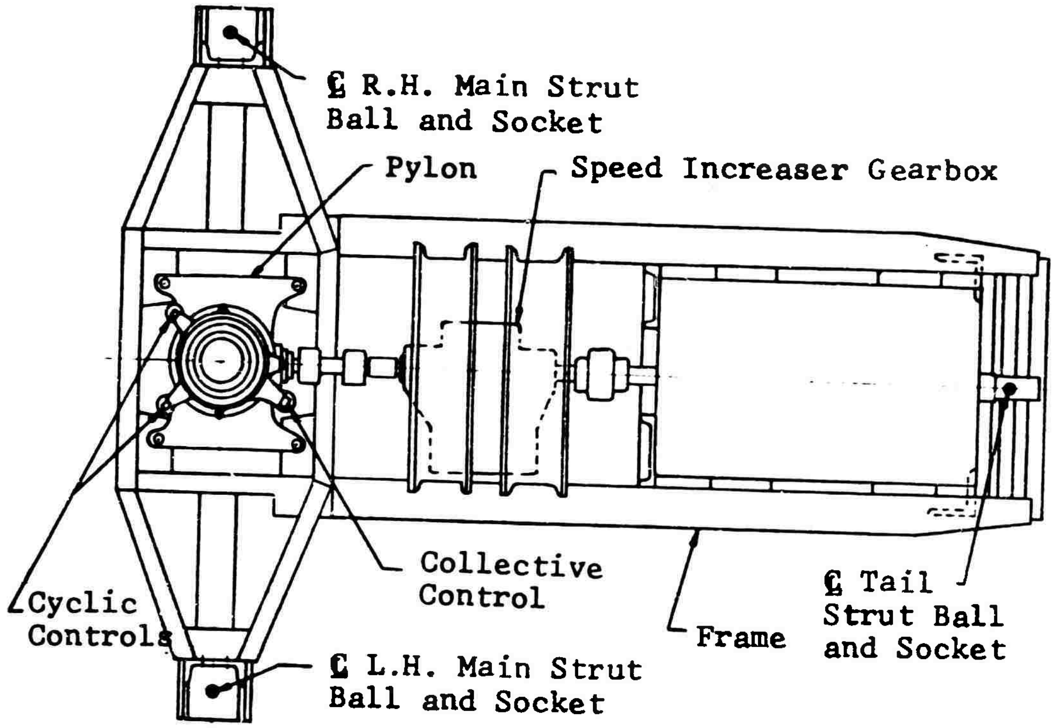

Figure 34. Plan View of Test Module.

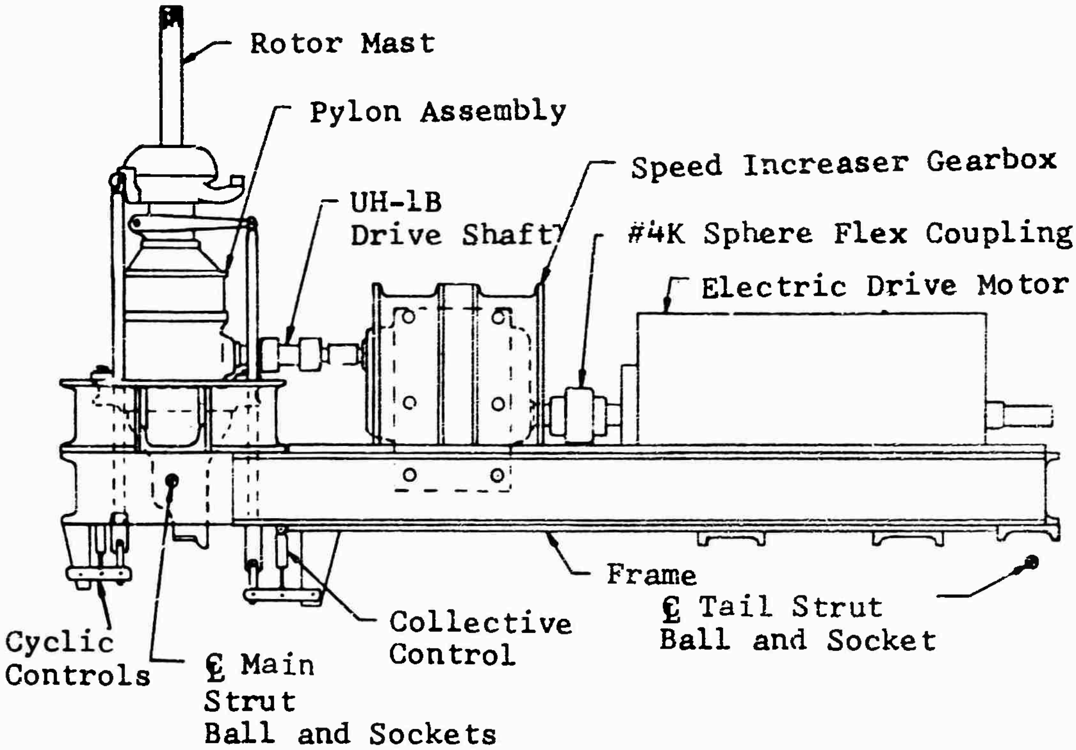

Figure 35. Side View of Test Module.

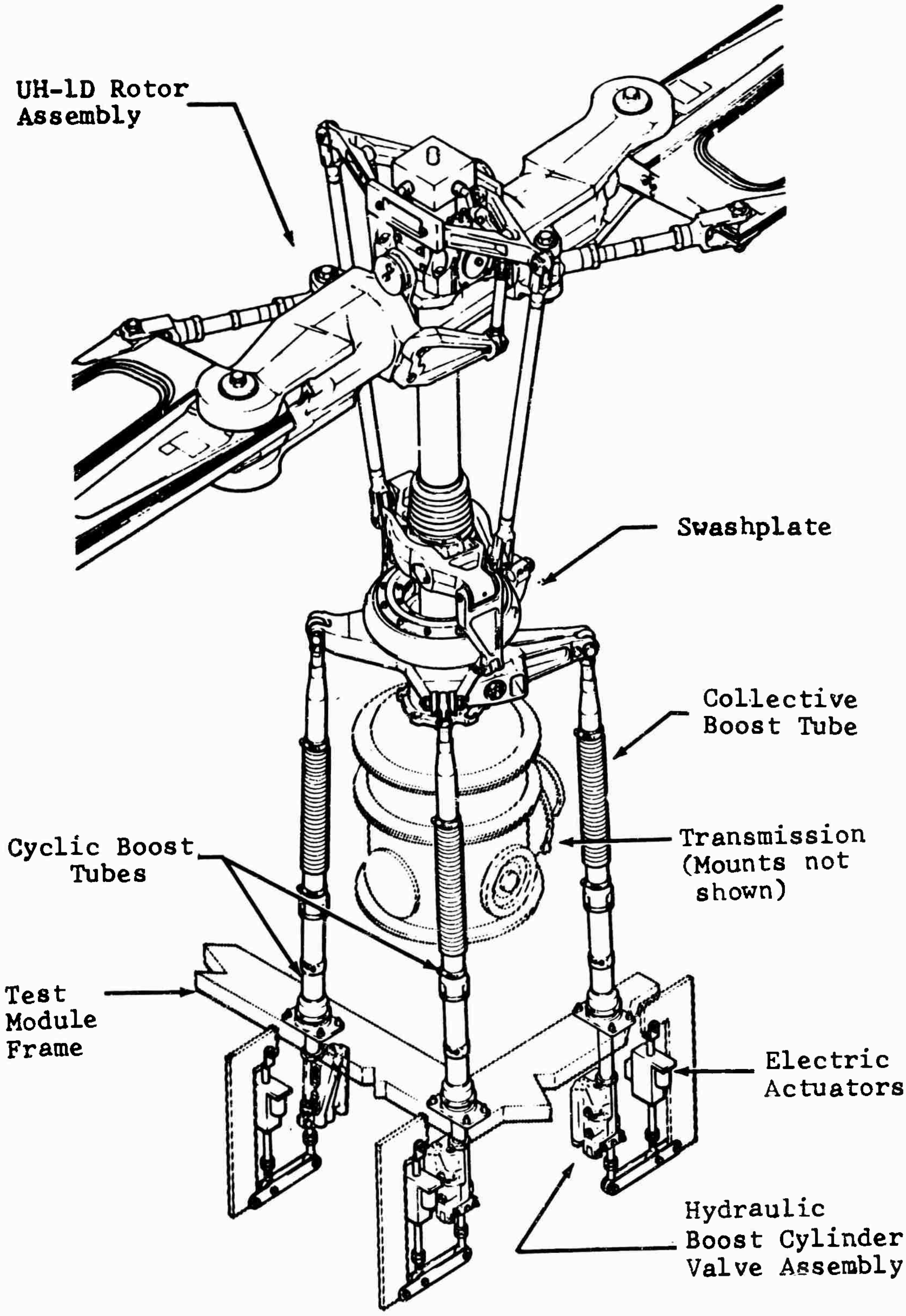

Figure 36. Control System Arrangement.

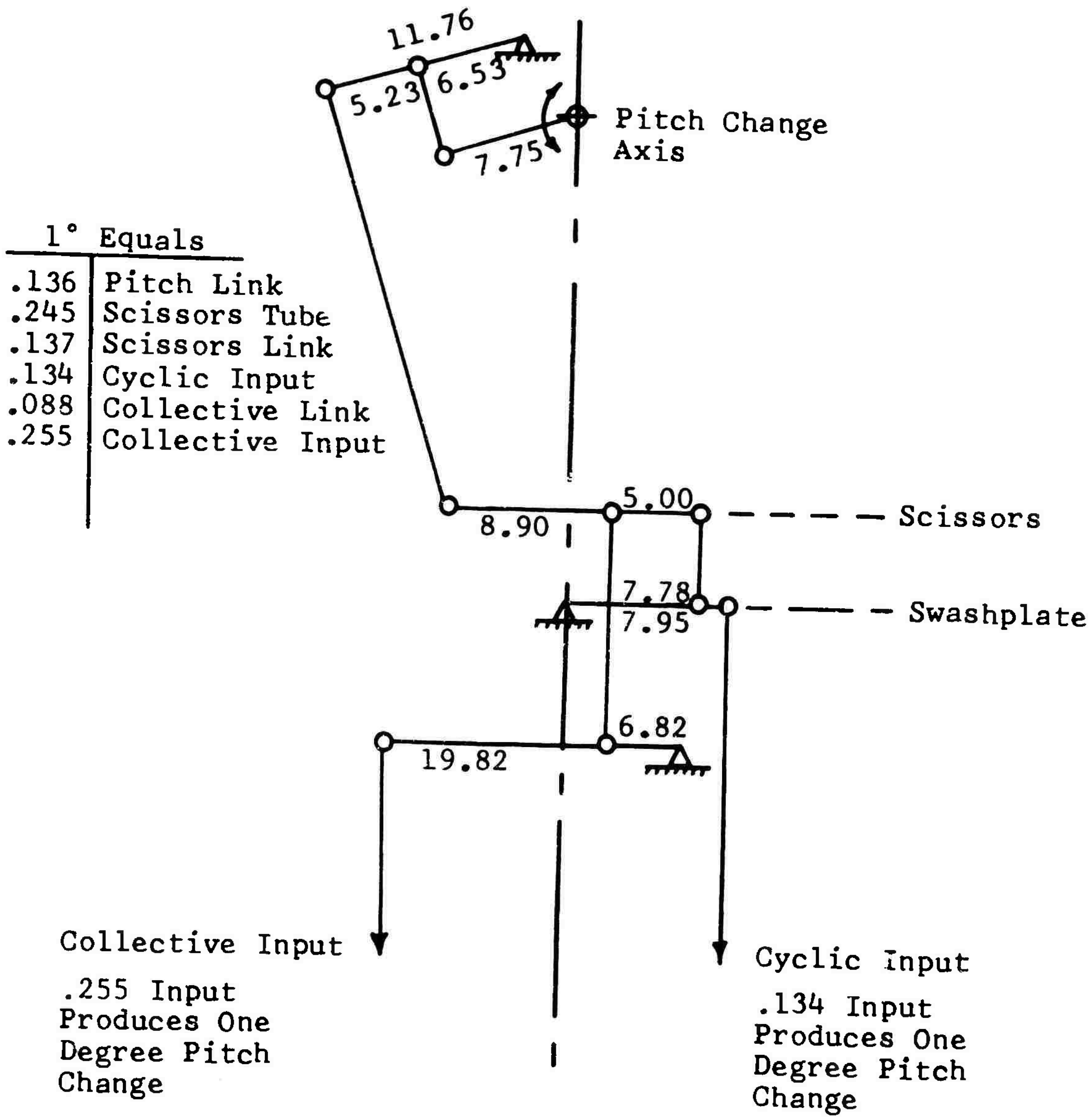

All Dimensions Are in Inches.

Figure 37. Rotor Control Motions.

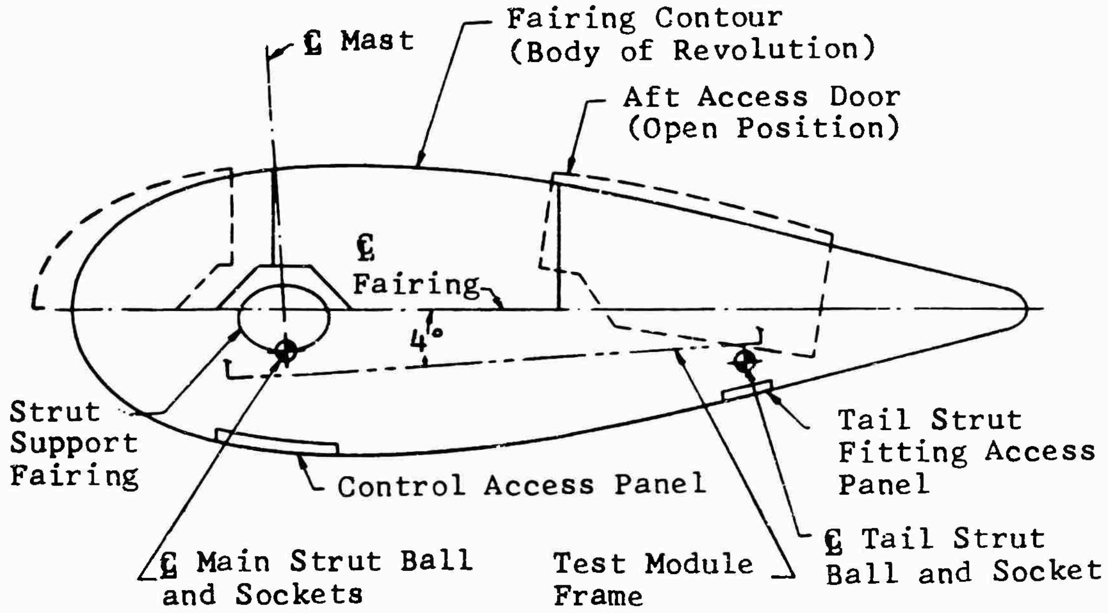

Figure 38. Profile View of Fairing.

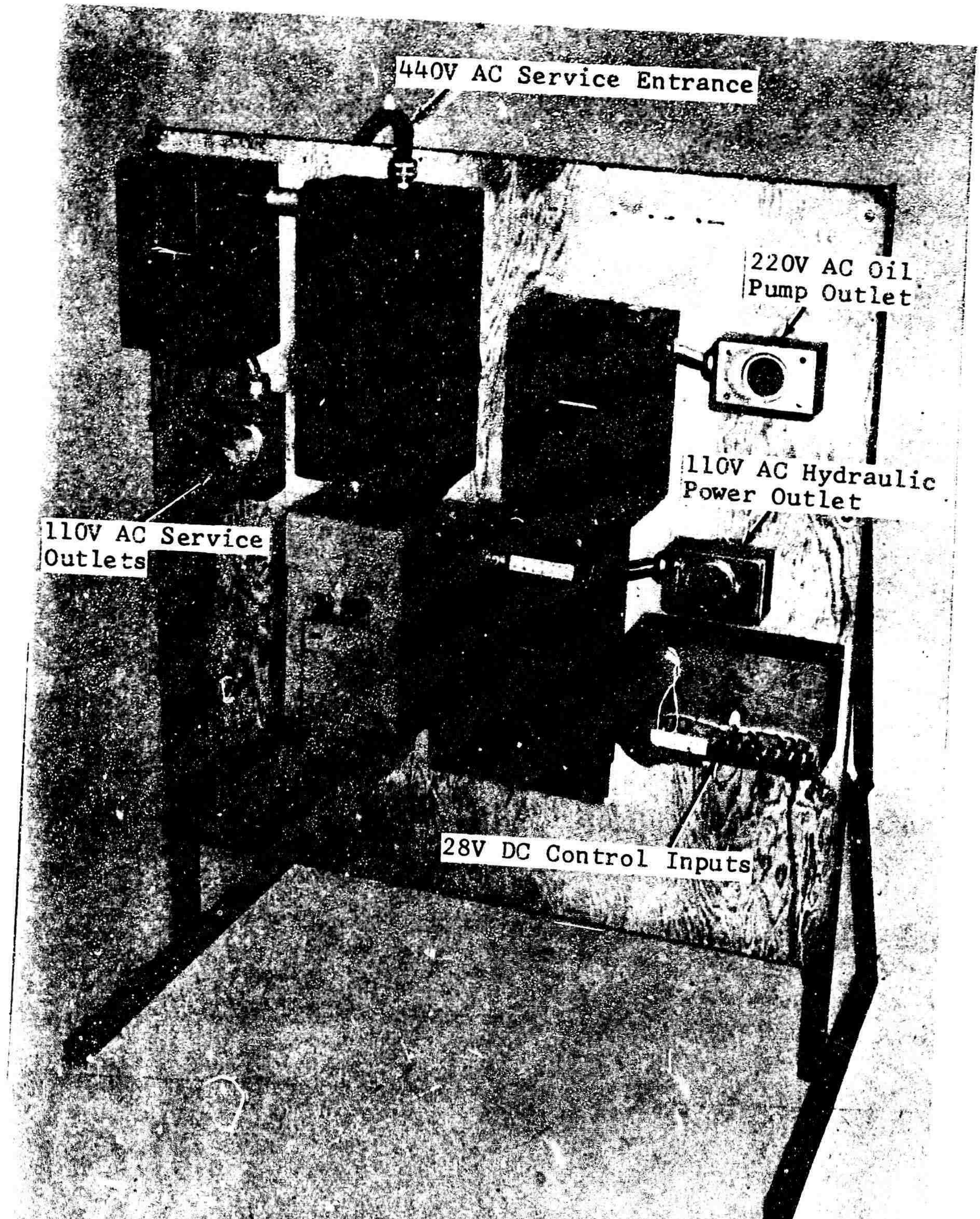

Figure 39. Power Distribution Panel.

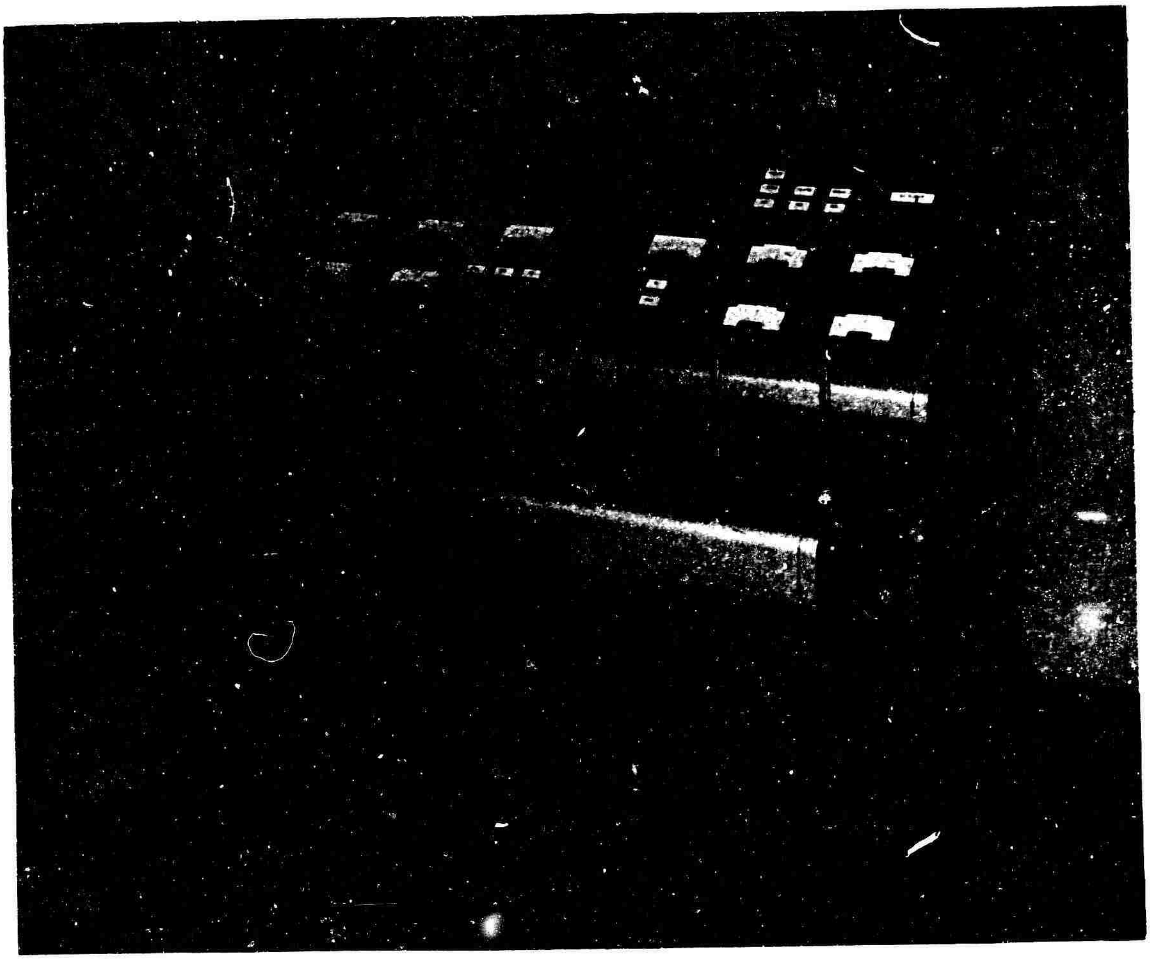

Figure 40. Control Module.

APPENDIX III
SHAKE TESTS

Two separate shake tests were conducted to determine the natural frequencies and mode shapes of the combined test module and support system. The purposes of the tests were to: (a) obtain data for predicting the dynamic behavior of the system during wind tunnel operation, (b) establish dynamic criteria for future test hardware designs, and (c) evaluate the effects of the tunnel balance system on the dynamics of the system. The initial test was conducted with the test module installed on a simulated support system located on the ground floor of the test facility as shown by Figure 41. The second test was conducted in the tunnel test section with the test module and support system mounted on the tunnel balance system.

SUPPORT SYSTEM CONFIGURATION

The test module was installed on the "light" main struts for both tests. The struts were attached to a welded steel mounting platform for the ground floor test and to the balance system for the wind tunnel test. The dimensional location of the attachments in the mounting base and the balance frame were the same. The principal differences between the two test configurations were in the mounting bases and the tail struts. The size and mass of the balance frame are extremely large compared to the mounting platform used for the floor test; however, the effects of these differences were at least partially compensated for by bolting the platform to the floor. The floor test was conducted with a fixed-length tail strut, and the tunnel test was conducted with the collapsible tail strut normally used with the primary support system. The fixed strut was mounted to the platform through a ball and socket to simulate the gimbal mounting of the collapsible test strut. The tail strut mounting dimensions were the same for both tests. The two tail strut installations were dynamically dissimilar, since the fixed tail strut did not extend below the base mounting plane as was the case for the collapsible strut. Upon completion of the initial tunnel shake tests, the support system was modified by removing a 30-inch section from the upper end of the lift struts.

TEST PROCEDURE

The same test procedures were used for both tests. Weights were installed in the main rotor blade grips to simulate the blade mass. The excitation forces were provided by externally driven, counterrotating, eccentric mass shakers. Three shakers were used for the tests. One shaker was installed in a blade grip to simulate rotor inplane excitations. A second shaker

was suspended, through a bungee chord, from the wind tunnel 15-ton hoist and connected to the rotor mast to simulate vertical excitations. A third shaker was mounted on the aft frame member of the test module to simulate rotor torque excitations. The shakers were driven separately through a flexible shaft coupled to a variable-speed motor mounted on the test module frame.

The motor speed was manually controlled to provide a 2-cps to 30-cps sweep in the excitation frequency. Accelerometers were installed on the rotor hub, pylon, and test module frame, and these data were recorded on magnetic tape for later playback through a Spectral Dynamic Analyzer. During the tests, the response of the test module was visually observed and the output of three selected accelerometers was recorded on direct-writing oscillographs for immediate readout and classification of mode shapes and frequencies. The tunnel scales were used as an additional source for visual observations of system response. Response data were not recorded for the final strut configuration. The natural frequencies of this configuration were obtained by visual observation only.

SHAKE TEST RESULTS

The natural frequencies determined by the tests are summarized in Table IV. The basic test results and comparison with rotor excitation frequencies are discussed in the following paragraphs.

Ground Floor Shake Test

The rotor inplane (lateral and longitudinal) excitations at the hub produced resonant frequencies of the pylon modes and bending modes of the vertical member of the lift struts. The pylon modes were near 3 cps, as expected, since the installation was similar to the normal helicopter installation. The first lateral mode of the main strut was located at 2.3 cps and was strongly coupled with the pylon mode. The second and third lateral modes were located at 6.3 and 7.8 cps respectively. These modes were not significant because of the pylon isolation. The first longitudinal mode was located from 4.6 to 5.5 cps, depending on the mounting platform stiffness. This mode was originally located at 4.6 cps and was raised to 5.5 cps by driving steel wedges between the floor and the platform and adding lead ballast to the platform. The bending frequencies of the forward and outboard diagonal members of the main struts were determined from decay records. These modes were located at approximately 17 cps for the forward diagonal and at 29 cps for the outboard diagonal.

TABLE IV. NATURAL FREQUENCIES DETERMINED IN WIND TUNNEL SHAKE TESTS

Mode Direction and Identification No.	Description of Mode	Natural Frequency - cps		
		Ground Floor Test	Initial Tunnel Test	Modified Strut Test
Longitudinal				
1	Balance Frame - Drag Scale		1.6 - 1.7	1.6 - 1.7
2	Pylon	2.9 - 3.1	2.9 - 3.1	2.9 - 3.1
3	1st Strut Bending	4.6 - 5.5(a)	5.3	6.5
Lateral				
4	Balance Frame - Rear Scale		1.8	1.8
5	Balance Frame - Fwd Scale		2.5(b)	(c)
6	1st Strut Bending	2.3	2.6(b)	(c)
7	Pylon	2.7 - 2.8	2.8(b)	(c)
8	2nd Strut Bending	6.3	6.0	7.5
9	3rd Strut Bending	12.8	10.5 - 11.5	(d)
Vertical				
10	Suspension System	14.5	(e)	(g)
11	Frame Mode	16.7	(e)	(g)

( ) Notes on page 91

TABLE IV - Continued

Mode Direction and Identification No.	Description of Mode		Natural Frequency - cps: Ground Floor Test	Natural Frequency - cps: Initial Tunnel Test	Natural Frequency - cps: Modified Strut Test
Lateral at Rear of Test Stand					
12	Tail Strut Bending			3.2	(g)
13	Main Strut Bending - 1st Bending Mode		6.25	6.3	(f)
Bending of Support Tubes					
14	Fwd Tubes Rt Side		16.0 - 18.0	(g)	(g)
	Lt Side		16.5	(g)	(g)
15	Diagonal Tubes Rt Side		23.0 - 24.5	(g)	(g)
	Lt Side		23.0 - 26.0		
Scale Modes in Balance Room		Scale			
16	Pendular Mode of Scale Balance Weight	Drag		.485	(g)
		Front		.485	(g)
		Rear		.493	(g)
17	Torsional Spring Mode	Drag		4.41	(g)
		Front		4.75	(g)
		Rear		4.55	(g)

( ) Notes on page 91

TABLE IV - Concluded

NOTES:

(a) In the ground floor test, the strut bending frequency was found to vary with the framework stiffness. Initially, the frequency was 4.6 cps. By adding mass on top and driving wedges beneath the frame, this frequency was raised to 5.5 cps.

(b) Modes 5, 6, and 7 are strongly coupled modes between 2.0 and 3.0 cps. Exact natural frequencies are not easily identified, since peaks occur in different elements at different frequencies.

(c) The three lateral modes with the struts cut off were still between 2.0 and 3.0 cps; however, no response data were taken and identification was not possible.

(d) This was a weak mode that was not visible in the test stand motion in the tunnel but was observed in the struts on the ground floor.

(e) The vertical test in the tunnel was stopped at 14.0 cps. No modes were apparent up to this frequency.

(f) The torsional frequency due to strut bending was undoubtedly increased by shortening the struts but was not re-evaluated.

(g) These frequencies were not measured, but they should be approximately the same as in earlier tests.

The vertical excitation at the hub produced resonant frequencies of the suspension system and the test module frame. The suspension system mode was located at 14.5 cps. This mode was determined by the stiffness of the lifting system external to the test system and was of no importance with respect to the test program. The test module frame mode was located at 16.7 cps and was not of sufficient strength to be considered of importance.

The excitation of the aft test module frame member produced a resonance of the main struts. This mode was located at 6.25 cps and was observed to be principally an out-of-phase longitudinal bending of the main strut vertical members. There were no other resonant frequencies observed as a result of the aft frame excitation.

Tunnel Shake Test

The same main strut modes observed during the ground test were also observed at the tunnel test but at slightly different resonant frequencies. The first lateral main strut mode was located at 2.7 cps and, as in the ground test, was strongly coupled with the pylon. The second and third lateral strut mode natural frequencies were slightly lower than in the ground test. The first longitudinal strut mode was located at 5.3 cps and resulted in a high response of the test module. These low-frequency balance frame modes were determined by visual observation of the balance frame scale responses during excitation sweeps. These frequencies are shown in Table IV. Because of the relatively small excitation force available below 3 cps, the frequencies could not be exactly defined; however, the modes were strongly coupled with the pylon.

The lateral excitations at the aft frame of the test module produced a 6.3-cps out-of-phase bending mode at the main struts and, additionally, the natural bending mode of the tail strut at 3.2 cps. The out-of-phase main strut bending was the same as in the ground floor test. The tail strut mode was not apparent during the ground test due to the lack of dynamic similarity between the two struts. This mode did not couple with the other support system modes, and the test module response to this mode was negligible.

The resonant frequency of the first longitudinal strut mode was known to be coincident within the rotor excitation range anticipated for the wind tunnel test prior to the tunnel shake test. It was also anticipated that this frequency would not be significantly changed in the tunnel and that modification of the struts would be required to eliminate the frequency coincidence. Preliminary calculation had indicated that

reducing the strut height approximately 30 inches would raise the resonance frequency sufficiently 't of the rotor excitation range. Although it was known th. c a strut modification would be necessary before rotor testing could proceed, it was also recognized that the basic differences between the ground and tunnel test could not be determined unless the support system effects were known.

Following the tunnel shake test of the basic configuration, the struts were removed and modified. To avoid unnecessary delays in the test program, the shake test instrumentation was removed and the rotor test instrumentation buildup was started while the struts were being modified. The modified struts were installed in the tunnel, and the rotor inplane excitation tests were repeated. The response data for this configuration were obtained by visual observations of the support system and balance frame scales. The lower frequency modes between 1.6 and 3.0 cps were the same as the original configuration. The first longitudinal and second lateral strut modes were observed to be significantly higher than those of the original configuration. The first longitudinal mode was located at 6.5 cps and was above the area of rotor excitation coincidence. The second lateral mode was raised from 6.0 to 7.5 cps.

The tunnel balance scales were hand excited to determine the natural frequencies of the scales. These tests were conducted with and without the dashpots connected. The observed natural frequencies are given in Table IV. With the dashpot disconnected, the first mode of vibration was lightly damped and could be excited by an internal excitation force. The dashpot installation prevented the first mode from being excited by balance frame motion. The second mode was also effectively damped out by the dashpot.

Discussion

In general, the ground floor test setup was a reasonable duplication of the tunnel system with respect to the struts and test module. The tunnel test verified that the principal conclusions reached from the floor test were realistic and identified the low-frequency balance frame modes that were not duplicated in the floor test. The significance of the various modes and responses is discussed in the following paragraphs.

Mode Characteristics - The tunnel balance frame modes located at 1.6 cps longitudinally, and at 1.8 and 2.4 cps laterally, are fundamental modes of the balance frame. These mode frequencies were probably not significantly affected by the installation of the support systems in the tunnel. The rotor pylon modes at 2.8 and 3.0 cps were strong modes with respect to the rotor hub on the test module, but they were generally weak with respect to the tunnel balance frame.

The first main strut lateral mode at 2.6 cps and the first main strut longitudinal mode at 5.3 cps were strong modes with respect to the test module and the balance frame. The resultant response at the rotor hub was high laterally due to pylon coupling and relatively low longitudinally due to pylon isolation. For the planned rotor tests, the longitudinal mode was of prime significance since it was within the expected rotor excitation range. The longitudinal mode was increased to 6.5 cps by shortening the struts. The second and third lateral strut bending modes at 6.0 and 11.0 cps were relatively weak modes in both the test module and the rotor hub. The principal response to this mode was in the vertical member of the main struts.

The natural frequency of the tail strut was observed to be at 3.2 cps. This mode had been observed in several rotor test programs conducted in the tunnel and was known to be located between 3.0 and 3.5 cps. The basic characteristic of this mode was a relatively high amplitude motion of the tail strut actuator motor at the lower end of the strut. The out-of-phase main strut mode at 6.3 cps had a mode shape similar to the first longitudinal mode at 5.3 cps. The natural frequency of this mode was undoubtedly increased when the main struts were shortened; however, the lateral frame excitation test was not repeated, and the actual magnitude of the change is unknown.

Response - Normalized response curves for the rotor hub, pylon, and test module frame are given in Figures 42 through 51 . The response curves are given for both the ground and tunnel tests with the original strut configuration. Measured data are not available for the short strut configuration since the modes were determined by visual observation only.

The hub response to longitudinal, lateral, and vertical excitations is shown by Figures 42 through 44. The highest response at the hub was at 3.1 cps longitudinally (Figure 42) and at 2.6 cps laterally (Figure 43). The response above these frequencies attenuated rapidly, indicating that the higher frequency modes of the support system had no significant effect on the hub response. The vertical response at the hub is shown by Figure 44. No significant vertical responses at the hub were observed during the test; however, the response curves indicate a weak resonant frequency between 8 and 10 cps. This response is believed to be the first vertical mode of the tunnel balance frame. The mass and damping of the balance frame was more than adequate to prevent any significant responses to vertical inputs.

The pylon response is shown by Figures 45 and 46. The response to longitudinal excitations of the rotor hub is shown by Figure 45 . The major responses are the pylon mode at

approximately 3.0 cps and the first longitudinal strut mode at approximately 5.3 cps. The lateral response data are shown by Figure 47. The principal pylon responses are the lateral pylon mode at approximately 2.8 cps and the lateral main strut mode at approximately 2.6 and 6.0 cps.

The test module frame response data are given by Figures 47 through 49. The longitudinal response is shown by Figure 47. The principal responses are the pylon mode at approximately 3.0 cps and the first longitudinal main strut mode at approximately 5.3 cps. The high response at approximately 3.0 cps is also characteristic of the pylon and rotor hub. The response at the first longitudinal main strut mode is characteristic of the pylon but not the rotor hub. This particular frequency was within the planned range of rotor operation for the test program and was the basic reason for reducing the height of the main struts.

The lateral response of the test module frame is shown by Figure 48. The basic responses are at the pylon and the lateral main strut mode frequencies. The response to first lateral strut and the pylon mode frequencies is also a characteristic of the pylon and rotor hub. The response to the second and third lateral strut modes is a characteristic of the test module frame and pylon only. The rotor hub response to these modes is insignificant due to the effectiveness of the pylon isolation.

The lateral response at the aft crossmember of the test module frame is shown by Figure 49. The principal response is located at 6.3 cps, which is the first torsional mode of the strut system. This mode is characterized by an out-of-phase bending of the vertical members of the main struts. Both a rotor excitation coincidence and higher-than-normal values of oscillatory rotor torque would be required to produce a significant excitation of this mode.

Balance Frame Damping - The effect of balance frame damping is shown by Figures 50 and 51. The response of the test module frame to the balance frame modes was significantly reduced by the addition of the dampers. The response of the pylon and main struts was higher with the dampers installed. These changes in response characteristics are attributed to the isolation effect of the balance frame modes on the higher frequencies. Without the dampers, the isolation was apparent above 3.0 cps. The pylon and strut modes were not isolated and exhibited a higher response with the dampers installed. This effect was observed on the test module frame during both the longitudinal and the lateral hub excitations.

Excitation Coincidence - The excitation coincidences for the original and shortened main strut configurations are shown by Figures 52 through 55. The operating ranges for the two different diameter rotors tested are also given in the figures. With the original strut configuration, the first longitudinal strut mode was coincident with one-per-rev rotor excitation of the 48-foot-diameter rotor at 320 rpm, as shown by Figure 52. The second lateral strut mode was coincident with one-per-rev excitations of the 48-foot rotor at 360 rpm and also two-per-rev excitations of the 34-foot rotor at 180 rpm, as shown by Figure 53. The 48-foot rotor coincidences were considered to be unacceptable, and the main struts were shortened to raise the strut modes. The strut modification shifted the frequency to remove these coincidences from the operating range, as shown by Figures 54 and 55.

The pylon modes were coincident with the one-per-rev rotor excitations of the 34-foot rotor at 180 rpm for both the original and the short strut configurations. The coincidence with the longitudinal pylon mode (Figure 52) was eliminated by removing the aft pylon mount, which lowered the pylon longitudal frequency to approximately 2.6 cps. The lateral pylon coincidence and the two-per-rev coincidence at 200 and 225 (Figures 53 and 55 respectively) could not be changed without additional modification to the main struts or the support system stiffness. The required changes would have caused further delays in the test program and also would unnecessarily complicate the support system. It was determined that the test program requirements could be satisfied by selecting specific rotor speeds to avoid the excitation coincidences, and the program proceeded on this basis.

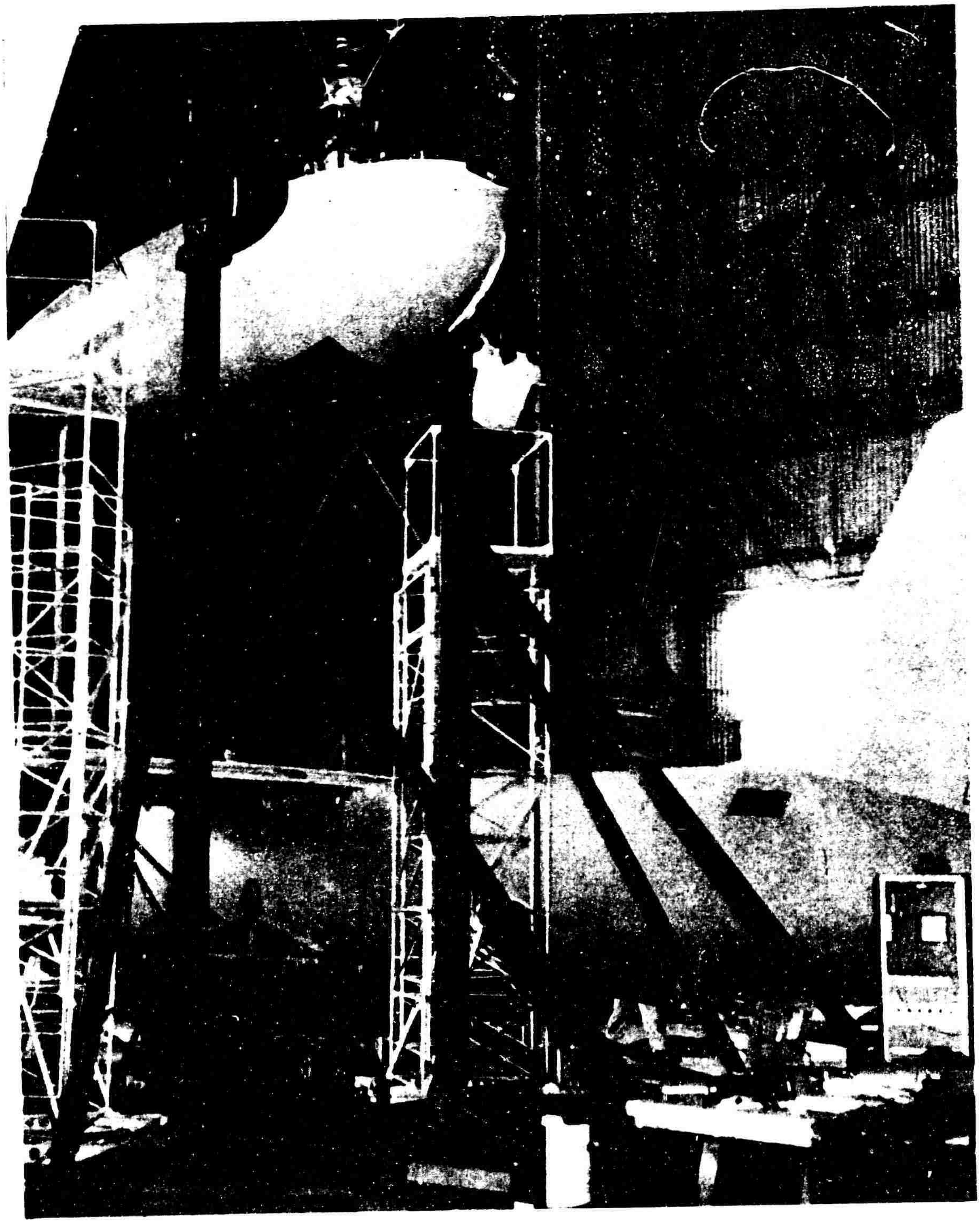

Figure 41. Photograph of Ground Floor Shake Test Facility.

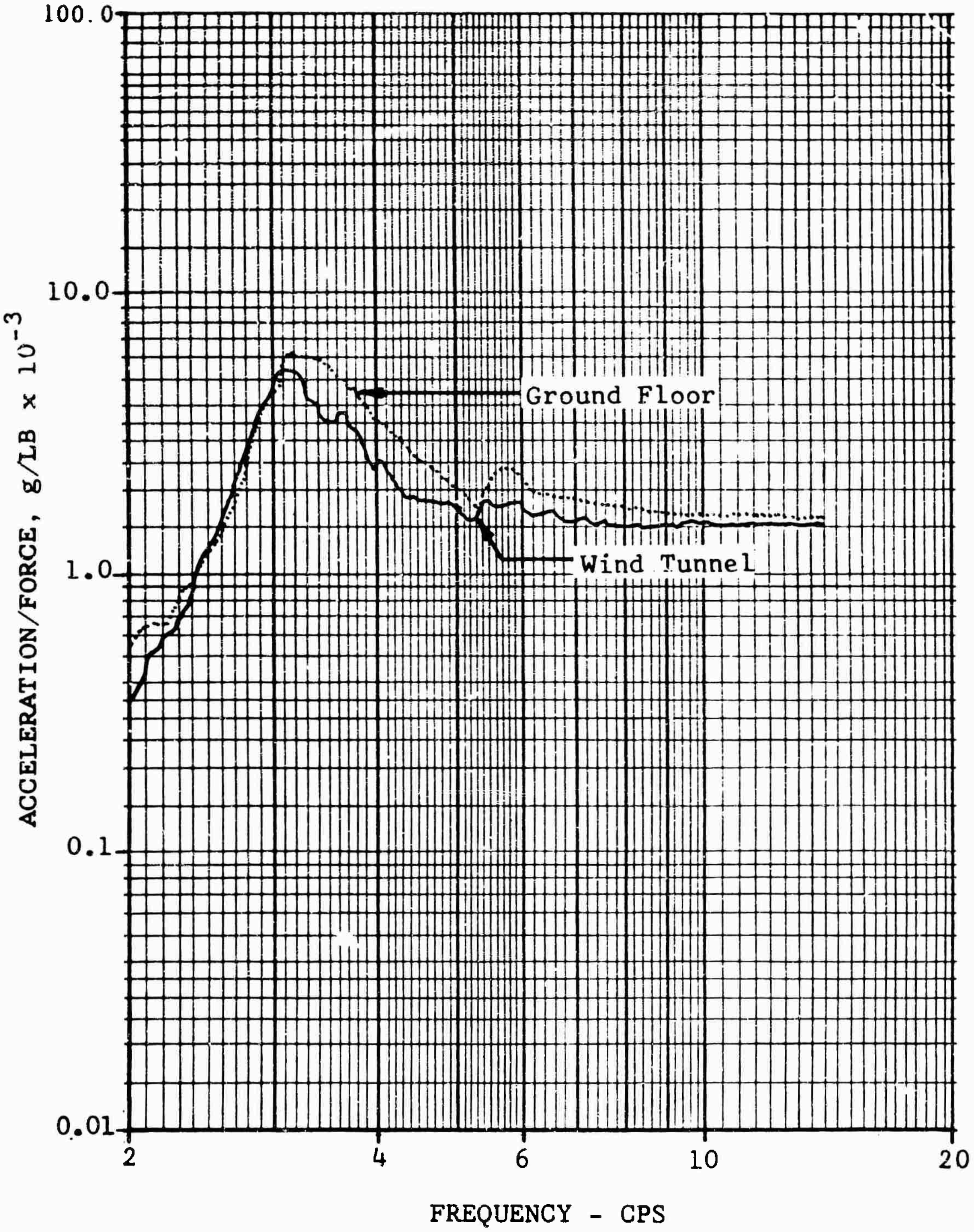

Figure 42. Hub Response to Longitudinal Excitation.

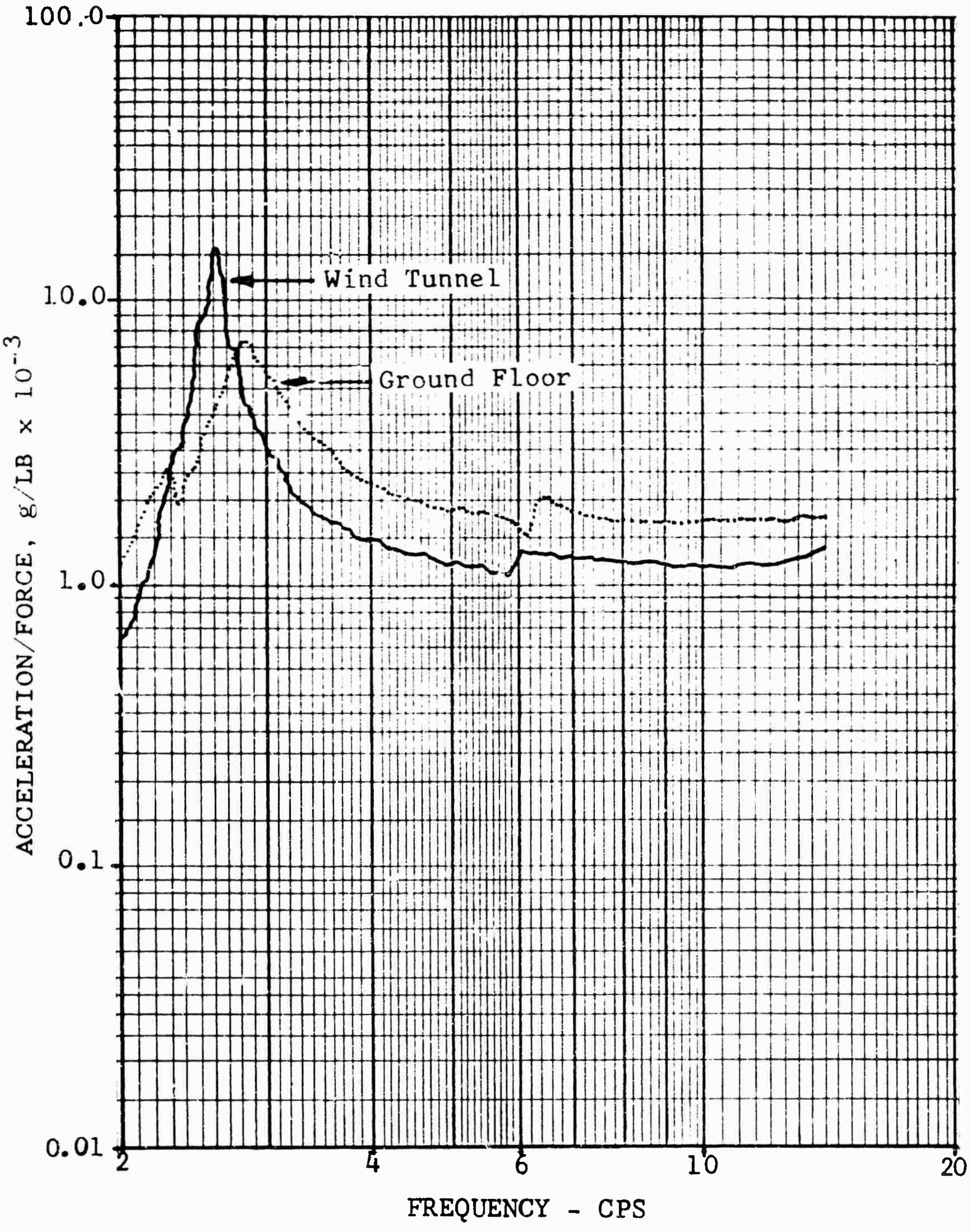

Figure 43. Hub Response to Lateral Excitation.

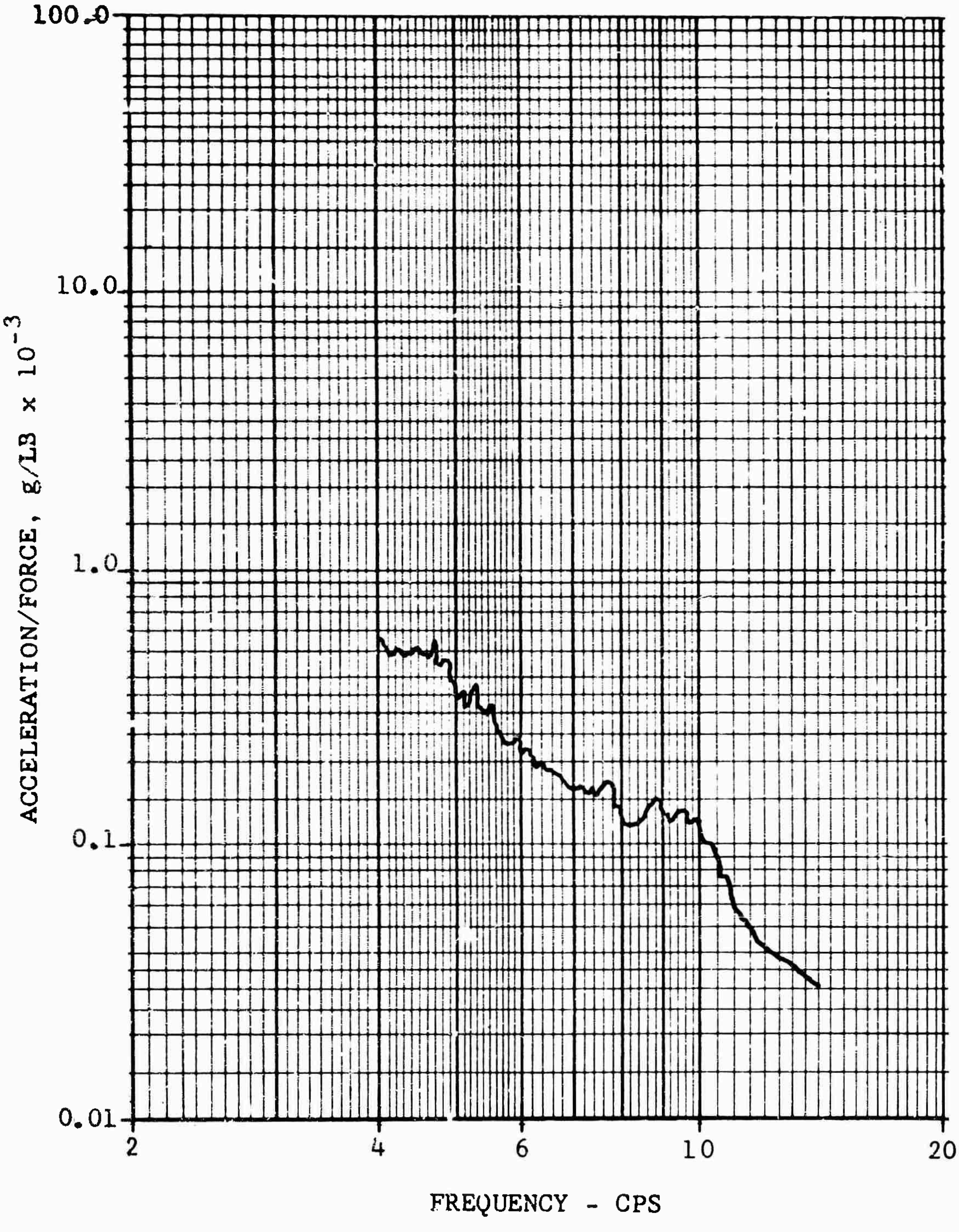

Figure 44. Hub Response to Vertical Excitation in the Wind Tunnel.

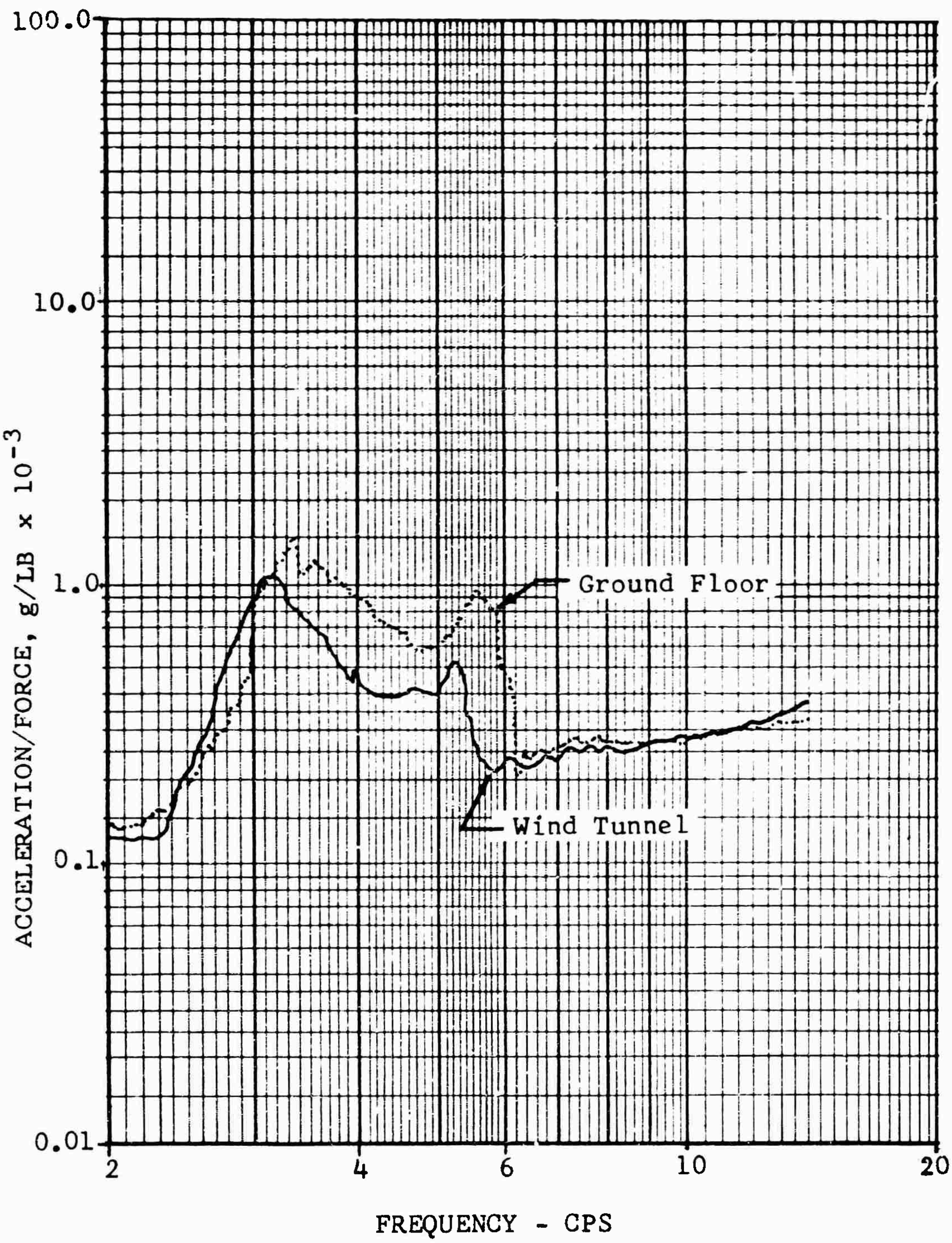

Figure 45. Pylon Response to Longitudinal Excitation.

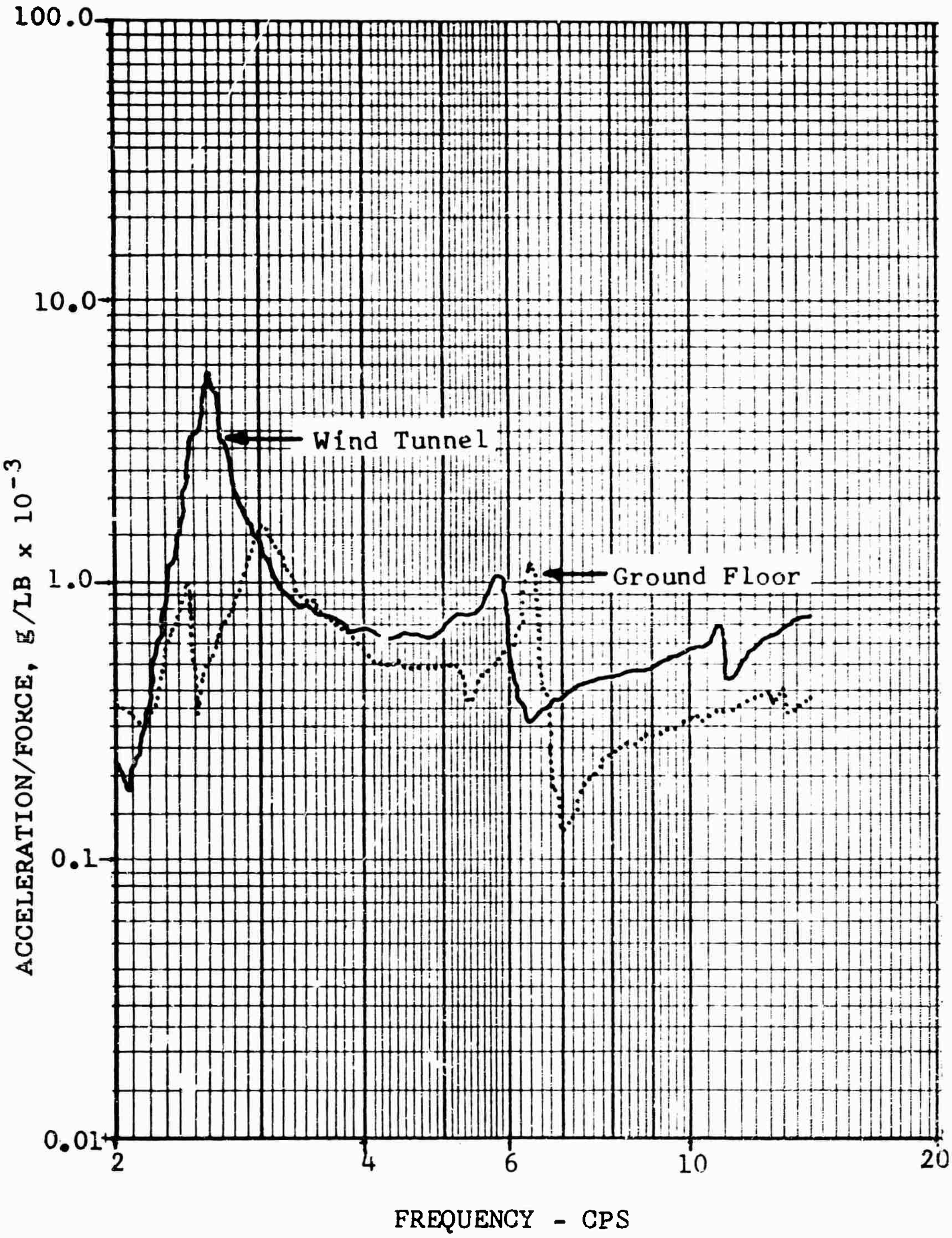

Figure 46. Pylon Response to Lateral Excitation.

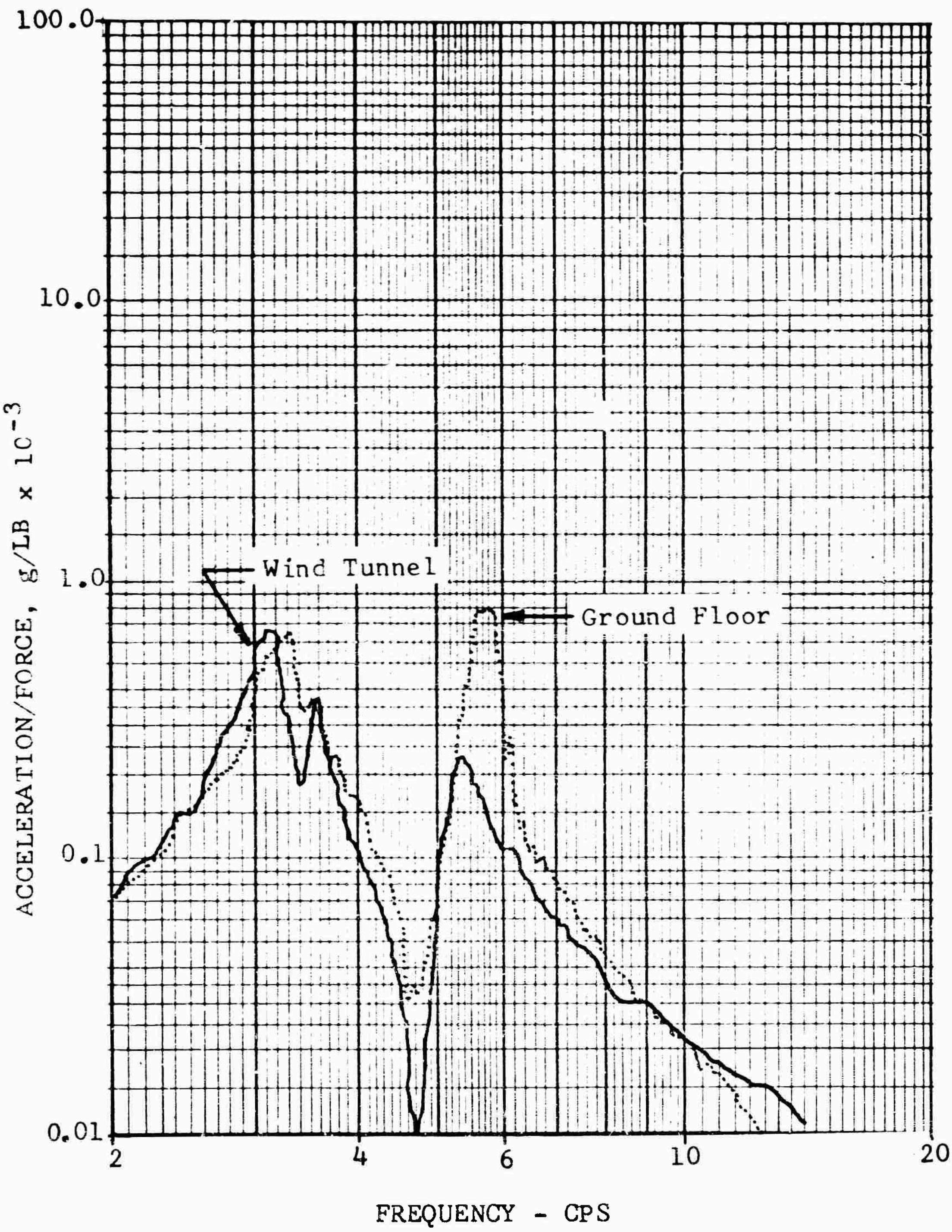

Figure 47. Module Response to Longitudinal Excitation.

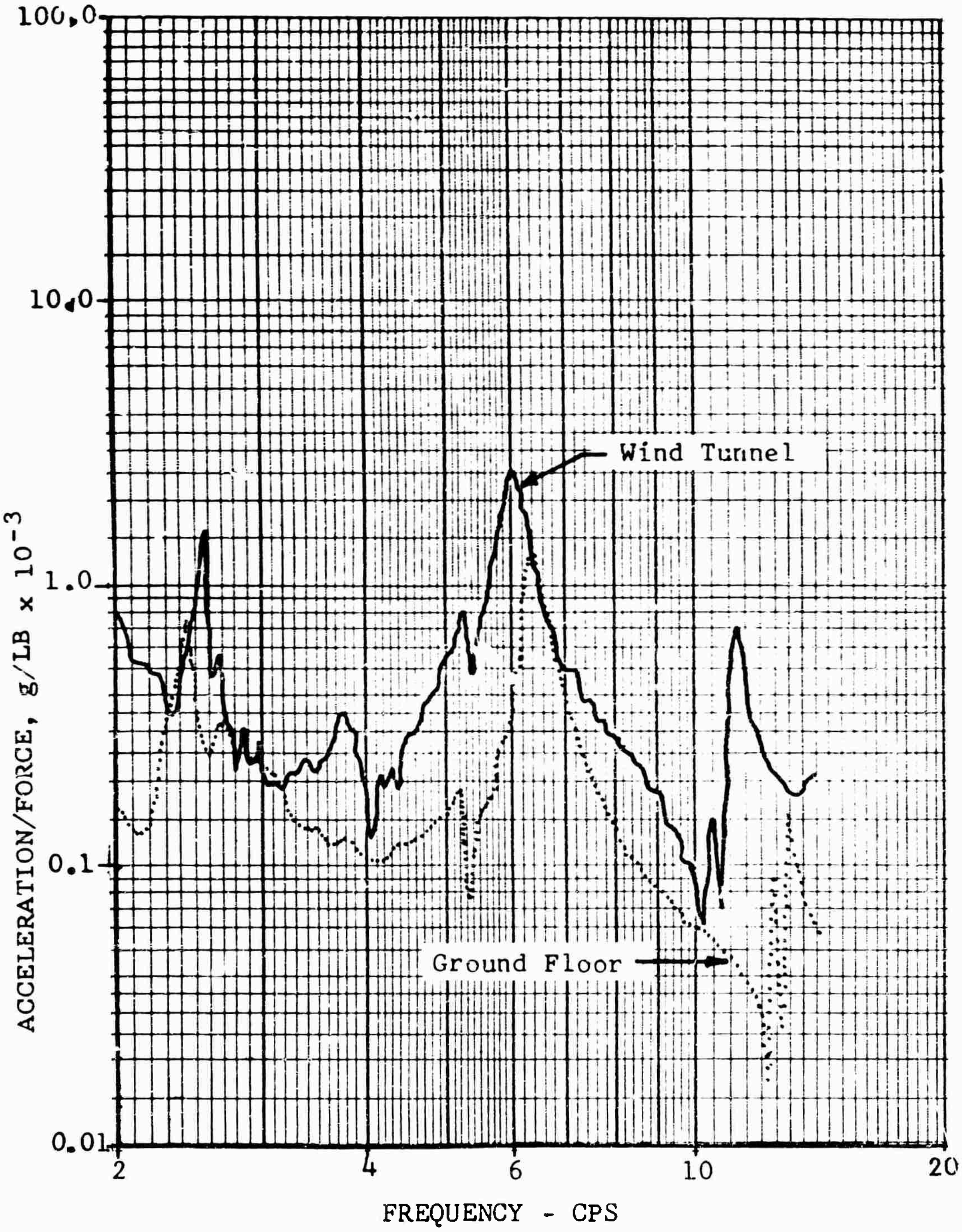

Figure 48. Module Response to Lateral Excitation.

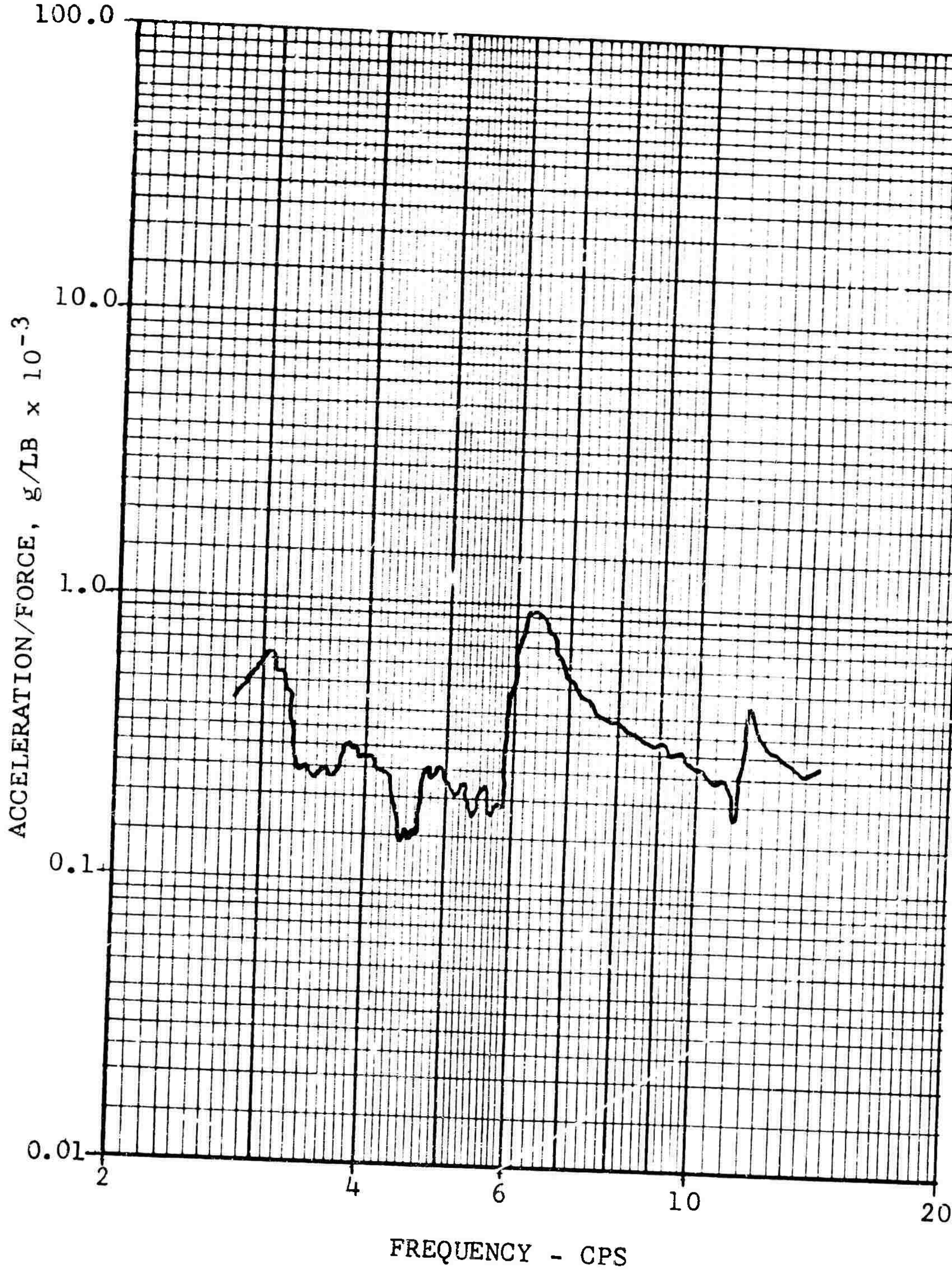

Figure 49. Module Response to Lateral Excitation at the Tail Strut in the Wind Tunnel.

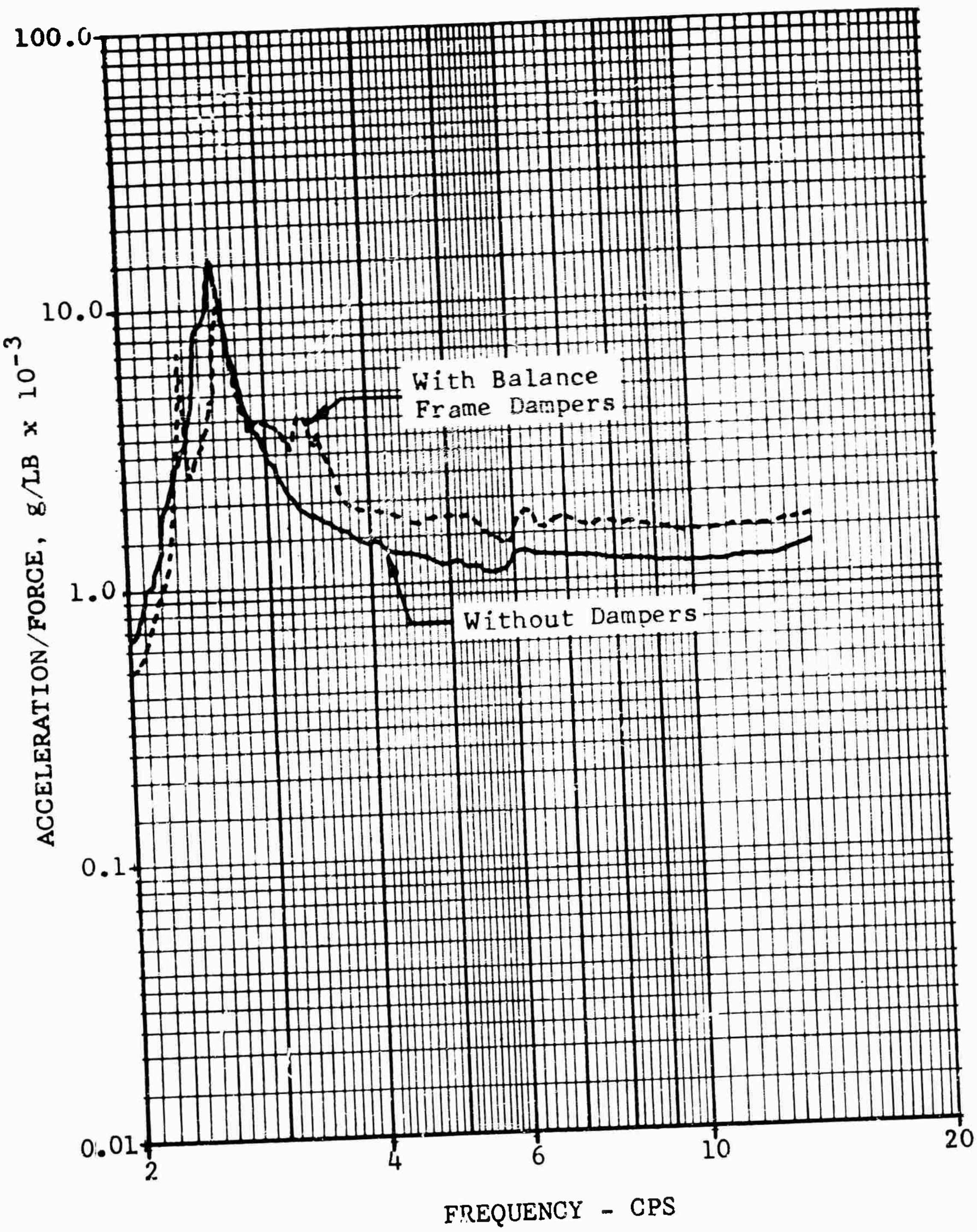

Figure 50. Effect of Damping on Hub Response to Lateral Excitation.

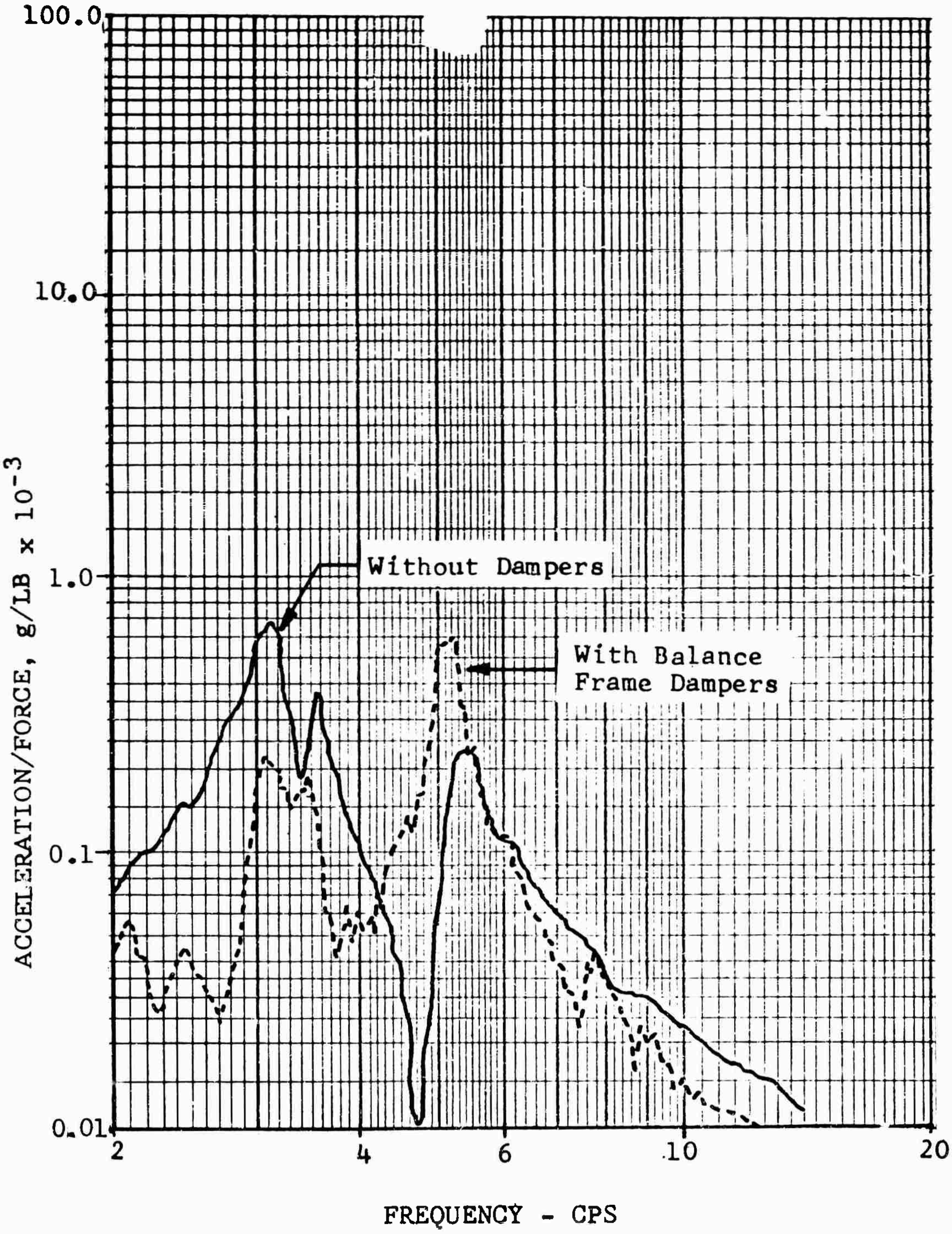

Figure 51. Effect of Damping on Module Response to Longitudinal Excitation.

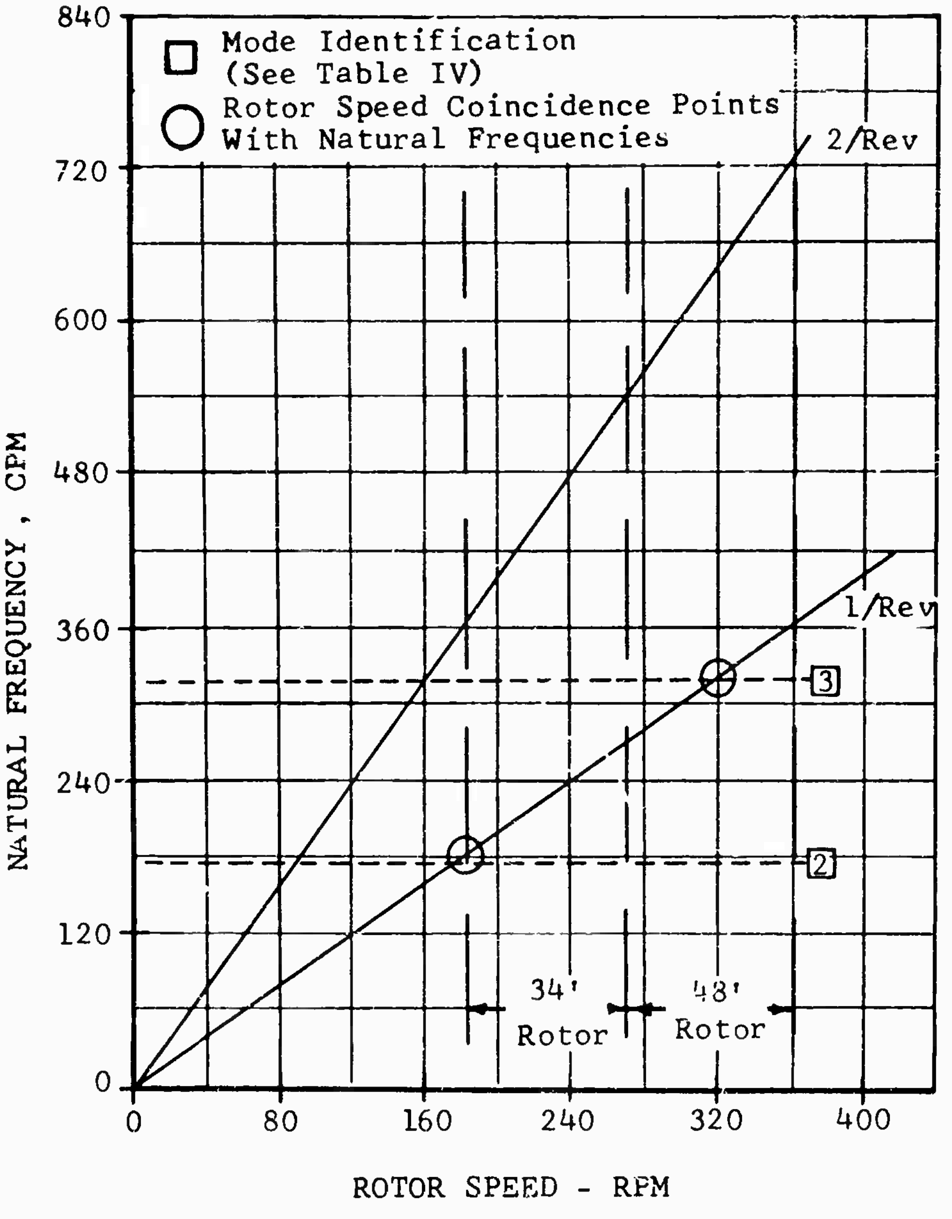

Figure 52. Longitudinal Natural Frequencies Versus Rotor Speed, Original Struts.

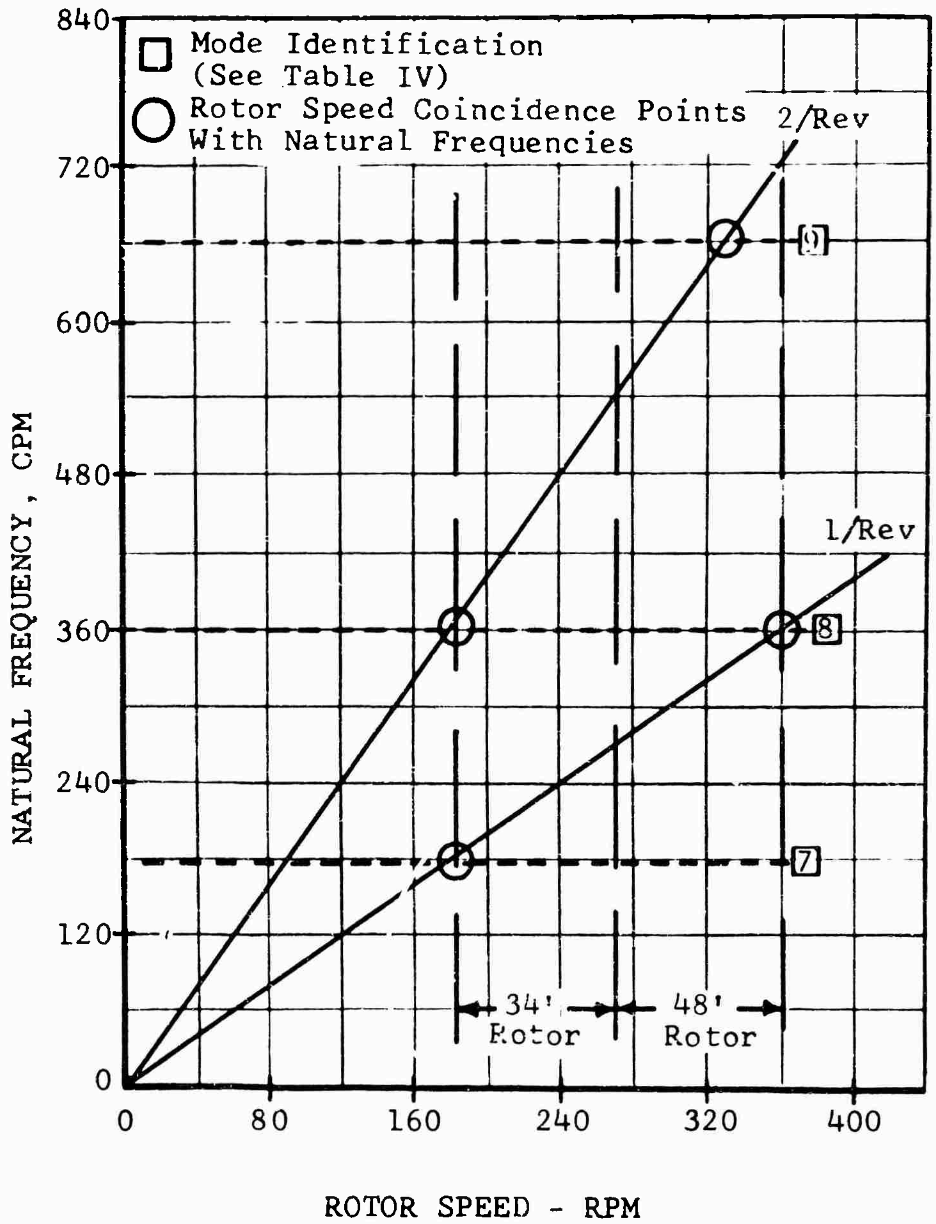

Figure 53. Lateral Natural Frequencies Versus Rotor Speed, Original Struts.

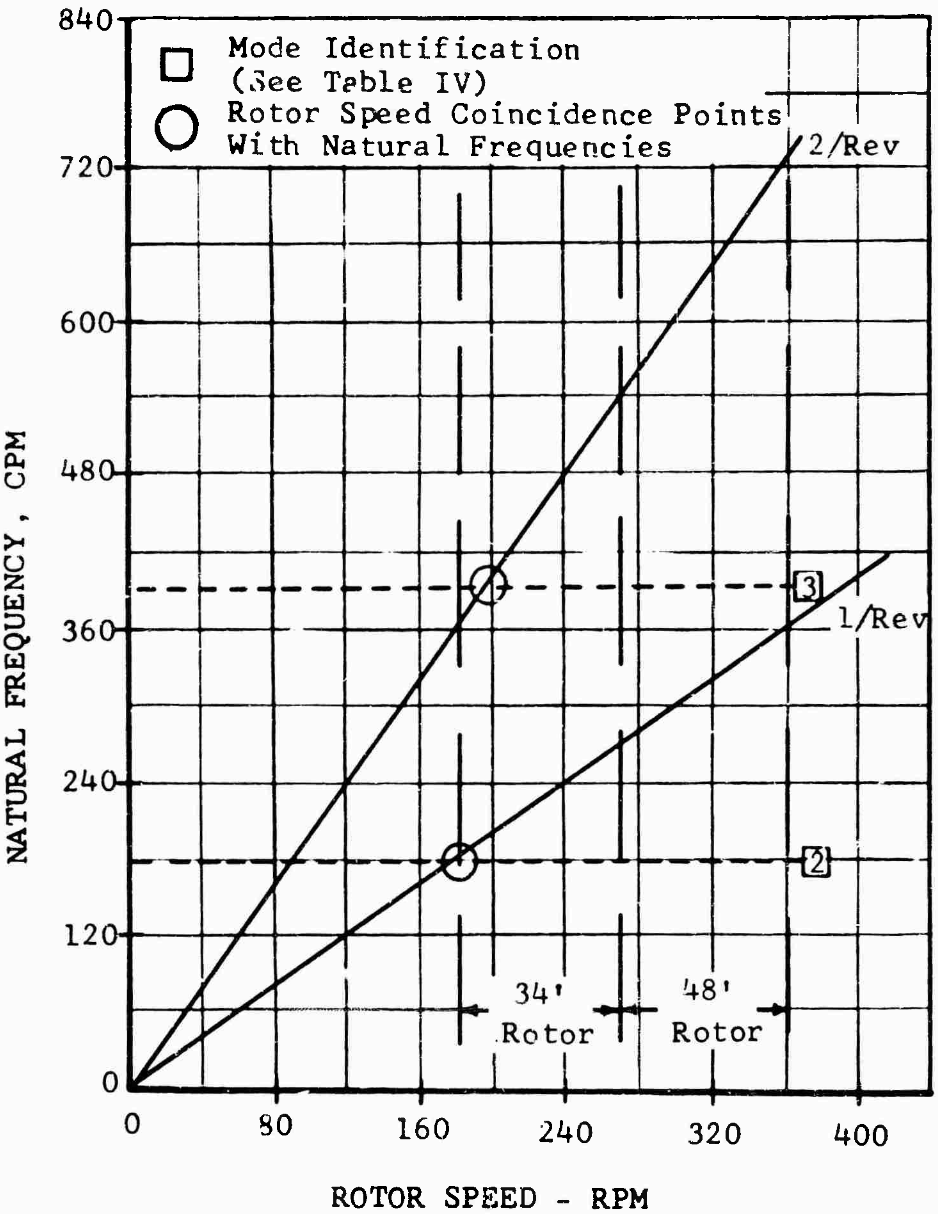

Figure 54. Longitudinal Natural Frequencies Versus Rotor Speed, Modified Struts.

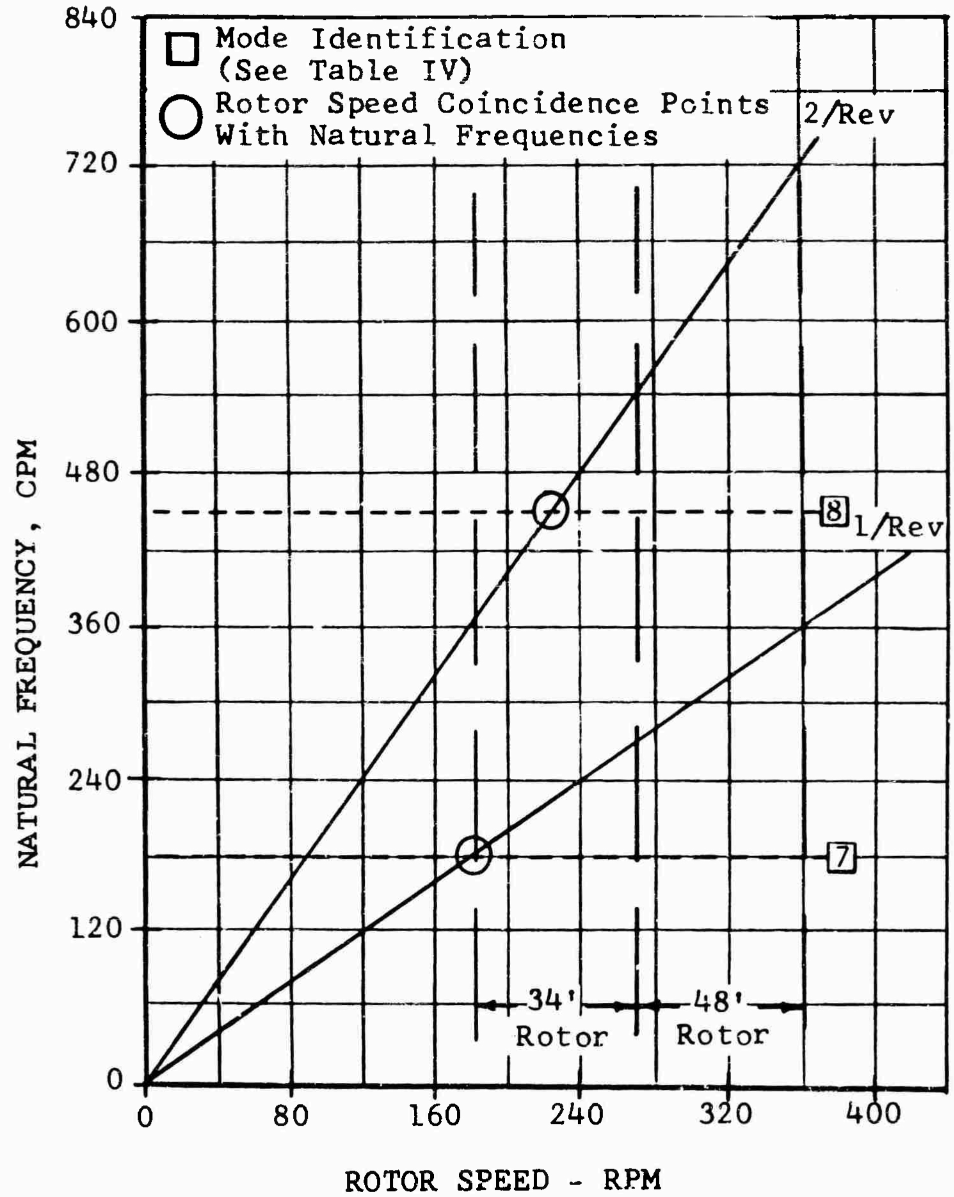

Figure 55. Lateral Natural Frequencies Versus Rotor Speed, Modified Struts.

APPENDIX IV
TABULAR DATA

The data presented in this appendix were recorded by the Large Scale Aerodynamic Branch of the NASA Ames Research Center. These data were taken during two separate test periods, and repetition of many test points will be noted. Table V relates the test conditions, rotor, and the page number of the data.

Data Reduction

Six-component forces and moments were measured by the wind tunnel balance system. Tare corrections were applied to the balance data to account for forces and moments produced by the exposed model support struts, the faired body, and the rotating hub. The rotating hub tares included all hardware inboard of the 2.66-foot radius station. The tares were applied based on wind tunnel dynamic pressure and shaft angle. Rotor downwash effects on the tares were neglected, and no data adjustments were made for wall effects.

TABLE V. WIND TUNNEL BALANCE TABULATED DATA

TABLE V - Continued

TABLE V-1. STANDARD BLADES, $\mu = 0.30$, $M_{(1.0,\ 90.)} = 0.79$

Test 274.0 Run 17

PT.	α_S	α_C	C_L/σ	C_D/σ	C_Y/σ	C_ℓ/σ	C_m/σ	C_Q/σ	θ_o	A_{1S}	μ	$M_{(1.0,90.)}$
1	-5.0	-8.7	0.030189	0.001406	-0.000464	0.000272	-0.000319	0.002004	12.0	0.60	0.299	0.787
2	-5.0	-7.3	0.012521	-0.000447	-0.000317	0.000217	-0.000173	0.001306	10.0	0.84	0.300	0.785
3	-5.0	-10.2	0.052881	0.003721	-0.000370	0.000304	-0.000588	0.002947	14.0	0.48	0.299	0.786
4	-5.0	-11.8	0.070891	0.006105	-0.001030	-0.000106	-0.000728	0.004119	16.0	-0.00	0.300	0.784
5	-5.0	-12.7	0.079485	0.007610	-0.001151	-0.000249	-0.000746	0.004787	17.0	-0.12	0.300	0.786
6	-10.0	-14.2	0.024645	0.002819	-0.000113	-0.000062	-0.000375	0.002385	14.0	0.60	0.300	0.786
7	-10.0	-12.8	0.006020	-0.000774	-0.000105	0.000100	-0.000335	0.001262	12.0	0.48	0.300	0.785
8	-10.0	-15.5	0.044780	0.006938	-0.000053	-0.000465	-0.000532	0.003790	16.0	0.36	0.300	0.787
9	-10.0	-16.5	0.054226	0.009047	-0.000222	-0.000601	-0.000676	0.004615	17.0	0.12	0.300	0.785
10	-10.0	-17.1	0.062509	0.010934	-0.000254	-0.000748	-0.000726	0.005367	18.0	0.12	0.300	0.785
11	-15.0	-19.7	0.017620	0.003123	-0.000040	-0.000376	-0.000142	0.002470	16.0	0.48	0.299	0.786
12	-15.0	-18.8	0.010097	0.000857	-0.000014	-0.000222	-0.000091	0.001804	15.0	0.72	0.300	0.785
13	-15.0	-21.0	0.036785	0.008970	-0.000243	-0.000859	-0.000416	0.004430	18.0	0.12	0.300	0.789
14	0.	-4.6	0.062302	-0.000985	-0.001620	0.000271	-0.000618	0.001630	12.0	-0.36	0.299	0.787
15	0.	-6.[illegible]	0.079271	0.000235	-0.001937	0.000290	-0.000774	0.002463	14.0	-0.36	0.299	0.787
16	0.	-3.0	0.041078	-0.001216	-0.001194	0.000308	-0.000457	0.001223	10.0	0.00	0.299	0.787
17	0.	-1.8	0.020380	-0.001299	-0.000940	0.000265	-0.000319	0.001078	8.0	0.00	0.298	0.788
18	0.	-0.5	0.003484	-0.001366	-0.000709	0.000208	-0.000221	0.001074	6.0	0.12	0.298	0.783
19	4.0	1.6	0.044860	-0.004407	-0.001591	0.000367	-0.000348	0.000383	8.0	-0.24	0.300	0.786
20	4.0	3.0	0.025323	-0.003120	-0.001313	0.000284	-0.000231	0.000602	6.0	0.00	0.299	0.786

TABLE V-2. STANDARD BLADES, $\mu = 0.30$, $M_{(1.0,\ 90.)} = 0.85$

Test 274.0 Run 16

PT.	α_S	α_C	C_L/σ	C_D/σ	C_Y/σ	C_ℓ/σ	C_m/σ	C_Q/σ	θ_o	A_{1S}	μ	$M_{(1.0,90.)}$
01	-5.0	-9.3	0.043314	0.002487	-0.000321	-0.000117	-0.000402	0.002518	13.0	0.60	0.302	0.847
02	-5.0	-8.5	0.033843	0.001507	-0.000287	-0.000025	-0.000437	0.002132	12.0	0.72	0.299	0.846
03	-5.0	-10.4	0.051805	0.003748	-0.000547	-0.000163	-0.000354	0.003092	14.0	0.36	0.302	0.846
04	-10.0	-14.1	0.073500	0.003033	-0.000017	-0.000195	-0.000321	0.002574	14.0	0.84	0.301	0.846
05	-10.0	-15.6	0.045795	0.007000	0.000234	-0.000600	-0.000468	0.003940	16.0	0.72	0.301	0.849
06	-15.0	-19.5	0.018718	0.003291	0.000088	-0.000433	-0.000120	0.002673	16.0	0.96	0.302	0.844
07	-15.0	-20.9	0.035858	0.008574	0.000208	-0.000850	-0.000221	0.004398	18.0	0.84	0.303	0.847
08	-15.0	-18.8	0.010126	0.000800	0.000034	-0.000278	-0.000183	0.001907	15.0	0.96	0.301	0.844
09	-10.0	-16.5	0.052919	0.008737	0.000210	-0.000702	-0.000505	0.004600	17.0	0.72	0.302	0.847
10	-10.0	-14.0	0.025629	0.002933	0.000086	-0.000277	-0.000309	0.002468	14.0	0.72	0.301	0.844
11	-10.0	-12.8	0.007088	-0.000650	-0.000008	-0.000010	-0.000341	0.001379	12.0	0.96	0.300	0.847
12	-5.0	-8.5	0.032068	0.001403	-0.000298	-0.000079	-0.000320	0.002076	12.0	0.60	0.300	0.847
13	-5.0	-7.0	0.014580	-0.000393	-0.000406	0.000127	-0.000377	0.001492	10.0	0.60	0.302	0.845
14	0.	-3.1	0.043786	-0.001367	-0.001011	0.000210	-0.000377	0.001331	10.0	0.36	0.302	0.845
15	0.	-4.7	0.062011	+0.000929	-0.001251	0.000217	-0.000409	0.001756	12.0	0.24	0.302	0.844
16	0.	-6.5	0.080557	0.000035	-0.001696	0.000203	-0.000437	0.002537	14.0	0.00	0.301	0.846
17	0.	-1.4	0.022328	-0.001581	-0.000677	0.000117	-0.000341	0.001172	8.0	0.72	0.302	0.844
18	0.	-0.4	0.004924	-0.001526	-0.000667	0.000134	-0.000608	0.001205	6.0	0.60	0.301	0.847
19	5.0	3.1	0.043639	-0.005437	-0.001623	0.000271	-0.000393	0.000215	7.0	0.00	0.302	0.844
20	5.0	3.8	0.033619	-0.004576	-0.001423	0.000201	-0.000445	0.000392	6.0	0.24	0.304	0.843
21	5.0	2.5	0.054309	-0.006415	-0.001702	0.000249	-0.000530	0.000049	8.0	0.00	0.301	0.847
22	0.	-6.5	0.082340	-0.000051	-0.001831	0.000217	-0.000494	0.002556	14.0	-0.12	0.303	0.843
23	-5.0	-11.2	0.062146	0.004985	-0.000456	-0.000248	-0.000395	0.003666	15.0	0.48	0.304	0.845

TABLE V-3. STANDARD BLADES, μ = 0.30, $M_{(1.0,\ 90.)}$ = 0.95

Test 274.0 Run 19

PT.	α_S	α_C	C_L/σ	C_D/σ	C_Y/σ	C_{ℓ}/σ	C_m/σ	C_Q/σ	θ_o	A_{1S}	μ	$M_{(1.0,90.)}$
1	-10.0	-13.1	0.027469	0.002052	0.000194	-0.000288	-0.000290	0.003526	14.0	0.84	0.298	0.951
2	-10.0	-14.1	0.034772	0.003252	0.000242	-0.000363	-0.000770	0.003961	15.0	1.08	0.300	0.949
3	-10.0	-14.6	0.045339	0.005088	0.000307	-0.000618	-0.000884	0.004840	16.0	0.84	0.298	0.952
4	-15.0	-18.6	0.019081	0.002235	0.000232	-0.000603	-0.000274	0.003523	16.0	1.08	0.298	0.953
5	-15.0	-19.5	0.027292	0.004404	0.000340	-0.000758	-0.000639	0.004308	17.0	1.08	0.298	0.954
6	-15.0	-19.8	0.036528	0.007069	0.000417	-0.001012	-0.000754	0.005206	18.0	1.08	0.300	0.950
7	-15.0	-17.9	0.011510	0.000150	0.000049	-0.000312	-0.000096	0.002886	15.0	1.08	0.298	0.952
8	-10.0	-13.0	0.025542	0.001680	0.000256	-0.000277	-0.000219	0.003488	14.0	1.08	0.297	0.954
9	-10.0	-12.3	0.017488	0.000130	0.000254	-0.000215	-0.000312	0.002953	13.0	1.08	0.298	0.950
10	-5.0	-9.0	0.052202	0.002084	-0.000445	-0.000016	-0.000079	0.003911	14.0	0.60	0.299	0.949
11	-5.0	-8.1	0.042904	0.001071	-0.000435	-0.000009	-0.000271	0.003496	13.0	0.72	0.298	0.951
12	-5.0	-7.3	0.032500	0.000032	0.000037	-0.000066	-0.000111	0.003134	12.0	1.20	0.297	0.952
13	-5.0	-6.6	0.024909	-0.000876	-0.000197	-0.000030	-0.000172	0.002917	11.0	0.96	0.298	0.954
14	0.	-3.2	0.062407	-0.002994	-0.001255	0.000349	-0.000636	0.002795	12.0	0.36	0.298	0.953
15	0.	-2.6	0.052515	-0.003092	-0.001098	0.000328	-0.000586	0.002456	11.0	0.36	0.299	0.949
16	0.	-1.9	0.042569	-0.003256	-0.000673	0.000228	-0.000434	0.002345	10.0	0.72	0.298	0.954
17	0.	-1.1	0.034478	-0.003357	-0.000607	0.000315	-0.000586	0.002243	9.0	0.84	0.298	0.951
18	2.0	0.5	0.044667	-0.005041	-0.000884	0.000375	-0.000380	0.001872	9.0	0.00	0.297	0.954
19	-5.0	-9.0	0.051255	0.002088	-0.000419	-0.000047	0.000053	0.004098	14.0	0.00	0.299	0.951
20	-5.0	-9.7	0.061862	0.003145	-0.000395	-0.000027	0.000294	0.004632	15.0	0.48	0.299	0.950
21	-5.0	-10.5	0.069841	0.004198	-0.000725	-0.000135	-0.000514	0.005210	16.0	0.24	0.300	0.949
22	-10.0	-15.4	0.052590	0.006809	0.000223	-0.000649	-0.000862	0.005642	17.0	0.60	0.299	0.954
23	-10.0	-16.1	0.059231	0.008521	0.000590	-0.000956	-0.000743	0.006253	18.0	0.72	0.298	0.951

TABLE V-4. STANDARD BLADES, μ = 0.35, $M_{(1.0,\ 90.)}$ = 0.85

Test 274.0 Run 17

PT.	α_S	α_C	C_L/σ	C_D/σ	C_Y/σ	C_{ℓ}/σ	C_m/σ	C_Q/σ	θ_o	A_{1S}	μ	$M_{(1.0,90.)}$
21	-5.0	-8.9	0.026294	0.000425	-0.000593	0.000089	-0.000615	0.002047	12.0	0.48	0.348	0.847
22	-5.0	-10.7	0.044276	0.002379	-0.000873	-0.000041	-0.000812	0.003014	14.0	0.24	0.350	0.846
23	-10.0	-14.4	0.018214	0.000969	-0.000114	-0.000186	-0.000412	0.002244	14.0	0.36	0.349	0.847
24	-10.0	-16.0	0.034674	0.004154	-0.000210	-0.000428	-0.000508	0.003559	16.0	0.48	0.349	0.847
25	-15.0	-19.5	0.008736	-0.000189	-0.000165	-0.000051	-0.000124	0.001960	16.0	0.60	0.349	0.845
26	-15.0	-20.2	0.017791	0.002468	-0.000180	-0.000374	-0.000239	0.002841	17.0	0.60	0.350	0.846
27	-15.0	-21.0	0.025547	0.004625	-0.000208	-0.000508	-0.000319	0.003772	18.0	0.60	0.349	0.847
28	-10.0	-17.0	0.048797	0.006950	-0.000262	-0.000603	-0.000793	0.004716	17.5	0.36	0.349	0.849
29	-10.0	-13.5	0.009019	-0.000804	0.000021	-0.000092	-0.000275	0.001591	13.0	0.72	0.349	0.849
30	-5.0	-11.4	0.056380	0.003457	-0.001071	-0.000153	-0.000726	0.003562	15.0	0.00	0.348	0.850
31	-5.0	-7.4	0.010417	-0.001193	-0.000404	0.000107	-0.000276	0.001472	10.0	0.36	0.348	0.848
32	0.	-5.1	0.057284	-0.001448	-0.001874	0.000196	-0.000617	0.001810	12.0	-0.00	0.349	0.849
33	0.	-3.5	0.039003	-0.001679	-0.001293	0.000179	-0.000592	0.001444	10.0	0.12	0.349	0.849
34	0.	-1.9	0.022603	-0.001824	-0.000997	0.000090	-0.000318	0.001262	8.0	0.12	0.348	0.850
35	0.	-0.5	0.006432	-0.001804	-0.000751	0.000045	-0.000176	0.001295	6.0	0.24	0.349	0.849
36	4.0	1.0	0.047713	-0.005111	-0.001973	0.000173	-0.000523	0.000388	8.0	-0.12	0.348	0.848
37	4.0	1.9	0.038856	-0.004684	-0.001944	0.000177	-0.000441	0.000435	7.0	-0.36	0.349	0.847
38	4.0	2.5	0.030361	-0.004030	-0.001609	0.000142	-0.000511	0.000564	6.0	-0.12	0.349	0.847
39	0.	-7.1	0.075409	-0.000656	-0.002533	0.000182	-0.000546	0.002601	14.0	0.36	0.349	0.847

TABLE V-5. STANDARD BLADES, $\mu = 0.35$, $M_{(1.0,\ 90.)} = 0.95$

Test 274.0 Run 20

PT.	α_S	α_C	C_L/σ	C_D/σ	C_Y/σ	C_ℓ/σ	C_m/σ	C_Q/σ	θ_o	A_{1S}	μ	$M_{(1.0,90.)}$
9	-5.0	-6.9	0.044738	-0.000835	0.000170	-0.000083	-0.000554	0.003446	12.5	1.56	0.350	0.947

Test 274.0 Run 21

PT.	α_S	α_C	C_L/σ	C_D/σ	C_Y/σ	C_ℓ/σ	C_m/σ	C_Q/σ	θ_o	A_{1S}	μ	$M_{(1.0,90.)}$
5	-5.0	-8.2	0.047342	0.000047	-0.000721	0.000121	-0.000931	0.003664	13.3	0.60	0.349	0.948
6	-5.0	-8.7	0.053799	0.000491	-0.000565	-0.000126	-0.000837	0.004109	14.0	0.60	0.350	0.947
7	-7.0	-10.2	0.043036	0.001111	-0.000186	-0.000262	-0.000854	0.004076	14.0	0.60	0.350	0.946
8	-10.0	-12.5	0.026645	0.000654	0.000396	-0.000324	-0.000911	0.003701	14.0	0.96	0.350	0.948
9	-10.0	-12.7	0.031651	0.001349	0.000375	-0.000408	-0.000785	0.004014	14.5	0.96	0.349	0.947
10	-10.0	-13.2	0.033094	0.001680	0.000368	-0.000407	-0.000666	0.004259	15.0	0.96	0.349	0.949
11	-10.0	-13.2	0.034128	0.001808	0.000342	-0.000405	-0.000861	0.004319	15.0	0.96	0.349	0.948
12	-10.0	-13.4	0.038875	0.002516	0.000532	-0.000667	-0.000869	0.004596	15.5	0.96	0.349	0.948

TABLE V-6. STANDARD BLADES, $\mu = 0.40$, $M_{(1.0,\ 90.)} = 0.85$

Test 274.0 Run 18

PT.	α_S	α_C	C_L/σ	C_D/σ	C_Y/σ	C_ℓ/σ	C_m/σ	C_Q/σ	θ_o	A_{1S}	μ	$M_{(1.0,90.)}$
1	-4.0	-10.4	0.044991	0.000745	-0.001028	0.000131	-0.000778	0.002840	14.0	0.48	0.399	0.846
2	-8.0	-13.1	0.021829	0.000165	-0.000168	-0.000015	-0.000553	0.002343	14.0	0.72	0.397	0.847
3	-8.0	-14.7	0.037953	0.002548	-0.000259	-0.000222	-0.000840	0.003546	16.0	0.72	0.401	0.843
4	-12.0	-17.5	0.014561	-0.000269	-0.000043	-0.000037	-0.000663	0.002283	16.0	0.84	0.399	0.844
5	-12.0	-18.2	0.023268	0.001176	0.000139	-0.000354	-0.001456	0.003123	17.0	0.84	0.400	0.844
6	-12.0	-19.2	0.029735	0.003208	-0.000033	-0.000557	-0.000961	0.003871	18.0	0.60	0.402	0.845
7	-12.0	-16.5	0.007338	-0.001894	0.000127	0.000006	-0.000641	0.001576	18.0	0.84	0.400	0.846
8	-8.0	-13.7	0.029497	0.001269	-0.000088	-0.000105	-0.000705	0.002878	15.0	0.84	0.399	0.846
9	-8.0	-12.0	0.014670	-0.000964	-0.000149	0.000021	-0.000651	0.001870	13.0	0.60	0.399	0.847
10	-4.0	-9.3	0.036901	0.000072	-0.000983	0.000244	-0.000784	0.002462	13.0	0.48	0.400	0.845
11	-4.0	-8.5	0.028915	-0.000447	-0.000994	0.000141	-0.000521	0.002077	12.0	-0.00	0.400	0.845
12	-4.0	-7.5	0.021224	-0.000891	-0.000795	0.000052	-0.000270	0.001785	11.0	-0.00	0.400	0.846
13	-4.0	-6.9	0.013786	-0.001431	-0.000850	0.000255	-0.000146	0.001540	10.0	-0.24	0.399	0.849
14	0.	-6.0	0.052218	-0.001924	-0.001955	0.000415	-0.000670	0.001809	12.0	0.24	0.398	0.849
15	0.	-4.0	0.038206	-0.002244	-0.001944	0.000299	-0.000413	0.001390	10.0	-0.48	0.399	0.847
16	0.	-4.9	0.045736	-0.002140	-0.001850	0.000447	-0.000334	0.001573	11.0	0.12	0.399	0.847
17	0.	[illegible]	0.029722	-0.002196	-0.001347	0.000361	-0.000142	0.001291	9.0	0.24	0.400	0.847
18	4.0	[illegible]	0.061307	-0.006142	-0.002901	0.000388	-0.000697	0.000370	10.0	-0.36	0.396	0.849
19	4.0	[illegible]	0.053606	-0.005888	-0.003050	0.000357	-0.000676	0.000295	9.0	-0.72	0.397	0.848
20	4.0	[illegible]	0.046025	-0.005574	-0.002497	0.000457	-0.000688	0.000263	8.0	-0.24	0.398	0.848
21	-4.0	[illegible]	0.052780	0.001441	-0.001072	0.000061	-0.000709	0.003395	15.0	0.60	0.399	0.846
22	-4.0	[illegible]	0.060543	0.002159	-0.001669	0.000073	-0.000699	0.003967	16.0	0.00	0.401	0.844

TABLE V-7. 48-FOOT TAPERED-TIP BLADES, $\mu = 0.13$, $M_{(1.0,\ 90.)} = 0.80$

Test 288.0 Run 14

PT	α_S	α_C	C_L/σ	C_D/σ	C_Y/σ	$C_{\mathcal{L}}/\sigma$	$C_{\mathcal{M}}/\sigma$	C_Q/σ	θ_o	A_{1S}	μ	$M_{(1.0,90.)}$
19	-2.0	-3.5	0.064289	0.002048	-0.000931	-0.000004	[illegible]	0.002135	13.2	0.80	0.129	0.802
20	-2.0	-3.5	0.072238	0.002067	-0.000934	0.000034	[illegible]	0.002348	13.7	0.80	0.130	0.797
21	-3.0	-4.5	0.070406	0.003042	-0.000933	-0.000046	-0.000245	0.002425	13.7	0.80	0.131	0.794
22	-3.0	-4.5	0.075747	0.003144	-0.000874	-0.000061	-0.000246	0.002624	14.2	0.80	0.130	0.797
23	-3.0	-4.5	0.061700	0.002814	-0.000922	-0.000032	-0.000169	0.002170	13.2	0.80	0.130	0.799
24	-1.0	-2.5	0.067530	0.000930	-0.000942	0.000045	-0.000203	0.002066	13.2	0.80	0.129	0.799
25	-1.0	-2.5	0.054014	0.000931	-0.000957	-0.000000	-0.000208	0.001759	12.2	0.80	0.130	0.799
26	-1.0	-2.5	0.061014	0.000937	-0.000939	-0.000003	-0.000291	0.001913	12.7	0.80	0.130	0.799
27	-2.0	-3.5	0.057811	0.001863	-0.000936	-0.000043	-0.000226	0.001961	12.7	0.80	0.130	0.799

Test 288.0 Run 16

PT	α_S	α_C	C_L/σ	C_D/σ	C_Y/σ	$C_{\mathcal{L}}/\sigma$	$C_{\mathcal{M}}/\sigma$	C_Q/σ	θ_o	A_{1S}	μ	$M_{(1.0,90.)}$
1	-4.0	-6.2	0.068100	0.004459	-0.001153	-0.000013	-0.000225	0.002555	13.2	1.00	0.130	0.798
2	-4.0	-6.2	0.074159	0.004741	-0.001152	-0.000047	-0.000310	0.002787	13.7	1.00	0.129	0.802
3	-5.0	-7.2	0.071174	0.005759	-0.001082	-0.000225	-0.000203	0.002863	13.7	1.00	0.129	0.801
4	-5.0	-7.2	0.077323	0.006080	-0.001093	-0.000203	-0.000198	0.003073	14.2	1.00	0.129	0.801
5	-5.0	-7.2	0.063794	0.005299	-0.001075	-0.000169	-0.000183	0.002566	13.2	1.00	0.130	0.800
6	-3.0	-5.2	0.069559	0.003336	-0.001122	-0.000047	-0.000181	0.002462	13.2	1.00	0.129	0.801
7	-3.0	-5.2	0.056528	0.002898	-0.001149	-0.000031	-0.000197	0.002056	12.2	1.00	0.129	0.804
8	-3.0	-5.2	0.063716	0.003123	-0.001136	-0.000041	-0.000265	0.002276	12.7	1.00	0.127	0.799
9	-3.0	-5.2	0.060332	0.004126	-0.001133	-0.000055	-0.000041	0.002297	12.7	1.00	0.129	0.801

TABLE V-8. 48-FOOT TAPERED-TIP BLADES, $\mu = 0.20$, $M_{(1.0,\ 90.)} = 0.85$

Test 288.0 Run 14

PT	α_S	α_C	C_L/σ	C_D/σ	C_Y/σ	$C_{\mathcal{L}}/\sigma$	$C_{\mathcal{M}}/\sigma$	C_Q/σ	θ_o	A_{1S}	μ	$M_{(1.0,90.)}$
10	-5.0	-7.8	0.064411	0.004901	-0.000969	-0.000027	-0.000296	0.002856	14.5	0.25	0.202	0.851
11	-5.0	-7.8	0.071570	0.005163	-0.001102	-0.000056	-0.000334	0.003108	15.0	0.25	0.203	0.848
12	-6.0	-8.8	0.066077	0.006022	-0.001010	-0.000212	-0.000303	0.003188	15.0	0.25	0.204	0.848
13	-6.0	-8.8	0.074469	0.006474	-0.001015	-0.000222	-0.000317	0.003498	15.5	0.25	0.203	0.848
14	-6.0	-8.8	0.058369	0.005565	-0.000980	-0.000156	-0.000199	0.002895	14.5	0.25	0.204	0.848
15	-4.0	-6.8	0.068127	0.003971	-0.001159	-0.000042	-0.000383	0.002808	14.5	0.25	0.201	0.852
16	-4.0	-6.8	0.055225	0.003579	-0.001105	-0.000007	-0.000232	0.002401	13.5	0.25	0.202	0.849
17	-4.0	-6.8	0.060959	0.003813	-0.001128	-0.000029	-0.000254	0.002571	14.0	0.25	0.201	0.852
18	-5.0	-7.8	0.055953	0.004432	-0.001034	-0.000075	-0.000241	0.002595	14.0	0.25	0.201	0.856

Test 288.0 Run 16

PT	α_S	α_C	C_L/σ	C_D/σ	C_Y/σ	$C_{\mathcal{L}}/\sigma$	$C_{\mathcal{M}}/\sigma$	C_Q/σ	θ_o	A_{1S}	μ	$M_{(1.0,90.)}$
10	-5.0	-8.3	0.065647	0.004855	-0.001011	-0.000065	-0.000412	0.002977	14.0	0.45	0.201	0.851
11	-5.0	-8.3	0.073275	0.005212	-0.001085	-0.000059	-0.000421	0.003214	14.5	0.45	0.201	0.850
12	-6.0	-9.3	0.068342	0.006124	-0.001019	-0.000110	-0.000447	0.003278	14.5	0.45	0.201	0.852
13	-6.0	-9.3	0.074735	0.006493	-0.000968	-0.000171	-0.000339	0.003545	15.0	0.45	0.201	0.850
14	-6.0	-9.3	0.060673	0.005715	-0.000944	-0.000194	-0.000166	0.003030	14.0	0.45	0.200	0.851
15	-4.0	-7.3	0.070084	0.004042	-0.001106	-0.000017	-0.000281	0.002922	14.0	0.45	0.201	0.851
16	-4.0	-7.3	0.055769	0.003527	-0.001043	-0.000013	-0.000311	0.002463	13.0	0.45	0.201	0.847
17	-4.0	-7.3	0.063371	0.003835	-0.001110	-0.000006	-0.000341	0.002683	13.5	0.45	0.201	0.851
18	-5.0	-8.3	0.058608	0.004539	-0.001008	-0.000077	-0.000377	0.002714	13.5	0.45	0.201	0.851

TABLE V-9. 48-FOOT TAPERED-TIP BLADES, $\mu = 0.24$, $M_{(1.0,\ 90.)} = 0.87$

Test 288.0 Run 14

PT	α_S	α_C	C_L/σ	C_D/σ	C_Y/σ	C_{ℓ}/σ	C_{m}/σ	C_Q/σ	θ_o	A_{1S}	μ	$M_{(1.0,90.)}$
1	-7.0	-11.0	0.065634	0.007368	-0.000948	-0.000102	-0.000265	0.003732	16.0	0.15	0.238	0.878
2	-7.0	-11.0	0.073267	0.007898	-0.000954	-0.000199	-0.000229	0.004105	16.5	0.15	0.238	0.880
3	-8.0	-12.0	0.066585	0.008542	-0.000841	-0.000308	-0.000245	0.004091	16.5	0.15	0.238	0.878
4	-8.0	-12.0	0.058279	0.007823	-0.000849	-0.000258	-0.000209	0.003718	16.0	0.15	0.237	0.881
5	-8.0	-12.0	0.074576	0.009249	-0.000825	-0.000352	-0.000352	0.004500	17.0	0.15	0.238	0.880
6	-7.0	-11.0	0.056628	0.006671	-0.000903	-0.000156	-0.000281	0.003413	15.5	0.15	0.238	0.876
7	-6.0	-10.0	0.063195	0.006133	-0.001011	-0.000115	-0.000331	0.003470	15.5	0.15	0.239	0.875
8	-6.0	-10.0	0.054435	0.005568	-0.001019	-0.000037	-0.000255	0.003116	15.0	0.15	0.238	0.877
9	-6.0	-10.0	0.071196	0.006578	-0.001009	-0.000176	-0.000299	0.003755	16.0	0.15	0.238	0.878

Test 288.0 Run 17

PT	α_S	α_C	C_L/σ	C_D/σ	C_Y/σ	C_{ℓ}/σ	C_{m}/σ	C_Q/σ	θ_o	A_{1S}	μ	$M_{(1.0,90.)}$
1	-7.0	-11.8	0.070455	0.007629	-0.001221	-0.000320	-0.000067	0.004161	16.0	0.25	0.242	0.872
2	-7.0	-12.0	0.078038	0.008739	-0.001336	-0.000400	-0.000037	0.004731	16.5	0.35	0.242	0.873
3	-8.0	-13.0	0.072511	0.009385	-0.001200	-0.000521	-0.000007	0.004683	16.5	0.35	0.241	0.874
4	-8.0	-13.3	0.079661	0.010596	-0.001398	-0.000532	0.000036	0.005216	17.2	0.35	0.243	0.870
5	-8.0	-12.2	0.062307	0.007740	-0.000779	-0.000406	0.000025	0.004006	17.8	0.15	0.241	0.873
6	-7.0	-10.8	0.061986	0.006116	-0.000954	-0.000278	-0.000072	0.003608	15.0	0.0	0.241	0.874
7	-6.0	-9.8	0.066823	0.005590	-0.001132	-0.000152	0.000015	0.003607	15.0	0.0	0.241	0.873
8	-6.0	-9.5	0.061838	0.005001	-0.001186	-0.000101	-0.000038	0.003341	14.5	0.0	0.242	0.872
9	-6.0	-10.7	0.078451	0.007351	-0.001288	-0.000297	-0.000013	0.004408	16.2	0.15	0.242	0.873

TABLE V-10. 48-FOOT TAPERED-TIP BLADES, $\mu = 0.27$, $M_{(1.0,\ 90.)} = 0.90$

Test 288.0 Run 13

PT	α_S	α_C	C_L/σ	C_D/σ	C_Y/σ	C_{ℓ}/σ	C_{m}/σ	C_Q/σ	θ_o	A_{1S}	μ	$M_{(1.0,90.)}$
17	-8.0	-13.1	0.068878	0.008818	-0.000989	-0.000472	-0.000410	0.004788	17.5	0.0	0.271	0.899
18	-8.0	-13.1	0.076147	0.009367	-0.001240	-0.000553	-0.000322	0.005175	18.0	0.0	0.270	0.903
19	-9.0	-14.1	0.070359	0.010036	-0.001078	-0.000646	-0.000306	0.005169	18.0	0.15	0.271	0.900
20	-9.0	-14.1	0.078458	0.010825	-0.001114	-0.000747	-0.000350	0.005673	18.5	0.15	0.271	0.902
21	-9.0	-14.1	0.060621	0.008900	-0.001040	-0.000561	-0.000274	0.004643	17.4	0.15	0.272	0.900
22	-8.0	-13.1	0.061572	0.008165	-0.001137	-0.000495	-0.000215	0.004414	17.0	0.15	0.271	0.899
23	-7.0	-12.1	0.068607	0.007654	-0.001374	-0.000317	-0.000242	0.004458	17.0	0.15	0.270	0.900
24	-7.0	-12.1	0.060242	0.007002	-0.001329	-0.000281	-0.000224	0.004072	16.5	0.15	0.270	0.901
25	-7.0	-12.1	0.078066	0.008292	-0.001473	-0.000359	-0.000386	0.004914	17.5	0.15	0.271	0.898
26	-8.0	-14.1	0.058392	0.009050	-0.001354	-0.000501	-0.000145	0.004618	17.5	0.35	0.272	0.901
27	-8.0	-15.1	0.053097	0.008906	-0.001399	-0.000495	-0.000140	0.004452	17.5	0.45	0.271	0.904
28	-9.0	-16.1	0.048024	0.008864	-0.001313	-0.000533	-0.000216	0.004359	17.5	0.45	0.271	0.902
29	-9.0	-13.8	0.063446	0.009130	-0.000433	-0.000601	-0.000402	0.004719	17.5	-0.60	0.271	0.901
30	-9.0	-12.8	0.072598	0.008736	-0.000308	-0.000619	-0.000508	0.004857	17.5	-0.45	0.269	0.904
31	-9.0	-11.8	0.082280	0.008238	-0.000331	-0.000585	-0.000569	0.005049	17.5	-0.45	0.270	0.902
32	-8.0	-10.8	0.088077	0.007250	-0.000288	-0.000474	-0.000577	0.005038	17.5	-0.45	0.269	0.904
33	-8.0	-12.8	0.069151	0.008831	-0.000780	-0.000531	-0.000255	0.004823	17.5	-0.10	0.272	0.902

TABLE V-10. CONT'D. 48-FOOT TAPERED-TIP BLADES, $\mu = 0.27$, $M_{(1.0,\ 90.)} = 0.90$

Test 288.0 Run 18

PT	α_S	α_C	C_L/σ	C_D/σ	C_Y/σ	C_ℓ/σ	C_m/σ	C_Q/σ	θ_o	A_{1S}	μ	$M_{(1.0,90.)}$
1	-8.0	-13.0	0.070915	0.009532	-0.001214	-0.000456	-0.000215	0.004672	16.5	0.35	0.239	0.873
	-8.0	-13.3	0.070917	0.008669	-0.000832	-0.000588	-0.000398	0.005215	17.25	0.0	0.272	0.895
3	-8.0	-13.7	0.077999	0.009878	-0.000967	-0.000721	-0.000425	0.005826	18.00	0.0	0.272	0.894
4	-8.0	-13.8	0.079988	0.010040	-0.001031	-0.000744	-0.000632	0.006302	18.25	0.0	0.273	0.891
5	-9.0	-14.8	0.075146	0.010599	-0.000951	-0.000856	-0.000525	0.006277	18.25	0.15	0.273	0.892
6	-9.0	-15.1	0.077747	0.011610	-0.000851	-0.000884	-0.000436	0.006695	18.75	0.15	0.271	0.896
7	-9.0	-13.8	0.063721	0.008490	-0.000550	-0.000625	-0.000402	0.005218	17.00	0.25	0.273	0.890
8	-8.0	-12.6	0.061590	0.007046	-0.000879	-0.000452	-0.000461	0.004641	16.00	0.10	0.272	0.892
9	-7.0	-11.6	0.067114	0.006578	-0.001028	-0.000349	-0.000395	0.004643	16.00	-0.10	0.273	0.892
10	-7.0	-11.0	0.057754	0.005232	-0.000809	-0.000259	-0.000393	0.003997	15.50	-0.10	0.272	0.892
11	-7.0	-12.4	0.076880	0.008063	-0.001249	-0.000463	-0.000466	0.005370	17.00	0.15	0.274	0.890

TABLE V-11. 48-FOOT TAPERED-TIP BLADES, $\mu = 0.30$, $M_{(1.0,\ 90.)} = 0.79$

Test 288.0 Run 7

PT	α_S	α_C	C_L/σ	C_D/σ	C_Y/σ	C_ℓ/σ	C_m/σ	C_Q/σ	θ_o	A_{1S}	μ	$M_{(1.0,90.)}$
14	-5.0	-8.4	0.051042	0.002568	-0.001276	0.000074	-0.001055	0.002799	14.0	-0.45	0.298	0.790
15	-5.0	-10.0	0.069612	0.004637	-0.001616	-0.000009	-0.001229	0.003850	16.0	-0.10	0.300	0.788
16	-5.0	-11.7	0.083975	0.006965	-0.002005	-0.000066	0.000475	0.005119	18.0	0.25	0.298	0.790
17	-10.0	-14.1	0.041437	0.005676	-0.000734	-0.000403	-0.001072	0.003689	16.0	-0.70	0.299	0.787
18	-10.0	-15.4	0.060330	0.009626	-0.000829	-0.000664	-0.001308	0.005212	18.0	-0.45	0.300	0.786
19	-10.0	-12.5	0.024051	0.002354	-0.000851	-0.000148	-0.000851	0.002502	14.0	-0.70	0.298	0.786
20	-10.0	-11.0	0.005556	-0.000825	-0.000783	-0.000087	-0.000559	0.001460	12.0	-0.70	0.297	0.789
21	-15.0	-18.2	0.017512	0.002733	-0.000712	-0.000497	-0.000837	0.002596	16.0	-0.60	0.299	0.788
22	-15.0	-19.3	0.034167	0.007581	-0.000511	-0.000848	-0.001018	0.004228	18.0	-0.80	0.300	0.788
23	-15.0	-20.9	0.050058	0.012464	-0.000577	-0.001292	-0.001320	0.005888	20.0	-0.45	0.300	0.786
24	-5.0	-6.9	0.030671	0.000862	-0.000943	0.000094	-0.000838	0.002030	12.0	-0.60	0.299	0.788
25	-5.0	-5.6	0.012428	-0.000611	-0.000849	0.000075	-0.000655	0.001498	10.0	-0.70	0.296	0.790
26	0.0	-1.5	0.040323	-0.001729	-0.001402	0.000250	-0.000789	0.001265	10.0	-0.70	0.299	0.788
27	0.0	-2.8	0.059234	-0.001814	-0.001919	0.000384	-0.001146	0.001558	12.0	-0.60	0.297	0.791
28	0.0	-4.5	0.078254	-0.001343	-0.002413	0.000440	-0.001197	0.002139	14.0	0.15	0.299	0.789
29	0.0	-6.4	0.094102	-0.000070	-0.002997	0.000428	-0.001402	0.003168	16.0	0.45	0.299	0.789
30	0.0	-0.3	0.019694	-0.001579	-0.001315	0.000192	-0.000589	0.001205	8.0	-0.60	0.297	0.792
31	4.0	3.4	0.042841	-0.004535	-0.002352	0.000482	-0.000721	0.000380	8.0	-0.10	0.297	0.791
32	4.0	1.8	0.061487	-0.005792	-0.002753	0.000535	-0.000950	0.000286	10.0	0.0	0.298	0.789
33	4.0	0.2	0.080812	-0.006906	-0.003299	0.000555	-0.001244	0.000494	12.0	0.35	0.298	0.789
34	4.0	-1.6	0.096365	-0.006799	-0.003751	0.000715	-0.001163	0.001163	14.0	0.60	0.300	0.786

TABLE V-12. 48-FOOT TAPERED-TIP BLADES, $\mu = 0.30$, $M_{(1.0,\ 90.)} = 0.85$

Test 288.0 Run 3

PT	α_S	α_C	C_L/σ	C_D/σ	C_Y/σ	C_{ℓ}/σ	C_m/σ	C_Q/σ	θ_o	A_{1S}	μ	$M_{(1.0,90.)}$
1	-5.0	-7.3	0.029615	0.001078	-0.001282	0.000380	-0.000334	0.002062	12.0	-0.95	0.302	0.848
2	-5.0	-8.7	0.048920	0.002887	-0.001518	0.000359	-0.000430	0.002843	14.0	-0.60	0.302	0.848
3	-5.0	-10.3	0.067184	0.005046	-0.001743	0.000265	-0.000415	0.003836	16.0	-0.45	0.301	0.852
4	-5.0	-12.0	0.084405	0.007658	-0.001996	0.000063	-0.000319	0.005237	18.0	-0.25	0.304	0.844
5	-7.0	-13.6	0.073726	0.008862	-0.001443	-0.000263	-0.000327	0.005302	18.0	-0.35	0.302	0.848
6	-12.0	-17.2	0.048236	0.009409	-0.000319	-0.000807	-0.000379	0.004811	18.0	-0.95	0.302	0.848
7	-10.0	-15.6	0.057903	0.010732	-0.000621	-0.000571	-0.000347	0.005053	18.0	-0.70	0.303	0.846
8	-10.0	-16.6	0.066472	0.011672	-0.000599	-0.000731	-0.000328	0.005890	19.0	-0.70	0.302	0.848
9	-8.0	-15.0	0.074956	0.011075	-0.000899	-0.000574	-0.000233	0.005943	19.0	-0.45	0.303	0.847
10	-6.0	-13.5	0.085678	0.009954	-0.001652	-0.000285	-0.000276	0.005923	19.0	-0.25	0.303	0.846
11	-7.0	-14.4	0.081135	0.010534	-0.001227	-0.000488	-0.000404	0.005948	19.0	-0.35	0.303	0.846
12	-7.0	-10.1	0.037511	0.003332	-0.000888	0.000059	-0.000419	0.002708	14.0	-0.80	0.303	0.846
13	-7.0	-8.5	0.019135	0.000972	-0.000895	0.000170	-0.000288	0.001883	12.0	-1.05	0.303	0.846
14	-7.0	-7.2	0.001754	-0.001026	-0.000771	0.000057	-0.000508	0.001205	10.0	-0.80	0.303	0.846
15	-7.0	-7.2	0.002315	-0.001203	-0.000864	0.000176	-0.000566	0.001261	10.0	-0.95	0.304	0.844
16	-3.0	-2.8	0.003543	-0.000988	-0.001381	0.000329	-0.000468	0.001328	8.0	-0.95	0.303	0.847
17	-3.0	-1.4	0.015453	-0.001743	-0.001444	0.000339	-0.000434	0.001247	6.0	-0.70	0.302	0.848
18	-3.0	-8.8	0.077304	0.003725	-0.002054	0.000280	-0.000355	0.003690	16.0	-0.35	0.303	0.846
19	-3.0	-10.6	0.092614	0.005961	-0.002367	0.000178	-0.000330	0.005048	18.0	0.0	0.305	0.843
20	0.0	-6.5	0.091997	0.000460	-0.003254	0.000647	-0.000524	0.003244	16.0	0.0	0.303	0.846
21	0.0	-7.7	0.096586	0.001739	-0.003494	0.000568	-0.000490	0.004078	17.0	0.35	0.304	0.845
22	0.0	-2.9	0.056426	-0.001257	-0.002227	0.000668	-0.000322	0.001600	12.0	-0.70	0.304	0.843
23	3.0	-1.7	0.073508	-0.004801	-0.003199	0.000902	-0.000413	0.000870	12.0	-0.25	0.304	0.843
24	3.0	0.8	0.053559	-0.004026	-0.002717	0.000829	-0.000404	0.000695	10.0	-0.60	0.303	0.847
25	3.0	2.2	0.034665	-0.003034	-0.002469	0.000807	-0.000321	0.000770	8.0	-0.70	0.304	0.844
26	3.0	3.6	0.016667	-0.001996	-0.002354	0.000791	-0.000312	0.001041	6.0	-0.70	0.305	0.843
27	3.0	-2.4	0.089094	-0.004410	-0.003860	0.000977	-0.000439	0.001500	14.0	0.25	0.303	0.846
28	3.0	-4.5	0.099900	-0.002802	-0.004146	0.000897	-0.000413	0.003114	16.0	0.35	0.302	0.848

Test 274.0 Run 4

PT	α_S	α_C	C_L/σ	C_D/σ	C_Y/σ	C_{ℓ}/σ	C_m/σ	C_Q/σ	θ_o	A_{1S}	μ	$M_{(1.0,90.)}$
4	0.	-3.5	0.059190	0.001435	-0.001826	0.000285	0.000160	0.001484	12.0	-00.48	0.301	0.844
5	0.	-1.8	0.039510	-0.001653	-0.001357	0.000202	0.000087	0.001138	10.0	-00.24	0.300	0.846
6	0.	-0.3	0.020436	-0.001560	-0.001003	0.000125	-0.000121	0.001070	8.0	-00.24	0.301	0.846
7	0.	-5.0	0.081876	-0.001117	-0.002625	0.000352	0.000175	0.002198	14.0	-00.72	0.299	0.844
8	-5.0	-7.3	0.032134	0.001139	-0.000506	-0.000055	-0.000216	0.001901	12.0	00.00	0.300	0.846
9	-5.0	-5.7	0.013562	-0.000544	-0.000300	-0.000060	-0.000584	0.001323	10.0	00.00	0.299	0.845
10	-5.0	-9.0	0.053802	0.003226	-0.000999	-0.000146	-0.000275	0.002846	14.0	-00.36	0.301	0.846

TABLE V-12. CONT'D. 48-FOOT TAPERED-TIP BLADES, $\mu = 0.30$, $M_{(1.0,\ 90.)} = 0.85$

Test 274.0 Run 5

PT	α_S	α_C	C_L/σ	C_D/σ	C_Y/σ	$C_{\mathcal{L}}/\sigma$	$C_{\mathcal{M}}/\sigma$	C_Q/σ	θ_o	A_{1S}	μ	$M_{(1.0,90.)}$
1	-10.0	-11.5	0.005116	-0.000888	0.000143	-0.000114	-0.000313	0.001221	12.0	00.36	0.302	0.840
2	-10.0	-13.2	0.024908	0.002787	0.000097	-0.000301	-0.000265	0.002380	14.0	00.24	0.307	0.832
3	-10.0	-14.8	0.043469	0.006517	-0.000114	-0.000566	-0.000260	0.003729	16.0	00.12	0.305	0.840
4	-10.0	-16.5	0.061462	0.010515	-0.000027	-0.000958	-0.000267	0.005269	18.0	00.00	0.305	0.843
5	-15.0	-18.5	0.017667	0.002996	0.000667	-0.000603	-0.000057	0.002330	16.0	00.36	0.303	0.843
6	-15.0	-20.1	0.035202	0.008330	0.000709	-0.001114	-0.000140	0.004078	18.0	00.24	0.306	0.840
7	-15.0	-18.0	0.008361	0.000371	0.000649	-0.000430	-0.000026	0.001569	15.0	00.60	0.304	0.838
8	-15.0	-17.1	0.000482	-0.001823	0.000493	-0.000156	-0.000092	0.000945	14.0	00.48	0.303	0.841
9	-5.0	-9.2	0.051513	0.003350	-0.000788	-0.000176	-0.000548	0.002364	14.0	-00.24	0.304	0.843
10	-5.0	-10.8	0.071583	0.005714	-0.001290	-0.000264	-0.000243	0.004018	16.0	-00.36	0.303	0.842
11	-5.0	-4.7	-0.007860	-0.002290	-0.000345	0.000049	-0.000138	0.000972	8.0	+00.12	0.303	0.841
12	0.	0.6	0.002054	-0.001331	-0.000775	0.000160	-0.000348	0.001230	6.0	00.00	0.301	0.844
13	5.0	5.0	0.031660	-0.004408	-0.001495	0.000101	-0.000297	0.000411	6.0	-00.24	0.301	0.843
14	5.0	3.6	0.050579	-0.006231	-0.002015	0.000146	-0.000269	0.000008	8.0	-00.48	0.300	0.843
15	5.0	1.7	0.069030	-0.007278	-0.002754	0.000245	-0.000334	0.000082	10.0	-00.72	0.301	0.844
16	5.0	0.1	0.088125	-0.008285	-0.003399	0.000384	-0.000298	0.000357	12.0	-00.84	0.301	0.841
17	4.0	-0.5	0.084094	-0.006820	-0.003276	[illegible]	-0.000352	0.000608	12.0	00.96	0.303	0.839
18	3.0	-1.3	0.078559	-0.005126	-0.002807	0.000279	-0.000308	0.000659	12.0	-00.72	0.304	0.840
19	0.	-3.6	0.061509	-0.001393	-0.001794	0.000199	-0.000351	0.001580	12.0	-00.48	0.306	0.836
20	-5.0	-7.5	0.031405	0.001215	-0.000470	-0.000041	-0.000280	0.001997	12.0	00.00	0.303	0.842
21	-10.0	-11.4	0.007824	-0.000553	0.000098	-0.000129	-0.000219	0.001360	12.0	00.12	0.301	0.844

Test 274.0 Run 11

PT	α_S	α_C	C_L/σ	C_D/σ	C_Y/σ	$C_{\mathcal{L}}/\sigma$	$C_{\mathcal{M}}/\sigma$	C_Q/σ	θ_o	A_{1S}	μ	$M_{(1.0,90.)}$
1	-5.0	-8.5	0.049827	0.002534	-0.000943	-0.000047	-0.000368	0.003027	14.0	-0.12	0.299	0.949
2	-10.0	-12.6	0.023865	0.002088	0.000135	-0.000273	-0.000372	0.002547	14.0	0.60	0.298	0.951
3	-10.0	-14.0	0.042665	0.005569	0.000077	-0.000537	-0.000625	0.003798	16.0	0.24	0.299	0.950
4	-15.0	-18.0	0.017089	0.002499	0.000295	-0.000386	-0.000295	0.002530	16.0	0.48	0.298	0.950
5	-15.0	-18.9	0.024906	0.004800	0.000512	-0.000757	-0.000324	0.003305	17.0	0.60	0.300	0.949
6	-15.0	-17.3	0.008598	0.000173	0.000326	-0.000216	-0.000430	0.001854	15.0	0.48	0.299	0.949
7	-10.0	-12.0	0.014639	0.000388	0.000165	-0.000119	-0.000642	0.001986	13.0	0.48	0.298	0.950
8	-10.0	-13.2	0.033404	0.003815	0.000175	-0.000411	-0.000761	0.003169	15.0	0.48	0.298	0.953
9	-5.0	-7.7	0.039998	0.001423	-0.000725	-0.000006	-0.000795	0.002558	13.0	0.00	0.298	0.951
10	-5.0	-7.0	0.030174	0.000569	-0.000472	0.000021	-0.000827	0.002221	12.0	0.12	0.298	0.950
11	-5.0	-6.3	0.021508	-0.000154	-0.000371	0.000070	-0.000767	0.001884	11.0	0.24	0.298	0.950
12	0.	-3.0	0.059723	-0.001880	-0.001855	0.000341	-0.000913	0.001823	12.0	-0.24	0.297	0.951
13	0.	-2.2	0.048358	-0.002028	-0.001486	0.000240	-0.000546	0.001607	11.0	-0.24	0.298	0.949
14	0.	-1.5	0.039922	-0.002078	-0.001426	0.000311	-0.000641	[illegible]	10.0	-0.12	0.299	0.951
15	0.	-0.9	0.030999	-0.002015	-0.001110	0.000217	-0.000628	[illegible]	9.0	-0.00	0.299	0.951
16	5.0	3.2	0.058853	-0.007322	-0.002363	0.000358	-0.000824	0.000286	9.0	-0.36	0.297	0.949

Test 274.0 Run 14

PT	α_S	α_C	C_L/σ	C_D/σ	C_Y/σ	$C_{\mathcal{L}}/\sigma$	$C_{\mathcal{M}}/\sigma$	C_Q/σ	θ_o	A_{1S}	μ	$M_{(1.0,90.)}$
1	-5.0	-7.8	0.028863	0.001134	-0.000422	-0.000034	-0.000585	0.001923	12.0	0.36	0.301	0.844
2	-5.0	-9.5	0.048316	0.003552	-0.000505	-0.000050	-0.000688	0.002836	14.0	0.36	0.301	0.846

TABLE V-12. CONT'D. 48-FOOT TAPERED-TIP BLADES, $\mu = 0.30$, $M_{(1.0,\ 90.)} = 0.85$

Test 274.0 Run 15

PT.	α_S	α_C	C_L/σ	C_D/σ	C_Y/σ	C_{ℓ}/σ	C_m/σ	C_Q/σ	θ_o	A_{1S}	μ	$M_{(1.0,90.)}$
1	-5.0	-7.9	0.027365	0.001023	-0.000201	-0.000256	-0.000753	0.002085	12.0	0.24	0.300	0.848
2	-5.0	-9.5	0.047940	0.003276	-0.000365	-0.000394	-0.000564	0.002955	14.0	0.24	0.300	0.848
3	-5.0	-11.1	0.066284	0.005699	-0.000580	-0.000506	-0.000406	0.004056	16.0	0.12	0.299	0.849
4	-5.0	-11.8	0.076953	0.007015	-0.000898	-0.000668	-0.000479	0.004752	17.0	-0.12	0.300	0.850
5	-3.0	-5.9	0.038909	0.000752	-0.000232	-0.000291	-0.000615	0.002037	12.0	0.36	0.300	0.849
6	-3.0	-6.8	0.049474	0.001529	-0.000398	-0.000247	-0.000668	0.002436	13.0	0.48	0.300	0.848
7	-3.0	-7.7	0.059786	0.002325	-0.000830	-0.000273	-0.000471	0.002850	14.0	-0.00	0.300	0.848
8	-3.0	-8.7	0.067131	0.003478	-0.000982	-0.000303	-0.000460	0.003358	15.0	-0.00	0.300	0.848
9	-3.0	-9.4	0.077887	0.004224	-0.001091	-0.000401	-0.000571	0.003916	16.0	-0.12	0.300	0.849
10	-3.0	-9.8	0.080970	0.004712	-0.001056	-0.000491	-0.000570	0.004170	16.5	0.00	0.301	0.849
11	-3.0	-10.2	0.086136	0.005270	-0.001145	-0.000411	-0.000525	0.004537	17.0	-0.12	0.301	0.849
12	0.	-3.5	0.055484	-0.001005	-0.001015	-0.000082	-0.000510	0.001763	12.0	0.12	0.300	0.848
13	0.	-4.5	0.068285	-0.000863	-0.001380	-0.000120	-0.000501	0.002068	13.0	-0.12	0.300	0.847
14	0.	-5.5	0.076500	-0.000167	-0.001594	-0.000180	-0.000432	0.002420	14.0	-0.24	0.299	0.850
15	0.	-6.2	0.085340	0.000065	-0.001859	-0.000222	-0.000229	0.002885	15.0	-0.36	0.299	0.850
16	0.	-6.5	0.089211	0.000299	-0.002016	-0.000192	-0.000195	0.003171	15.5	-0.36	0.299	0.850
17	0.	-7.5	0.088459	0.001160	-0.002220	-0.000248	0.001662	0.003609	16.0	-0.48	0.300	0.851

TABLE V-13. 48-FOOT TAPERED-TIP BLADES, $\mu = 0.30$, $M_{(1.0,\ 90.)} = 0.95$

Test 288.0 Run 8

1	-5.0	-7.8	0.049643	0.002083	-0.001365	0.000120	-0.000400	0.003044	14.0	-0.35	0.297	0.952
2	-5.0	-6.5	0.031727	0.000432	-0.001188	0.000260	-0.000411	0.002413	12.0	-0.60	0.300	0.953
3	-5.0	-9.2	0.067771	0.003868	-0.001843	0.000083	-0.000422	0.004109	16.0	-0.25	0.300	0.953
4	-5.0	-10.2	0.075513	0.005012	-0.002260	0.000101	-0.000431	0.004774	17.0	0.0	0.300	0.951
5	-5.0	-10.8	0.083909	0.006477	-0.002516	0.000161	-0.000503	0.005633	18.0	0.15	0.300	0.950
6	-10.0	-13.3	0.040517	0.004937	-0.000655	-0.000317	-0.000534	0.003784	16.0	-0.80	0.299	0.952
7	-10.0	-14.8	0.056855	0.008451	-0.000808	-0.000598	-0.000608	0.005304	18.0	-0.45	0.300	0.952
8	-10.0	-14.1	0.049353	0.006779	-0.000641	-0.000469	-0.000533	0.004574	17.0	-0.70	0.301	0.948
9	-15.0	-17.6	0.017051	0.002301	-0.000505	-0.000399	-0.000407	0.002769	16.0	-1.05	0.299	0.948
10	-15.0	-18.8	0.033473	0.006913	-0.000349	-0.000868	-0.000436	0.004328	18.0	-0.95	0.301	0.948
11	-15.0	-19.4	0.041103	0.009203	-0.000262	-0.001092	-0.000455	0.005129	19.0	-0.95	0.300	0.951
12	-17.0	-20.5	0.022761	0.004843	-0.000102	-0.000825	-0.000250	0.003521	18.0	-1.15	0.299	0.950
13	-17.0	-21.1	0.028974	0.006998	0.000119	-0.001116	-0.000374	0.004181	19.0	-1.05	0.300	0.950
14	-17.0	-21.5	0.037228	0.009667	0.000123	-0.001422	-0.000489	0.005098	20.0	-0.95	0.300	0.950
15	-17.0	-20.0	0.015199	0.002473	-0.000301	-0.000637	-0.000268	0.002751	17.0	-1.15	0.298	0.949
16	-17.0	-19.3	0.007663	0.000048	-0.000529	-0.000230	-0.000280	0.002109	16.0	-1.05	0.298	0.948

TABLE V-13. CONT'D. 48-FOOT TAPERED-TIP BLADES, μ = 0.30, $M_{(1.0,\ 90.)}$ = 0.95

Test 274.0 Run 15

PT.	α_S	α_C	C_L/σ	C_D/σ	C_Y/σ	$C_{\mathcal{L}}/\sigma$	$C_{\mathcal{M}}/\sigma$	C_Q/σ	θ_o	A_{1S}	μ	$M_{(1.0,90.)}$
18	-5.0	-8.7	0.049546	0.002717	-0.000641	-0.000306	-0.000559	0.003091	14.0	-0.12	0.298	0.947
19	-5.0	-9.3	0.060165	0.003738	-0.000761	-0.000383	-0.000562	0.003730	15.0	0.12	0.299	0.951
20	-5.0	-10.0	0.069405	0.004787	-0.000935	-0.000490	-0.000714	0.004318	16.0	-0.00	0.299	0.950
21	-5.0	-10.2	0.073377	0.005314	-0.000957	-0.000490	-0.000571	0.004641	16.5	-0.00	0.299	0.948
22	-3.0	-5.2	0.041884	0.000282	-0.000540	-0.000274	-0.000436	0.002306	12.0	0.12	0.298	0.949
23	-3.0	-6.0	0.052528	0.000930	-0.000779	-0.000245	-0.000395	0.002720	13.0	0.12	0.297	0.951
24	-3.0	-7.0	0.061069	0.001752	-0.001010	-0.000242	-0.000358	0.003124	14.0	-0.00	0.297	0.951
25	-3.0	-7.5	0.069888	0.002348	-0.001302	-0.000354	-0.000078	0.003599	15.0	-0.12	0.297	0.951
26	0.	-3.0	0.057761	-0.001666	-0.001317	0.000015	-0.000509	0.001968	12.0	-0.00	0.297	0.949
27	0.	-3.5	0.070441	-0.001733	-0.001393	-0.000142	-0.000354	0.002247	13.0	-0.00	0.297	0.948
28	0.	-4.2	0.072013	-0.001136	-0.001709	-0.000139	-0.000011	0.002514	13.5	-0.24	0.298	0.949
29	0.	-4.5	0.078514	-0.001281	-0.001848	-0.000120	-0.000176	0.002761	14.0	-0.12	0.298	0.950
30	0.	-4.7	0.083275	-0.001057	-0.002033	-0.000131	-0.000114	0.003057	14.5	-0.24	0.297	0.952

TABLE V-14. 48-FOOT TAPERED-TIP BLADES, μ = 0.30, $M_{(1.0,\ 90.)}$ = 1.0

Test 288.0 Run 11

1	-5.0	-6.1	0.032471	-0.000348	-0.001252	0.000168	-0.000477	0.002870	12.0	-0.80	0.309	0.990
2	-6.0	-6.9	0.026653	-0.000282	-0.001064	0.000165	-0.000500	0.002857	12.0	-0.80	0.309	0.989
3	-6.0	-7.2	0.035456	0.000491	-0.001079	0.000057	-0.000547	0.003216	13.0	-0.60	0.308	0.992
4	-6.0	-7.9	0.045178	0.001292	-0.001303	0.000067	-0.000820	0.003626	14.0	-0.45	0.310	0.989
5	-6.0	-8.6	0.053029	0.002146	-0.001232	-0.000075	-0.000894	0.004182	15.0	-0.45	0.310	0.991
6	-6.0	-9.5	0.060671	0.003230	-0.001512	-0.000079	-0.000802	0.004711	16.0	-0.35	0.310	0.989
7	-9.0	-10.6	0.029126	0.001277	-0.000692	-0.000161	-0.000669	0.003415	14.0	-0.80	0.309	0.990
8	-9.0	-11.2	0.037116	0.002580	-0.000648	-0.000282	-0.000707	0.003940	15.0	-0.80	0.310	0.990
9	-9.0	-11.8	0.046723	0.003991	-0.000773	-0.000374	-0.000844	0.004601	16.0	-0.70	0.309	0.992
10	-9.0	-12.5	0.055362	0.005366	-0.000870	-0.000416	-0.001114	0.005302	17.0	-0.60	0.310	0.991
11	-12.0	-13.8	0.022260	0.001529	-0.000591	-0.000376	-0.000627	0.003402	15.0	-0.95	0.308	0.992
12	-12.0	-14.3	0.030262	0.003301	-0.000534	-0.000493	-0.000696	0.003974	16.0	-0.95	0.309	0.990
13	-12.0	-15.0	0.039036	0.005051	-0.000547	-0.000672	-0.000811	0.004819	17.0	-0.80	0.309	0.993
14	-12.0	-13.2	0.013491	-0.000154	-0.000576	-0.000282	-0.000418	0.002845	14.0	-1.05	0.308	0.990
15	-9.0	-9.9	0.020624	0.000150	-0.000567	-0.000169	-0.000632	0.002926	13.0	-1.05	0.307	0.991
16	-3.0	-6.7	0.052676	-0.000639	-0.001710	0.000281	-0.000713	0.003062	13.0	-0.45	0.308	0.991
17	-3.0	-4.7	0.054202	-0.000924	-0.001690	0.000312	-0.000808	0.003355	13.0	-0.45	0.304	1.002
18	-6.0	-7.2	0.038219	0.000291	-0.000987	0.000024	-0.000698	0.003461	13.0	-0.60	0.304	1.002
19	-6.0	-7.7	0.046604	0.001107	-0.001026	-0.000067	-0.000767	0.003866	14.0	-0.45	0.305	1.000
20	-6.0	-8.5	0.054744	0.001993	-0.001240	-0.000066	-0.000832	0.004425	15.0	-0.25	0.305	1.002
21	-6.0	-9.2	0.062730	0.003023	-0.001423	0.000065	-0.000491	0.004965	16.0	-0.10	0.305	1.000
22	-9.0	-11.8	0.047482	0.003988	-0.000623	-0.000445	-0.000664	0.004805	16.0	-0.45	0.304	1.002
23	-9.0	-11.1	0.039178	0.002597	-0.000481	-0.000368	-0.000699	0.004174	15.0	-0.80	0.304	1.002
24	-9.0	-10.4	0.029298	0.001196	-0.000414	-0.000316	-0.000542	0.003519	14.0	-0.80	0.305	0.999
25	-9.0	-9.8	0.022933	0.000131	-0.000338	-0.000301	-0.000567	0.003134	13.0	-0.80	0.304	1.000
26	-6.0	-7.1	0.038329	0.000282	-0.000872	-0.000048	-0.000687	0.003516	13.0	-0.60	0.303	1.004

TABLE V-14. CONT'D. 48-FOOT TAPERED-TIP BLADES, $\mu = 0.30$, $M_{(1.0,\ 90.)} = 1.0$

Test 274.0 Run 12

PT.	α_S	α_C	C_L/σ	C_D/σ	C_Y/σ	C_{ℓ}/σ	C_m/σ	C_Q/σ	θ_o	A_{1S}	μ	$M_{(1.0,90.)}$
1	0.	-2.8	0.059227	-0.002587	-0.001402	0.000161	-0.000547	0.002381	12.0	0.00	0.301	0.994
2	0.	-2.8	0.063700	-0.002655	-0.001565	0.000207	-0.000613	0.002462	12.5	0.00	0.302	0.990
3	-1.0	-3.8	0.052312	-0.001661	-0.001260	0.000171	-0.000515	0.002512	12.0	0.24	0.302	0.989
4	-2.0	-4.5	0.046231	-0.000865	-0.001006	0.000096	-0.000387	0.002616	12.0	0.12	0.303	0.989
5	-3.0	-5.3	0.040948	-0.000397	-0.000751	0.000008	-0.000323	0.002637	12.0	0.24	0.303	0.988
6	-4.0	-6.2	0.034551	-0.000148	-0.000635	0.000005	-0.000413	0.002695	12.0	0.24	0.304	0.987
7	-5.0	-6.9	0.030143	-0.000023	-0.000465	-0.000057	-0.000328	0.002676	12.0	0.36	0.304	0.988
8	-6.0	-7.8	0.025232	-0.000126	-0.000254	-0.000136	-0.000499	0.002617	12.0	0.36	0.304	0.987
9	-6.0	-8.1	0.030834	0.000566	-0.000184	-0.000185	-0.000305	0.002796	12.5	0.48	0.305	0.987
10	-6.0	-8.4	0.035733	0.001040	-0.000276	-0.000138	-0.000426	0.003027	13.0	0.48	0.305	0.986
11	-6.0	-9.0	0.044562	0.002002	-0.000350	-0.000209	-0.000559	0.003530	14.0	0.48	0.306	0.986
12	-6.0	-9.5	0.054968	0.002906	-0.000487	-0.000335	-0.000609	0.004274	15.0	0.12	0.301	0.996
13	-7.0	-9.0	0.030972	0.000788	-0.000127	-0.000259	-0.000496	0.003162	13.0	0.48	0.301	0.996
14	-7.0	-9.7	0.040470	0.002024	-0.000136	-0.000271	-0.000594	0.003598	14.0	0.48	0.301	0.995
15	-9.0	-11.3	0.030289	0.001799	0.000065	-0.000390	-0.000462	0.003381	14.0	0.60	0.302	0.995
16	-9.0	-12.0	0.038256	0.003246	0.000177	-0.000499	-0.000595	0.003844	15.0	0.60	0.302	0.994
17	-9.0	-10.6	0.020039	0.000132	0.000147	-0.000276	-0.000397	0.002836	13.0	0.72	0.301	0.993
18	-9.0	-10.1	0.011824	-0.001142	0.000065	-0.000223	-0.000412	0.002409	12.0	0.72	0.301	0.993
19	-6.0	-6.7	0.017183	-0.001082	-0.000238	-0.000067	-0.000359	0.002448	11.0	0.48	0.301	0.993
20	-6.0	-6.3	0.009154	-0.001924	-0.000268	0.000023	-0.000371	0.002220	10.0	0.60	0.300	0.995
21	-3.0	-5.6	0.052279	0.000066	-0.000897	0.000013	-0.000630	0.003098	13.0	0.12	0.302	0.990
22	-3.0	-4.9	0.042503	-0.000640	-0.000766	-0.000007	-0.000426	0.002861	12.0	0.24	0.303	0.994
23	-3.0	-4.2	0.032503	-0.001096	-0.000587	-0.000003	-0.000330	0.002576	11.0	0.24	0.299	0.997
24	-3.0	-3.5	0.023706	-0.001576	-0.000520	0.000050	-0.000422	0.002415	10.0	0.36	0.299	0.997
25	0.	-1.6	0.050257	-0.002989	-0.001257	0.000229	-0.000706	0.002329	11.0	0.00	0.299	0.996
26	0.	-1.0	0.040680	-0.003010	-0.000951	0.000159	-0.000475	0.002145	10.0	0.24	0.297	0.999

TABLE V-15. 48-FOOT TAPERED-TIP BLADES, $\mu = 0.35$, $M_{(1.0,\ 90.)} = 0.85$

Test 288.0 Run 4

PT.	α_S	α_C	C_L/σ	C_D/σ	C_Y/σ	C_{ℓ}/σ	C_m/σ	C_Q/σ	θ_o	A_{1S}	μ	$M_{(1.0,90.)}$
1	-5.0	-7.6	0.023610	0.003516	-0.000707	0.000124	-0.000444	0.001898	12.0	-0.60	0.347	0.849
2	-5.0	-6.1	0.007668	-0.000897	-0.000589	0.000122	-0.000394	0.001369	10.0	-1.05	0.346	0.849
3	-5.0	-11.0	0.056771	0.004128	-0.000982	0.000024	-0.000586	0.003675	16.0	-0.80	0.346	0.848
4	-5.0	-13.0	0.071727	0.006495	-0.001353	-0.000147	-0.000661	0.004558	18.0	-0.35	0.350	0.844
5	-5.0	-14.5	0.082621	0.008897	-0.001686	-0.000320	-0.000170	0.006433	20.0	-0.25	0.347	0.848
6	-10.0	-14.7	0.030283	0.003654	-0.000058	-0.000373	-0.000540	0.003073	16.0	-1.05	0.347	0.849
7	-10.0	-16.2	0.045940	0.007054	0.000137	-0.000611	-0.000737	0.004490	18.0	-0.95	0.346	0.851
8	-10.0	-17.8	0.060293	0.010363	-0.000107	-0.000924	-0.000751	0.006030	20.0	-0.70	0.346	0.850
9	-12.0	-16.2	0.020177	0.002349	0.000071	-0.000388	-0.000468	0.002571	16.0	-1.05	0.347	0.848
10	-12.0	-17.7	0.035338	0.006238	0.000111	-0.000730	-0.000591	0.004027	18.0	-1.05	0.347	0.848
11	-12.0	-19.2	0.048421	0.009760	-0.000172	-0.000991	-0.000652	0.005553	20.0	-0.80	0.346	0.850
12	-15.0	-19.9	0.020873	0.003682	0.000031	-0.000651	-0.000376	0.003124	18.0	-1.05	0.346	0.850
13	-15.0	-21.4	0.033549	0.007583	-0.000072	-0.000957	-0.000471	0.004705	20.0	-0.95	0.347	0.846
14	-15.0	-18.4	0.005736	-0.000667	-0.000049	-0.000327	-0.000236	0.001562	16.0	-1.05	0.346	0.849
15	-12.0	-14.5	0.003187	-0.001340	0.000293	-0.000230	-0.000552	0.001207	14.0	-1.15	0.347	0.849
16	0.0	-5.4	0.067680	-0.000392	-0.002576	0.000702	-0.000641	0.002186	14.0	-0.45	0.346	0.850
17	0.0	-7.5	0.082532	0.000561	-0.003145	0.000557	-0.000761	0.003168	16.0	-0.10	0.346	0.849
18	0.0	-9.5	0.091155	0.002701	-0.003595	0.000576	-0.000125	0.004880	18.0	0.0	0.346	0.849
19	0.0	-3.9	0.050050	-0.000953	-0.002197	0.000643	-0.000781	0.001630	12.0	-0.60	0.346	0.848
20	2.0	-2.1	0.061886	-0.002824	-0.003126	0.000876	-0.000813	0.001216	12.0	-0.35	0.346	0.843
21	2.0	-3.0	0.068944	-0.002808	-0.003491	0.000829	-0.000844	0.001396	14.0	-0.25	0.346	0.847
22	2.0	-6.1	0.089849	-0.001365	-0.004242	0.000854	-0.000225	0.003067	16.0	0.15	0.346	0.850
23	2.0	-0.8	0.044836	-0.002526	-0.002663	0.000712	-0.000696	0.001040	10.0	-0.60	0.347	0.847

Test 274.0 Run 6

PT.	α_S	α_C	C_L/σ	C_D/σ	C_Y/σ	C_{ℓ}/σ	C_m/σ	C_Q/σ	θ_o	A_{1S}	μ	$M_{(1.0,90.)}$
1	0.	0.7	0.004132	-0.001650	-0.000938	0.000160	-0.000552	0.001242	6.0	0.24	0.349	0.851
2	0.	-0.6	0.021443	-0.001910	-0.001168	0.000164	-0.000544	0.001163	8.0	0.00	0.350	0.847
3	0.	-2.3	0.038385	-0.001899	-0.001471	0.000211	-0.000850	0.001257	10.0	0.00	0.351	0.845
4	0.	-4.0	0.057006	-0.001767	-0.001930	0.000222	-0.000924	0.001589	12.0	0.00	0.352	0.845
5	0.	-6.0	0.074851	-0.001248	-0.002636	0.000291	-0.000629	0.002261	14.0	-0.36	0.351	0.846
6	-5.0	-6.0	0.008023	-0.001306	-0.000482	0.000110	-0.000672	0.001303	10.0	0.36	0.351	0.847
7	-5.0	-7.6	0.027743	0.000367	-0.000610	-0.000015	-0.000595	0.001930	12.0	0.36	0.352	0.847
8	-5.0	-9.5	0.046127	0.002100	-0.000855	-0.000093	-0.000884	0.002841	14.0	0.12	0.352	0.847
9	-5.0	-11.2	0.061822	0.004097	-0.001180	-0.000207	-0.000391	0.003930	16.0	0.00	0.352	0.849
10	-10.0	-14.6	0.035420	0.004131	0.000016	-0.000491	-0.000295	0.003399	16.0	0.36	0.351	0.848
11	-10.0	-13.0	0.017362	0.000660	0.000147	-0.000277	-0.000387	0.002056	14.0	0.48	0.349	0.850
12	-10.0	-11.4	0.000829	-0.002312	-0.000098	0.000125	-0.000698	0.000977	12.0	0.48	0.349	0.850
13	-15.0	-18.4	0.008389	-0.000282	0.000494	-0.000226	-0.000061	0.001673	16.0	0.60	0.351	0.849
14	-15.0	-20.0	0.024035	0.004364	0.000694	-0.000911	0.000206	0.003457	18.0	0.48	0.353	0.848
15	-10.0	-16.4	0.051504	0.007569	-0.000030	-0.000777	-0.000316	0.004935	18.0	0.36	0.351	0.851
16	2.0	2.1	0.014648	-0.002121	-0.001096	0.000043	-0.000182	0.001127	6.0	0.00	0.351	0.846
17	2.0	1.0	0.032937	-0.002983	-0.001471	0.000178	-0.000372	0.000878	8.0	0.12	0.351	0.847

TABLE V-16. 48-FOOT TAPERED-TIP BLADES, $\mu = 0.35$, $M_{(1.0,\ 90.)} = 0.94$

Test 274.0 Run 9

PT.	α_S	α_C	C_L/σ	C_D/σ	C_Y/σ	C_ℓ/σ	C_m/σ	C_Q/σ	θ_o	A_{1S}	μ	$M_{(1.0,90.)}$
1	-5.0	-9.2	0.043538	0.001350	-0.000615	-0.000130	-0.000641	0.003040	14.0	0.60	0.352	0.942
2	-10.0	-13.0	0.016497	0.000165	0.000255	-0.000231	-0.000548	0.002215	14.0	0.72	0.350	0.943
3	-10.0	-13.8	0.024041	0.001550	0.000283	-0.000335	-0.000541	0.002794	15.0	0.72	0.353	0.938
4	-10.0	-14.5	0.032308	0.003183	0.000450	-0.000579	-0.000615	0.003369	16.0	0.72	0.355	0.935
5	-15.0	-18.2	0.006624	-0.000974	0.000535	-0.000230	-0.000359	0.001859	16.0	0.96	0.350	0.941
6	-5.0	-9.2	0.042150	0.001399	-0.000662	0.000011	-0.000670	0.002949	14.0	0.48	0.354	0.933
7	-5.0	-8.1	0.033208	0.000375	-0.000571	0.000025	-0.000745	0.002598	13.0	0.60	0.354	0.942

Test 274.0 Run 10

PT.	α_S	α_C	C_L/σ	C_D/σ	C_Y/σ	C_ℓ/σ	C_m/σ	C_Q/σ	θ_o	A_{1S}	μ	$M_{(1.0,90.)}$
1	-5.0	-9.2	0.042109	0.001306	-0.000666	-0.000058	-0.000568	0.003084	14.0	0.48	0.351	0.942
2	-5.0	-8.2	0.034130	0.000428	-0.000628	-0.000058	-0.000807	0.002608	13.0	0.36	0.349	0.944
3	-5.0	-7.5	0.024768	-0.000321	-0.000439	0.000029	-0.000935	0.002191	12.0	0.48	0.348	0.945
4	-4.0	-6.7	0.031134	-0.000205	-0.000680	0.000137	-0.000575	0.002216	12.0	0.60	0.351	0.940
5	-3.0	-6.0	0.034878	-0.000334	-0.000871	0.000170	-0.000587	0.002196	12.0	0.36	0.351	0.937
6	0.	-3.7	0.055235	-0.002549	-0.001738	0.000251	-0.000384	0.001811	12.0	0.12	0.354	0.940
7	0.	-2.9	0.046148	-0.002443	-0.001355	0.000274	-0.000453	0.001619	11.0	0.24	0.354	0.939
8	-5.0	-6.6	0.015978	-0.001088	-0.000479	0.000133	-0.000661	0.001877	11.0	0.46	0.355	0.939
9	-10.0	-13.0	0.016179	0.000158	0.000206	-0.000206	-0.000662	0.002270	14.0	0.60	0.354	0.941
10	-10.0	-12.0	0.007322	-0.001427	0.000045	-0.000002	-0.000744	0.001777	13.0	0.60	0.353	0.942

TABLE V-17. 48-FOOT TAPERED-TIP BLADES, $\mu = 0.35$, $M_{(1.0,\ 90.)} = 0.95$

Test 288.0 Run 9

PT.	α_S	α_C	C_L/σ	C_D/σ	C_Y/σ	C_ℓ/σ	C_m/σ	C_Q/σ	θ_o	A_{1S}	μ	$M_{(1.0,90.)}$
1	-3.0	-4.1	0.029508	-0.002273	-0.001621	0.000350	0.000293	0.002054	11.0	-0.70	0.298	0.955
2	-3.0	-3.5	0.024994	-0.001235	-0.001476	0.000303	-0.000612	0.001823	10.0	-0.60	0.300	0.950
3	-3.0	-6.9	0.071268	0.001237	-0.002359	0.000352	-0.000680	0.003386	15.0	-0.25	0.301	0.949
4	-3.0	-7.7	0.077988	0.002069	-0.002457	0.000283	-0.000782	0.003975	16.0	-0.10	0.300	0.951
5	-3.0	-8.5	0.085815	0.003008	-0.002714	0.000381	-0.001020	0.004721	17.0	-0.10	0.299	0.953
6	-3.0	-9.2	0.091049	0.004339	-0.003180	0.000287	-0.000729	0.005621	18.0	0.25	0.298	0.955
7	-5.0	-9.8	0.077569	0.004590	-0.002358	0.000066	-0.000885	0.004824	17.0	0.0	0.301	0.952
8	-5.0	-10.5	0.085415	0.005816	-0.002566	-0.000180	-0.000827	0.005638	18.0	0.15	0.300	0.953
9	2.0	1.0	0.051624	-0.004649	-0.002470	0.000557	-0.000416	0.001124	10.0	-0.35	0.298	0.950
10	2.0	1.5	0.044324	-0.004591	-0.002435	0.000609	-0.000410	0.001064	9.0	-0.45	0.301	0.951
11	0.0	-4.3	0.086850	-0.002286	-0.003234	0.000541	-0.000263	0.003007	15.0	0.0	0.302	0.951
12	0.0	-5.2	0.092140	-0.001200	-0.003460	0.000693	-0.000096	0.003839	16.0	0.15	0.301	0.954
13	0.0	-5.9	0.097581	-0.000703	-0.003371	0.000511	-0.000211	0.004874	17.0	0.35	0.300	0.953
14	5.0	4.1	0.060643	-0.008553	-0.003250	0.000722	-0.000626	0.000158	9.0	-0.25	0.300	0.947
15	5.0	3.4	0.071095	-0.009384	-0.003476	0.000771	-0.000136	0.000233	10.0	-0.25	0.299	0.950
16	5.0	1.7	0.085233	-0.009764	-0.003889	0.000926	-0.000268	0.000730	12.0	0.0	0.301	0.951

TABLE V-17. CONT'D. 48-FOOT TAPERED-TIP BLADES, μ = 0.35, $M_{(1.0,\ 90.)}$ = 0.95

Test 288.0 Run 9 Cont'd.

PT.	α_S	α_C	C_L/σ	C_D/σ	C_Y/σ	C_{ℓ}/σ	C_m/σ	C_Q/σ	θ_o	A_{1S}	μ	$M_{(1.0,90.)}$
17	-5.0	-6.7	0.031134	-0.000297	-0.001281	0.000228	-0.000600	0.002520	13.0	-0.95	0.350	0.952
18	-5.0	-7.3	0.039128	0.000390	-0.001436	0.000259	-0.000629	0.002841	14.0	-0.80	0.350	0.952
19	-5.0	-8.0	0.047723	0.000977	-0.001703	0.000260	-0.000724	0.003201	14.0	-0.60	0.350	0.953
20	-5.0	-8.8	0.054762	0.001740	-0.001519	0.000139	-0.000879	0.003638	15.0	-0.95	0.350	0.952
21	-7.0	-9.5	0.035794	0.001404	-0.001157	0.000140	-0.000782	0.003157	14.0	-0.95	0.350	0.951
22	-7.0	-11.0	0.052213	0.003468	-0.001222	-0.000087	-0.000798	0.004248	16.0	-0.70	0.351	0.952
23	-7.0	-12.7	0.067350	0.005770	-0.001482	-0.000247	-0.000935	0.005531	18.0	-0.60	0.351	0.951
24	-7.0	-8.3	0.018210	-0.000447	-0.000932	0.000119	-0.000618	0.002282	12.0	-0.95	0.349	0.949
25	-7.0	-7.5	0.009631	-0.001367	-0.000894	0.000129	-0.000481	0.001992	11.0	-1.05	0.351	0.949
26	-10.0	-13.5	0.034463	0.003144	-0.000529	-0.000209	-0.000585	0.003847	16.0	-0.80	0.350	0.955
27	-10.0	-14.1	0.041936	0.004585	-0.000576	-0.000395	-0.000670	0.004478	17.0	-0.80	0.352	0.952
28	-10.0	-15.0	0.049159	0.006084	-0.000493	-0.000620	-0.000690	0.005135	18.0	-0.95	0.352	0.952
29	-10.0	-15.6	0.058559	0.007722	-0.000939	-0.000748	-0.000684	0.006082	19.0	-0.70	0.352	0.953

Test 288.0 Run 10

PT.	α_S	α_C	C_L/σ	C_D/σ	C_Y/σ	C_{ℓ}/σ	C_m/σ	C_Q/σ	θ_o	A_{1S}	μ	$M_{(1.0,90.)}$
7	-12.0	-15.2	0.023934	0.001967	-0.000972	-0.000167	-0.000568	0.003405	16.0	-1.15	0.350	0.948
8	-12.0	-16.5	0.040197	0.005603	-0.000893	-0.000541	-0.000704	0.004901	18.0	-1.05	0.351	0.948
9	-12.0	-17.2	0.046198	0.007090	-0.000688	-0.000660	-0.000766	0.005523	19.0	-1.15	0.352	0.946
10	-15.0	-17.5	0.008784	-0.000722	-0.001054	-0.000109	-0.000384	0.002349	16.0	-1.25	0.350	0.948
11	-15.0	-19.1	0.024610	0.003490	-0.001042	-0.000554	-0.000562	0.004067	13.0	-1.25	0.351	0.948
12	-15.0	-19.7	0.030797	0.005285	-0.000819	-0.000663	-0.000542	0.004718	19.0	-1.25	0.352	0.946
13	-15.0	-20.2	0.037121	0.007096	-0.000720	-0.001002	-0.000621	0.005475	20.0	-1.25	0.353	0.942
14	-12.0	-13.7	0.007753	-0.001318	-0.001049	0.000083	-0.000501	0.002138	14.0	-1.25	0.351	0.949
15	-10.0	-12.0	0.017538	0.000217	-0.000848	-0.000012	-0.000439	0.002618	14.0	-1.15	0.352	0.944
16	-5.0	-9.7	0.062713	0.002421	-0.001729	0.000130	-0.000877	0.004213	16.0	-0.70	0.352	0.948
17	-5.0	-11.5	0.076562	0.004513	-0.002254	-0.000013	-0.000830	0.005617	18.0	-0.35	0.350	0.949
18	-2.0	-5.9	0.062374	-0.000711	-0.002381	0.000568	-0.000803	0.002948	14.0	-0.45	0.351	0.947
19	-2.0	-7.5	0.079165	0.000283	-0.003070	0.000578	-0.000705	0.004019	16.0	-0.25	0.352	0.945
20	-2.0	-4.4	0.045218	-0.001351	-0.002061	0.000592	-0.000553	0.002353	12.0	-0.80	0.351	0.947
21	0.0	-2.6	0.058889	-0.003087	-0.002742	0.000706	-0.000630	0.002012	12.0	-0.45	0.351	0.945
22	0.0	-4.6	0.073448	-0.002651	-0.003250	0.000789	-0.000838	0.002670	14.0	-0.35	0.351	0.948
23	0.0	-6.2	0.088303	-0.001686	-0.003768	0.000776	-0.000327	0.003905	16.0	-0.10	0.353	0.943

TABLE V-18. 48-FOOT TAPERED-TIP BLADES, μ = 0.35, $M_{(1.0,\ 90.)}$ = 1.0

Test 288.0 Run 12

PT.	α_S	α_C	C_L/σ	C_D/σ	C_Y/σ	C_ℓ/σ	C_m/σ	C_Q/σ	θ_o	A_{1S}	μ	$M_{(1.0,90.)}$
1	-9.0	-11.8	0.033323	0.000827	-0.000727	-0.000219	-0.001077	0.004215	15.0	-1.05	0.353	0.996
2	-9.0	-11.0	0.025396	-0.000811	-0.000785	0.000069	-0.001559	0.003927	14.0	-1.05	0.350	1.003
3	-9.0	-12.2	0.042084	0.001623	-0.000843	-0.000028	-0.001649	0.005144	16.0	-0.80	0.352	0.998
4	-9.0	-13.0	0.049369	0.002692	-0.001037	-0.000157	-0.001827	0.005831	17.0	-0.60	0.350	1.002
5	-9.0	-10.0	0.017947	-0.001739	-0.000718	0.000038	-0.001351	0.003414	13.0	-1.15	0.349	1.003
6	-9.0	-9.9	0.009032	-0.002730	-0.000649	-0.000013	-0.000928	0.002947	12.0	-1.15	0.351	1.003
7	-12.0	-14.6	0.025147	0.000798	-0.000556	-0.000371	-0.001070	0.004279	16.0	-1.15	0.350	1.002
8	-12.0	-15.3	0.032855	0.002395	-0.000609	-0.000435	-0.001171	0.005009	17.0	-0.95	0.351	1.003
9	-12.0	-14.0	0.017319	-0.000546	-0.000522	-0.000345	-0.000835	0.003585	15.0	-0.95	0.349	1.002
10	-12.0	-13.2	0.010439	-0.001898	-0.000706	-0.000117	-0.000667	0.002998	14.0	-1.25	0.351	1.001
11	-12.0	-12.5	0.002874	-0.003202	-0.000578	-0.000086	-0.000557	0.002472	13.0	-1.15	0.349	1.003
12	-15.0	-17.1	0.010694	-0.001387	-0.000536	-0.000467	-0.000468	0.003271	16.0	-1.15	0.351	1.002
13	-15.0	-17.7	0.018403	0.000538	-0.000664	-0.000597	-0.000643	0.004085	17.0	-1.05	0.350	1.005
14	-15.0	-18.4	0.026390	0.002529	-0.000558	-0.000729	-0.000816	0.004939	18.0	-1.05	0.353	0.999
15	-15.0	-16.4	0.003068	-0.003257	-0.000691	-0.000311	-0.000352	0.002608	15.0	-1.25	0.351	1.001
16	-12.0	-16.0	0.038999	0.003802	-0.000569	-0.000645	-0.001069	0.005695	17.0-18.0	-0.95	0.352	1.002
17	-13.0	-16.8	0.038004	0.003998	-0.000693	-0.000687	-0.001030	0.005746	18.0	-0.95	0.352	1.000
18	-14.0	-17.8	0.030445	0.003164	-0.000471	-0.000834	-0.000891	0.005150	18.0	-0.95	0.351	1.003
19	-6.0	-8.1	0.041862	-0.000306	-0.001239	0.000229	-0.001047	0.004123	14.0	-0.80	0.352	0.999
20	-6.0	-8.9	0.051300	0.000467	-0.001388	0.000118	-0.001171	0.004731	15.0	-0.70	0.352	1.000
21	-6.0	-9.7	0.059704	0.001236	-0.001691	0.000101	-0.001216	0.005413	16.0	-0.45	0.353	1.000
22	-6.0	-7.4	0.035716	-0.000961	-0.001114	0.000122	-0.000943	0.003733	13.0	-0.80	0.351	1.001
23	-6.0	-6.7	0.026919	-0.001558	-0.001070	0.000143	-0.000898	0.003338	12.0	-0.95	[illegible]	0.999
24	-6.0	-6.2	0.018195	-0.002151	-0.000954	0.000157	-0.000889	0.003034	11.0	-0.95	0.351	1.002
25	-3.0	-6.0	0.059447	-0.001873	-0.002166	0.000539	-0.001310	0.004080	14.0	-0.60	0.351	1.002
26	-3.0	-6.5	0.067565	-0.001496	-0.002150	0.000481	-0.001221	0.004678	15.0	-0.35	0.351	1.001
27	-3.0	-5.1	0.050920	-0.002331	-0.002049	0.000610	-0.001306	0.003675	13.0	-0.45	0.351	1.001
28	-3.0	-4.3	0.043578	-0.002687	-0.001780	0.000532	-0.001225	0.003412	12.0	-0.60	0.352	1.001
29	-3.0	-3.7	0.034536	-0.002878	-0.001442	0.000469	-0.001178	0.003158	11.0	-0.70	0.352	1.001

TABLE V-19. 48-FOOT TAPERED-TIP BLADES, μ = 0.35, $M_{(1.0,\ 90.)}$ = 1.025

Test 288.0 Run 15

1	-12.0	-15.4	0.033266	0.002486	-0.000149	-0.000682	-0.000636	0.005051	17.0	-1.05	0.352	1.017
2	-12.0	-15.2	0.033456	0.002440	-0.000254	-0.000711	-0.000565	0.005221	17.0	-0.95	0.350	1.024
3	-12.0	-14.4	0.027293	0.001019	-0.000078	-0.000628	-0.000575	0.004575	16.0	-1.05	0.351	1.022
4	-12.0	-13.5	0.019153	-0.000654	-0.000094	-0.000480	-0.000619	0.003890	15.0	-1.15	0.350	1.020
5	-12.0	-12.8	0.012027	-0.002102	-0.000037	-0.000441	-0.000679	0.003352	14.0	-1.15	0.352	1.020
6	-9.0	-10.2	0.027565	-0.000529	-0.000209	-0.000366	-0.000641	0.004066	14.0	-1.05	0.352	1.022
7	-9.0	-9.6	0.019757	-0.001608	-0.000113	-0.000287	-0.000752	0.003633	13.0	-0.95	0.351	1.023
8	-9.0	-11.2	0.034926	0.000655	-0.000228	-0.000387	-0.000508	0.004618	15.0	-0.80	0.352	1.020
9	-9.0	-12.1	0.043378	0.001949	-0.000182	-0.000581	-0.000592	0.005289	16.0	-0.70	0.352	1.022
10	-15.0	-16.7	0.011735	-0.001590	0.000151	-0.000711	-0.000492	0.003573	16.0	-1.25	0.350	1.024
11	-15.0	-17.3	0.019647	0.000485	0.000070	-0.000818	-0.000460	0.004332	17.0	-1.15	0.350	1.024

TABLE V-19. CONT'D. 48-FOOT TAPERED-TIP BLADES, μ = 0.35, $M_{(1.0,\ 90.)}$ = 1.025

Test 288.0 Run 15 Cont'd.

PT	α_S	α_C	C_L/σ	C_D/σ	C_Y/σ	C_ℓ/σ	C_m/σ	C_Q/σ	θ_o	A_{1S}	μ	$M_{(1.0,90.)}$
12	-15.0	-18.1	0.026347	0.002357	0.000275	-0.001081	-0.000405	0.004974	18.0	-1.05	0.351	1.022
13	-13.0	-16.8	0.031172	0.003843	0.000278	-0.001248	-0.000586	0.005724	19.0	-0.95	0.351	1.024
14	-13.0	-15.9	0.029001	0.001986	-0.000060	-0.000803	-0.000390	0.005001	17.0	-1.05	0.350	1.023

TABLE V-20. 48-FOOT TAPERED-TIP BLADES, μ = 0.40, $M_{(1.0,\ 90.)}$ = 0.84

Test 274.0 Run 7

PT	α_S	α_C	C_L/σ	C_D/σ	C_Y/σ	C_ℓ/σ	C_m/σ	C_Q/σ	θ_o	A_{1S}	μ	$M_{(1.0,90.)}$
1	-4.0	-7.3	0.028193	-0.000495	-0.000797	0.000180	-0.000629	0.001965	12.0	0.48	0.399	0.846
2	-4.0	-9.2	0.044789	0.000794	-0.001045	0.000058	-0.000688	0.002733	14.0	0.24	0.401	0.844
3	-8.0	-11.9	0.021366	0.000146	-0.000069	-0.000011	-0.000639	0.002212	14.0	0.48	0.401	0.843
4	-8.0	-13.5	0.037794	0.002486	-0.000092	-0.000173	-0.000761	0.003390	16.0	0.60	0.403	0.842
5	-12.0	-16.2	0.014696	-0.000067	0.000238	0.000094	-0.000731	0.002216	16.0	0.72	0.401	0.844
6	-12.0	-18.0	0.029574	0.003329	0.000353	-0.000403	-0.000677	0.003751	18.0	0.72	0.403	0.843
7	-8.0	-15.3	0.052280	0.005030	-0.000178	-0.000450	-0.000926	0.004760	18.0	0.60	0.403	0.843
8	-4.0	-10.8	0.059777	0.002045	-0.001376	0.000065	-0.000688	0.003682	16.0	0.36	0.402	0.843
9	-4.0	-12.0	0.067206	0.002957	-0.001512	0.000166	-0.000867	0.004358	17.0	0.24	0.403	0.841
10	0.	-4.5	0.051270	-0.002032	-0.002075	0.000416	-0.000612	0.001634	12.0	0.00	0.402	0.844
11	0.	-6.5	0.068744	-0.001777	-0.002495	0.000529	-0.000607	0.002244	14.0	0.00	0.400	0.845
12	0.	-2.5	0.035900	-0.002264	-0.001562	0.000347	-0.000455	0.001255	10.0	0.00	0.400	0.845
13	0.	-0.8	0.019073	-0.002101	-0.001123	0.000286	-0.000545	0.001137	8.0	0.12	0.401	0.844
14	4.0	1.9	0.045410	-0.005526	-0.002247	0.000384	-0.000746	0.000209	8.0	0.00	0.398	0.847
15	4.0	-0.1	0.059835	-0.006383	-0.003007	0.000415	-0.001053	0.000323	10.0	-0.36	0.400	0.846
16	-4.0	-5.3	0.012128	-0.001580	-0.000625	0.000076	-0.000602	0.001546	10.0	0.36	0.403	0.842
17	-8.0	-9.9	0.005026	-0.002199	-0.000071	-0.000029	-0.000535	0.001377	12.0	0.36	0.402	0.845

Test 274.0 Run 15

PT	α_S	α_C	C_L/σ	C_D/σ	C_Y/σ	C_ℓ/σ	C_m/σ	C_Q/σ	θ_o	A_{1S}	μ	$M_{(1.0,90.)}$
31	-2.0	-7.7	0.053944	-0.000207	-0.001356	0.000108	-0.000816	0.002617	14.0	0.48	0.399	0.847
32	-2.0	-8.7	0.060952	0.000259	-0.001537	-0.000011	-0.000697	0.002995	15.0	0.24	0.401	0.846
33	-2.0	-9.5	0.070202	0.000684	-0.001800	-0.000002	-0.000791	0.003504	16.0	0.24	0.401	0.845

TABLE V-21. 48-FOOT TAPERED-TIP BLADES, μ = 0.40, $M_{(1.0,\ 90.)}$ = 0.85

Test 288.0 Run 5

PT	α_S	α_C	C_L/σ	C_D/σ	C_Y/σ	C_ℓ/σ	C_m/σ	C_Q/σ	θ_o	A_{1S}	μ	$M_{(1.0,90.)}$
1	-4.0	-8.7	0.039962	0.000916	-0.001126	0.000163	-0.000660	0.002682	14.0	-0.80	0.401	0.852
2	-4.0	-10.6	0.054461	0.002205	-0.001486	0.000197	-0.000724	0.003519	16.0	-0.80	0.396	0.859
3	-4.0	-12.5	0.069525	0.003919	-0.001811	0.000052	-0.000767	0.004812	18.0	-0.70	0.401	0.850
4	-8.0	-15.2	0.047449	0.004913	-0.000205	-0.000535	-0.000592	0.004555	18.0	-1.05	0.399	0.852
5	-8.0	-16.8	0.058799	0.007126	-0.000214	-0.000687	-0.000841	0.005803	20.0	-0.95	0.397	0.857
6	-12.0	-17.8	0.025729	0.002908	0.000153	-0.000588	-0.000624	0.003415	18.0	-1.25	0.397	0.856
7	-12.0	-19.4	0.038319	0.005997	0.000133	-0.000789	-0.000652	0.005017	20.0	-1.25	0.399	0.853

TABLE V-21. CONT'D. 48-FOOT TAPERED-TIP BLADES, μ = 0.40, $M_{(1.0,\ 90.)}$ = 0.85

Test 288.0 Run 7

PT.	α_S	α_C	C_L/σ	C_D/σ	C_Y/σ	C_ℓ/σ	C_m/σ	C_Q/σ	θ_o	A_{1S}	μ	$M_{(1.0,90.)}$
1	-4.0	-12.2	0.076035	0.002944	-0.002899	0.000536	-0.001161	0.004894	18.0	-0.60	0.401	0.845
2	-4.0	-13.1	0.081044	0.004087	-0.002909	0.000369	-0.001344	0.005704	19.0	-0.45	0.396	0.853
3	-4.0	-14.0	0.085398	0.005007	-0.003104	0.000360	-0.001309	0.006660	20.0	1.40	0.398	0.850
4	-4.0	-3.3	-0.001140	-0.002049	-0.001617	0.000459	-0.001158	0.001326	8.0	-1.05	0.399	0.849
5	-2.0	-5.0	0.043550	-0.001147	-0.002479	0.000723	-0.000340	0.001950	12.0	-0.70	0.396	0.853
6	-2.0	-3.5	0.027193	-0.001475	-0.002198	0.000757	-0.000144	0.001537	10.0	-0.95	0.398	0.848
7	-2.0	-2.0	0.010925	-0.001746	-0.001868	0.000520	-0.000159	0.001451	8.0	-1.05	0.400	0.847
8	-2.0	-9.9	0.080477	0.001158	-0.003413	0.000652	-0.000710	0.004190	17.0	-0.45	0.398	0.850
9	-2.0	-11.0	0.084170	0.002159	-0.003762	0.000639	-0.000697	0.005017	18.0	-0.25	0.398	0.851
10	0.0	-7.6	0.083656	-0.001384	-0.004335	0.000830	-0.000698	0.003334	16.0	-0.25	0.399	0.848
11	0.0	-8.8	0.087839	-0.000399	-0.004628	0.000848	-0.000786	0.004182	17.0	-0.10	0.398	0.849
12	0.0	-9.7	0.092076	0.000599	-0.004998	0.001015	-0.000711	0.005188	18.0	0.15	0.398	0.849
13	0.0	-9.7	0.071532	-0.002381	-0.004007	0.000971	-0.000722	0.002217	14.0	-0.35	0.398	0.849

TABLE V-22. 48-FOOT TAPERED-TIP BLADES, μ = 0.40, $M_{(1.0,\ 90.)}$ = 0.95

Test 288.0 Run 13

1	-9.0	-12.4	0.026799	0.000248	-0.000476	0.000015	-0.000510	0.003153	15.0	-1.25	0.404	0.947
2	-9.0	-13.1	0.034482	0.001380	-0.000664	0.000062	-0.000378	0.003801	16.0	-1.15	0.404	0.948
3	-9.0	-11.6	0.019715	-0.000792	-0.000632	0.000142	-0.000491	0.002677	14.0	-1.25	0.403	0.948
4	-9.0	-10.9	0.012847	-0.001753	-0.000612	0.000167	-0.000265	0.002235	13.0	-1.25	0.404	0.948
5	-12.0	-14.6	0.011369	-0.001578	-0.000292	-0.000029	-0.000289	0.002349	15.0	-1.25	0.404	0.947
6	-12.0	-15.2	0.018260	-0.000168	-0.000298	-0.000088	-0.000302	0.002997	16.0	-1.25	0.404	0.948
7	-12.0	-16.1	0.025255	0.001360	-0.000231	-0.000294	-0.000323	0.003587	17.0	-1.15	0.402	0.949
8	-12.0	-16.8	0.031335	0.002680	-0.000377	-0.000302	-0.000301	0.004371	18.0	-1.25	0.405	0.947
9	-12.0	-17.7	0.038236	0.003964	-0.000419	-0.000564	-0.000720	0.005229	19.0	-1.15	0.404	0.947
10	-12.0	-13.9	0.003491	-0.003199	-0.000383	0.000065	-0.000448	0.001716	14.0	-1.25	0.404	0.946
11	-15.0	-18.3	0.009813	-0.001550	-0.000400	-0.000282	-0.000137	0.002576	17.0	-1.35	0.403	0.948
12	-15.0	-19.0	0.015745	0.000067	-0.000369	-0.000449	-0.000137	0.003244	18.0	-1.35	0.402	0.951
13	-15.0	-19.7	0.022658	0.001875	-0.000356	-0.000616	-0.000160	0.003992	19.0	-1.25	0.401	0.952
14	-15.0	-17.8	0.001979	-0.003535	-0.000298	-0.000125	-0.000077	0.001663	16.0	-1.25	0.401	0.950
15	-7.0	-9.8	0.031850	-0.000098	-0.000798	0.000127	-0.000559	0.003122	14.0	-1.15	0.403	0.949
16	-7.0	-10.8	0.038698	0.000707	-0.000805	0.000029	-0.000632	0.003640	15.0	-1.05	0.403	0.946

TABLE V-23. 34-FOOT-DIAMETER BLADES, μ = 0.51, $M_{(1.0,\ 90.)}$ = 0.65

Test 274.0 Run 23

PT.	α_S	α_C	C_L/σ	C_D/σ	C_Y/σ	$C_{\mathcal{L}}/\sigma$	$C_{\mathcal{M}}/\sigma$	C_Q/σ	θ_o	A_{1S}	μ	$M_{(1.0,90.)}$
1	-4.0	-9.6	0.029793	-0.001943	-0.001352	0.000436	-0.000416	0.002533	12.0	-0.36	0.508	0.651
2	-4.0	-11.5	0.043524	-0.001430	-0.001942	0.000401	-0.000123	0.003467	14.0	-0.36	0.508	0.651
3	-4.0	-13.5	0.052638	-0.000799	-0.002382	0.000365	-0.000662	0.004621	16.0	-0.24	0.509	0.650
4	-4.0	-7.7	0.018401	-0.002224	-0.001100	0.000308	-0.000124	0.001939	10.0	-0.72	0.509	0.650
5	-4.0	-12.5	0.048248	-0.001306	-0.001987	0.000164	-0.000685	0.003890	15.0	-0.24	0.510	0.650
6	-6.0	-12.8	0.032110	-0.001279	-0.000900	-0.000238	-0.000528	0.003393	14.0	-0.24	0.509	0.648
7	-6.0	-10.9	0.020478	-0.001979	-0.000650	-0.000241	-0.000254	0.002291	12.0	-0.36	0.509	0.648
8	-6.0	-14.6	0.044590	-0.000235	-0.001530	-0.000036	-0.000749	0.004588	16.0	-0.12	0.509	0.648

Test 274.0 Run 26

PT.	α_S	α_C	C_L/σ	C_D/σ	C_Y/σ	$C_{\mathcal{L}}/\sigma$	$C_{\mathcal{M}}/\sigma$	C_Q/σ	θ_o	A_{1S}	μ	$M_{(1.0,90.)}$
7	-4.0	-10.8	0.039924	-0.001627	-0.001795	0.000353	-0.000162	0.003233	13.0	-0.36	0.508	0.652
8	-4.0	-11.8	0.045328	-0.001458	-0.002071	0.000347	-0.000415	0.003707	14.0	-0.36	0.509	0.650
9	-4.0	-12.7	0.051313	-0.001092	-0.001934	0.000047	-0.000027	0.004033	15.0	-0.24	0.510	0.648
10	-4.0	-13.5	0.058421	-0.000716	-0.002539	0.000254	-0.000154	0.004705	16.0	-0.36	0.511	0.648
11	-2.0	-8.5	0.043574	-0.002552	-0.00218	0.000449	0.000335	0.002655	12.0	-0.60	0.510	0.649
12	-2.0	-10.5	0.057079	-0.002402	-0.00277	0.000511	0.000418	0.003418	14.0	-0.48	0.511	0.648
13	-2.0	-8.5	0.043643	-0.002635	-0.002044	0.000239	0.000517	0.002596	12.0	-0.60	0.511	0.648
14	-2.0	-6.6	0.032804	-0.002662	-0.001270	-0.000201	0.001272	0.001984	10.0	-0.72	0.510	0.648
15	-2.0	-7.7	0.038594	-0.002532	-0.002038	0.000620	0.000737	0.002433	11.0	-0.60	0.511	0.647
16	-2.0	-5.0	0.019549	-0.002570	-0.001041	0.000398	0.001086	0.001716	8.0	-0.84	0.512	0.648
17	0.	-7.3	0.056057	-0.004106	-0.002669	0.000160	0.000440	0.002220	12.0	-0.84	0.512	0.648
18	0.	-5.4	0.044194	-0.003711	-0.002360	0.000462	0.000572	0.001730	10.0	-0.84	0.512	0.648
19	0.	-3.7	0.031124	-0.003269	-0.001494	0.000371	0.001284	0.001443	8.0	-0.84	0.512	0.648
20	0.	-9.2	0.065880	-0.003694	-0.003548	0.000648	0.001213	0.003260	14.0	-0.60	0.515	0.646
21	2.0	-4.1	0.054716	-0.005593	-0.003154	0.000750	0.000657	0.001286	10.0	-0.96	0.512	0.647
22	2.0	-2.3	0.043638	-0.005041	-0.002295	0.000360	0.000502	0.000907	8.0	-0.96	0.513	0.646
23	2.0	-0.8	0.032084	-0.004419	-0.001962	0.000599	0.001469	0.000983	6.0	-1.2	0.513	0.646
24	2.0	-6.0	0.068288	-0.006240	-0.003463	0.000081	0.001172	0.001975	12.0	-0.96	0.514	0.646
25	2.0	-8.0	0.077860	-0.005931	-0.004445	0.000790	0.001122	0.003163	14.0	-0.84	0.515	0.645
26	0.	-11.0	0.078046	-0.003865	-0.003656	0.000427	0.000908	0.004605	16.0	-0.24	0.517	0.644
27	-2.0	-11.4	0.062101	-0.002497	-0.002650	0.000045	0.000526	0.003932	15.0	-0.60	0.517	0.644

TABLE V-24. 34-FOOT-DIAMETER BLADES, μ = 0.66, $M_{(1.0,\ 90.)}$ = 0.55

Test 274.0 Run 27

PT.	α_S	α_C	C_L/σ	C_D/σ	C_Y/σ	$C_{\mathcal{L}}/\sigma$	C_m/σ	C_Q/σ	θ_o	A_{1S}	μ	$M_{(1.0,90.)}$
3	0.	-8.4	0.034002	-0.005523	-0.003018	0.001042	0.002759	0.001777	12.0	-0.48	0.652	0.556
4	0.	-6.2	0.029013	-0.004954	-0.003125	0.001644	0.002152	0.001848	10.0	-0.60	0.653	0.555
5	0.	-4.1	0.022101	-0.004698	-0.002417	0.000833	0.002090	0.001524	8.0	-1.08	0.653	0.554
6	0.	-2.5	0.012812	-0.004042	-0.001786	0.000963	0.001460	0.001671	6.0	-1.20	0.654	0.554
7	0.	-10.4	0.042426	-0.006537	-0.004611	0.002040	0.004753	0.002615	14.0	-0.36	0.655	0.552
8	0.	-8.4	0.034672	-0.005892	-0.003623	0.001548	0.002443	0.001965	12.0	-0.60	0.655	0.553
9	-2.0	-9.4	0.025905	-0.005298	-0.002126	0.001025	0.000201	0.001746	12.0	-0.36	0.663	0.550
10	-2.0	-7.4	0.017451	-0.005056	-0.002139	0.001413	-0.001044	0.001753	10.0	-0.72	0.662	0.550
11	-2.0	-5.1	0.011458	-0.004403	-0.002096	0.001144	-0.000633	0.001519	8.0	-0.96	0.664	0.550
12	-2.0	-11.7	0.028681	-0.006305	-0.002909	0.001462	0.000900	0.002187	14.0	-0.24	0.663	0.550
13	-4.0	-11.5	0.020578	-0.006435	-0.001933	0.001638	-0.001914	0.002088	13.0	-0.36	0.665	0.549
14	-4.0	-12.7	0.023335	-0.006873	-0.002052	0.001481	-0.001733	0.002147	14.0	-0.12	0.666	0.549
15	-4.0	-13.5	0.028335	-0.006586	-0.002493	0.001939	-0.000049	0.002643	15.0	0.00	0.666	0.549
16	-4.0	-14.5	0.032142	-0.006982	-0.001935	0.000906	-0.000253	0.002591	16.0	0.00	0.666	0.549
17	-4.0	-10.5	0.015771	-0.006364	-0.001611	0.001209	-0.001102	0.001785	12.0	-0.36	0.666	0.549
18	2.0	-5.2	0.042321	-0.006331	-0.004032	0.001919	0.000742	0.001430	10.0	-0.84	0.666	0.548
19	2.0	-3.0	0.035765	-0.006018	-0.003564	0.001905	0.001691	0.001184	8.0	-1.08	0.667	0.548
20	2.0	-1.2	0.028333	-0.005342	-0.001829	0.000032	0.001288	0.001125	6.0	-1.32	0.668	0.548
21	2.0	-8.5	0.051621	-0.008063	-0.005192	0.002114	0.002338	0.002086	13.0	-0.84	0.668	0.548
22	2.0	-7.3	0.050186	-0.007537	-0.003877	0.000884	0.001516	0.001613	12.0	-0.84	0.667	0.548
23	4.0	-2.1	0.047956	-0.007430	-0.004067	0.001132	0.002071	0.000249	8.0	-1.44	0.670	0.548
24	4.0	-0.2	0.042675	-0.006952	-0.002248	-0.000472	0.001774	-0.000032	6.0	-1.56	0.668	0.548
25	4.0	-4.2	0.053789	-0.008436	-0.004300	0.001158	0.003084	0.000321	10.0	-1.08	0.667	0.547
26	4.0	-5.4	0.059673	-0.009058	-0.005201	0.002201	0.000961	0.000875	11.0	-0.96	0.667	0.547

TABLE V-25. 34-FOOT-DIAMETER BLADES, μ = 0.79, $M_{(1.0,\ 90.)}$ = 0.52

Test 274.0 Run 29

PT.	α_S	α_C	C_L/σ	C_D/σ	C_Y/σ	$C_{\mathcal{L}}/\sigma$	C_m/σ	C_Q/σ	θ_o	A_{1S}	μ	$M_{(1.0,90.)}$
6	0.	-9.5	0.031178	-0.009999	-0.003442	0.001102	0.002000	0.001374	12.0	-0.48	0.785	0.528
7	0.	-8.3	0.030857	-0.009479	-0.004031	0.001343	0.002954	0.001111	11.0	-0.96	0.787	0.527
8	0.	-7.1	0.029976	-0.008726	-0.003761	0.002411	0.002489	0.001384	10.0	-0.96	0.786	0.526
9	0.	-6.1	0.023137	-0.007974	-0.002090	-0.000395	0.002025	0.001157	9.0	-1.08	0.787	0.526
10	0.	-5.0	0.020888	-0.006787	-0.002337	0.000774	0.002071	0.001793	8.0	-1.20	0.787	0.526
11	2.0	-6.2	0.039647	-0.010028	-0.003583	0.001255	0.002300	0.000779	10.0	-0.96	0.789	0.524
12	2.0	-5.2	0.035874	-0.009461	-0.004759	0.002092	0.002630	0.001067	9.0	-1.20	0.792	0.524
13	2.0	-4.1	0.040683	-0.007894	-0.003609	0.000732	0.005380	0.000680	8.0	-1.44	0.792	0.523
14	2.0	-7.6	0.037808	-0.010249	-0.004786	0.001395	0.001554	0.001239	11.0	-0.72	0.792	0.523
15	2.0	-6.3	0.039812	-0.010278	-0.004718	0.001879	0.001203	0.000606	10.0	-1.20	0.789	0.523
16	0.	-7.1	0.027435	-0.008690	-0.003789	0.002183	0.001909	0.001768	10.0	-1.32	0.791	0.523

Unclassified

Security Classification

DOCUMENT CONTROL DATA - R & D

(Security classification of title, body of abstract and indexing annotation must be entered when the overall report is classified)

1. ORIGINATING ACTIVITY (Corporate author) Bell Helicopter Company Fort Worth, Texas	2a. REPORT SECURITY CLASSIFICATION Unclassified 2b. GROUP

3. REPORT TITLE

WIND TUNNEL TESTS OF FULL-SCALE ROTORS OPERATING AT HIGH ADVANCING TIP MACH NUMBERS AND ADVANCE RATIOS

4. DESCRIPTIVE NOTES (Type of report and inclusive dates)

Final

5. AUTHOR(S) (First name, middle initial, last name)

Watson H. Tanner
James F. Van Wyckhouse

6. REPORT DATE July 1968	7a. TOTAL NO. OF PAGES 150	7b. NO. OF REFS 15
8a. CONTRACT OR GRANT NO. DA 44-177-AMC-291(T) DAAJ02-67-C-0018 b. PROJECT NO. IF125901A13903 c. IF125901A14231 d.	9a. ORIGINATOR'S REPORT NUMBER(S) USAAVLABS Technical Report 68-44 9b. OTHER REPORT NO(S) (Any other numbers that may be assigned this report) BHC Report 576-099-001	

10. DISTRIBUTION STATEMENT

This document has been approved for public release and sale; its distribution is unlimited.

11. SUPPLEMENTARY NOTES	12. SPONSORING MILITARY ACTIVITY U. S. Army Aviation Materiel Laboratories, Fort Eustis, Va.

13. ABSTRACT

A joint U. S. Army Aviation Materiel Laboratories/NASA-Ames/Bell Helicopter Company experimental investigation of three full-scale sets of rotor blades was conducted in the NASA-Ames Large Scale Wind Tunnel. Tested were: (1) production UH-1D (NACA 0012 profile) 48-foot-diameter blades, (2) modified UH-1D blades reduced in thickness at the tip, and (3) UH-1D blades reduced in diameter to 34 feet. The production blades were evaluated at Mach numbers up to 0.95, the thin-tipped blades to Mach 1.025, and the 34-foot rotor to advance ratios of 0.79. The production and thin-tipped blades are compared to show the compressibility effects. At higher tip Mach numbers, a significant reduction in power required was obtained with the thin-tipped blades. Additionally, the state of the art of calculating rotorcraft performance at high tip speeds and advance ratio is reviewed, and limited experimental data obtained with special boundary layer instrumentation installed at the 3/4 radius and surface pressure instrumentation installed near the blade tip are presented.

DD FORM 1 NOV 65 1473 REPLACES DD FORM 1473, 1 JAN 64, WHICH IS OBSOLETE FOR ARMY USE.

Unclassified

Security Classification

Unclassified
Security Classification

14. KEY WORDS	LINK A		LINK B		LINK C	
	ROLE	WT	ROLE	WT	ROLE	WT
Rotor performance Thin-tipped main rotor blades High advance ratio High advancing tip Mach number Surface pressure distribution Boundary layer						

Unclassified
Security Classification

7162-68